DISSIPATIVE FLOW IN THE SUPERFLUID HELIUM FILM IN THE TEMPERATURE REGION 1.63K TO 0.01K

Michael W. Toft

A Thesis Submitted for the Degree of PhD
at the
University of St Andrews

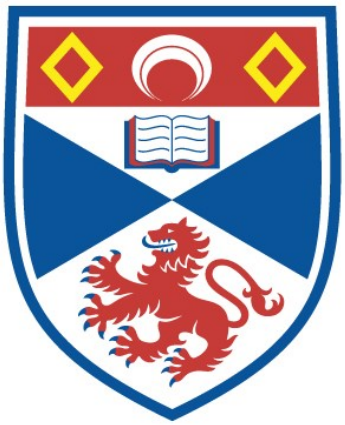

1978

DISSIPATIVE FLOW OF THE SUPERFLUID HELIUM FILM IN THE TEMPERATURE REGION 1.63K TO 0.01K

A thesis

presented by

Michael W. Toft, BSc,

to the

University of St. Andrews

in application for the Degree of

Doctor of Philosophy.

ProQuest LLC.
789 East Eisenhower Parkway
P.O. Box 1346
Ann Arbor, MI 48106 – 1346

ABSTRACT

Experiments on helium film flow over a stainless steel beaker rim were carried out in the temperature region 1.63K to 11mK. No previous measurements have been made below 36mK. The results of other studies of film flow below 1K are mutually conflicting; this is thought to originate from poor temperature stability, inadequate vibration isolation and contamination of the substrate. Careful attention was paid to these points in the design and construction of a demagnetisation cryostat, full details of which are given.

Flow experiments from initial level differences of ∿8mm confirmed the existence of a range of metastable transfer rates at all temperatures. The variation of the mean rate with rim height suggests that the film profile should be calculated using a van der Waals' exponent, n, of 2.85 $\pm$ .25. The low temperature increase in transfer rate reported by others was observed, but did not extend below 1K. Instead, the mean transfer rate was approximately constant from 1K to 400mK, in direct conflict with the predictions of thermal fluctuation theories of superfluid dissipation. Below 250mK the results corroborated closely those of Crum et al in that the transfer rate fell sharply with decreasing temperature. Discrepancies arose between runs below 60mK, some showing the transfer rate to decrease monotonically with temperature down to 20mK whilst others indicated a levelling out of the transfer rate, followed by a slight increase at the lowest temperatures. These effects were thought to originate from changes in the concentration of the ^{3}He impurity in the film.

Steady state driven flow experiments at level differences of

<500μm provided the first evidence for the existence of dissipation at subcritical transfer rates at temperatures below 1K. That is, superfluid flow was shown to be never strictly frictionless. Above 1K, the form of the subcritical dissipation curve conformed to the predictions of thermal fluctuation theories, but the values of the parameters β and f_o for flow over stainless steel were considerably smaller than those reported for flow over glass. The parameter f_o was also found to be strongly temperature dependent. Below 1K, the onset of dissipation was seen to be much more gradual, and the form of the subcritical dissipation curve was independent of temperature down to 20mK.

These findings were corroborated by measurements of the damping of the inertial oscillations occurring at the end of each flow experiment. At the lowest temperature attained, 11mK, a change in subcritical dissipative behaviour was observed; exponential damping of the oscillations indicated that the frictional force on unit mass of superfluid was now directly proportional to the superfluid velocity, and was of magnitude $(4.56 \pm .28) \times 10^{-3}$ dynes $g^{-1} cm^{-1} s$. Exponential damping was also observed at temperatures above 1K, where Robinson type thermal dissipation was the dominant mechanism at small transfer rates.

DECLARATION

I hereby certify that this thesis has been composed by me, and is a record of work done by me, and has not previously been presented for a Higher Degree.

The research was carried out in the School of Physical Sciences in the University of St Andrews, under the supervision of Professor J.F. Allen, FRS.

Michael W. Toft.

CERTIFICATE

I certify that Michael W. Toft, BSc, has spent nine terms at research work in the School of Physical Sciences in the University of St. Andrews under my direction, that he has fulfilled the conditions of the Resolution of the University Court, 1967, No 1, and that he is qualified to submit the accompanying thesis in application for the Degree of Doctor of Philosophy.

Research Supervisor

PERSONAL PREFACE

After three years as an undergraduate at the University of Bristol I graduated in 1972 with an Upper Second Class Honours Bachelor of Science degree in Physics.

From October 1972 to July 1976 I held an SRC Studentship in the School of Physical Sciences at the University of St Andrews, under the supervision of Professor J.F. Allen. In October 1972 I enrolled under resolution of the University Court, 1967, No 1, as a candidate for a PhD.

From December 1976 to September 1977 I held an SRC Research Assistantship in the School of Physical Sciences at the University of St Andrews.

ACKNOWLEDGEMENTS

I should like to thank Professor J.F. Allen and Mr J.G.M. Armitage for their most valuable guidance and support during the supervision of this project.

I should also like to express my gratitude to the Physics Department Trust for the provision of a maintenance grant during a period of this work.

I am also indebted to Professor J.T. Tough of the Ohio State University, with whom I worked for one year on the prototype model of the cryostat. Professor Tough very kindly supplied part of the experimental cell and many of the specialist materials used during the construction of the cryostat.

I would like to thank Dr Fracetti of the CNRS (Grenoble) for his generosity in providing a calibrated carbon resistance thermometer.

My thanks are also due to Mr R. McCraw, Mr D. Jones, Mr W. Cargill and Mr A. Mackie of the Physics Department Workshop, who skilfully manufactured many parts of the cryostat.

I am especially indebted to Mr T. Marshall for always keeping pace with the insatiable demands made upon him for liquid helium.

Finally, I would like to thank my wife Linda for her unfailing patience and encouragement during the course of this work, and also for her help in the preparation of many of the diagrams in this thesis.

CONTENTS

CHAPTER ONE

INTRODUCTION

1.1. THE GENERAL PROPERTIES OF LIQUID HELIUM

Helium is the only substance to remain a liquid under its own vapour pressure down to a temperature of absolute zero. This is true of both the stable isotopes, ^4He and ^3He, and it results from the large zero point energy of the atoms due to their small mass and the weakness of the interatomic attractive forces. We are thus presented with a unique opportunity to study a liquid state at low energy, exhibiting very little thermal disorder.

Helium-4 was first liquefied by Kamerlingh Onnes in 1908 and was found to boil at 4,21K under one atmosphere pressure. An indication that the liquid possessed unusual properties came with the observation that the density passed through a maximum at a temperature of 2.17K. This temperature, termed the λ-point, was also found to characterise, amongst other things, a logarithmic infinity in the specific heat and a maximum in the dielectric constant, and is understood as marking a phase transition of at least 2nd order in the liquid. The phases of helium above and below the λ-point are designated HeI and HeII respectively.

Early experiments on transport properties of the new phase revealed remarkable and unexpected behaviour. In particular determinations of the viscosity as a function of temperature gave different results according to the experimental method employed. Rotation viscometer measurements showed that, below the λ-point, the viscosity decreased rapidly to a small but finite value and then rose sharply again below 1K. On the other hand, capillary flow experiments by Allen and Misener (1938) and Kapitza (1938) indicated that under certain conditions the viscosity

below the λ-point became vanishingly small, with an upper limit of 10^{-11} poise. Such behaviour led to the new phase being termed a superfluid.

No satisfactory interpretation of this and other phenomena was afforded until the introduction by London (1939) and Tisza (1938) and later, in a different form by Landau (1941) of a "Two-Fluid Model" for HeII.

1.2. THE TWO-FLUID MODEL OF LONDON AND TISZA

This "early" two-fluid model proposed that, since the ^{4}He nucleus is even-numbered and has zero spin, it should obey Bose-Einstein statistics. Thus, the λ-transition exhibited by a system of He-4 atoms can be identified with the theoretically predicted condensation of an ideal Bose gas. Below the transition temperature T_λ the liquid can be thought of as a mixture of two fluids, the "superfluid" consisting of the condensate, that is, atoms all in the same momentum ground state, and the "normal fluid", constituted by the remaining atoms of higher momenta. The relative amounts of normal and superfluid are functions of the temperature, and at $T = 0$, the liquid is thought of as being entirely composed of atoms in the condensed state. This interpretation was encouraged by the apparent absence of a superfluid transition in the other isotope, ^{3}He, which obeys Fermi-Dirac statistics. Also a substitution of the appropriate parameters for ^{4}He into the theoretical expression for the transition temperature of an ideal Bose gas yielded $T_c = 3.14$K, which, allowing for the non-ideal nature of liquid He-4, was reasonably close to the observed value.

However, this model has certain undesirable features. Its predictions include that the λ-transition should be of first order, that is,

accompanied by a latent heat; that T_λ should increase with increasing pressure; and that the specific heat at low temperatures should vary as $T^{3/2}$. None of these features are observed in liquid ^{4}He. Also it would seem impossible for the condensate of an ideal Bose gas to exhibit superfluidity since there is no energy gap between the ground state and the first excited state. Thus an atom in the condensate could gain energy in arbitrarily small amounts through collisions and so become part of the normal fluid.

1.3. THE LANDAU TWO-FLUID MODEL

In 1941, three years after the London-Tisza two-fluid model had been proposed, Landau (1941) gave an alternative approach to the problem. He stressed the importance of treating the whole fluid as a quantum mechanical system at low temperatures, and studied the form that the lowest energy excitations of this system would take. He at first concluded that the excitation spectrum of the liquid would exhibit two branches separated by an energy gap. The lower energy excitations were phonons, with energy ε related to momentum p by $\varepsilon = cp$, c being the velocity of sound in the liquid. The higher energy branch of the spectrum represented excitations of a "free particle" nature, which he termed "rotons". These he envisaged as having angular momentum and involving the collective motion of several atoms, with an energy-momentum relationship given by $\varepsilon = \Delta + \frac{p^2}{2\mu}$. Δ is the energy gap and μ is an effective mass.

Landau (1947) later modified the form of his proposed spectrum by combining the roton and phonon branches as shown in figure 1.3.1. This led to the interpretation of rotons as higher energy phonons, with wavelengths of the order of the interatomic spacing . The "roton"

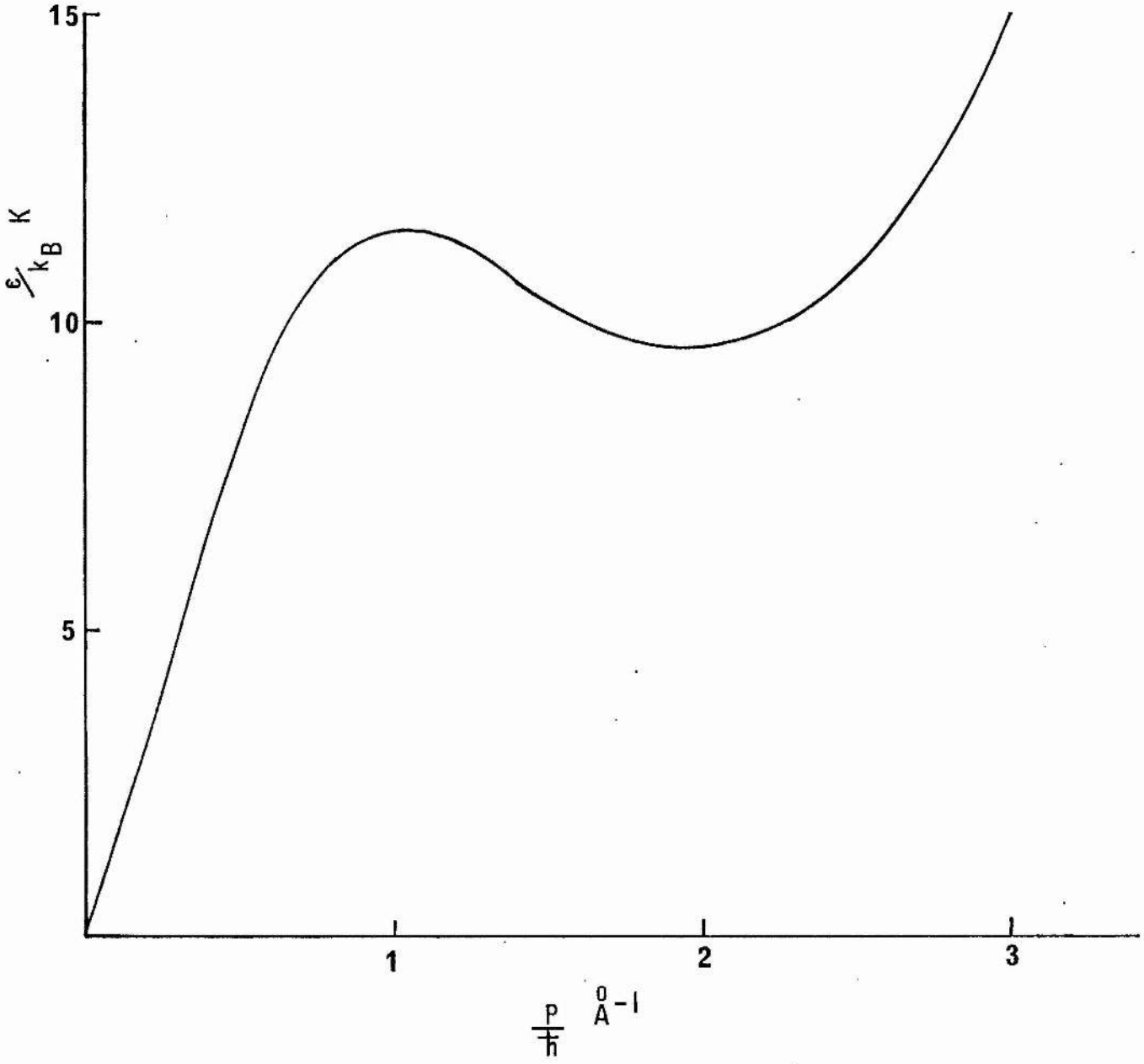

Figure 1.3.1.
The excitation spectrum of HeII

part of the spectrum is now described by $\varepsilon = \Delta + \frac{(p-p_o)^2}{2\mu}$, where p_o is an additional parameter determined from the known thermodynamic data.

If a sample of liquid helium is considered at some finite temperature there will exist in the liquid an appropriate population of excitations. Landau argued that these will come into equilibrium with the walls of the container and will have zero net drift momentum in the frame of reference in which the container walls are stationary. This frame of reference can in general have a velocity v_n with respect to the laboratory frame. The net drift momentum $\bar{p}$ of the excitations as seen in the laboratory frame can be calculated for small velocities to be

$$\bar{p} = -\frac{4\pi V}{3h^3} v_n \int_0^\infty \frac{\partial n(\varepsilon)}{\partial \varepsilon} p^4 \, dp, \tag{1.3.1}$$

where V is the volume of the system, h is Planck's constant and $n(\varepsilon)$ is the Planck distribution function;

$$n(\varepsilon) = (\exp \varepsilon/kT - 1)^{-1} \tag{1.3.2}$$

Thus for small velocities the liquid exhibits an effective density given by

$$\rho_n = -\frac{4\pi}{3h^3} \int_0^\infty \frac{\partial n(\varepsilon)}{\partial \varepsilon} p^4 \, dp. \tag{1.3.3}$$

Knowledge of the form of the excitation spectrum $\varepsilon(p)$ allows the integral to be evaluated, and one finds that $\rho_n \propto \rho$, the total density of the liquid, for $T \propto T_\lambda$.

A two-fluid model can now be formulated in which the normal fluid fraction is constituted by the excitation gas of phonons and rotons, and the superfluid fraction is simply the background against which these excitations occur. It follows that the normal fluid carries all the entropy of the system and can be assigned a viscosity η_n. The superfluid, on the other hand, has zero entropy, zero viscosity and

a density ρ_s, given by

$$\rho = \rho_n + \rho_s, \tag{1.3.4}$$

where ρ is the total density of the liquid.

If the excitations are considered as an ideal gas obeying Bose statistics, with closely spaced energy levels, then the partition function of the system can be evaluated by integration, once the form of the excitation spectrum is known:-

$$\ell n\, Z = -\frac{V}{2\pi^2} \int_0^\infty \ell n(1 - e^{-\beta\varepsilon(k)}) k^2\, dk. \tag{1.3.5}$$

One can then obtain expressions for the free energy, entropy and specific heat in the low temperature approximation where interactions between the excitations are negligible. Comparison with experimental data then allows the parameters μ, Δ and p_o of the excitation spectrum to be determined.

On the basis of this two fluid model, explanations of many of the phenomena observed in He II can be given. In particular, the conflicting viscosity measurements are resolved once it is realised that the different experimental methods in fact determine different quantities. The rotating viscometer gives, for low angular velocities, a direct measurement of the normal fluid viscosity η_n. In the capillary flow experiment, however, the normal fluid is virtually immobilised by its own viscosity and only superfluid flow occurs. The explanation of the apparent lack of viscosity of the superfluid component in terms of the Landau two-fluid model will be discussed in chapter 2.

1.4. THE EQUATIONS OF MOTION OF THE TWO FLUIDS

For small relative velocities, the velocity fields of the two fluids are assumed independent of each other. Also, the absolute velocity of each fluid with respect to the container is assumed small

enough to preclude any dissipative forces due to the onset of turbulence. Under these conditions, Landau derived the following equations to describe the macroscopic motions of the two fluids. For the normal fluid component:-

$$\rho_n \frac{d\underline{v}_n}{dt} = -\frac{\rho_n}{\rho} \underline{\nabla} p - \rho_s S \underline{\nabla} T + \eta_n \nabla^2 \underline{v}_n, \tag{1.4.1}$$

where v_n is the normal fluid velocity and S is the entropy per unit mass. For the superfluid component

$$\frac{d\underline{v}_s}{dt} = - \text{grad } \mu. \tag{1.4.2}$$

Here v_s is the superfluid velocity and μ is the chemical potential per unit mass, which can be written as

$$\mu = \mu_o - \tfrac{1}{2} \frac{\rho_n}{\rho} (\underline{v}_n - \underline{v}_s)^2 + U. \tag{1.4.3}$$

U is the potential energy per unit mass due to the presence of external fields and μ_o is the chemical potential in the absence of external fields and relative motion. Landau also postulated that superfluid flow must be irrotational, so that curl $v_s = 0$. In this case $\frac{d\underline{v}_s}{dt}$ is given by

$$\frac{d\underline{v}_s}{dt} = \frac{\partial \underline{v}_s}{\partial t} + \text{grad } (\tfrac{1}{2} v_s^2). \tag{1.4.4}$$

Using equations 1.4.3 and 1.4.4, the superfluid equation of motion becomes

$$\frac{\partial \underline{v}_s}{\partial t} = - \text{grad } \{\mu_o + \tfrac{1}{2} v_s^2 - \tfrac{1}{2} \frac{\rho_n}{\rho} (\underline{v}_n - \underline{v}_s)^2 + U\}. \tag{1.4.5}$$

1.5. FEYNMAN'S MICROSCOPIC THEORY

The derivation of Landau's excitation spectrum proceeds from his formulation of quantum hydrodynamics. This approach, however, is not entirely satisfactory since the average variables of the quantum

hydrodynamics cannot describe with accuracy an excitation spectrum, the parameters of which are related to the atomic structure of the liquid. To overcome this difficulty, Feynman (1953, 1954 and 1955) approached the problem on an atomic scale. The wave function ψ of a many-boson system can be represented in configuration space as a function of the position co-ordinates of all the atoms. The energy of any particular state of the system is related to the curvature of the wave function representing that state; if the system point in configuration space only moves a small distance between configurations of maximum and minimum probability, the amplitude of the wave function will be changing rapidly and the energy of that particular state will be high. Using this criterion Feynman showed that states of the system corresponding to density fluctuations or phonons were of a lower energy than the states involving stirring motions of the atoms at constant density.

He then developed a trial wave function describing the excited states of the liquid and from this calculated the shape of the excitation spectrum. Feynman's spectrum exhibited a minimum in the energy for wavelengths of the order of the interatomic separation, but this minimum energy was approximately double that of Landau's proposed spectrum. A later calculation by Feynman and Cohen (1956), in which the wave function was modified to conserve current, gave good agreement with the Landau spectrum.

Cohen and Feynman (1957) also proposed that the form of the excitation spectrum could be determined experimentally by a neutron scattering experiment. This prediction was subsequently verified by three independent groups:- Henshaw (1958), Palevsky et al (1957) and Yarnell et al (1959).

1.6 THE WAVE FUNCTION OF FLOWING HELIUM

Consider a mass of liquid helium at rest in some frame of reference. Its wave function will be some function in configuration space of the co-ordinates of all the atoms in the system:

$$\psi_o = \psi_o (\underline{r}_1, \underline{r}_2 \ldots\ldots \underline{r}_n). \tag{1.6.1}$$

A uniform translational velocity can be imposed on the entire system by a Galilean transformation to a frame of reference having velocity $\underline{v}$ with respect to the initial one. The wave function of the system in the new frame becomes;

$$\psi = \{e^{i\underline{k}\sum_j \underline{r}_j}\} \psi_o (\underline{r}_1 \ldots\ldots \underline{r}_n), \tag{1.6.2}$$

where $\underline{r}_j$ is the position vector of the jth atom and the summation extends over all atoms. $\hbar\underline{k}$ is the momentum imparted to each atom by the macroscopic translation. If the velocity field is not quite uniform throughout the liquid the wave function of any small region considered separately will be of the above form, but now $\underline{k}$ will be a slowly varying function of position. It must therefore be brought inside the summation:

$$\psi = (e^{i\sum_j \underline{k}(\underline{r}_j).\underline{r}_j}) \psi_o (\underline{r}_1 \ldots\ldots \underline{r}_n) . \tag{1.6.3}$$

This can be written more generally as

$$\psi = \{e^{i\sum_j \phi(\underline{r}_j)}\} \psi_o (\underline{r}_1 \ldots\ldots \underline{r}_n). \tag{1.6.4}$$

The relationship between the phase ϕ and the superfluid velocity $\underline{v}_s$ can be derived by substitution of equation 1.6.4 into the expression for the current density $\underline{J}$ of a many particle system;

$$\underline{J} = \frac{i\hbar}{2m} \sum_j \int_v (\psi \underline{\nabla}_j \psi^* - \psi^* \underline{\nabla}_j \psi) \, dr' = \rho_o \underline{v}_s, \tag{1.6.5}$$

where dr' is the product of the differentials of co-ordinates of all

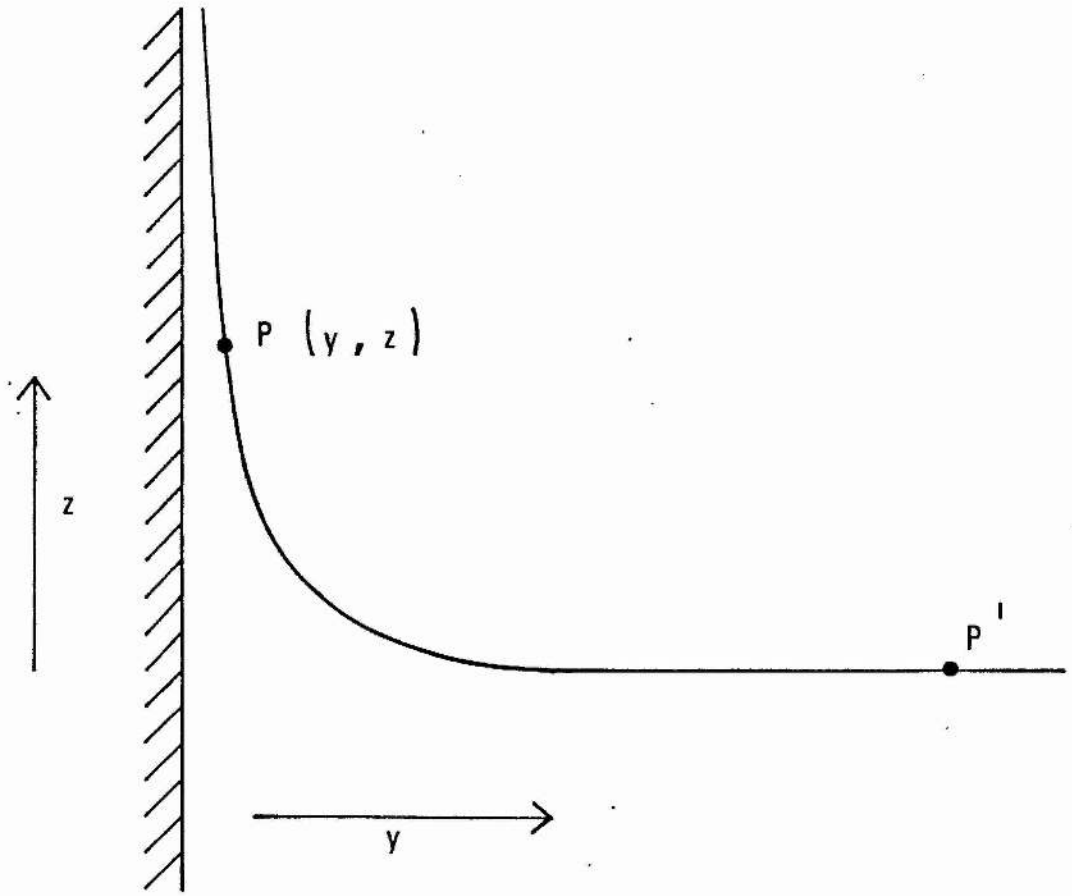

Figure 1.7.1.
Schematic diagram showing the situation at the wall of a vessel containing liquid HeII

particles except the jth, ∇_j operates on the co-ordinates of the jth particle and the summation extends over all particles. ρ_o is the number density and m is the mass of a single particle. One obtains

$$\underline{J} = \frac{\hbar}{m} \rho_o \underline{\nabla} \phi = \rho_o \underline{v}_s , \qquad (1.6.6)$$

from which:

$$\underline{v}_s = \frac{\hbar}{m} \underline{\nabla} \phi . \qquad (1.6.7)$$

Thus the superfluid velocity at any point $\underline{r}$ in the liquid can be related quite simply to the gradient of the phase ϕ at that point.

1.7 THE HELIUM FILM

The van der Waals forces between helium atoms and a solid substrate are sufficiently strong to cause the formation on the substrate of a thin film of liquid at low temperatures. The hydrostatic pressure in the film will increase towards the substrate and it is thought that the first two atomic layers of the film may in fact consist of solid helium. As the temperature is lowered below the λ-point an appropriate fraction of the film becomes superfluid and consequently exhibits an extremely high mobility, flowing in a direction such as to equalise the chemical potential throughout the system. In fact this property of the film was first observed in 1922 by Kamerlingh Onnes, who noted that an open container partially immersed in a bath of liquid helium would rapidly fill to the same level as the bath. However, Onnes attributed the effect to an anomalously efficient distillation process, and it was not until the work of Rollin (1936) that the existence of the film was firmly established.

A simple theory put forward by Frenkel (1940) and Schiff (1941) accounts fairly successfully for the observed profile of the static film. Consider the situation at the wall of a container which holds a sample of bulk liquid as shown in fig. 1.7.1. For any point

P(y,z) in the surface of the film we have from equation 1.4.2 the equilibrium condition

$$\underline{\nabla}\mu = \underline{\nabla}\,(\mu_o + U(y,z)) = 0. \qquad (1.7.1)$$

If the pressure and temperature are constant along the liquid-vapour interface, then $\underline{\nabla}\mu_o = 0$. Also, at a point P' located in the surface of the bulk liquid, far from the wall, the potential energy due to van der Waals' and gravitational forces can be taken as zero. Thus at all points in the surface of the film

$$U(y,z) = gz - \frac{\alpha}{y^3} = 0, \qquad (1.7.2)$$

where α is a constant that characterises the strength of the van der Waals' forces. The equilibrium film profile is therefore given by

$$y = \sqrt[3]{\frac{\alpha}{gz}} = \frac{k}{z^{1/3}} \quad . \qquad (1.7.3)$$

The constant k will vary according to the substrate and represents the film thickness at unit height above the bulk liquid, (typically 300Å at 1 cm height). The static film profile has been measured experimentally by various techniques and reasonable quantitative agreement with the above formula has been obtained, although the exponent of z is usually found to be slightly larger than 0.33.

Kontorovich (1956) advanced a theory that the flowing film should be thinner than the stationary one. Consider a situation of dissipation-free, steady-state film flow, in which it is assumed that the normal fluid is effectively locked in place by its own viscosity, owing to the very small film thickness. According to the superfluid equation of motion (1.4.5),

$$\underline{\nabla}\,\{\mu_o + \tfrac{1}{2}v_s^2 - \tfrac{\rho_n}{2\rho}v_s^2 + U(y,z)\} = 0. \qquad (1.7.4)$$

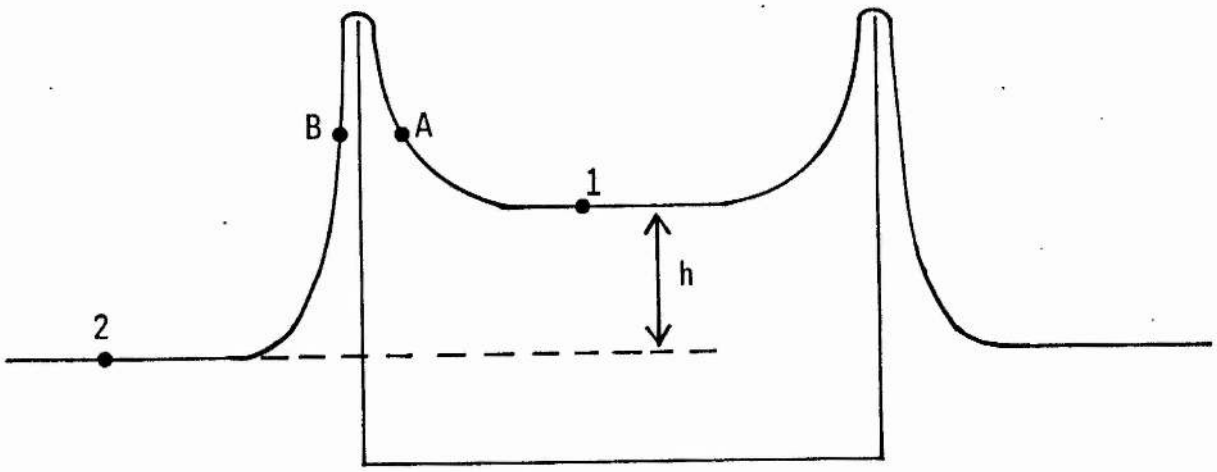

Figure 1.8.1.
Schematic diagram of the beaker film flow experiment.

With reference to figure 1.7.1 integration along the surface of the liquid from P to P' yields

$$(\mu_o + \tfrac{1}{2}\frac{\rho_s}{\rho} v_s^2 + U(y,z))_P = \mu_{oP'} \ . \qquad (1.7.5)$$

If $\mu_{oP} = \mu_{oP'}$, which step is open to some question (Campbell 1975), then

$$\tfrac{1}{2}\frac{\rho_s}{\rho} v_s^2 + gz - \frac{\alpha}{y^3} = 0, \qquad (1.7.6)$$

or

$$y = \left(\frac{\alpha}{gz + \tfrac{1}{2}\frac{\rho_s}{\rho} v_s^2} \right)^{1/3} \ . \qquad (1.7.7)$$

Thus for zero v_s we obtain the static film thickness equation, and for non-zero v_s the film thickness decreases. Early experimental evidence for this effect was conflicting but recent work has provided qualitative confirmation of the theory. This subject will be discussed in more detail in Chapter 3.

1.8 BEAKER FILM FLOW

Consider an open container partially immersed in a bath of liquid helium at a temperature below T_λ, and let there be a level difference between the inside and outside as shown in figure 1.8.1. The two bulk reservoirs will be linked by a superfluid helium film which will be thicker at point A on the inside wall of the beaker than at the equivalent point B on the outside. The pressure and temperature will be constant over the surface of the film, so that in equation 1.7.1 $\nabla\mu_o = 0$. However, the potential energy of an atom in the surface will be greater at point A than at point B owing to the change in the film thickness. There is thus a resultant gradient in the chemical potential, causing acceleration of the film in a direction such as to bring about equalisation of the levels. At the end of such a flow, inertial over-

shoot occurs owing to the small but finite mass of the film and the inner and outer levels execute very slow, lightly damped oscillations about a mean equilibrium position. These inertial oscillations were first observed by Allen and Misener (1939) during experiments on superfluid flow through narrow channels.

The so-called "beaker film flow experiment" is therefore one of the most easily observed and striking manifestations of the superfluid properties of HeII. It provides a very convenient tool for probing the equation of motion of the superfluid fraction, since the normal fluid is effectively immobilised by its own viscosity in such a narrow channel. Observation of the rate of change of one liquid level together with a knowledge of the experimental geometry determines the volume transfer rate per unit length of perimeter, usually referred to as σ. This quantity can be related to the superfluid velocity v_s at any height, given the appropriate film thickness d:

$$\sigma = \frac{\rho_s}{\rho} v_s \, d. \qquad (1.8.1)$$

According to the superfluid equation of motion, which contains no dissipative terms, the film should accelerate continuously under such a chemical potential gradient until the levels equilibrate. However, the pioneering work of Daunt and Mendelssohn (1939) revealed that this was not the case. Instead, the transfer rate σ was found to be virtually independent of level difference. This implies that under these conditions superfluidity is breaking down in the film and the gradient of the chemical potential is being exactly balanced by some form of frictional dissipation. At any instant, the work done against these dissipative forces in transporting unit mass from the inner level to the outer level is given by

$$- \int_1^2 \underline{\nabla}\mu \cdot \underline{d\ell} = \mu_1 - \mu_2 = gh. \qquad (1.8.2)$$

Thus a measurement of the level difference, h, simultaneously with its rate of change, $\dot{h}$, enables the work done against the frictional forces to be calculated as a function of the superfluid velocity.

The characteristic rate at which film transfer proceeds led to the concept of a "critical velocity" below which the frictional forces opposing the flow of the liquid were thought to be entirely absent, and above which the frictional dissipation is seen as an extremely rapidly increasing function of velocity. The ingenious double beaker experiment of Daunt and Mendelssohn (1946) in which it was shown that a film transfer rate of 90% of the critical value proceeded at a level difference of less than 100μm, this being the limit of experimental resolution, lent support to this viewpoint. However, the results of more recent work, both theoretical and experimental, have called the whole concept of a critical velocity into question, and a present school of thought maintains the existence of dissipation for all superfluid velocities, the so-called "critical velocity" being that velocity at which this dissipation becomes experimentally observable. A more detailed discussion of this question will be given in chapter 2.

CHAPTER TWO

THEORIES OF SUPERFLUID DISSIPATION

2.1 Introduction

Dissipation effects manifested during superfluid flow fall into two distinct categories. If the flow sets up a temperature gradient between different regions of the fluid then "thermal" dissipation will occur as the ensuing irreversible heat exchange takes place. This can be minimised by careful choice of experimental conditions. In addition, if the flow proceeds at a relatively high velocity with respect to the containing vessel, then an "intrinsic" type of dissipation will occur in the superfluid itself. The magnitude of this dissipation may be affected by such factors as the shape and size of the container.

Theories of the latter type of dissipation are of two main types: "mechanical" theories postulate mechanisms whereby the kinetic energy of the superflow is used directly in the formation of excitations in the fluid, whilst "thermal fluctuation" theories require the nucleation of excitations from the thermal energy of the fluid before these excitations can take part in dissipative processes.

In this chapter the mechanical and thermal fluctuation theories are reviewed in turn, followed by a brief discussion of the much better understood thermal dissipation. The chapter concludes with a summary of the theoretical viewpoint, against which background the aims of the present research are presented.

2.2 "Mechanical" Theories of Dissipation

a) The Landau Criterion

In his paper of 1941, Landau argued that the shape of his proposed excitation spectrum was sufficient in itself to explain the basic phenomenon of superfluidity. Consider the case of helium flowing

through a capillary at a temperature of absolute zero, for simplicity. Let dissipation occur by means of an interaction between the liquid and the tube wall, in which momentum from the superflow is transferred to the tube. The effect of this interaction on the liquid can be represented by the creation of an excitation in the liquid with momentum directed oppositely to the main direction of flow. The type of this excitation, be it phonon, roton or otherwise, is unimportant. If the energy and momentum of the excitation are ϵ and $\underline{p}$ respectively in the frame in which the liquid is stationary, the corresponding quantities in the laboratory frame are, by the Galilean transformation, $\epsilon + \underline{p}.\underline{v}_s$ and $\underline{p}$. $\underline{v}_s$ is the velocity of superflow. Since the total energy of the liquid is the sum of its initial energy and that of the excitation, this latter quantity must be negative if a dissipative process takes place. That is, $\epsilon + \underline{p}.\underline{v}_s < 0$. Taking the direction of $\underline{p}$ into account, we have

$$\epsilon - p v_s < 0 , \qquad (2.2.1)$$

or

$$v_s > \epsilon/p . \qquad (2.2.2)$$

In a classical liquid, the excitations can be of the free particle type, so that $\epsilon = p^2/2m$, where m is the mass of the particle. Hence $\epsilon/p = p/2m$, which can take all values continuously to zero. This agrees with the observation that dissipation occurs at all finite velocities in a classical fluid. However, with reference to figure 1.3.1 it can be seen that the proposed excitation spectrum for superfluid helium exhibits the property of a non-zero minimum value of ϵ/p for rotons of momentum slightly greater than p_o. Landau's theory therefore predicts that superfluid flow will be dissipation-free up to a "critical velocity" given by $(\epsilon/p)_{\text{minimum}}$.

The actual value of $(\epsilon/p)_{min.}$ corresponds to a critical velocity of 60 m s^{-1} which is two orders of magnitude greater than that observed experimentally. One possible explanation is that Landau's excitation spectrum is incomplete, in that there should exist some other form of excitation at higher momentum and lower energy, such that the minimum value of ϵ/p is reduced. One such excitation will now be described.

b) Quantised Vortex Lines

According to the discussion of section 1.6, the superfluid velocity is related to the phase of the wavefunction by $\underline{v}_s = \frac{\hbar}{m} \underline{\nabla}\phi$. Considering any closed contour in the fluid, the circulation κ is given by

$$\kappa = \oint \underline{v}_s . \underline{ds} = \int \text{curl } \underline{v}_s . \underline{da} \ . \qquad (2.2.3)$$

If the contour encloses a simply-connected region of superfluid, curl $\underline{v}_s = 0$ everywhere, and hence $\kappa = 0$. However, for a multiply-connected region containing a hole or a non-superfluid obstruction, κ can take a non-zero value whilst the superfluid velocity field remains irrotational. In particular,

$$\kappa = \oint \underline{v}_s . \underline{ds} = \oint \frac{\hbar}{m} \underline{\nabla}\phi . \underline{ds} = \frac{\hbar}{m} (\phi_1 - \phi_2) \ , \qquad (2.2.4)$$

where $(\phi_1 - \phi_2)$ must be an integral multiple of 2π, to keep the wave-function single-valued. Thus

$$\kappa = \frac{h}{2\pi m} . 2n\pi = n(\frac{h}{m}) \ , \qquad (2.2.5)$$

where n is an integer. That is, in any multiply-connected region of superfluid, circulation around the non-superfluid regions is quantised in units of h/m ($\sim 10^{-3}$ $cm^2 s^{-1}$). This suggestion was first put forward by Onsager (1949) and developed by Feynmann (1955).

Circulation around a non-superfluid region of atomic dimensions constitutes a quantised vortex line, which, from hydrodynamic consider-

ations, must either extend to the fluid boundaries or close on itself to form a vortex ring. It is possible that such a flow configuration corresponds to the excitation that is missing from the Landau spectrum, and that dissipation in superfluid flow consists of the formation of quantised vortices with cores that are either hollow, or composed of normal fluid.

This argument can be made quantitative by a direct application of the Landau criterion. Following Roberts and Donnelly (1970), the energy and impulse of a vortex ring are given by

$$\epsilon = \tfrac{1}{2}\rho\kappa^2 R[\ell n \frac{8R}{a} - \frac{3}{2}] , \qquad (2.2.6)$$

$$p = \rho\kappa\pi R^2 , \qquad (2.2.7)$$

where ρ is the density of the fluid, R is the radius of the ring, a is the radius of the vortex core and κ is the circulation. The core of the vortex is assumed to be hollow and the fluid is assumed unbounded and at rest at infinity. Applying the Landau criterion gives for the critical velocity

$$v_c = (\frac{\epsilon}{p})_{min.} = \frac{\kappa}{2\pi R}[\ell n \frac{8R}{a} - \frac{3}{2}] , \qquad (2.2.8)$$

the minimum value of which corresponds to the maximum value of R compatible with the size of the channel. The model therefore predicts a critical velocity inversely proportional to the diameter d of the channel in which the superflow takes place. This conflicts with the experimental observation that $v_c \propto d^{-\frac{1}{4}}$ (Van Alphen et al (1966)). Also, taking $\kappa = 10^{-3}\text{cm}^2\text{s}^{-1}$, $R = 1.5 \times 10^{-6}$cm, a = 1.28Å, which values correspond to the film flow situation, v_c is given by equation 2.2.8 as 567 cm s^{-1}. This is an improvement over the original Landau estimate by an order of magnitude, but it still remains an order of magnitude greater than experimentally observed values.

c) The Effects of Boundaries

The above approach can be criticised on the grounds that the vortex rings having the minimum value of ϵ/p are very close to the boundaries of the flow, whilst the formulae employed in the derivation are only valid in the absence of such boundaries. Two studies of the energy of a vortex ring of radius R in a cylindrical tube of radius R_o have been made in an attempt to remove this inconsistency. Fineman and Chase (1963) considered the case of a hollow-cored ring in which the vorticity was concentrated on an infinitesimal source circle. Their analysis predicted that $\epsilon \to 0$ as $R \to R_o$. On the other hand, Gopal (1963) considered a vortex ring with a fluid-filled core over which the vorticity was uniformly distributed. He showed that, in agreement with Fineman and Chase, the energy passed through a maximum for a certain value of R/R_o, although it approached a finite limit as $R \to R_o$, given by

$$\epsilon = \tfrac{1}{2}\rho_s \kappa^2 R_o (\ell n\, 2 + \tfrac{1}{4}) . \qquad (2.2.9)$$

When this is used in the Landau criterion, we obtain

$$v_c = \left(\frac{\epsilon}{p}\right)_{min.} = \frac{\kappa(\ell n\, 2 + \frac{1}{4})}{2\pi R_o} . \qquad (2.2.10)$$

For the film flow situation, equation 2.2.10 predicts a critical velocity of $\sim 100\ cm\ s^{-1}$, which is some improvement over the result obtained from "unbounded" formulae, but it is still too high by a factor of approximately three. Again, the experimental variation of v_c with channel size is not reproduced.

It would thus seem that the results of any study of the above type, besides predicting the wrong dependence of v_c on d, are very sensitive to the model assumed for the core structure; either vortex rings can be formed very easily at velocities well below experimental values, in which case there must be some additional mechanism

preventing their taking part in dissipative processes, or they can be formed at velocities considerably greater than those observed. However, despite these conflicting and rather disappointing results, it seems highly probable that superfluid dissipation is in some way connected with the production of quantised vorticity, even though this may not be understandable in terms of the Landau criterion.

d) Phase Relations

An alternative approach that supported the connection between dissipation and quantised vorticity was provided by Anderson (1966). He showed that the number N of atoms in a superfluid sample and the appropriate phase ϕ of the wavefunction are conjugate variables. Hence the time rate of change of ϕ at any point is given by

$$-\hbar \frac{d\phi}{dt} = \frac{dE}{dN} = \mu_p \ , \qquad (2.2.11)$$

where μ_p is the chemical potential per particle.

Consider a superfluid in which there is a chemical potential gradient. Equation (2.2.11) then gives for the time rate of change of the phase difference between two points 1 and 2

$$\frac{d}{dt} (\phi_2 - \phi_1) = \frac{1}{\hbar} (\mu_{p_1} - \mu_{p_2}) \ . \qquad (2.2.12)$$

That is, for $\mu_{p_1} > \mu_{p_2}$ the gradient of the phase between 1 and 2 is increasing with time, indicating that the superfluid must accelerate under the chemical potential gradient. However, in dissipative superfluid flow the situation obtains where v_s is constant whilst $\mu_{p_1} > \mu_{p_2}$. This implies that the dissipative process involves some mechanism which cancels the rate of change of $(\phi_2 - \phi_1)$ with time. Such a cancellation could be effected by the transport of vorticity across the stream. In particular, consider a vortex ring positioned between 1 and 2 with its plane perpendicular to a line joining the two points. The line integral of $\underline{\nabla}\phi$ along a path passing through the

centre of the ring differs by 2π from the line integral taken around the outside of the ring. Thus if a ring of negative κ expands across the stream, or conversely if a ring of positive κ contracts across the stream, the phase difference between 1 and 2 is reduced by 2π. This "phase slippage" process can balance the effect of the chemical potential gradient provided the number $\dot{N}$ of vortex rings crossing the stream in unit time is given by

$$2\pi\dot{N} = \frac{d}{dt}(\phi_2 - \phi_1) = \frac{1}{\hbar}(\mu_{p_1} - \mu_{p_2}) ,$$

or

$$\dot{N} = \frac{1}{\hbar}(\mu_{p_1} - \mu_{p_2}) . \qquad (2.2.13)$$

In terms of μ, the chemical potential per unit mass, $\mu_p = m\mu$, where m is the mass of a helium atom. Equation (2.2.13) then becomes

$$\dot{N} = \frac{\mu_1 - \mu_2}{\kappa} . \qquad (2.2.14)$$

Thus superfluid dissipation, as envisaged by Anderson, necessarily involves the transport of quantised vorticity across the stream at a rate specified by the gradient of the chemical potential.

e) Superfluid Vortex Dynamics

Campbell (1970) has taken the ideas of the previous section a stage further by considering the equation of motion of a vortex in a superfluid system, and proposing a detailed mechanism for the transportation of vorticity across the stream.

The forces which act on unit length of vortex line consist of

(i) a Magnus force;-

$$\rho_s (\underline{v}_s - \underline{v}_L) \times \underline{\kappa} , \qquad (2.2.15)$$

(ii) a frictional force due to scattering of normal fluid excitations by the core;-

$$\nu(\underline{v}_n - \underline{v}_L) + \nu' \frac{\underline{\kappa}}{|\underline{\kappa}|} \times (\underline{v}_n - \underline{v}_L) . \qquad (2.2.16)$$

$\underline{v}_s$ and $\underline{v}_n$ are the superfluid and normal fluid velocities at the core and $\underline{v}_L$ is the velocity of the core itself. ν and ν' are the friction constants describing the anisotropic scattering process. Since the vortex is simply a flow configuration, the sum of the above forces must be zero. This condition leads to the following expression for $\underline{v}_L$;-

$$\underline{v}_L = \frac{1}{1+(\gamma\sigma)^2}\left[\gamma\sigma^2(\underline{v}_s-\underline{v}_n) + \underline{\sigma}\times(\underline{v}_n-\underline{v}_s) + \gamma\underline{\sigma}.(\underline{v}_n-\underline{v}_s)\underline{\sigma}\right] + \underline{v}_n \ , \quad (2.2.17)$$

where γ and $\underline{\sigma}$ are dimensionless functions of temperature given by

$$\gamma = 1 - \frac{\nu'}{\rho_s\kappa} \ , \quad \text{and} \quad (2.2.18)$$

$$\underline{\sigma} = \frac{\rho_s}{\nu}\underline{\kappa} \ . \quad (2.2.19)$$

In the two dimensional case where $\underline{\kappa}$ is perpendicular to $\underline{v}_s$ and $\underline{v}_n$, and if, for ease, $\underline{v}_n$ is taken as zero (narrow channel flow), equation (2.2.17) can be expressed in complex notation as

$$v_L = \frac{\sigma(\gamma\sigma-i)}{1+(\gamma\sigma)^2}\, v_s \ , \quad (2.2.20)$$

where $v = v_x + iv_y$.

v_s is composed of contributions from the background flow, self-induced velocities, and images, and will always remain parallel to the boundaries if they themselves are parallel to each other. Hence v_L will be at a constant angle θ to v_s, given from (2.2.20) by

$$\tan\theta = -\left(\frac{1}{\gamma\sigma}\right) \ . \quad (2.2.21)$$

That is, in superfluid flow down a parallel-sided narrow channel, a vortex core does not move with the local superfluid velocity v_s, as would be the case in a classical fluid, but instead crosses the stream at a temperature dependent angle θ, through the interaction with normal fluid excitations. Careful consideration shows that if κ is positive, θ is a negative angle and vice versa.

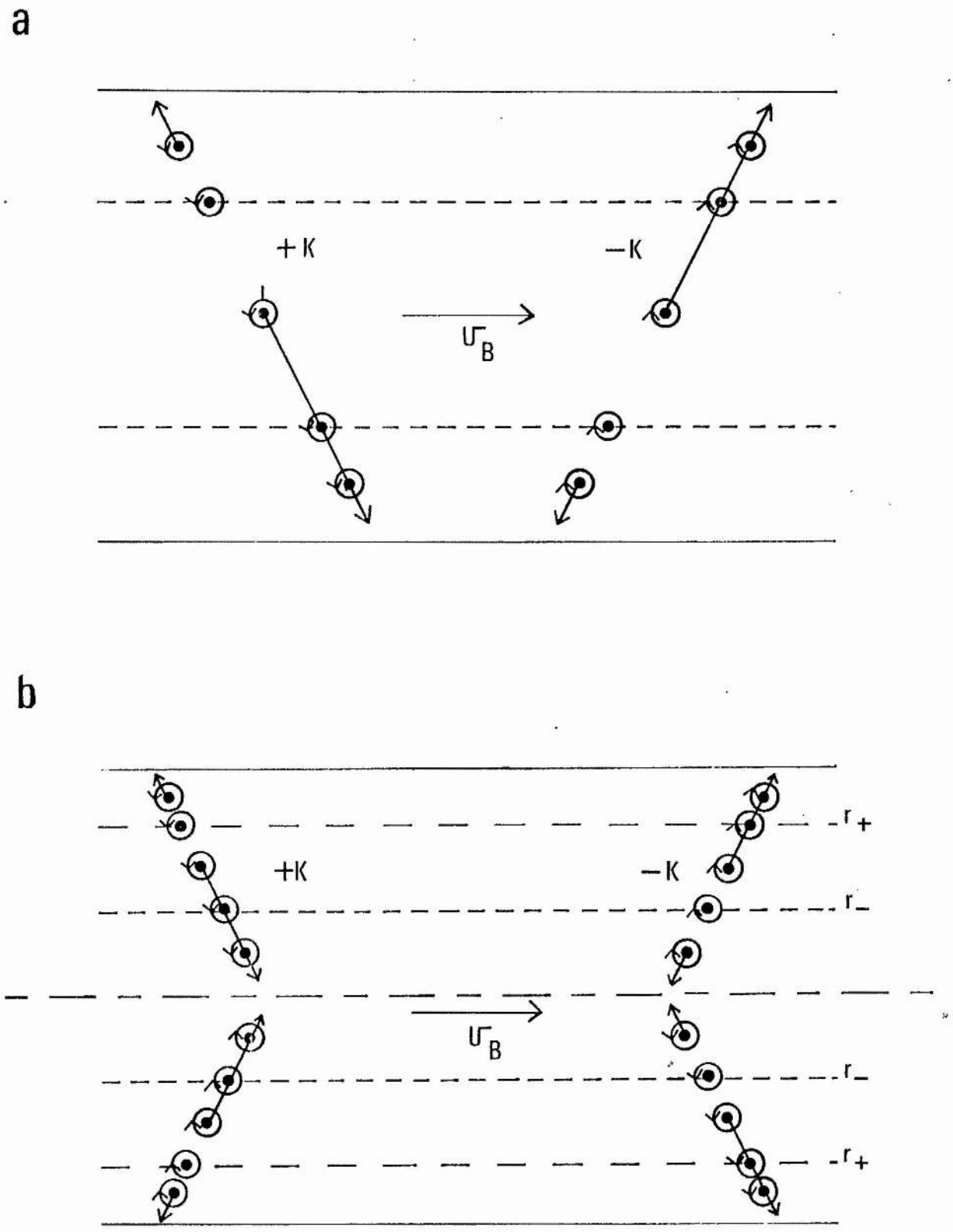

Figure 2.2.1.
The motion of (a) vortex lines and (b) vortex rings during superfluid flow down a parallel sided narrow channel.

In the absence of a background superfluid flow, the centre of a narrow channel marks a line of metastability for a vortex core of either circulation; along this line all image contributions to $\underline{v}_s$ cancel, so by (2.2.20) $\underline{v}_L = 0$. If a background flow is now introduced, the line of metastability splits in two, one for each sign of κ. Along each line of metastability the background flow $\underline{v}_B$ cancels the sum of the image contributions $\underline{v}_I$ to give $\underline{v}_s = 0$ and $\underline{v}_L = 0$. This situation is illustrated in figure (2.2.1(a)) where vortex lines of both directions of circulation are shown in various positions and the subsequent direction of motion is indicated. The vortices are assumed to be non-interacting.

This treatment for vortex lines is also a reasonable approximation to the case of vortex rings in a channel of twice the width; the image of the line is taken as the other half of the ring in the absence of the boundary. The behaviour of vortex rings of both directions of circulation in the presence of a background flow v_B is illustrated in figure (2.2.1(b)). (A vortex ring of positive κ is defined as one whose self-induced velocity in an unbounded fluid is in the direction signifying positive velocity.)

With reference to figure (2.2.1(b)) it can be seen that the lines of metastability have been replaced by radii of metastability, marked r_+ and r_- for $+\kappa$ and $-\kappa$ respectively. In general, the rings either contract or expand along the surface of a right circular cone. Rings nucleated with radii less than the smaller radius of metastability will always shrink to zero, irrespective of the sign of κ. Likewise rings nucleated with radii greater than the larger radius of metastability will always expand to the walls. Such rings can therefore never accomplish a complete crossing of the stream.

In contrast, if a pair of rings of opposite circulation are nucleated in the region between the two radii of metastability, one ring will shrink to zero while the other will expand to the walls.

The Anderson phase relations will now be satisfied, and it is presumably these rings which cause dissipation in the superfluid. A similar argument can be made for vortex lines or pairs, but will not be stated here since the literature deals mainly with the case of rings.

f) Energy Considerations

In a later paper Campbell (1972) considered the energy loss of such a pair of rings in crossing a narrow channel in the presence of a background flow v_B. He showed that this is given by

$$\Delta E = \rho_s \kappa \pi v_B \left[(R-a)^2 - a^2\right] + 2 \int_{r_-}^{r_+} E_o(r)\, f(r)\, dr \ , \qquad (2.2.22)$$

where R is the channel radius and a the vortex core radius. Again, r_+ and r_- are the two radii of metastability; $f(r)\,dr$ is the probability of nucleating a pair of rings within dr of radius r and $E_o(r)$ is the energy of a vortex ring in a tube, with background velocity zero. The last term in (2.2.22) is therefore the mean nucleation energy of the rings in a fluid at rest at infinity.

If we have a situation of steady-state dissipation in the narrow channel, and the chemical potential difference across this region is $\Delta\mu$, then the Anderson phase slippage relation (2.2.14) requires that vortices must cross the stream with a frequency of $\Delta\mu/\kappa$. Hence the energy loss per unit time from such a ring system will be

$$\Delta\mu \rho_s v_B \pi \left[(R-a)^2 - a^2\right] + \frac{2\Delta\mu}{\kappa} \int_{r_-}^{r_+} E_o(r)\, f(r)\, dr \ . \qquad (2.2.23)$$

Now the first term in this expression is simply the energy gained per unit time by the stream in flowing through a chemical potential difference $\Delta\mu$. Thus it can be seen from (2.2.23) that more energy is lost per unit time from the superfluid than can be provided by the drop in chemical potential, and the difference is simply the mean nucleation energy of the vortices in the absence of a background flow. That is, in any situation of steady state dissipative flow the nucleation energy

of the vortices can not be derived from the chemical potential difference existing across the dissipative region if the phase slippage relation is to be obeyed.

Campbell concludes that the only alternative source of energy is the thermal energy of the fluid, and that vortex nucleation and growth must always occur by means of thermal fluctuations. This energy is eventually returned to the fluid as heat when the vortex decays.

g) Pinned Vorticity and the Vortex Mill

Glaberson and Donnelly (1966) have suggested a vortex nucleation mechanism which rests on the idea that pinned vortex lines anchored to protuberances on the channel wall are always present, even in the absence of a flow. (The lines could be nucleated thermally as the liquid is cooled through the λ point.) The initial vortex line is imagined as taking on a configuration such that at any point on the core the self-induced velocity balances the velocity field of the images in the walls. If the background flow is then increased from zero, the line is gradually bent into a new configuration, again corresponding to the situation of zero velocity at the core. However, there comes a point, when the line is approximately semi-circular, where any further increase in the stream velocity can not be balanced by image and self-induced velocities. The line will then grow continually and move in accordance with equation 2.2.17, causing the energy of the superfluid system to be dissipated. The critical velocity predicted in this way is of the same form as equation 2.2.8, again showing the wrong dependence on channel diameter. Glaberson and Donnelly speculate that in fact a "vortex mill" may be formed at the pinning site. A length of line feeding out down the channel may "pinch off" into vortex rings, leaving the site once more occupied by a line in a subcritical configuration, ready for the whole process to begin again.

According to section 2.2.f. the initial growth of the subcritical line can only be brought about by thermal fluctuations. Such a "thermally activated" vortex mill has been described by Donnelly and Roberts and will be discussed in the next section.

2.3 Thermal Fluctuation Theories of Dissipation

a) Origins

It was Vinen (1963) who first suggested that the nucleation energy of the vortices could be provided from the thermal energy of the liquid. However, he did not develop this notion to any great extent; crude calculations indicated that the process was extremely improbable, except perhaps for temperatures very close to the λ-point or for rough channels where local superfluid velocities could be extremely high.

b) Iordanskii Model

A more detailed study of the mechanism was carried out by Iordanskii (1965), who considered the case of the nucleation of vortex rings in an unbounded fluid having a background velocity v_s. The energy ϵ of such rings in the laboratory frame of reference is given by the Galilean transformation as $\epsilon_o + \underline{p}.\underline{v}_s$ where ϵ_o is the ring energy in a fluid at rest at infinity and p is the impulse. For a ring of negative circulation, the momentum is directed against that of the flow and so $\epsilon = \epsilon_o - p\, v_s$. Taking the classical expressions (Lamb 1965) for ϵ_o and p as a function of the radius R, Iordanskii showed that such a ring of negative circulation had a maximum energy for a critical radius R_c given implicitly by

$$R_c = \frac{\kappa}{4\pi v_s}\left[\ell n \frac{8R_c}{a} - \frac{3}{4}\right] . \qquad (2.3.1)$$

The translational velocity of this "critical" ring is zero in the laboratory frame of reference, and it follows that R_c corresponds to the "radius of metastability" discussed in section 2.2.e. The maximum

ring energy at radius R_c thus represents a barrier to the thermal nucleation of vortex rings that are capable of crossing the stream and satisfying the phase slippage condition.

Iordanskii considered that the direct formation of a ring of critical size by a single thermal fluctuation was improbable, since this would require large scale organisation of rapidly fluctuating quantities. He went on instead to calculate the probability of a ring growing to critical size as a result of repeated collisions with normal fluid excitations, after the manner of a particle undergoing Brownian motion. This probability was found to be appreciable for background velocities in excess of 60 cm s^{-1}, and to fall off extremely sharply with decreasing v_s, giving the impression of a "critical" velocity. The probability was also found to be a very strong function of temperature.

c) Donnelly-Roberts Model

Donnelly and Roberts (1971) have also studied this problem with the additional assumption that the vortex ring energy spectrum forms a continuation of the roton spectrum, so that at any finite temperature there is an equilibrium population of vortex rings in the fluid. The rate of creation ν of critical rings from rotons, per unit volume, is given by

$$\nu = PN_r \ , \qquad (2.3.2)$$

where P is the nucleation probability per second and N_r is the roton density.

Three situations are discussed; the Iordanskii case of vortex rings in an unbounded fluid, the thermally activated vortex mill and the thermal nucleation of vortex rings coaxial to a cylindrical tube. The first case yields critical velocities still an order of magnitude greater than those observed, the critical velocity being defined as that velocity for which, at a given temperature, $\nu \sim 1$. The two subsequent studies of the possible effects of the boundaries on the flow were undertaken in the

hope of reducing this estimate of v_c, but no substantial reduction was obtained. In all cases, the probability of forming a critical vortex ring either from a roton or a pinned vortex line was found to be of the form

$$P = f \exp(-\Delta F/kT) \quad . \tag{2.3.3}$$

Hence the rate of production, ν, of such rings per unit volume is given by

$$\nu = Nf \exp(-\Delta F/kT) \tag{2.3.4}$$

where N is either the density of rotons or pinned vortex lines. The factor Nf can thus be regarded as an "attempt frequency" per unit volume, whilst ΔF represents the energy barrier opposing the production of critical rings. k is Boltzmann's constant. Note that there is a fundamental difficulty in the case of the thermally excited vortex mill, it being impossible to estimate the pinned line density N, as this depends on the microscopic structure of the boundaries.

Although the exact functional forms of f and ΔF vary in each of the examples discussed by Roberts and Donnelly, certain common features are retained. f and ΔF are both seen to be decreasing functions of v_s; in fact they are approximately proportional to $1/v_s$. The temperature dependence of ΔF is given by $\rho_s(T)$ and that of f approximately by $\alpha(T)$, the Rayfield and Reif (1964) drag coefficient. Thus equation 2.3.4 can be approximately written as

$$\nu = N(T)A \frac{\alpha(T)}{v_s} \exp\left[-\frac{B}{v_s}\frac{\rho_s(T)}{T}\right] \tag{2.3.5}$$

where A and B are the constant parts of f and ΔF respectively. ν is thus an extremely strong function of the superfluid velocity due to the appearance of v_s in the exponential term. It is this feature which renders thermal fluctuation theories attractive for the interpretation of superfluid dissipation, in that to all external appearances a critical

velocity is manifested, below which ν is immeasurably small and above which ν becomes exceedingly large. However, the theory departs radically from traditional thinking on superfluidity in that a finite amount of dissipation now accompanies all superfluid flow, no matter how small the velocity. The concept of the critical velocity is therefore modified in this view to that velocity at which dissipation effects rise above the threshold of experimental detection.

The temperature dependence of ν as predicted by 2.3.5 is of considerable interest: as T is reduced, both N(T) and α(T) decrease rapidly, as does the exponential term. (N(T) is taken here as signifying the roton density; it is not clear what temperature dependence, if any, the pinned vortex line density would exhibit.) Typically, for a variation in T from 1.3K to 0.2K, the product αN_r decreases by 22 orders of magnitude! If ν is to be held constant at some observable value corresponding to the "critical" velocity, a substantial increase of v_s in the exponential is required. The theory therefore predicts that the observed critical velocity should increase rapidly with decreasing temperature.

d) Langer-Fisher Model

Langer and Fisher (1967) have independently considered the thermal nucleation problem in an unbounded fluid and adopt a somewhat similar approach. They regard states of superflow as being metastable to the creation of critical sized vortex rings, the transitions between states occurring as the result of isolated thermal fluctuations. This contrasts with the Brownian motion type theories of Iordanskii, and Donnelly and Roberts.

A fundamental characteristic frequency f_o for atomic processes is assumed and equated to $\frac{cN}{d_a}$, where c is the velocity of sound, d_a is the atomic diameter and N is the number of atoms per unit volume. This gives $f_o \sim 10^{35} cm^{-3} s^{-1}$ which is in agreement with the equivalent quantity

$f N_r$, in the Donnelly-Roberts theory for an unbounded fluid at 2.1K, with $v_s = 700\ \mathrm{cm\,s^{-1}}$. However, Langer and Fisher ignore any possible temperature dependence of f_o. The rest of the theory is developed along similar lines to that of Iordanskii and predicts critical velocities that are too high by approximately an order of magnitude.

A full account of the thermal fluctuation theory as propounded by Langer and Fisher, and its application to the decay of superfluid persistent currents has been given by Langer and Reppy (1970).

e) The Form of the Dissipation Curve

Notarys (1969) has extended the thermal fluctuation theory to include a prediction of the size of the chemical potential difference across any region of steady-state dissipation, as a function of the superfluid velocity v_s. If the volume of the dissipation region is V, then by 2.3.4, the number of critical vortices produced per second must be $VNf \exp(-\Delta F/kT)$. In the steady state, this must equal the number of vortices crossing the stream per unit time, so by 2.2.14 and 2.3.5,

$$\Delta\mu = \kappa VNf \exp(-\Delta F/kT) = \kappa VNf \exp(-B\rho_s/v_s T) \ . \qquad (2.3.6)$$

2.4 Dissipation due to Irreversible Heat Exchange

In many experimental situations, superfluid flow is accompanied by changes in the entropy density and the consequent appearance of temperature gradients. Unless either perfectly adiabatic or perfectly isothermal conditions prevail, the ensuing flow of heat will be an irreversible process and the energy of the superfluid system will be dissipated.

Consider, as a specific example, the case of film flow from a beaker to a bath. Only the superfluid, which has zero entropy, is transported through the film. Thus the temperature of the beaker reservoir is increased, and that of the bath is decreased. Heat flow

between the two will then take place, possibly in the form of a distillation process, although experimental conditions could favour conduction through the beaker walls. No intrinsic dissipation need occur in the superfluid itself, and so a level difference could develop between the reservoirs in order to balance the chemical potential gradient across the film caused by the temperature difference. In experimental studies of intrinsic superfluid dissipation, the above level difference should be either minimised by making the conditions sufficiently isothermal, or very carefully allowed for, if misleading results are to be avoided (Keller 1965).

The damping of the inertial oscillations that accompany beaker film flow may be explained by this model above 1K, and a full discussion for the case of small displacements has been given by Robinson (1951). The differential equation governing the level difference x is

$$\dddot{x} + L\ddot{x} + \omega_i^2(1+\alpha)\dot{x} + L\omega_i^2 x = 0 \ , \qquad (2.4.1)$$

where L is a constant related to the thermal conductance between the reservoirs, α is a temperature dependent quantity and ω_i is the angular frequency of the oscillations in the perfectly isothermal case. Three types of solution exist, appropriate to different ranges of L. Two of these, corresponding to the isothermal and adiabatic limits, are similar and represent damped oscillations about an aperiodically decreasing level difference:

$$x = C_1 e^{-bt}\cos(at-\phi) + C_2 \exp\{-L\omega_i^2 t/(a^2+b^2)\} \ . \qquad (2.4.2)$$

C_1, C_2 and ϕ are arbitrary constants. a and b are the imaginary and real parts of the complex conjugate roots of

$$\lambda^3 + L\lambda^2 + \omega_i^2(1+\alpha)\lambda + L\omega_i^2 = 0 \ , \qquad (2.4.3)$$

which is the secular equation corresponding to 2.4.1. Note that, from 2.4.2, in both the isothermal and adiabatic limits the damping of the oscillations is exponential. Between these limits a third solution obtains. This is aperiodic and has the form

$$x = Ae^{\lambda_1 t} + Be^{\lambda_2 t} + Ce^{\lambda_3 t} , \qquad (2.4.4)$$

where A, B and C are arbitrary constants and λ_1, λ_2 and λ_3 are the three real roots of 2.4.3.

For the case of small damping in the isothermal limit, equation 2.4.1 can be approximated to the second order equation of a damped oscillator;

$$\ddot{x} + 2k\dot{x} + \omega_i^2 x = 0 , \qquad (2.4.5)$$

with solution

$$x = x_o e^{-kt} \sin\omega t , \qquad (2.4.6)$$

where

$$\omega^2 = \omega_i^2 - k^2 . \qquad (2.4.7)$$

The damping constant k is given by

$$k = \frac{\omega_i^2 S^2 T\rho A}{2g\kappa} . \qquad (2.4.8)$$

S is the entropy per unit mass, A the cross-sectional area of the beaker, ρ the total density and κ the thermal conductance from beaker to bath.

The damping constant k exhibits an unusual dependence on ω_i^2 and an interesting temperature dependence, both of which have been confirmed experimentally, (Allen et al, 1974 and Hoffer et al, 1974). The temperature dependence is contained in the terms S, T, ω_i and κ and causes the damping to pass through a maximum just below the λ-point. At very low temperatures in the isothermal limit, the damping should become

very small; the liquid is now virtually pure superfluid, so that the temperature gradients accompanying superfluid flow will be minute, giving virtually no dissipation by irreversible heat exchange.

2.5 Summary

The present consensus of opinion favours the interpretation of intrinsic superfluid dissipation in terms of the transportation of quantised vorticity across the stream. The two main problems inherent in this viewpoint are to account for the nucleation energy of the vortices and to describe a plausible mechanism whereby the vortices can cross the stream. In recent years it has become popular to seek the answer to the first of these problems in theories of the thermal fluctuation type. However, the success of these theories has been limited in that comparison between predicted and observed values of the critical velocity is very poor. The second problem has been treated convincingly by Campbell in terms of the scattering of normal fluid excitations by the cores of the vortices.

Both of these approaches are rather sensitive to the temperature of the superfluid system. As was seen in section 2.3(c), the probability of nucleating a "critical" vortex diminishes rapidly with temperature, and from section 2.2(e), the angle at which vortices traverse the stream becomes effectively zero at low temperatures. [From Campbell (1970), $\theta = 6 \times 10^{-5}$ at $T = 0.4K$.] For these reasons it would seem that, according to currently held opinions, intrinsic superfluid dissipation should be severely inhibited in the very low temperature region. (The occurrence of extrinsic thermal dissipation is also automatically precluded in this region.)

The present work was undertaken with the aim of investigating this possibility. The experiments were of the beaker film flow type and included determinations of the critical transfer rate, the form of the dissipation curve and the damping of the inertial oscillations. The measurements were made over the temperature range 1.62K to 0.01K.

CHAPTER THREE

RECENT EXPERIMENTS ON SUPERFLUID FLOW

3.1 INTRODUCTION

The basic properties of superfluid flow in films and channels were established in the early experiments of Daunt and Mendelssohn (1939), Allen and Misener (1939) and Atkins (1950). Subsequent studies of flow phenomena were numerous, but the results obtained were irreproducible and often conflicting, emphasising the difficulties inherent in this type of work.

The most easily measured transport property of the superfluid is the so-called "critical velocity", v_c, which early experimenters found to be virtually independent of pressure head, although measurements at very low heads were precluded by the limitations of the optical techniques current at that time. The values obtained for v_c varied both between different groups of workers, and also from day to day in the same experiment. This unsatisfactory situation was clarified somewhat by the work of Bowers and Mendelssohn (1950), who demonstrated that anomolously high, or "enhanced" flow rates, could be caused through contamination of the substrate by grease, dirt, or more probably, condensed gases. It is now known that the flow rate is also extremely sensitive to extraneous vibration. In all probability, therefore, much of the aforesaid irreproducibility stemmed from either or both of these sources, although it must be admitted that more recent work, in which great care has been taken on these counts, still reveal facets of behaviour which are unpredictable. This apparent capriciousness on the part of liquid helium only serves to reflect the general inadequacy of our understanding of the phenomenon of superfluidity.

Some of the more recent experimental studies of aspects of superfluid flow that are relevant to the present work will now be reviewed.

3.2 THE DEPENDENCE OF v_c ON TEMPERATURE AND CHANNEL WIDTH

Until recently it was thought that two regimes of dissipation existed for flow through narrow channels. For channel diameters d less than 10^{-3} cm the critical velocity was found to vary as $d^{-\frac{1}{4}}$ (Keller and Hammel, 1965), remaining temperature independent until close to the λ point; for larger channels, v_c varied inversely as d and became temperature dependent.

This latter relation conformed with the predictions of the Feynman vortex ring model (section 2.2b) and hence gained widespread acceptance, whilst the behaviour of the critical velocity in smaller channels was considered anomalous. This viewpoint has recently been reversed by the work of Van Alphen et al (1966), who showed that the measurements made in channels with $d \triangleright 10^{-3}$ cm were indicative of the onset of turbulence in the normal fluid; when suitable precautions were taken to immobilise the normal fluid, critical superfluid velocities were obtained which formed a continuation of the $v_c \propto d^{-\frac{1}{4}}$ relation. The current experimental evidence now indicates that this law remains valid for channel sizes ranging through eight orders of magnitude.

The superfluid film can be regarded as a narrow channel, and for the case of beaker film flow, the channel width in the dissipative region is simply the film thickness at the rim. This varies according to the height of the rim above the bulk fluid levels. Allen and Armitage (1966) carried out a series of beaker film flow experiments in which the variation of the film transfer rate σ with rim height H was given by

$$\sigma(H,T) = 6.5\ \rho_s/\rho\ H^{-\frac{1}{4}} \times 10^{-5}\ cm^2 s^{-1}. \qquad (3.2.1)$$

If the static film thickness equation $d = kH^{-1/3}$ and the relation $\sigma = \frac{\rho_s}{\rho} v_c d$ are substituted into 3.2.1., it is seen that, again v_c varies as $d^{-\frac{1}{4}}$, and is independent of temperature over the range investigated, (1.19K to 1.8K).

3.3 PREFERRED FLOW RATES

In an early study of film flow, Eselson and Laserev (1951,1952) discovered that the history of the helium film had some bearing on the observed transfer rate. If, prior to a flow experiment, the beaker was filled by immersion in the bath, the subsequent transfer rate was found to be higher than if the beaker had been allowed to fill slowly via the film. A detailed investigation of this effect was carried out by Allen (1960, 1963) and Allen and Matheson (1966), who interpreted their results in terms of an increased film thickness following the drainage of liquid from a previously immersed substrate.

The appearance of such "enhanced" rates is not, however, dependent on immersion of the substrate, as is seen from the film flow experiments of Mate et al. (1965), Allen and Armitage (1966) and Harris-Lowe et al (1966). Rather, there appears to exist at all times a structure of "preferred flow rates", between which spontaneous changes can occur during the course of a single flow. Furthermore, the preferred rates are apparently evenly spaced, although agreement between different researchers as to the size of the spacing is not good. In a recent series of experiments employing high resolution techniques, Harris-Lowe and Turkington (1971 and 1973) suggest that this spacing may, in fact, be a gross structure superimposed on a much finer set of preferred rates, found at intervals of $0.16 \times 10^{-5}\ cm^2 s^{-1}$. Unfortunately, the

authors were working very close to the limit of resolution of their apparatus, and the question remains open as to whether a further increase in sensitivity would have revealed further detail.

Some light has been shed on the problem of preferred rates by the work of Keller and Hammel (1966(a), 1969, 1974). In an elegant series of experiments the chemical potential profile accompanying beaker film flow was determined by means of special capillary probes inserted at certain points on the beaker wall. Keller and Hammel demonstrated that in the case of an outflow, most of the drop in chemical potential occurred at the inside edge of the rim, indicating that the dissipation was normally confined to a very narrow region. However, it was seen that for inflows, the dissipation region extended down the inside wall from just below the rim almost to the liquid level. Of particular interest were the observations that, during outflows, the occurrence of a discontinuous drop in transfer rate was always accompanied by a change in the chemical potential profile; the dissipation region was seen to spread from the rim down the inner wall of the beaker. This implies that throughout the dissipation region the gradient of the chemical pontential is now reduced, and since it is this quantity which provides the force on unit mass of superfluid, it is maybe not surprising that the flow rate should simultaneously drop.

These observations would seem to bear some relation to the earlier measurements made by Keller and Hammel (1966(b)) on isothermal flow through narrow channels. In these experiments, it was seen that if the flow was initiated by setting up a relatively large gravitational head of liquid, a certain critical velocity would be observed and the dissipation region would be uniformly distributed along the entire length of the channel. On the other hand, if a "driven flow" technique

was employed, whereby the flow rate was slowly increased from zero, substantially higher velocities were obtained for the same pressure heads. By the above argument, the dissipation regions were now presumably localised at favoured sites. Furthermore, there seemed to be some instability in the number and location of these sites, as the driven flow data exhibited the same kind of preferred rate structure as is seen in beaker film flow.

3.4 THE THICKNESS OF THE STATIC FILM

The earliest reliable measurements of the thickness of the static film as a function of height above the bulk liquid level were made by Jackson and co-workers, using an optical technique (Burge and Jackson 1951; Ham and Jackson 1957; Grimes and Jackson 1959). The film was formed on a polished stainless steel substrate on which plane polarised light was incident. The reflected beam was elliptically polarised and the thickness of the film could be inferred from the angle between the initial plane of polarisation and the major axis of the ellipse. The results conformed to the simple Frenkel-Schiff theory, in the form of equation 1.7.3. with $k \sim 296\text{Å}$ and the exponent of $z \sim 0.39$, both quantities exhibiting a small temperature dependence. It was also found that if the substrate was contaminated by a thin layer of solid air, the film thickness could be as much as three times the normal value. This corroborated the observations of Bowers and Mendelssohn (1950) of anomolously high transfer rates over contaminated substrates.

The theoretical profile $d = kH^{-1/3}$ stems from the fact that the Frenkel-Schiff theory assumes a van der Waals potential of the form $-\alpha/d^3$. This is only true very close to the substrate; at greater distances the time lag between the polarisation of molecules due to the finite velocity of light becomes important. The retardation effects

have been treated by Lifshitz (1956), and the predictions of this theory for helium films on cleaved surfaces of alkaline-earth fluoride crystals have been tested by Sabisky and Anderson (1973) using a sensitive acoustic interferometry technique. Excellent agreement with the theory was obtained.

3.5 THE THICKNESS OF THE MOVING FILM

As mentioned in section 1.7 the prediction by Kontorovich (1956) that a flowing helium film should be thinner than a stationary one has caused a certain amount of controversy, both theoretical and experimental. The main theoretical difficulty lies in deciding whether or not the effect of kinetic film thinning will be cancelled out by condensation from the vapour above the film. (Campbell 1975). Experimental investigations into the thickness of the flowing film are reviewed briefly below.

Atkins (1950(a)) employed a dynamic method to determine the film thickness. From his calculations it can be shown that the period τ of the inertial oscillations following a beaker film flow experiment is given by

$$\tau = 2\pi \left(\frac{\rho}{\rho_s} \frac{A^*}{2\pi r^* g} \int_0^H \frac{dz}{d(z)}\right)^{\frac{1}{2}}, \qquad (3.5.1)$$

where H is the height of the beaker rim above the liquid level, $d(z)$ is the film thickness as a function of height z, r^* is the reduced radius of the beaker, given by $r^* = \frac{r_{in} r_{out}}{r_{in} + r_{out}}$, and A^* is the reduced area, given by $A^* = \frac{A_{in} A_{out}}{A_{in} + A_{out}}$.

Atkins assumed a film profile of the form $d = kz^{-1/n}$, which gives

$$\int_0^H \frac{dz}{d(z)} = \frac{n}{k(1+n)} H^{(n+1)/n}. \qquad (3.5.2)$$

Substitution of 3.5.2 into 3.5.1 then shows that a graph of $\ell n\ \tau$ against $\ell n\ H$ should be a straight line of slope $\frac{1}{2}(\frac{n+1}{n})$, with intercept

$$\tfrac{1}{2}\ell n\ \{4\pi^2\ \frac{\rho}{\rho s}\ \frac{A^*}{2\pi r^* g}\ \frac{n}{k(1+n)}\}.$$

From his measurements of τ and H, Atkins obtained values for k and n of 167Å and 7.1 respectively. These results are very different from currently accepted values, and it seems probable that they were produced by an undetected experimental artifact. The method itself is of considerable merit and has been used successfully by subsequent workers (Crum et al 1974; Kwoh and Goodstein 1977). Crum et al used a retarded van der Waals potential to predict an approximate film profile on stainless steel of the form $d = 284\ H^{-1/3.5}$ Å. This compared well with their experimental results, despite the fact that the theoretical profile is that of a static film whilst the "oscillation" method employs a moving film.

An early experiment by Gribbon and Jackson (1963) using the ellipsometry technique for film flow out of a metal beaker gave confirmation of film thinning, although the size of the effect was somewhat smaller than the Kontorovich prediction. However, Keller (1970) investigated the film thickness under similar conditions by a capacitative technique and observed no thinning. A null result has also come from Telschow et al (1975) who measured the velocity of third sound in an unsaturated film as a function of the superfluid velocity; only the expected Doppler shift was observed, with no extra contributions that should have been present if film thinning had occurred.

At the time of these experiments, it was thought that vapour condensation was responsible for the apparent absence of kinetic

thinning. Consequently, experiments were undertaken in which the flow of the vapour was restricted by the geometry of the apparatus. Van Spronsen et al (1973) observed inertial oscillations between liquid reservoirs linked by a helium film which covered the inside of a glass spiral 120 m in length. The narrow bore of the spiral (0.33mm) presented a high impedance to vapour flow, and any kinetic thinning over such a length of film should have been observable as a change in the net amount of liquid present in the reservoirs. The experiment was successful in that kinetic thinning was indeed detected and the size of the effect was found to be in order of magnitude agreement with the prediction of Kontorovich.

Williams and Packard (1974) reduced the effect of vapour in their film thickness experiment by working at a temperature of 0.9K. The thickness was measured using a capacitor and film thinning was observed that agreed with the Kontorovich prediction to within 30%.

These preliminary indications that inhibition of vapour flow was necessary to achieve kinetic thinning were contradicted by the work of Graham and Vittoratos (1974). The thickness of a horizontal helium film in radial flow was measured, again by a capacitative technique, and the Kontorovich effect was observed. The experiments were performed between 1.2K and 2.0K and the vapour had free access to the film surface. Graham (1977) has extended this experiment to the case of a persistent current in the saturated film. (Persistent currents will be discussed in section 3.6.) The film was formed on the inner surface of a torus of rectangular cross-section, and the presistent current was achieved by rotation of the torus. The film thickness was measured by a capacitor, and the vapour was given maximum possible access to the film

surface. Film thinning was observed to be a steady-state phenomenon in currents that were allowed to persist for as long as several hours, which times greatly exceeded any possible relaxation times of a vapour condensation mechanism.

The original experiment by Keller in which no film thinning was observed has been duplicated by Kwoh and Goodstein (1977), and this time a positive result was obtained; film thinning was observed at all temperatures in the range 0.5K to 1.9K in approximate quantitative agreement with Kontorovich. The static film thickness profile was determined as $d = 335 \times H^{-1/3}$ Å as compared to Keller's value of $464H^{-0.35}$ Å, and film transfer rates over the stainless steel substrate were found to be significantly lower than those found by Keller. Taken together, these factors strongly suggest that Keller's null result could in some way be connected with surface contamination.

It would now seem that the weight of experimental evidence has established kinetic film thinning as a basic property of superfluid flow although convincing explanations for some of the earlier null results remain to be found. In particular, the vapour condensation mechanism causing re-thickening of the film has been shown not to operate.

3.6 PERSISTENT CURRENTS

It has been known for some time that persistent flow of helium both in the bulk and in completely filled porous material can be achieved experimentally using a rotational method; (Reppy and Depatie 1964; Mehl and Zimmerman 1965). The same phenomenon has also been observed for an unsaturated helium film adsorbed onto a porous substrate; (Henkel et al 1968).

However, early attempts to duplicate this result for both unsaturated and saturated films covering relatively smooth cylindrical surfaces were not successful; (Wang and Rudnick 1974; Wagner 1973).

The first persistent currents in the saturated film were observed by Verbeek et al (1974(a)). In this experiment, film flow took place along the inner wall of a glass spiral 130m long and .035cm bore. Unfortunately the results were not entirely clear-cut as part of the flow circuit consisted of a rouge plug containing bulk fluid , in which vorticity could have been trapped. A similar experiment by Galkiewicz and Hallock (1974) with a flow path consisting entirely of the saturated film again gave positive results. In this latter experiment the substrate was of stainless steel, not glass, and the shorter, wider flow tube presented far less impedance to vapour flow over the film. A modified version of this experiment has recently been performed (Galkiewicz et al (1977)) in which the existence of the persistent flow was demonstrated by means of Doppler-shifted third sound.

Both of these successes with the saturated film employed a multiply-connected geometry to obtain the persistent current, as opposed to the rotational methods of the earlier attempts. However, experiments by Verbeek et al (1974(b)), Wagner (1976) and Graham (1977) have demonstrated that the rotational technique can be used successfully.

Persistent currents would therefore seem to be an established phenomenon for unsaturated and saturated films, and for bulk liquid, in both microscopic and macroscopic geometries. As in the case of film thinning, there do, however, remain some puzzling null results which are at present unexplained.

3.7 EXPERIMENTAL EVIDENCE FOR A THERMAL FLUCTUATION APPROACH TO SUPERFLUID DISSIPATION

The outstanding prediction of the thermal fluctuation theories (section 2.3) is that superfluid flow is never really frictionless; a small chemical potential gradient will be present across all flows, no matter how slow. Early experiments on sub-critical flow by Daunt and Mendelssohn (1946) and Chandrasekhar and Mendelssohn (1955) did not reveal this effect, although the resolution of small pressure heads was limited by the experimental techniques employed at that time. However, in a series of experiments in which beaker film flow was driven at a sub-critical rate, Picus (1954) concluded that "a finite but small level difference is always necessary to sustain film flow, even at rates less than the critical value." Seki (1962) studied thermally driven sub-critical film transfer and by careful consideration of both the temperature and pressure contributions to the chemical potential gradient showed that transfer rates slightly below the critical value were indeed accompanied by a small effective pressure head.

The work of Reppy and co-workers on the properties of persistent currents in fluid-filled porous annuli has done much to support the thermal fluctuation approach. Clow and Reppy (1967) showed that the "critical velocity", or that velocity at which dissipation effects suddenly become extremely large, is proportional to ρ_s/ρ near the λ point. This agrees with the predictions of thermal fluctuation theory. In addition, Kukich, Henkel and Reppy (1968) have shown that the velocity of a superfluid persistent current actually decays logarithmically with time, again qualitatively in agreement with the thermal fluctuation

approach; quantitatively the observed rate of decay is much too large.

Notarys (1969) interpreted the results of his experiments on pressure-driven superfluid flow through porous mica in terms of the fluctuation theory and obtained good functional agreement with equation 2.3.6:

$$\Delta\mu = \tfrac{1}{2}kVNf \exp(-\frac{\Delta F}{kT}). \qquad (2.3.6)$$

Writing this as

$$\Delta\mu = kVf_o \exp(-\frac{\beta}{v_s}\frac{\rho_s}{\rho}\frac{1}{kT}), \qquad (3.7.1)$$

Notarys found values for f_o and β of $5 \times 10^{27} cm^{-3}s^{-1}$ and 1.3×10^{-12} cgs respectively, for flow through 800Å pores. These values were independent of temperature over the range 1.27K to 2.09K. The theoretical values of f_o and β from the Langer-Fisher model are $f_o \sim 10^{35}\ cm^{-3}s^{-1}$, $\beta \sim 50 \times 10^{-12}$ cgs, so again numerical comparison is poor.

A similar study of superflow through porous mica has been carried out by Harrison and Mendelssohn (1974) who found, for 800Å pores, a value for β of 1.4×10^{-12} cgs, which is very close to the result of Notarys, whilst f_o was a factor of 10 lower at $5 \times 10^{26}\ cm^{-3}s^{-1}$. These values were virtually constant from 1.72K to 1.34K, but for temperatures below this, f_o increased rapidly.

Banton (1974) has carried out extensive measurements on superflow through small orifices and observed behaviour compatible with the predictions of the fluctuation theory for a 5μ hole at a temperature of 1.25K. The value of β obtained was 0.89×10^{-12} cgs which again agrees reasonably well with Notarys' value. The fact that this hole had a diameter of 50,000 Å whilst those used by Notarys' were approximately 800Å in diameter suggests that β is independent of channel width.

A study of thermally driven film flow has been made by Liebenberg

(1971(a) and (b)). The temperature difference across the region of dissipation was measured in one case by a sensitive thermometric technique, and in another by vapour pressure capillary probes. The functional form of equation 3.7.1 was found to be obeyed, with $f_o = 2.2 \times 10^{17}$ cm^{-3}s^{-1} and $\beta = 4.4 \times 10^{-13}$ cgs for temperatures over the range 1.7K to 2.03K.

The temperature independence of the parameter f_o has been questioned by Cannon, Chester and Jones (1972) who found that in a beaker film flow experiment f_o increased substantially with decreasing temperature. A similar observation has been made by Saunders (1974). In this experiment, whilst β was observed to remain roughly constant around a value of 2.9×10^{-13} cgs, the value of f_o increased by ten orders of magnitude as the temperature decreased from 2.1K to 1.5K. Hoffer et al (1974) have independently arrived at a similar conclusion, with f_o increasing by 20 orders of magnitude for a decrease in temperature of 1.14K! The parameter β was also observed to be slightly temperature dependent, taking values from 7.2×10^{-14} to 3.3×10^{-13} cgs over the temperature range 2.12K to 1.17K.

Keller and Hammel (1974) have determined the chemical potential profile along the inner wall of a beaker during film flow by means of eight capillary probes inserted into the wall at regular intervals. From these profiles the chemical potential gradient at any height can be estimated and by assuming a film thickness profile of $d = 300 \times H^{-1/3}$ Å, the corresponding value of v_s can be determined from the transfer rate σ. At a temperature of 1.585K, using appropriate values of f_o and β from the work of Hoffer et al (1974), the relation between $\underline{\nabla}\mu$ and v_s was seen to agree with the fluctuation model, as expressed in equation 3.7.1.

An extensive investigation into beaker film flow at temperatures above 1K has recently been carried out by Campbell et al (1976). High accuracy data was obtained, enabling a comparison of different fluctuation theories to be made. The best fit to the data was consistently given by equation 3.7.1. although, again, the quantity f_o was found to be strongly temperature dependent, whilst β was weakly so.

It would therefore seem to be experimentally established that above 1K superfluid flow does not proceed at one characteristic velocity v_c, but rather that v_s takes on values over a narrow range as the chemical potential gradient passes through the entire spectrum of values observable in the laboratory. The exponential relation given in equation 3.7.1. can be made to describe this variation satisfactorily at all temperatures between 1K and 2.2K by a suitable choice of the parameters f_o and β. To proceed beyond this point and seek an interpretation of this phenomenological model in terms of a thermal fluctuation theory would appear to be justified only in the immediate vicinity of the λ transition, for the case of films. At temperatures between 1K and 2K, where the "critical" velocity is observed to be more or less independent of temperature, the consequence of fitting the particular form of equation 3.7.1. to the data is to make the quantity f_o temperature dependent to an almost ridiculous degree; an increase of 20 orders of magnitude for a decrease in temperature of 1.14K is a rather extreme variation in any physical quantity. Furthermore, to describe f_o as an "attempt frequency" in this temperature region would seem to be doubly inappropriate, as all microscopic fluctuation theories to date show that f_o should have the opposite temperature dependence

(Jordanskii 1965; Donnelly and Roberts 1971; Chester and Ziff 1971).

3.8 EXPERIMENTAL STUDIES OF DISSIPATION DUE TO IRREVERSIBLE HEAT EXCHANGE

Many studies of the damping of the inertial oscillations observed during beaker film flow experiments have been undertaken in order to test the Robinson theory of thermal dissipation as described in section 2.4. Early attempts suffered the usual inconsistencies common to experimental superfluidity, but in recent years a number of groups have obtained good agreement with the theory.

Allen, Armitage and Saunders (1974) studied beaker film flow driven at low rates, and demonstrated the predicted dependence of the damping constant on the square of the oscillation frequency. Also, by directly measuring the thermal conductance between the beaker and the bath, the authors showed that the observed maximum in the damping constant just below the λ point was in good quantitative agreement with the theory. The same conclusions were reached independently by Hoffer et al (1974) in an experiment on the near isothermal oscillations of the helium film covering the surface of an inverted U-tube between two liquid reservoirs.

The irreversible heat flow of the Robinson theory results from the small temperature oscillations that accompany the oscillations in the liquid levels. These temperature oscillations were observed by Hallock and Flint (1973) and were shown to be consistent in magnitude and phase with the theoretical predictions. The observations of Allen et al and Hoffer et al concerning the temperature dependence of the damping constant were also corroborated.

During experiments investigating Kontorovich film thinning, using

extremely long (∿200m) glass capillary spirals, van Spronsen et al (1974) measured the temperature dependence of the damping of the inertial oscillations occurring in this system. A direct determination of the thermal conductance between the reservoirs was not possible, but by assuming a reasonable value for this parameter, a good fit between theory and experiment was achieved.

3.9 FILM FLOW EXPERIMENTS AT TEMPERATURES BELOW 1K

Ambler and Kurti (1952) were the first to investigate the flow of the helium film in this region. Cooling was achieved by a demagnetisation technique, giving a bottom temperature of 0.15K. Unfortunately the optical method of determining the position of the liquid levels led to large heat inputs and rapid warm-up times of around half an hour. Temperature stability during measurements was therefore not good. The film flow took place over a glass substrate and the transfer rate obtained above 1K (11-13 x 10^{-5} $cm^2 s^{-1}$) was somewhat high compared to accepted values (8 x $10^{-5} cm^2 s^{-1}$). This fact, together with the observation that run to run reproducibility was poor, suggested that some contamination was present on the flow surface. However, interesting results were obtained in that the transfer rate was seen to rise steadily below 0.8K, amounting to an increase of 30% at a temperature of 0.2K.

An attempt was made by Lesensky and Boorse (1952), to repeat these measurements for film flow over copper, avoiding the problem of a rapid warm-up by measuring the liquid levels using a capacitative technique. Unfortunately problems were encountered with thermal isolation and results were only obtained down to 0.75K. The rates were again rather high at 1K, but corroborated the observation by Ambler and Kurti of an upward trend below about 0.8K.

Waring (1955) obtained measurements of thermally driven transfer rates over glass down to a temperature of 0.14K, using a demagnetisation cryostat. A novel technique of determining the flow rate was employed, in that the film was allowed to flow into the warmer region of the cryostat where it was pumped away; the fore-pressure at the pump was related to the rate at which gas was evolved from the film, yielding a value for the flow rate. However, these values were anomalously high at 1K, suggesting that either the measuring technique was faulty or the substrate was badly contaminated. At 0.14K the flow rate was observed to have increased by 10% over its 1K value.

The first convincing measurements below 1K came from Hebert, Chopra and Brown (1957). To overcome the difficulties of thermally isolating a volume of helium at low temperatures, a "sealed capsule" technique was employed: enough gas was sealed into the experimental chamber at room temperature to provide the liquid for the experiment. The liquid levels were viewed optically, which again limited the experimental time after demagnetisation to about half an hour. Also, the experimental chamber was raised mechanically from the demagnetisation position to the viewing position, which operation caused additional warming. A respectably low transfer rate of $7 \times 10^{-5} cm^2 s^{-1}$ was obtained above 1K, and good reproducibility was reported. Again the flow rate was seen to increase below 1K, and at the lowest temperature obtained, 0.3K, its value was around $9 \times 10^{-5} cm^2 s^{-1}$, representing a 30% increase.

A common fault of these early experiments employing the demagnetisation method was the poor temperature stability during measurements. In an attempt to improve on this situation, Mate et al (1965) used a ^3He

cryostat to study film flow over glass down to 0.35K. The low flow rate of 7.8×10^{-5} $cm^2 s^{-1}$ obtained above 1.2K was indicative of a clean substrate and at 0.35K the mean rate had increased by 65%. The experimental method was sufficiently accurate to show that the observed scatter in the results, which became worse at lower temperatures, was larger than the experimental error. This was the first indication that the preferred rate structure, commented on by others above 1K, persisted into the very low temperature region.

Allen, Matheson and Walker (1965), again using a ^{3}He cryostat formed a composite picture of the flow behaviour from T_λ down to 0.5K. The "enhanced" rates (see section 3.3), obtained by filling the beaker by immersion prior to an emptying, were shown to lie on a well defined curve extending from 1.8K to 0.8K. This curve increased smoothly with decreasing temperature and did not exhibit the plateau region seen in the "normal" flow rate above 1K. Below 0.8K the scatter in both the enhanced and normal rates increased to such an extent that the two modes of flow were no longer distinct; most of the points fell in the region bounded by extrapolations of the "enhanced" and "normal" curves. The mean rate at 0.5K was found to be 62% greater than the normal rate at 1K.

Film flow over a stainless steel substrate has been studied by Crum et al (1974) down to a temperature of 0.036K, which is a substantial reduction over previous measurements. A He-3,4 dilution refrigerator was employed to give extended running times with very stable temperatures. The results obtained above 1K are unusual, in that the plateau region normally observed for flow over other substrates

was absent; the transfer rate increased smoothly with decreasing temperature from T_λ to 0.4K. That this effect is not a peculiarity of flow over stainless steel can be seen from the work of Smith and Boorse (1955) who indeed observed the usual plateau region, albeit with substantially higher transfer rates than those observed by Crum et al. when the different film heights in the two experiments are taken into account. The 1K data of Crum et al is in fact reminiscent of the enhanced rates discussed earlier. Also the fact that the rates recorded by Crum et al were the initial high rates at which film flow commenced, and that these subsequently decayed by abrupt transitions to lower rates lends substance to this conjecture.

Below 0.3K an interesting effect was observed by Crum, in that the flow rate started to drop steeply. This behaviour was attributed to the formation of a layer of ^{3}He on the surface of the film, ^{3}He being contained in commercially available ^{4}He at a concentration of approximately 2 parts in 10^7. (The formation of a surface state of ^{3}He at very low temperatures has been suggested by Andreev (1966), and experimental evidence has been provided by Zinov'eva and Boldarev (1969) and Guo et al (1971)). Further increase of the ^{3}He concentration caused the drop in flow rate to set in at progressively higher temperatures in accordance with theoretical predictions. Also measurements performed during the same experiment showed that the surface tension γ decreased progressively as the ^{3}He layer was formed, and that the flow rate σ in this region was related to γ by $\sigma \propto \sqrt{\gamma}$, in accordance with a theory of Ark hipov (1958).

The dependence of flow rate on level difference observed in beaker film flow experiments above 1K was not seen by Crum et al.

In fact no dependence at all was reported for level differences greater than 100μm, which suggests that the results can no longer be fitted to the form of equation 3.7.1. in the low temperature region. The profile of the film was also investigated using the oscillation technique of Atkins, and was found to be independent of temperature below 1K to within the experimental error of 3%.

The main conclusions to be drawn from the seven experiments briefly reviewed in this section is that a rise in the transfer rate definitely occurs below 1K, although considerable confusion exists as to the size of this increase due to contamination in some of the experiments. Also, the occurrence of "preferred" and "enhanced" rates has done much to complicate the situation. Both the superfluid fraction and the film profile remain constant below 1K, so it seems that the increase in rate must be attributed to an increase in the "critical" velocity v_c. This is maybe indicative that a different dissipation mechanism comes into force at these low temperatures. The "critical velocity" type behaviour observed by Crum et al, where no dependence of the flow rate on level difference was detected for pressure heads as small as 100μm supports this idea.

It therefore appeared desirable to carry out further investigations into beaker film flow at very low temperatures, and the remainder of this thesis is devoted to a description of such an experimental study. The specific aims of the work were as follows:-

(i) to establish the size of the increase in flow rate below 1K on a clean substrate, in as far as the preferred rate structure would allow;

(ii) to make more observations of the behaviour of preferred rates so that a better understanding might be gained of the processes involved in this phenomenon;

(iii) to study the sub-critical flow of the helium film, both in the steady state and during the inertial oscillations, so that possible evidence of sub-critical dissipation in the form of small pressure heads or damping could be obtained. This would be helpful in establishing possible differences between dissipation mechanisms operating above and below 1K;

(iv) to investigate the behaviour of the flow rate at temperatures below 36mk to see if the strong downward trend observed by Crum et al continues.

CHAPTER FOUR

THE DESIGN STUDY FOR THE CRYOSTAT

4.1 INTRODUCTION

The experiments outlined in Chapter 3 required stable temperatures below 36mk. Temperatures of this order can be attained either by dilution refrigeration or adiabatic demagnetisation of a paramagnetic salt. The latter method is better suited for the present work in that the level of vibration in the experimental region can be kept very low. The temperature stability is admittedly a problem, but this can be made sufficiently good by the use of adequate thermal guards and of salt specimens with large residual heat capacities.

The demagnetisation cryostat to be described in the next two chapters was designed to cool 140 cm^3 of liquid ^4He to a bottom temperature of 10mK with minimal warming over a period of several hours.

4.2 THEORY OF MAGNETIC COOLING

The discussion given here will be confined to fundamentals since many excellent reviews exist in the literature. See for example Ambler and Hudson (1955), DeKlerk (1956), Mendoza (1961), Little (1964).

(a) The entropy of a paramagnetic salt in zero applied magnetic field

For a substance to be a potential coolant below 1K, it must still possess a substantial amount of entropy at this temperature. Most solids are not very useful in this respect since their lattice entropy is generally very small at 1K. However, in the case of a paramagnetic salt, considerable entropy may be retained in the spin system down to temperatures as low as several hundredths of a degree.

The entropy of a spin system derives from the number of possible

orientations of the magnetic moment vectors of the paramagnetic ions. As a specific example, consider the case of potassium chrome alum ($Cr_2(SO_4)_3K_2SO_4.24H_2O$). The paramagnetic properties are due to the $3d^3$ state of the chromium ion. The total angular momentum quantum number j is made up solely from spin contributions from each of the three unpaired electrons. (The strong electric field of neighbouring oxygen ions constrains the electrons to occupy levels with a resultant orbital angular momentum of zero). The spins are aligned due to the exchange interaction, giving a value for j of 3/2. At 1K the thermal energy per spin is much greater than the interaction energy with the crystalline electric field. The 2j+1 orientations of the angular momentum vector of each ion are therefore equally probable, which leads to a simple expression for the entropy per mole:

$$S = R \ln(2j + 1) = R \ln 4, \qquad (4.2.1)$$

where R is the gas constant. As the temperature is lowered to a few tenths of a degree this four fold degeneracy is reduced by further interaction with the crystalline electric field. The remaining entropy is removed by the dipole-dipole interaction at a few hundredths of a degree; a co-operative ordering of spins along some axis of symmetry within the crystal comes into play at these temperatures.

The dependence of the zero field entropy of a paramagnetic salt on temperature has not yet been predicted theoretically. However, experimental determinations have been carried out for the most commonly used salts and are given in the references quoted at the beginning of the section. See also Vilches and Wheatley (1966a).

(b) The entropy of a paramagnetic salt in a large external magnetic field

If a paramagnetic salt is placed in a large external magnetic field,

the interaction energies due to internal constraints become negligible in comparison with those due to the external field. The paramagnetic salt therefore behaves as an assembly of N non-interacting magnetic dipoles, each of moment $\underline{\mu}$. A theoretical form can now be obtained for the entropy as a function of the applied field strength and temperature.

The energy ε of each dipole in the external field $\underline{H}$ is given by

$$\varepsilon = -\underline{\mu}.\underline{H} = -g\mu_o J_z H \qquad (4.2.2)$$

where μ_o is the Bohr magneton, g is the "g-factor" of the ion and $\hbar\underline{J}$ is the total angular momentum of the ion. $\underline{H}$ is taken in the z-direction. J_z can take values in integral steps over the range $-j \leq J_z \leq +j$ where j is the total angular momentum quantum number. The partition function z of a single dipole can be written as

$$z = \sum_{J_z=-j}^{J_z=+j} \exp\left(\frac{g\mu_o J_z H}{kT}\right) \qquad (4.2.3)$$

$$\text{Defining } \eta = \frac{g\mu_o H}{kT} \quad , \qquad (4.2.4)$$

the summation in equation 4.2.3 can be evaluated to give

$$z = \frac{\sinh(j+\frac{1}{2})\eta}{\sinh\frac{\eta}{2}} \quad . \qquad (4.2.5)$$

Since the dipoles are assumed to be non-interacting, the partition function $\mathcal{Z}$ of the whole system of N molecules is given by

$$\mathcal{Z} = z^N = \left\{\frac{\sinh(j+\frac{1}{2})\eta}{\sinh\frac{1}{2}\eta}\right\}^N \quad . \qquad (4.2.6)$$

All the other thermodynamic functions of the system can now be evaluated. In particular, the free energy F and the entropy S are

given by

$$F = -kT\ell nZ = -NkT\ell n \{\frac{\sinh (j+\frac{1}{2})\eta}{\sinh \frac{1}{2}\eta}\} \qquad (4.2.7)$$

and

$$S = -(\frac{\partial F}{\partial T})_H =$$

$$Nk\eta\{\frac{1}{\eta} \ell n (\frac{\sinh(j+\frac{1}{2})\eta}{\sinh \frac{1}{2}\eta}) - ((j+\tfrac{1}{2})\coth(j+\tfrac{1}{2})\eta - \tfrac{1}{2}\coth\tfrac{1}{2}\eta)\} \qquad (4.2.8)$$

The latter function has been tabulated by several authors for different values of j; Hull and Hull (1941), Giauque et al (1941), Schmid and Smart (1954).

(c) The Magnetic Cooling Cycle

The basic principle of the magnetic cooling cycle can be stated quite simply. A paramagnetic salt is cooled by some means to a temperature of $\sim$ 1K. Considerable entropy remains in the spin system. The salt is magnetised whilst in thermal contact with a heat bath at $\sim$1K and the entropy of the spin system falls as the heat of magnetisation is removed. The thermal link between the salt and the heat bath is then broken and the salt is demagnetised. As long as this latter process is carried out slowly compared with spin-spin and spin-lattice relaxation times, the entropy will remain constant at a low value. At the end point of the demagnetisation this highly ordered spin configuration in zero applied magnetic field corresponds to an extremely low final temperature.

Given the original temperature at which the isothermal magnetisation was carried out and the value of the applied magnetic field, the final entropy of the system can be calculated. This knowledge, together with an experimental determination of the zero field entropy curve of the paramagnetic salt enables the final temperature of the system

to be predicted. (See figure 4.5.4)

4.3 THE CHOICE OF REFRIGERANT

Several factors had to be taken into account when deciding which paramagnetic salt or salts would be most suitable in this experiment. The thermal load was initially estimated as $100cm^3$ of liquid ^4He, which suggested that the main refrigerant should be of large cooling power. That is, the spin per molecule should be great enough to give considerable entropy at 1K. On the other hand, the requirement for a very low final temperature could not be met if the interaction between spins was too strong, leading to cooperative ordering at relatively high temperatures. The final choice decided upon was chrome potassium alum which, with a spin of 3/2 per molecule, would enable the desired final temperature of 10mk to be attained, given a starting temperature of ∿0.9K, and an applied magnetic field of ∿20,000 Gauss. Starting temperatures down to 0.75K can be obtained with a vortex "refrigerator" the operation of which will be described in section 4.6.

The time consuming nature of the experiments demanded good temperature stability following a demagnetisation. This is difficult to achieve if only a single salt is used. It was therefore decided to incorporate a second paramagnetic salt, ferric ammonium alum, as a thermal guard, to be demagnetised simultaneously with the main cooling salt. Ferric alum has a very large specific heat peak at a temperature of ∿26mK. (Vilches and Wheatley:1966a) Heat leaks from the warmer parts of the cryostat can therefore be absorbed with a negligible rise in temperature. The heat leak to the main salt from the guard will remain extremely small until the guard exceeds a temperature of ∿0.5K.

4.4 THE THERMAL LINK

To keep the magnetisation process as isothermal as possible, a thermal link of high conductivity between the salts and the heat sink at ∿1K was desirable. The thermal link either had to be of the "mechanical" type, which could be made and broken manually, or made of a material whose thermal conductivity could be controlled in some way. An example of the latter type of "heat switch" is a superconductor, which is a good thermal conductor when the metal is in the normal state, but a poor one when the metal is in the superconducting state. The transition from superconducting to normal states can be brought about by the application of a large enough magnetic field. Superconducting heat switches are often used in demagnetisation cryostats since they can be operated in the end field of the main solenoid. Unfortunately, the conductivity in the "off" state is still relatively high if the "hot" end is at a temperature of ∿0.9K. For successful operation, the switch should really be positioned between a ^{3}He evaporator and the salts, so that the highest temperature seen by the superconductor is ∿0.3K. This was undesirable in the present application since the operation of an additional pumping system would have increased the level of vibration in the experimental environment. It was therefore decided not to use a heat switch of this type.

Mechanical heat switches, in which thermal contact is made and broken manually between two metal surfaces, were also considered to be unsuitable; considerable force is necessary to establish good thermal contact between the surfaces in question, and utmost cleanliness of the surfaces must be maintained at all times. It was thought that

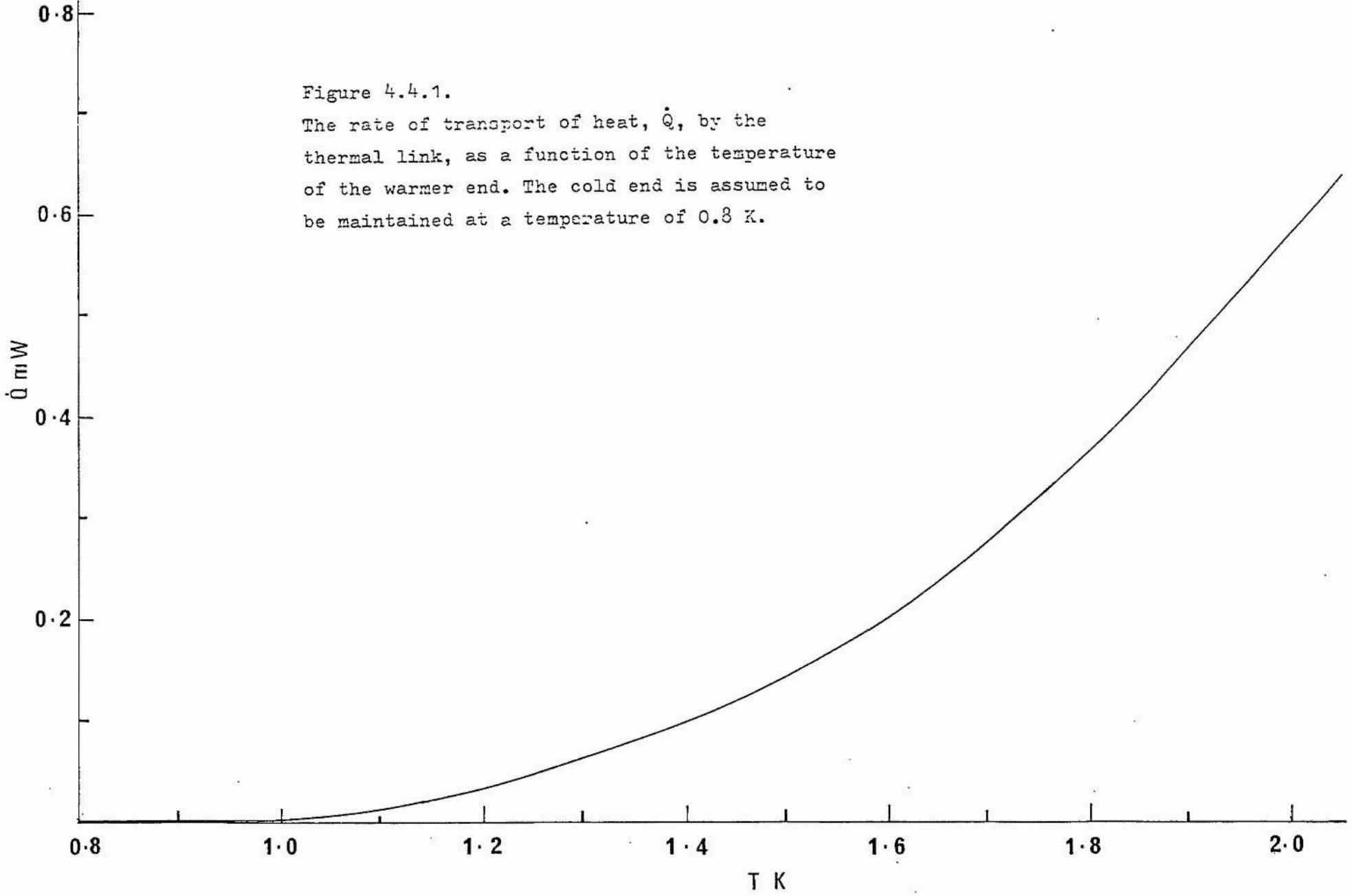

Figure 4.4.1.
The rate of transport of heat, $\dot{Q}$, by the thermal link, as a function of the temperature of the warmer end. The cold end is assumed to be maintained at a temperature of 0.8 K.

the requirement for high contact pressures would involve a large, highly engineered switch housing for which space was not available.

The final decision as to the best type of thermal switch to use was greatly influenced by certain design features incorporated into the experimental region of the cryostat. The liquid sample of 140 ccs of ^{4}He was contained, together with the main refrigerant, in a cell made from Epibond 100A epoxy resin. The liquid was condensed into the cell via a long narrow capillary thermally anchored at each cooling stage by a sintered copper heat exchanger, and wound into isolation spirals between the various stages. To allow changes of the liquid level during the course of the experiments, the cell terminated in a stainless steel bellows, operated directly from the cryostat top plate through a mechanical linkage. At temperatures above 1K, the thermal conductivity of superfluid ^{4}He is extremely high. By a careful choice of cell geometry and bellows size, the cell filling capillary was made to function as a thermal switch. Full compression of the bellows forced the liquid ^{4}He back up the capillary to make thermal contact between cell, guard salt and vortex refrigerator.

The thermal conductivity of superfluid-filled capillaries of various dimensions and temperatures has been calculated by Bertman and Kitchens (1968). To give adequate thermal isolation between the guard salt and the vortex fridge after a demagnetisation, a capillary 300cm long and 0.22mm bore was chosen. (Vilches and Wheatley 1966). The rate of transport of heat, $\dot{Q}$, by this capillary, when filled with superfluid helium, is shown in figure 4.4.1. as a function of the temperature of the "hot" end, with the "cold" end maintained at 0.8K. It can be seen that to give a reasonably isothermal magnetisation, the

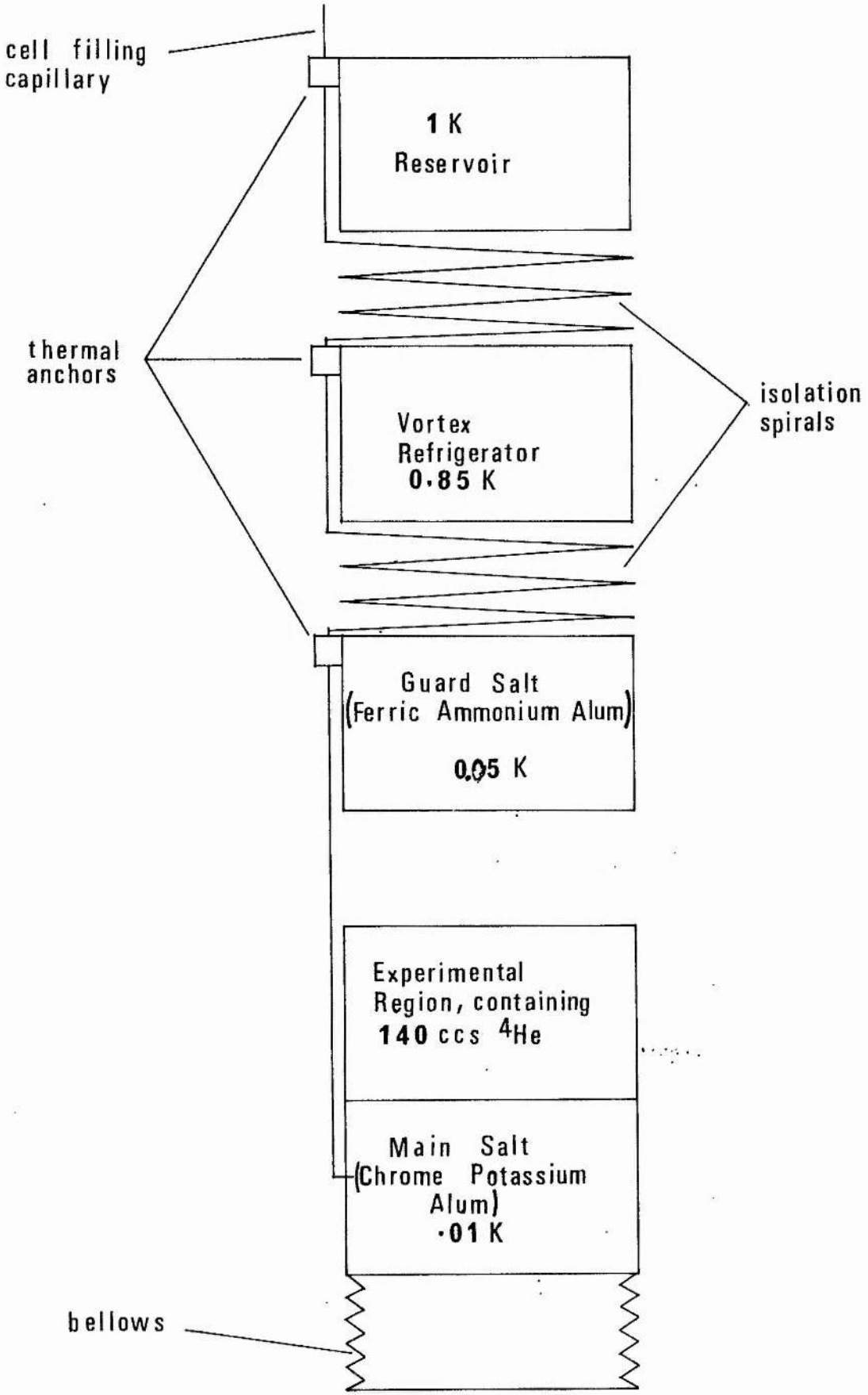

Figure 4.5.1.

A schematic diagram showing the essential features of the cryostat.

rate of production of heat must be of the order of a milliwatt. This, however, would correspond to a magnetisation time of several hours. Unfortunately such a long magnetisation period would have been hard to achieve in practice owing to the large heat leak into the main helium bath from the leads of the superconducting solenoid. (The solenoid design will be described in chapter 5.) Luckily the large heat capacity of the thermal load of 140 cm^3 of liquid helium can be used to great advantage here; if the magnetisation were carried out rapidly, the rise in temperature of the system comprising salts and helium would in fact be quite small. A calculation for the worst case, corresponding to adiabatic conditions, with the exact values for the quantities of materials used in the cryostat, will be given in the next section.

4.5 THE THEORETICAL PERFORMANCE OF THE CRYOSTAT

(a) Technical data

A schematic diagram showing the essential features of the cryostat is given in figure 4.5.1. The quantities of ferric ammonium alum and chrome potassium alum actually used were 0.33 mole (159 gm) and 0.34 mole (170 gm), respectively. The experimental cell contained 5.11 moles of ^4He.

To obtain comparison between the actual performance of the cryostat and theoretical predictions, all the thermal paths existing between the guard salt and the vortex fridge had to be taken into account. These consisted of:-

(i) The epibond former of the isolation spiral, 6.8 cm diameter, 2 cm long and $\sim$0.1mm thick;

(ii) 18 manganin wires, 10 cm long and .002" diameter with a .0002" thick coating of lead;

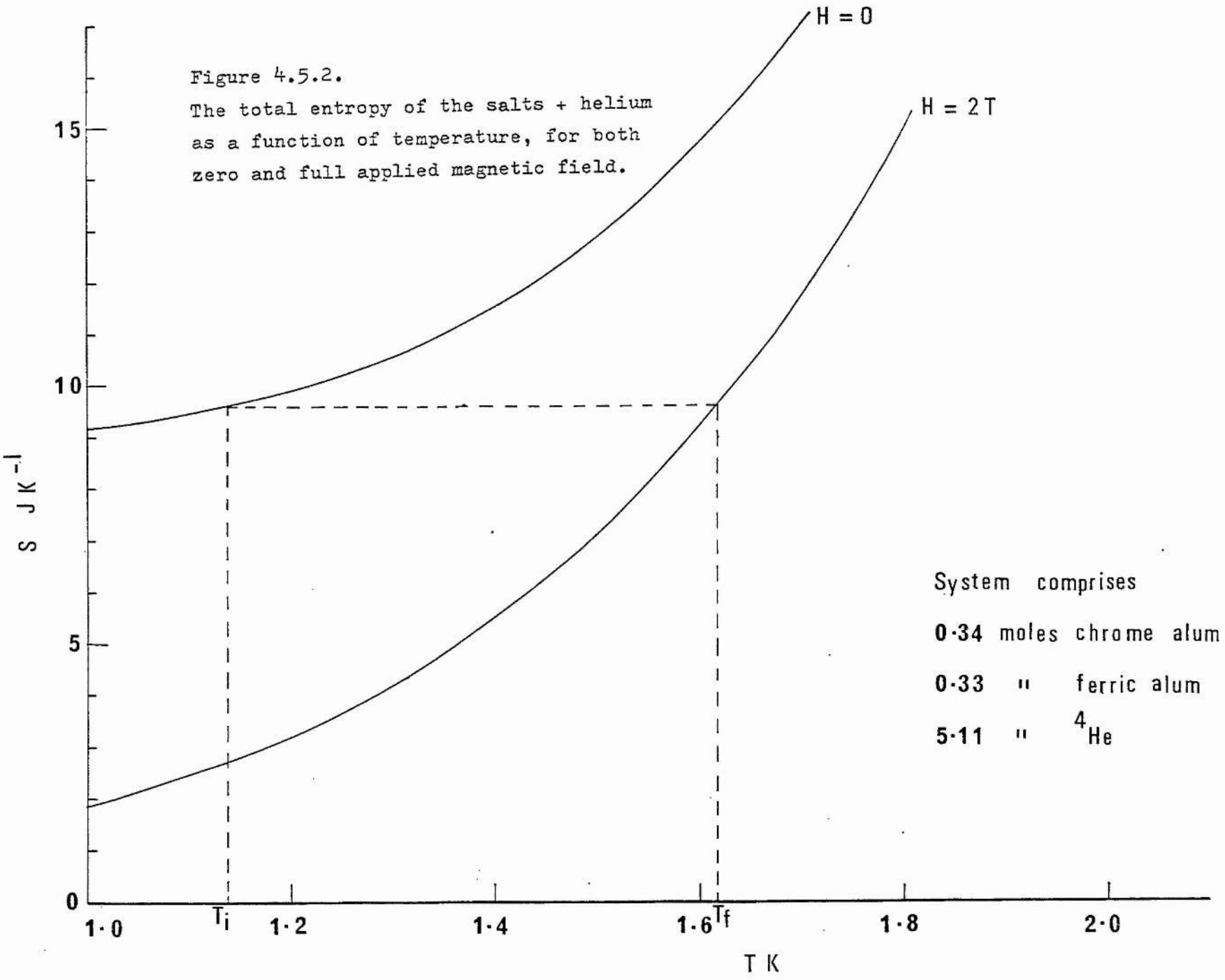

Figure 4.5.2.
The total entropy of the salts + helium as a function of temperature, for both zero and full applied magnetic field.

(iii) 3 stainless steel tubes, 6.5cm long, 3/16" in diameter with a wall thickness of .006".

The thermal conductivities of epibond and stainless steel were taken as $0.28T^{1.95}$ mWcm^{-1}K$^{-1.95}$ (Anderson et al 1963) and $(0.45T + 0.14T^{2})$mWcm^{-1} (Probert 1964) respectively. That of lead in the normal and superconducting states was taken as 4T Wcm^{-1}K^{-1} and 8 x10^{-2}T^{3}Wcm^{-1}K^{-3}(Heer et al 1954).

(b) The rise in temperature of the system on magnetisation

A magnetisation carried out quite rapidly on the two salts along with the liquid sample can be considered as nearly adiabatic. The total entropy should therefore remain approximately constant. By plotting curves of entropy versus temperature for the two cases of zero applied field and maximum applied field, the final temperature of the system can be found for any initial temperature.

In the zero applied field case, for the temperature range 1K to 2K, both salts will have a constant entropy of

$$S = N_i R \ln(2j+1) \qquad (4.5.1)$$

where N_i is the number of moles. (Lattice contributions to the entropy are negligible at these temperatures.) The entropy of ^{4}He as a function of temperature can be found from tables. (Van Dijk and Durieux 1958).

For an applied field of 20,000 Gauss, the entropy of the two salts as a function of temperature is of the form of equation 4.2.8 and can be found from tables (Hull and Hull 1941). The total entropy versus temperature curves for the quantities of salt and helium used here are given in figure 4.5.2. The starting temperature T_i prior to magnetisation was in practice $\sim$ 1.14K. This is indicated in the figure. It can be seen that this leads to a final temperature T_f for the system of 1.62K.

(c) The time needed to remove the heat of magnetisation

In order for the operation of the cryostat to be practical, the thermal link must be able to cool the salts and helium from 1.6K back down to 0.9K in a reasonable length of time. The length of this cooling period can be estimated as follows.

If the salts are in a constant magnetic field H and cool by an amount -dT, the increase in the mean magnetic moment M of one of the salts is given by

$$dM = \left(\frac{\partial M}{\partial T}\right)_H \cdot (-dT). \qquad (4.5.2)$$

M can be found from the partition function Z:-

$$M = kT \frac{\partial}{\partial H} (\ell nZ)$$

$$= N_i g \mu_o \{(j_i+\tfrac{1}{2}) \coth(j_i+\tfrac{1}{2})\eta - \tfrac{1}{2}\coth \eta/2\}, \qquad (4.5.3)$$

From equation 4.5.2. dM can now be evaluated:-

$$dM = \frac{N_i g^2 \mu_o^2 H}{kT^2} \left\{\frac{1}{4\sinh^2 \frac{\eta}{2}} - \frac{(j_i+\frac{1}{2})^2}{\sinh^2(j_i+\frac{1}{2})\eta}\right\} dT. \qquad (4.5.4)$$

The heat of magnetisation, đQ given out is simply equal to the magnetic work term HdM. Consider now the whole system, consisting of both salts, suffixed 1 and 2, and the liquid ^{4}He sample. The amount of heat given out for a temperature drop of dT is given by

$$đQ = N_1 k\eta^2 \left\{\frac{1}{4\sinh^2 \eta/2} - \frac{(j_1+\frac{1}{2})^2}{\sinh^2(j_1+\frac{1}{2})\eta}\right\} dT$$

$$+ N_2 k\eta^2 \left\{\frac{1}{4\sinh^2 \eta/2} - \frac{(j_2+\frac{1}{2})^2}{\sinh^2(j_2+\frac{1}{2})\eta}\right\} dT + C_{He}\, dT. \qquad (4.5.5)$$

where C_{He} is the heat capacity of the ^{4}He sample. Putting $j_1 = 3/2$, $j_2 = 5/2$ and writing đQ as $\dot{Q}(T,T_o)dt$, where $\dot{Q}(T,T_o)$ is the rate of heat conduction through the thermal link for the hot end at temperature

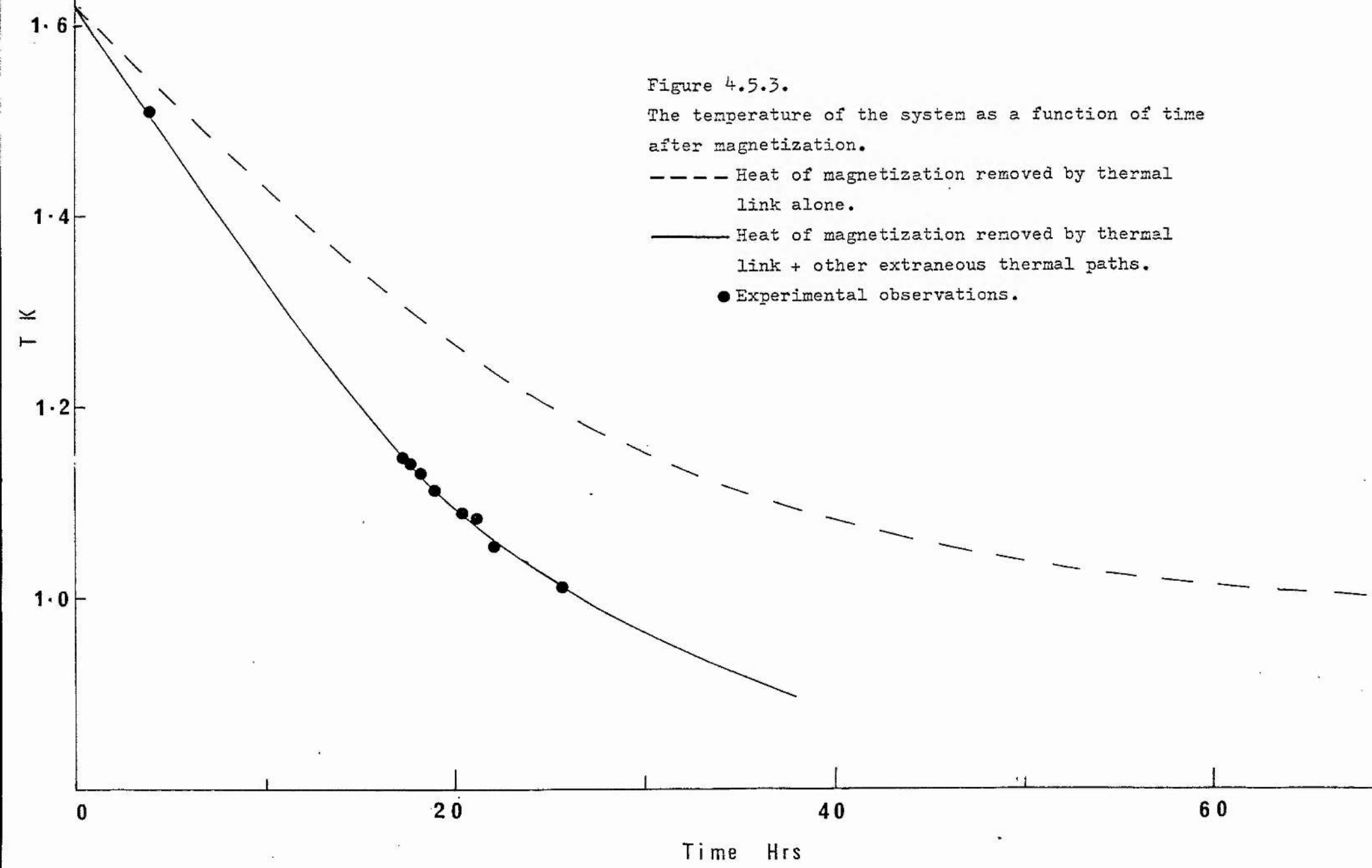

Figure 4.5.3.
The temperature of the system as a function of time after magnetization.
– – – – Heat of magnetization removed by thermal link alone.
——— Heat of magnetization removed by thermal link + other extraneous thermal paths.
● Experimental observations.

T and the cold end at a constant temperature T_o:

$$dt = \frac{1}{\dot{Q}(T,T_o)} \{C_{He} + k\eta^2 \left(\frac{N_1+N_2}{4\sinh^2\eta/2} - \frac{4N_1}{\sinh^2 2\eta} - \frac{9N_2}{\sinh^2 3\eta}\right)\} dT \qquad (4.5.6)$$

This equation was integrated numerically in steps of .01K, to give the temperature of the system as a function of time after magnetisation. The heat capacity of 5.11 moles of ^{4}He as a function of temperature was found from tables. (Van Dijk and Durieux 1958) and the rate of transport of heat through the thermal link was calculated from the data of Bertman and Kitchens (1968). The result is shown in figure 4.5.3. If $\dot{Q}(T,T_o)$ includes heat leaks through the epibond former, the electrical leads and the mechanical supports, then the solid line is obtained. Heat conduction through the superfluid-filled capillary alone would lead to behaviour as indicated by the dashed line. The experimental points are seen to agree well with the predicted behaviour.

In most of the experiments envisaged, a bottom temperature of ∿20mK immediately after demagnetisation would be quite adequate. It will be shown in the next section that this would correspond to an initial temperature of ∿1.14K, and from figure 4.5.3, the time needed to cool to this temperature after magnetisation is ∿18 hours. The operation of the cryostat is therefore quite convenient in the majority of cases; magnetisation can be carried out one day in preparation for a demagnetisation the next. In the small number of cases where a very low temperature of ∿10mK is required, a post-magnetisation cooling period of ∿36 hours is necessary.

(d) Calculation of the lowest temperature attainable on demagnetisation

During demagnetisation the guard salt and main salt are thermally

Figure 4.5.4.
The magnetic cooling cycle for the guard salt (0.33 mole ferric ammonium alum). Zero field data taken from Vilches and Wheatley (1966a).

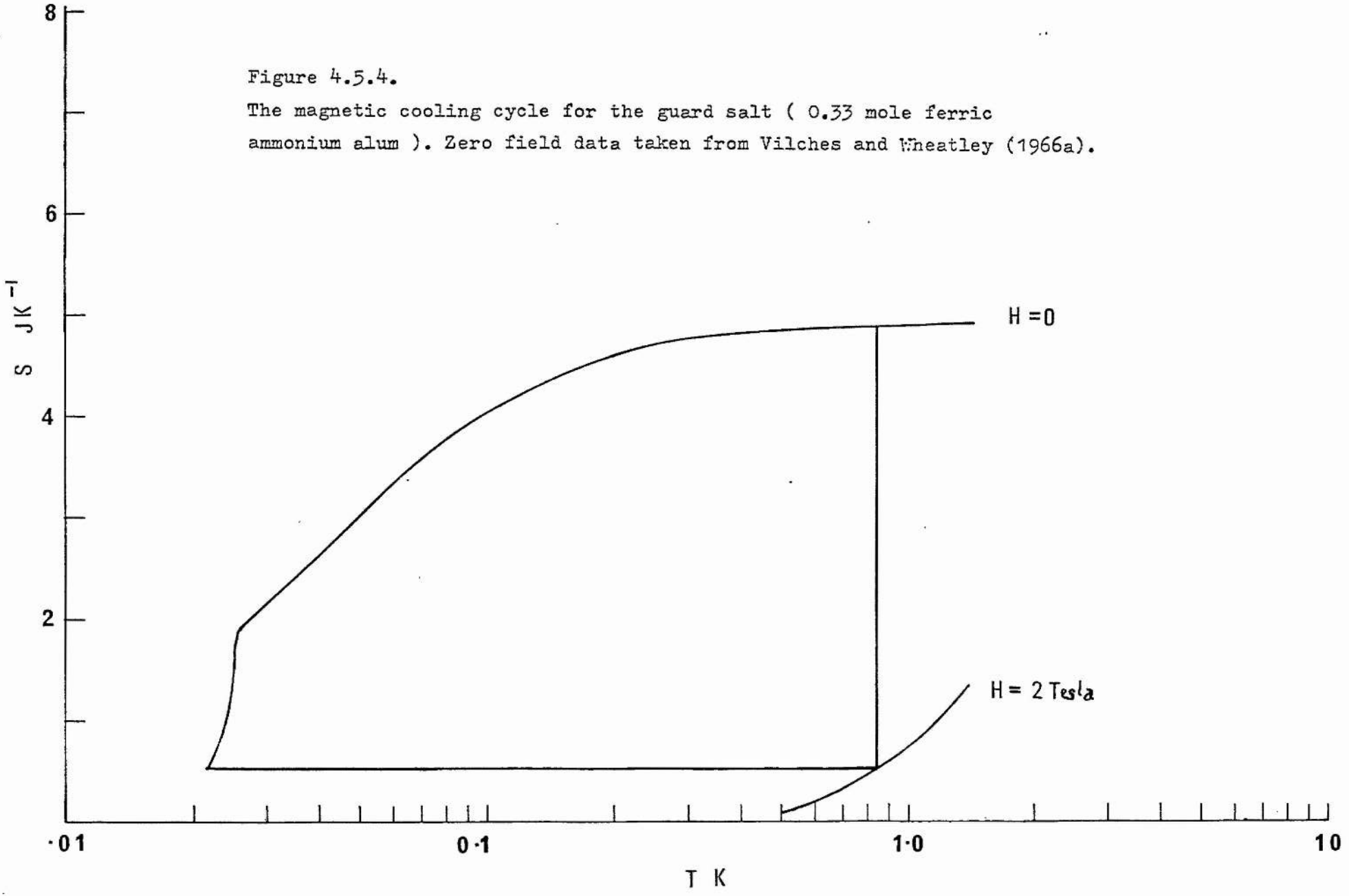

Figure 4.5.5.
The magnetic cooling cycle for the main salt (0.34 mole chrome potassium alum.) + liquid helium sample (5.11 moles). Zero field data taken from Vilches and Wheatley (1966a).

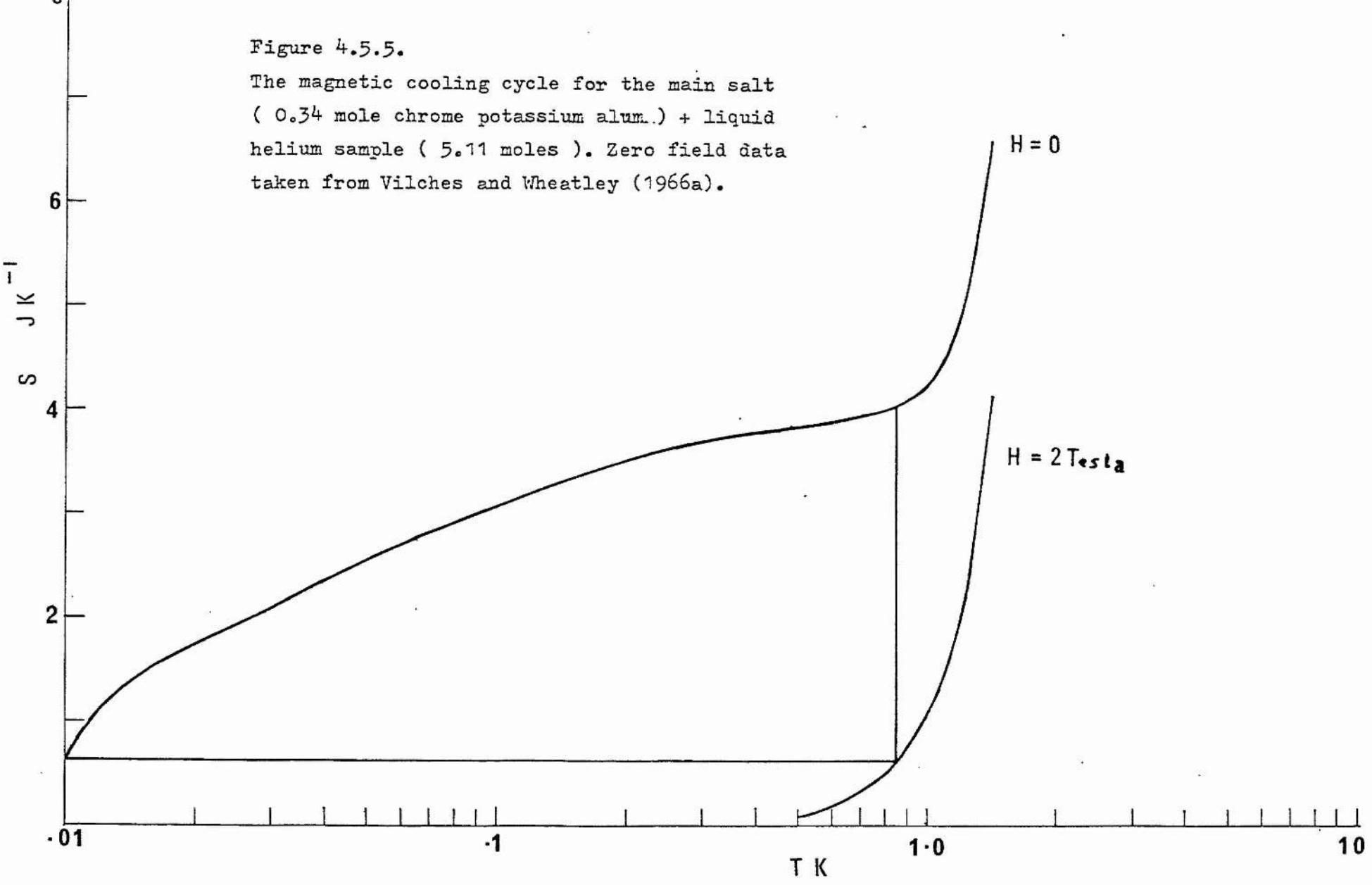

isolated from each other. (The heat leaks that do exist at temperatures of ∿1K, such as the refluxing of the superfluid film in the cell-filling capillary, disappear rapidly as the temperature falls below ∿0.5K.) There are thus two separate systems, the one comprising the main salt and the thermal load of ^{4}He, the other the guard salt alone.

In figures 4.5.4 and 4.5.5 the magnetic cooling cycles for these two systems are illustrated. It can be seen that, provided the demagnetisation is executed reversibly, given a starting temperature of 0.85K the helium sample should be cooled to 10mK whilst the guard salt should cool to 22mK.

(e) The cold performance of the cryostat

The heat leaks to the guard salt were calculated assuming a vortex fridge temperature of 0.85K and a guard salt temperature of 50mK. The contributions from the isolation spiral former, the stainless steel supporting tubes and the electrical leads were 69 ergs s^{-1}, 17 ergs s^{-1} and 1.5 ergs s^{-1} respectively. Radiation from the walls of the vacuum chamber at 4.2K contributed a further 2 ergs s^{-1}, giving a total of 89.5 ergs s^{-1}. From the data of Vilches and Wheatley (1966(b)) the change in the heat content of 159 gms of ferric ammonium alum between 50 mK and 0.5K is 2.3×10^6 ergs. Assuming that the heat leak remains constant at 89.5 ergs s^{-1}, the time taken for the guard salt to warm through this interval is 7.2 hours. The heat leak will in fact diminish as the guard salt warms, so the above estimate will be pessimistic.

One of the major heat leaks into the experimental cell arises from the mobile superfluid film which covers the entire inside surface

of the filling capillary. The film will flow up from the colder to the warmer regions of the cryostat under the influence of the chemical potential gradient caused by the temperature difference. This process will be accompanied by a counterflow of warm vapour down the capillary, constituting a heat leak into the colder regions. Below 0.5K the heat leak from the guard to the main salt by this thermal path is in fact negligible, since the vapour pressure of ^{4}He at these temperatures becomes extremely small. For this reason, the useful experimental time corresponded to the period during which the guard salt remained below 0.5K, which, from the estimate given above, should be at least 7 hours.

In addition to the refluxing of the superfluid film, other heat leaks into the experimental cell will occur. The most serious of these is a contribution of 8 ergs s^{-1} from the absorption of 4.2K radiation over the considerable surface area of the cell. This problem could be obviated by the inclusion of preferably two radiation shields, one operating from the vortex refrigerator and the other from the guard salt. Provision was in fact made for two such shields in the present design, but it will be seen that the performance of the cryostat is still satisfactory in their absence. Other thermal paths to the cell exist through the mechanical supports, the walls of the filling capillary and the bellows actuating mechanism. Their contributions to the total heat leak were assessed as 0.15 ergs minute^{-1}, 0.08 ergs minute^{-1}, and 3 ergs minute^{-1} respectively. (Construction details relevant to these calculations will be given in chapter 5.) In the absence of radiation shields the total heat leak is dominated by 4.2K radiation. Using the data of Vilches and Wheatley (1966(b)) the

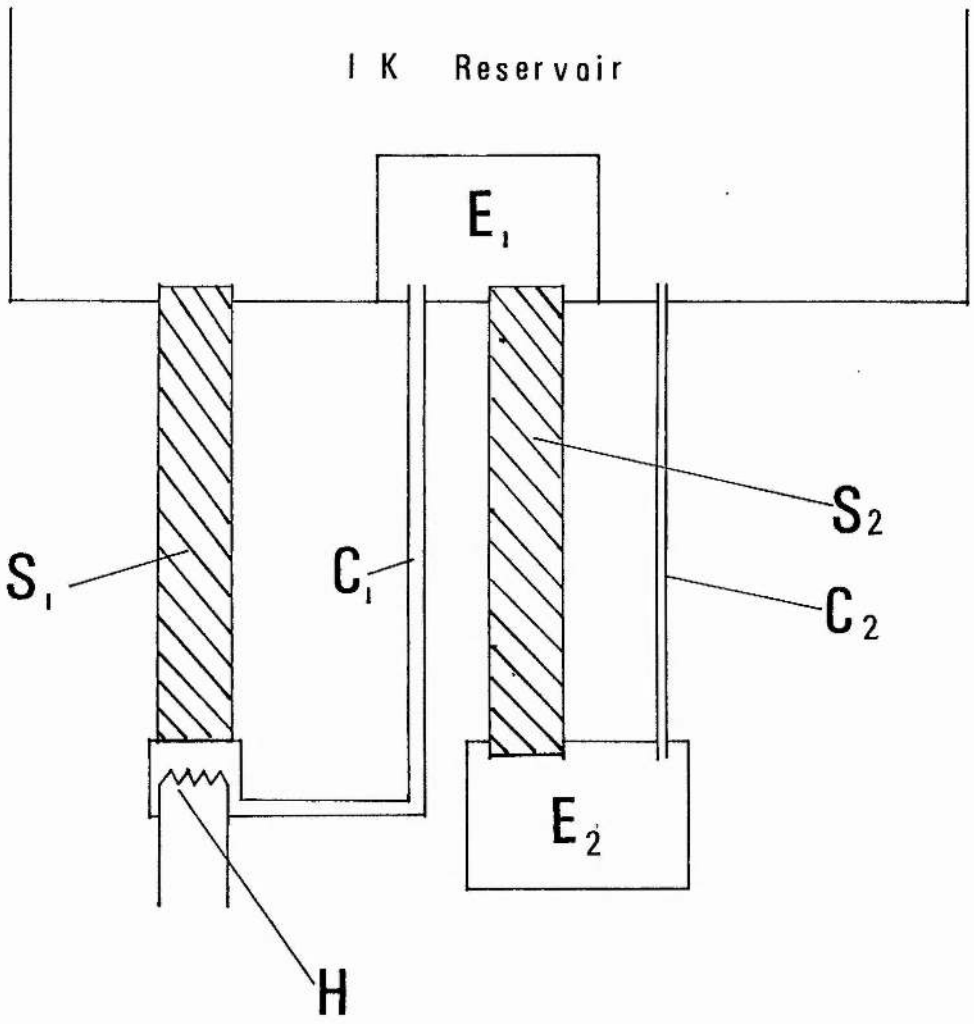

Figure 4.6.1.

A schematic diagram of the vortex refrigerator.

S_1 ; Fountain pump superleak.

S_2 ; " Fridge " superleak.

C_1 ; Fountain pump capillary.

C_2 ; " Fridge"capillary.

E_1 ; 1K heat exchanger.

E_2 ; " Fridge " heat exchanger.

H ; Wire-wound heater.

warming rate of the main coolant under these conditions was estimated as 3.3 mK $hour^{-1}$ over the temperature range 10 mK to 100 mK, which was considered adequate for the purposes of the experiments. The inclusion of radiation shields would reduce this rate to 0.02 mK $hour^{-1}$.

4.6 THE VORTEX REFRIGERATOR

The essential details of this cooling stage are shown schematically in figure 4.6.1. S_1 and S_2 are two "superleaks", formed by compressing a fine powder, such as jewellers rouge (Fe_2O_3) into a metal tube. Only the superfluid fraction of ^4He is able to flow through such a material; the interstices are sufficiently small to immobilise the normal fluid. The combination of superleak S_1 and capillary C_1 functions as a "fountain pump" when heat is applied via the heater H. The pressure and temperature gradients established by H cause a steady flow of superfluid to enter the "pump chamber" via S_1, whilst a combined flow of normal and superfluid passes from the pump chamber through C_1 to the heat exchanger E_1. The extra heat imparted to the fluid by H is removed at this point. The fluid then passes through the second superleak S_2 to the "fridge chamber" E_2, from which it is returned to the 1K reservoir via the capillary C_2. By a suitable choice of the diameters of C_2 and C_1 and the size of the heat input to H, the superfluid velocity in C_2 can be made high enough for intrinsic dissipation to take place. This can bring about the transport of normal fluid excitations from the chamber E_2 to the 1K reservoir by two possible mechanisms. The initial onset of dissipation in C_2 will cause a pressure difference to develop across the capillary, under the influence of which the normal fluid will flow to the 1K reservoir. Mutual friction coupling between superfluid vortices and normal fluid

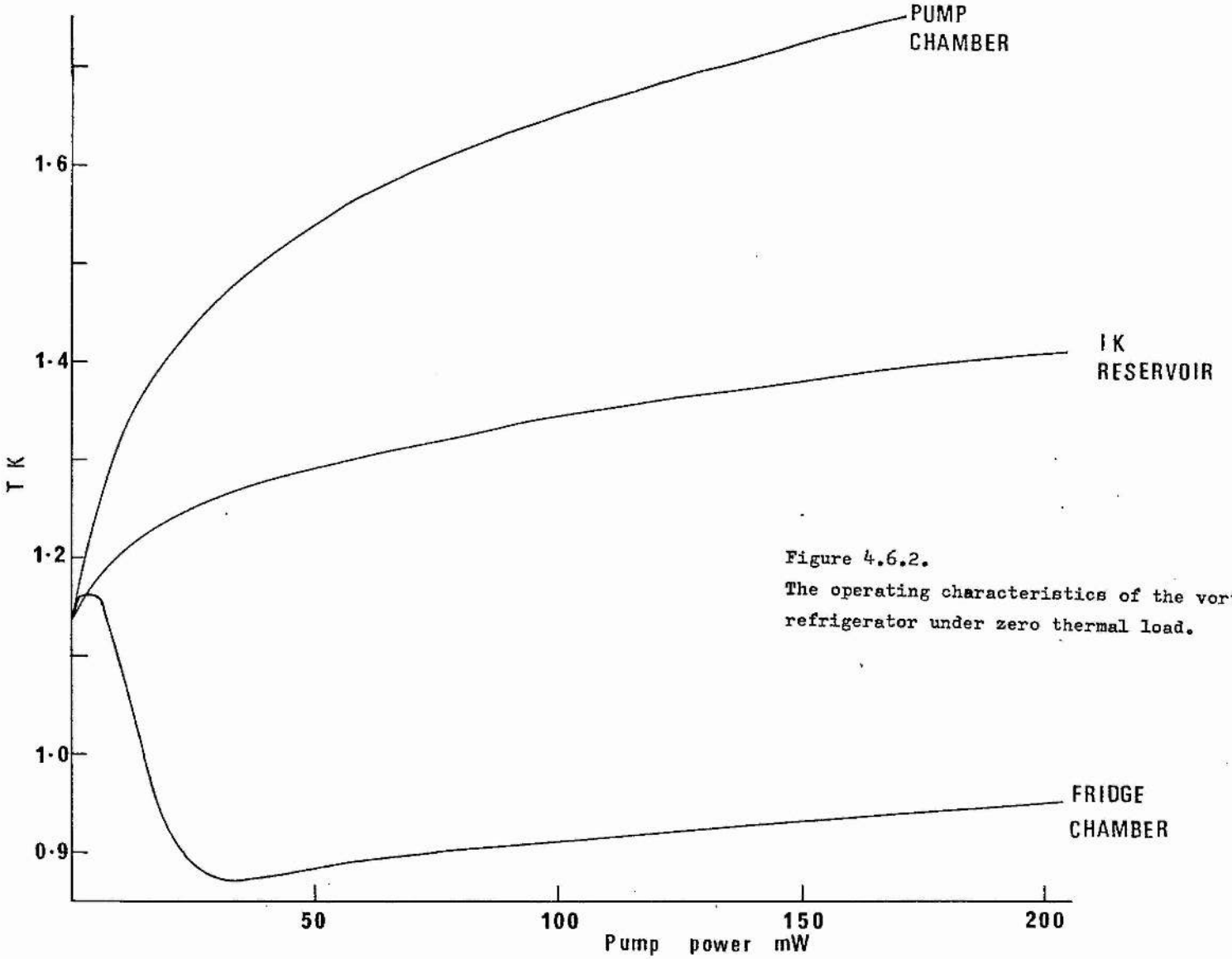

Figure 4.6.2.
The operating characteristics of the vortex refrigerator under zero thermal load.

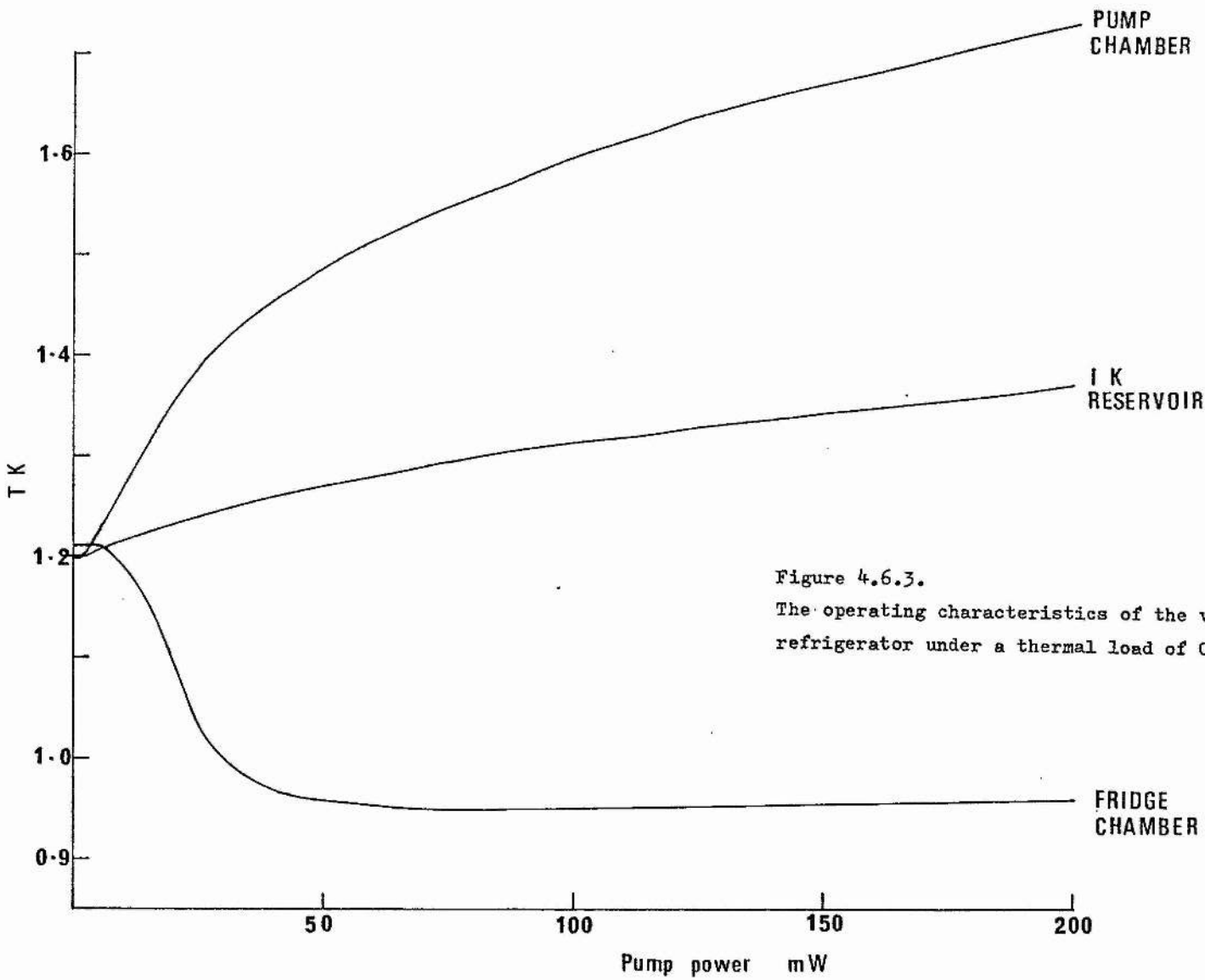

Figure 4.6.3.
The operating characteristics of the vortex refrigerator under a thermal load of 0.25mW.

excitations could also take place, with the same end result. Cooling of chamber E_2 is bound to follow since the liquid entering through S_2 is almost pure superfluid. As cooling progresses, the initial pressure difference across C_2 will decay; the chemical potential difference needed to support the dissipative processes in C_2 will now be provided mainly by the temperature difference existing between the ends of the capillary. However, no superfluid dissipation should occur in the narrow channels of superleak S_2 and hence, as the temperature of E_2 falls a pressure gradient must develop across the superleak to maintain the net chemical potential gradient at zero.

At first sight it might appear that a temperature arbitrarily close to absolute zero might be obtained by this means. Unfortunately this is not the case, as was demonstrated by the experiments of Olijhoek et al (1967), Staas and Severijns (1969) and Olijhoek et al (1973 a and b). The lowest temperature attainable in the chamber E_2 is found to be in the region of 0.75K, which coincides with the temperature below which the roton density becomes very small. The mutual friction process is known to involve primarily the scattering of rotons by vortex rings; it therefore seems highly probable that at temperatures of 0.75K and below, the scattering cross-section for phonons is insufficiently large to maintain the flow of normal fluid away from chamber E_2 against the temperature gradient. It is also possible that the heat input from the dissipative processes occurring in capillary C_2 plays some role in preventing cooling below 0.75K, although the situation here is not entirely clear. (Olijhoek et al (1973 a and b)).

The cooling characteristics of the vortex refrigerator incorporated into the present cryostat are given in figures 4.6.2 and 4.6.3.

Figure 4.6.2 shows the temperatures of the "fridge chamber" E_2, the "pump" chamber and the 1K reservoir as functions of the power applied to heater H, whilst figure 4.6.3 shows the behaviour of the same quantities in the presence of a thermal load of 0.25 mW applied to chamber E_2. The rather high bottom temperature of 0.87K was thought to result from a "mismatch" between the diameters of capillaries C_1 and C_2, leading to low superfluid velocities in C_2. This temperature was, however, found to be adequate for the purposes of the experiments, and no modifications to the capillary sizes were carried out. The construction details of the vortex refrigerator will be given in chapter 5.

5.1.1. A general view of the laboratory.

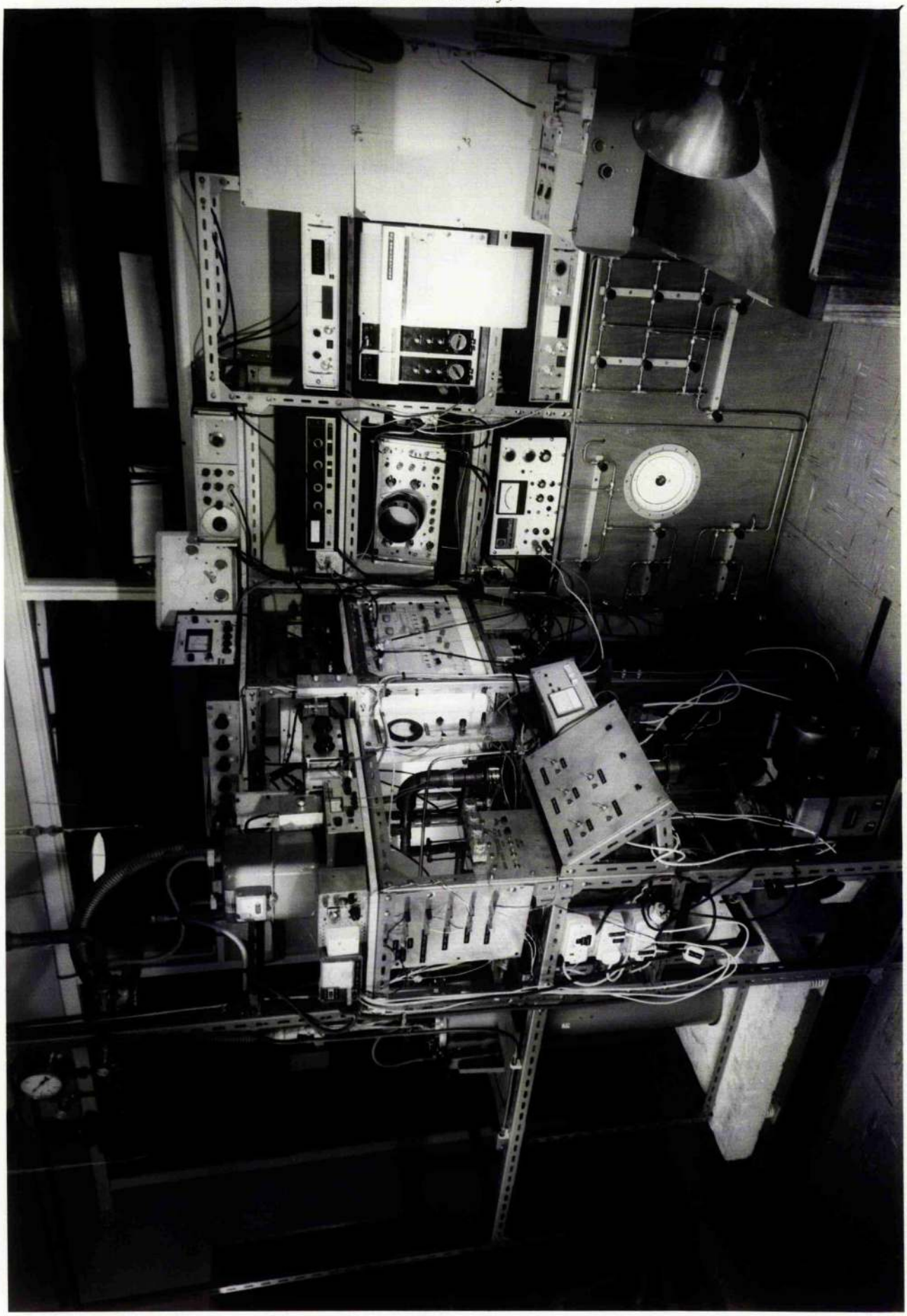

CHAPTER FIVE

CONSTRUCTIONAL DETAILS OF THE APPARATUS

5.1 THE DEWAR ASSEMBLY

The cryostat was housed in a metal dewar of conventional design, supplied by Oxford Instruments Ltd. Careful precautions were taken to isolate the dewar from external sources of vibration; at very low temperatures vibration can have a serious heating effect, and can also disturb the liquid levels. The dewar was mounted on a sprung concrete block weighing approximately ½ton and having a natural frequency of ∿2Hz. No rigid connections were made to this system. The main ^{4}He pump acting on the 1K pot was sited remotely. The residual vibration on the liquid level in the experimental cell was less than 0.2μm in amplitude.

Plate 5.1.1. shows a general view of the laboratory, with the dewar assembly on the left of the picture, partly hidden by the rack of instruments.

5.2 THE MAIN BATH AND INNER VACUUM CHAMBER

The four cooling stages shown schematically in figure 4.5.1. were contained in a stainless steel vacuum jacket which was suspended in the main helium space of the dewar from a top flange. This main bath, containing helium at 4.2K, was of 16 ℓ capacity and was replenished every 14 hours in order to keep the inner vacuum chamber continuously submerged. Liquid helium level detectors provided an automatic alarm if the bath level fell below the top of the inner vacuum chamber.

The top flange of the cryostat, made from 5mm thick stainless steel, carried, amongst other things, pumping lines to the inner vacuum chamber and to the 1K pot. These pumping lines were fitted with radiation traps situated in the main helium bath. The top flange also carried feed-throughs for 21 unscreened electrical leads and 8 miniature coaxial leads. The unscreened leads passed directly through the main bath before entering the inner vacuum chamber, ensuring good thermal anchoring at 4.2K. The 8 screened cables were treated differently owing to the difficulty of making a fully screened, low temperature feed-through at the flange of the inner vacuum chamber. A thin-walled stainless steel tube carried the leads to the top plate, this tube forming an extension of the inner vacuum space. On the top plate a room temperature screened feed-through was constructed using standard B.N.C. coaxial sockets made leak-tight with Stycast 2850 epoxy resin. The screens of the coaxial leads were isolated from the cryostat ground and from each other, to prevent unwanted earth loops in the measuring systems. Because this design did not allow direct thermal anchoring of the leads to 4.2K in the main bath, they were anchored to the underside of the vacuum chamber flange, using a method to be described in section 5.4.

The body of the inner vacuum chamber was made from two sections of seam-welded stainless steel pipe, the diameter of the bottom section being smaller than that of the top in order to provide a "tail" around which the superconducting solenoid could be positioned. The seal between this vacuum can and the flange forming the top of the chamber was of the demountable indium 'O' ring type. The flange was made from stainless steel sheet; a thickness of 1 cm was necessary to

prevent distortion occurring at low temperatures.

All ports in the vacuum chamber flange were fitted with stand-off collars, which were welded in. When all welding operations had been completed, the flange was faced off to remove the effects of any warping that may have occurred. The stand-off collars allowed pipes and lead-throughs to be soft soldered in position one by one, without having to heat the entire flange each time. Great care was taken at all stages of construction of the cryostat to prevent corrosive soldering flux being left on the surfaces of thin-walled pipes. The flux would have quickly corroded the pipe walls, such that after a number of months the cryostat would have been riddled with pin holes.

5.3 THE MAGNET ASSEMBLY

A superconducting magnet consisting of two solenoids screwed together at a central flange was made to order by Thor Cryogenics Ltd. The magnet was wound from fully stabilised niobium-titanium superconductor embedded in a copper matrix, and produced a field of at least 20,000 Gauss over the entire volume of both paramagnetic salts, for an operating current of 55A. Both solenoids were fitted with persistent mode switches. The unit was powered from a B.O.C. Cryoproducts 60A supply. The magnet assembly was positioned around the lower half of the inner vacuum chamber in the main bath of helium, and was secured by three bolts to a flange projecting from the vacuum chamber. In this way, the cryostat and magnet could be removed as a single unit from the dewar.

The dimensions of the magnet leads were optimised according to the calculations of McFee (1958). During energisation of the solenoids

5.3.1. The cryostat with the superconducting solenoid in position.

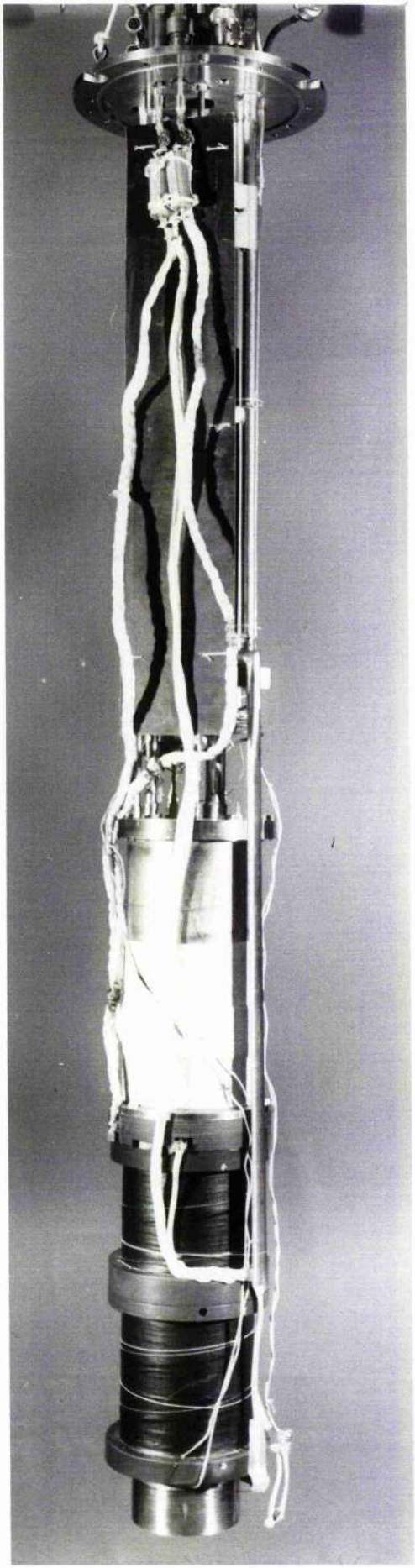

the heat leak into the helium bath from this source has two components; thermal conduction and Joule heating. These two contributions have opposite dependences on the diameter d of the lead, and consequently, for a given current and length of lead, an optimum value of d exists. This was found to be 2.9mm for a lead 60 cm long, carrying 55A.

In order to economise further on the use of liquid helium, a technique first introduced by Lavrova et al (1973) was used. Flexible leads were made by plaiting together the screens from several coaxial cables, taking care to maintain the total cross-sectional area at the optimum value given above. The tops of the leads were soldered to brass rods which projected through nylon bushes set into the top flange of the cryostat. Contact was made to each rod with a small copper clamp which was in turn connected to the power supply. When the magnet was not in use, or in the persistent mode, the clamps were removed and lengths of thin-walled stainless steel tubing were screwed into the tops of the brass rods. The tubes and rods were of the same diameter. The copper leads could then be slowly lowered into the bath on the ends of the thin-walled stainless steel tubes, bringing about a substantial reduction in the heat leak. When energisation of the solenoid was required, the leads could be recovered from the bath by a reversal of this procedure.

In the event of a malfunction causing the magnet to turn normal, the system was suitably protected. A voltage sensor in the power supply detected the increased resistance of the solenoids and automatically reduced the energising current to zero. Two 1Ω, 50W safety resistors connected across the current leads and situated in the

Figure 5.4.1

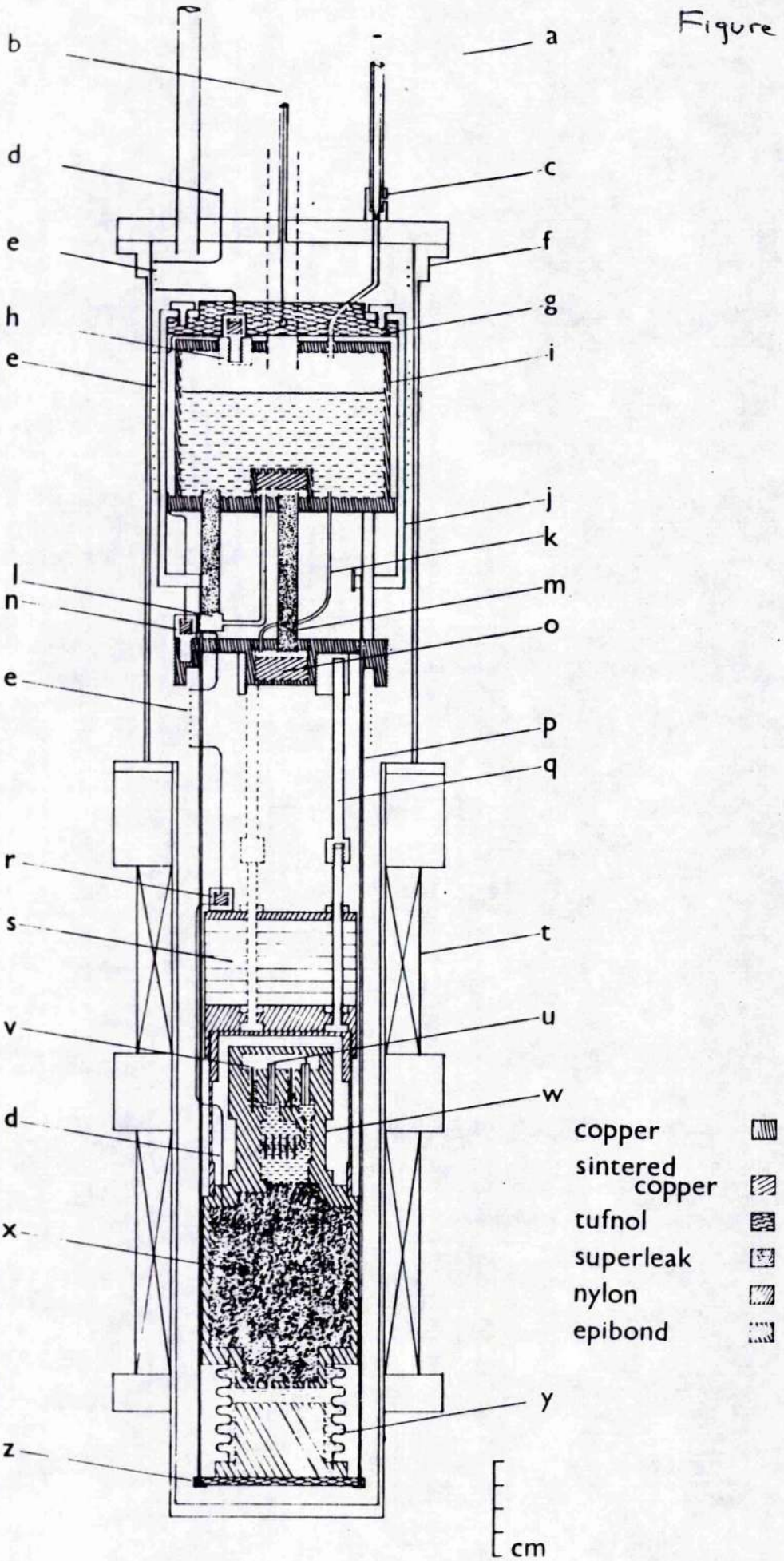
a
b
c
d
e
f
g
h
i
j
k
l
m
n
o
p
q
r
s
t
u
v
w
x
y
z
copper
sintered copper
tufnol
superleak
nylon
epibond
cm

Figure 5.4.1.

A scale drawing of the low temperature region of the cryostat, showing the four main cooling stages.

Caption

a. Main helium bath

b. Stainless steel wire, movement of which lowers or raises bellows on cell.

c. Needle valve for filling 1K pot.

d. Capillary through which liquid sample is condensed into cell.

e. Isolation spiral

f. Inner vacuum chamber

g. Tufnol lifting arm

h. Thermal sink at 1K for cell filling capillary

i. 1K pot

j. Steel stirrups

k. Vortex fridge capillary

l. Fountain pump

m. Vortex fridge superleak

n. Thermal sink at 0.8K for cell filling capillary

o. Vortex fridge heat exchanger

p. Braided dacron strings by which bellows on cell are raised or lowered

q. Thin-walled stainless steel supports

r. Thermal sink at 50mK for cell filling capillary

s. Guard salt (ferric ammonium alum)

t. Superconducting solenoid

u. Liquid level sensors

v. Stainless steel beaker

w. Experimental cell

x. Main salt (potassium chrome alum)

y. Stainless steel bellows

z. Tufnol cradle

cold gas at the top of the cryostat then allowed the magnetic field to decay smoothly, without the induction of dangerously high voltages.

Plate 5.3.1. shows the cryostat, removed from the dewar, with the magnet assembly in position and the flexible leads pulled up in the "energising" configuration.

5.4 THE 1K POT

Those components of the cryostat contained within the inner vacuum chamber can be loosely classified as "the low temperature parts". Plate 5.4.1. shows the cryostat with the vacuum can removed, and a close-up of the low temperature parts is given in Plate 5.4.2. Figure 5.4.1. is a scale drawing of this region.

The first of the low temperature cooling stages was the ^{4}He evaporator, henceforth referred to as the 1K pot. This was a copper chamber of 269ccs capacity situated immediately below the flange of the inner vacuum chamber and thermally isolated from it by short lengths of thin-walled stainless steel tubing. The main body of the pot was turned from a solid piece of copper to reduce the number of solder joints. The pot was filled through a capillary from a needle valve situated on the vacuum chamber flange. The needle valve, consisting of a commercial stainless steel needle mating into a brass seat, was operated from the cryostat top plate. Cooling of the pot was produced by pumping on the helium via a 1" pumping line, and under typical operating conditions a temperature of 1.15K was achieved. The residual heat leak into the pot was $\sim$6mW, giving a lifetime of $\sim$48hours between refilling operations.

The 1K pot had several functions; to provide a thermal anchor at 1K for the electrical leads and the cell filling capillary and to

5.4.1. The cryostat with the vacuum can removed.

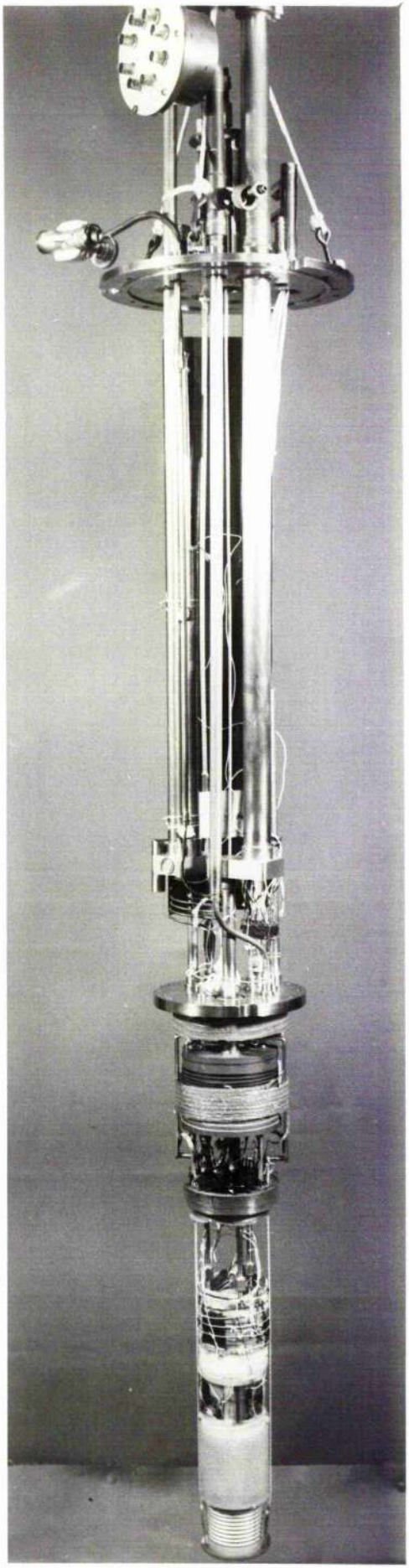

provide a source of ^{4}He at ∿1K for the operation of the vortex refrigerator.

Thermal anchoring of electrical leads was achieved by making a section of each lead out of thin copper strip. These strips were then tightly bound to the wall of the pot with thread and G.E. varnish, electrical insulation being provided by a single layer of greased cigarette paper. Thermal impedances, in the form of short-sections of Pb-coated manganin wire, .002" in diameter, were inserted on either side of each strip. This reduced the total heat leak and also ensured that the comparative resistance to "ground" of the thermal anchor was very small.

A similar system was used to thermally ground the coaxial leads at 4.2K. The copper strips were, in this instance, glued to a thin copper sheet, covered by a single layer of cigarette paper. The copper sheet was soldered onto a copper tube with Woods metal, and the tube was itself soldered into a socket on the underside of the vacuum chamber flange. By bending the sheet in a corrugated fashion, the centre conductors of the coaxial cables were afforded a certain degree of shielding.

The cell filling capillary was thermally anchored at the 1K pot by means of a small heat exchanger which screwed into a threaded plug let into the top of the pot. (See figure 5.4.1.). The heat exchanger consisted of a copper chamber, of volume ∿0.2 cm^3, connected in line with the filling capillary. A small sintered copper plug made a tight push-fit into the chamber. A Speer 220Ω carbon resistance thermometer was mounted on the lid of the chamber.

5.4.2. The low temperature region of the cryostat.

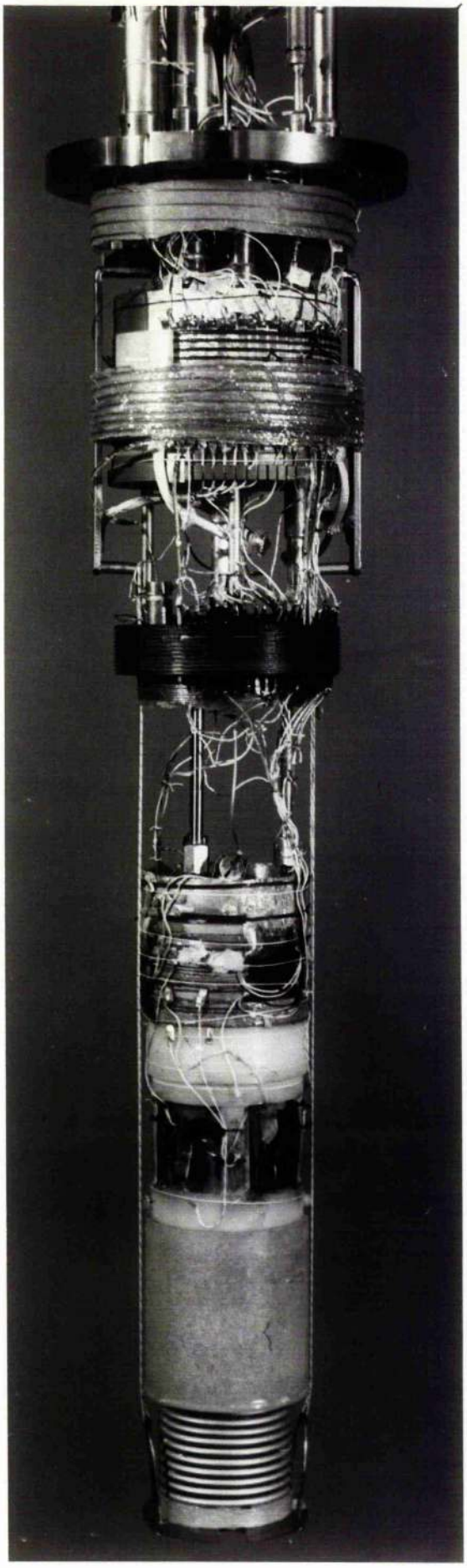

A second sintered copper heat exchanger was let into the base of the 1K pot, as shown in figure 5.4.1. This chamber was separate from the main volume of the pot and served to cool the helium in the vortex fridge circuit.

Plate 5.4.3. shows a close up of the 1K pot and vortex refrigerator.

5.5 THE VORTEX REFRIGERATOR

The technique of cooling by convective heat transport, as discussed in section 4.6, was used to cool a copper block suspended beneath the 1K pot by three thin walled stainless steel tubes. The working components were situated between this copper piece and the 1K pot and consisted of two superleaks, a wire-wound heater and two capillaries. The superleaks were made by packing jewellers rouge into 5/16" diameter thin-walled stainless steel tubes, a little at a time. The tubes were mounted in a special jig and the rouge was hammered down quite hard with a piston. Pads of felt were placed at each end to prevent any loose rouge being carried into the capillaries. The fountain pump superleak was $5\frac{1}{2}$ cm long and one end was let directly into the base of the 1K pot. The other end terminated in a small brass chamber, which contained a manganin heating coil, of resistance 80Ω. The heater leads left the chamber through a small port which was sealed with Stycast 2850 epoxy resin. The length of manganin lead in the vacuum space outside the chamber was kept to an absolute minimum; manganin is such a poor thermal conductor that the heat generated by the passage of a current can not be easily conducted away. Copper leads were used to connect the heater to the 1K thermal anchor. The mixture of superfluid and normal fluid set in motion by the fountain pump was carried to the 1K sintered copper heat exchanger by a german silver capillary,

5.4.3. A close-up of the 1K pot and vortex refrigerator, showing the thermal anchors for the electrical leads.

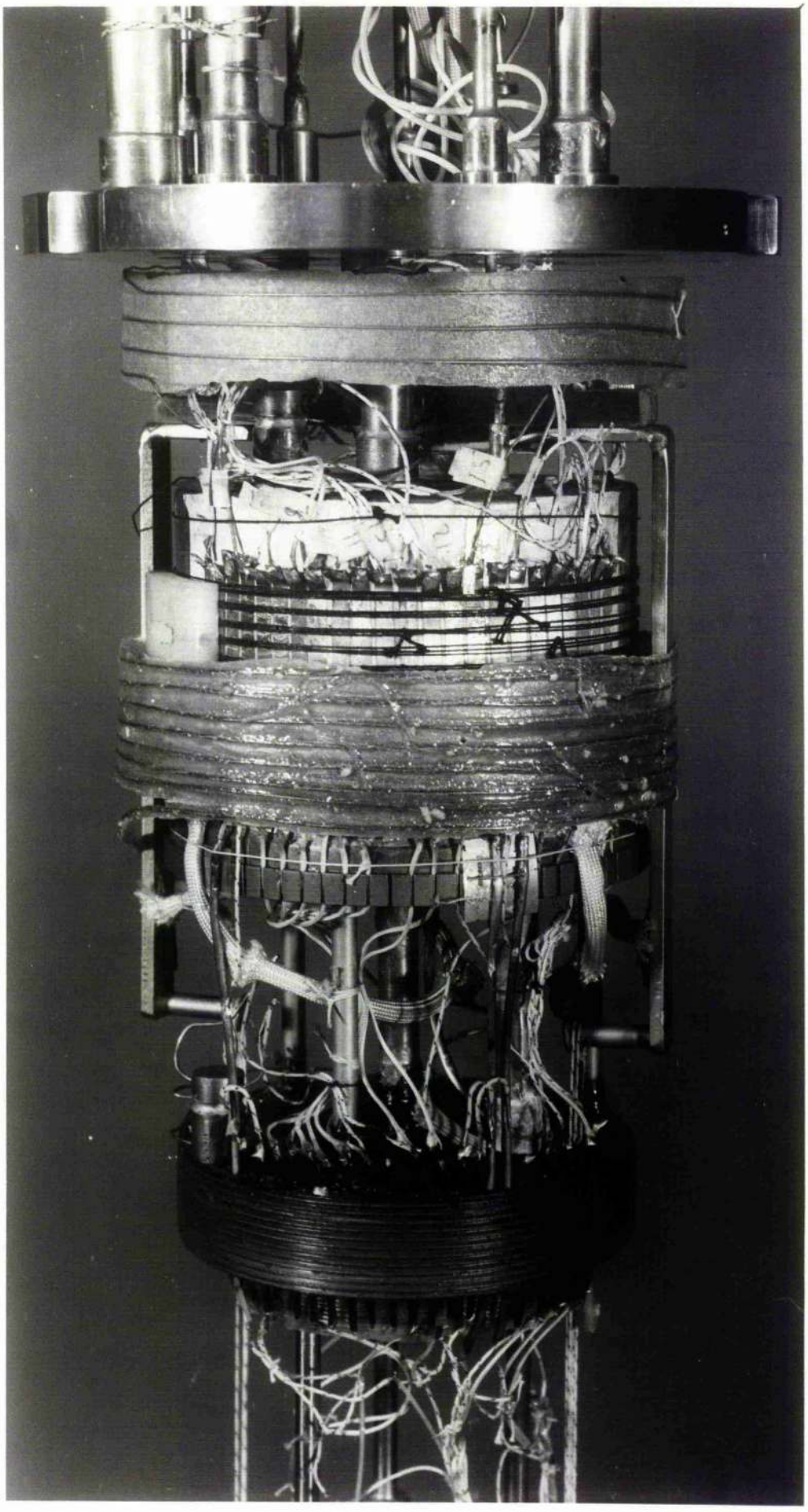

5.5.1. A close-up of the 1K pot and vortex refrigerator, showing the arrangement of superleaks and capillaries.

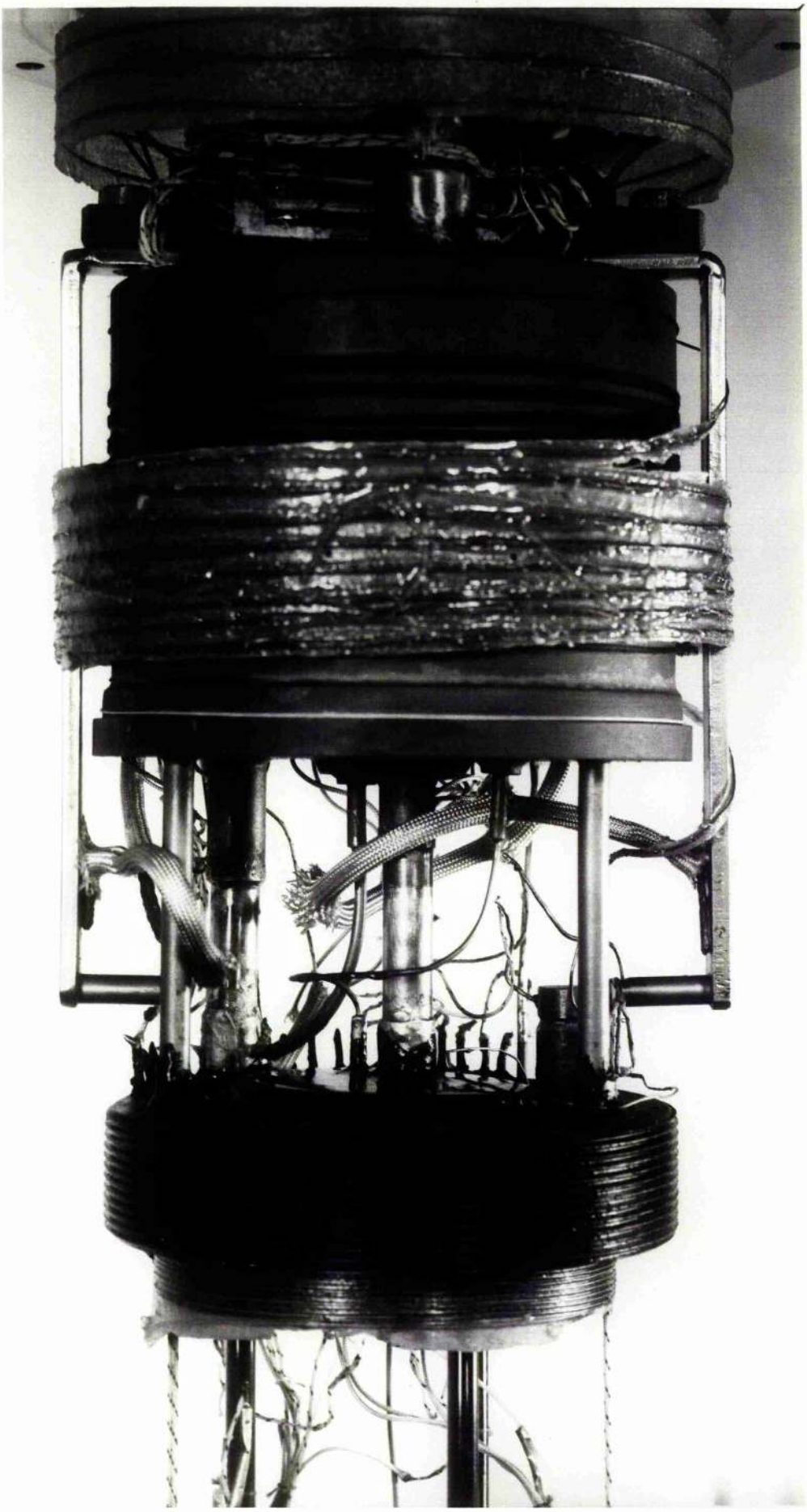

2mm in diameter. The main superleak was positioned directly between this heat exchanger and an identical heat exchanger set in the centre of the copper block, as shown in figure 5.4.1. This superleak was 7 cm in length and it was essential that it entered the 1K heat exchanger directly, and that no lengths of capillary tubing were interposed at this point. The fluid was returned from the fridge heat exchanger to the 1K pot via a 1mm diameter german silver capillary.

All electrical leads travelling to colder parts of the cryostat were thermally anchored to the copper block. A different design of thermal anchor from that used at 1K was employed here, as the outside of the block was threaded to take a radiation shield. Lengths of heavy gauge copper wire were cemented into close fitting holes in the block with a very thin layer of Stycast 2850. This served both as electrical insulator and thermal contact agent. The holes were drilled through the thickest part of the block to provide a 2 cm length over which thermal contact could be made. The cell filling capillary was also thermally anchored to the copper block, with a heat exchanger identical to that used on the 1K pot. Plate 5.5.1. is a photograph of the 1K pot and vortex fridge from behind, showing the arrangement of superleaks and capillaries. The thermal anchors on the vortex fridge are more clearly seen in plate 5.4.3.

5.6 THE GUARD SALT

The underside of the vortex fridge heat exchanger formed a threaded boss from which the guard salt was suspended. Three thin-walled stainless steel tubes made tight push-fits into a stainless steel piece which mated onto the boss. The tubes had a wall thickness

of .006" and a free length of 6.5 cm, and terminated in long brass nuts. These mated onto the threaded rods of the guard salt assembly proper. This arrangement was very convenient for bringing the tail of the cryostat into correct alignment. In a prototype version, graphite rods were used in place of the stainless steel tubes, since these provided better thermal isolation. Unfortunately, they proved too weak to withstand the sideways forces that could occur if the salts were not positioned centrally in the magnetic fields.

The guard salt itself consisted of a number of salt "pills" stacked to form a squat cylinder. The pills were made by crushing ferric alum crystals to an even consistency with a pestle and mortar, rehydrating them by covering the mortar with a damp cloth, and then mixing a shellac varnish, such that the ratio of salt to shellac was 14:1 by weight. The mixture obtained had the consistency of soft brown sugar. This mixture was left to stand for $\sim$1 hour such that the shellac became fairly tacky. It was then compressed in a mould using a 5 ton hydraulic press. On removal from the mould, the pill was coated with a thin layer of shellac. A second coat was applied after 12 hours. This protective coating prevented dehydration of the salt at room temperature. (The loss of water of crystallisation would have caused stronger interactions between the paramagnetic ions, leading to co-operative spin ordering setting in at higher temperatures. The salt would therefore have lost its usefulness as an ultra-low temperature refrigerant.) The salt pills obtained were 6.4 cm in diameter and 0.5 cm high, and contained ferric alum at an effective density of 1.44 gms cm^{-3}, that is 84% of the crystalline density. Seven pills were used to produce a guard salt containing 159 gms of ferric alum.

Thermal contact to the salt was achieved by interposing discs and strips of "coil-foil" between the pills. "Coil-foil" is a very useful thermal contact material which does not exhibit eddy current heating when placed in a varying magnetic field. It consists of many fine insulated copper wires glued to a mylar backing strip with G.E. varnish. This backing strip is removed when the coil-foil is required for use, the G.E. varnish being sufficiently strong to hold the wires together in a continuous sheet. A disc of coil-foil smeared with Apiezon N grease was placed on the top of each individual salt pill. A long strip of coil foil was similarly greased and laid over each disc, such that the copper wires in the disc and strip were mutually perpendicular. In this way thermal, but not electrical, contact was made between each wire in the disc and each wire in the strip. A single sheet of greased cigarette paper was placed over each strip and several flat copper strips were laid on top. The salt pills were then stacked up and placed between two nylon pieces. Three stainless steel bolts were passed through holes that had previously been drilled through each component of the salt pill assembly, and the whole unit was compressed. The holes in the nylon pieces were made slightly oversize to allow for thermal contraction. The coil-foil strips projecting from between the salt pills were brought up to the top of the pill assembly where they were soldered to a copper strip running three quarters of the way round the circumference. Non-superconducting solder was used for these joints. The cell filling capillary made thermal contact to this copper strip via a sintered copper heat exchanger of similar design to those used at 1K. This heat exchanger was soldered to the strip with Woods metal. By this rather complicated

5.6.1. A close-up of the guard salt.

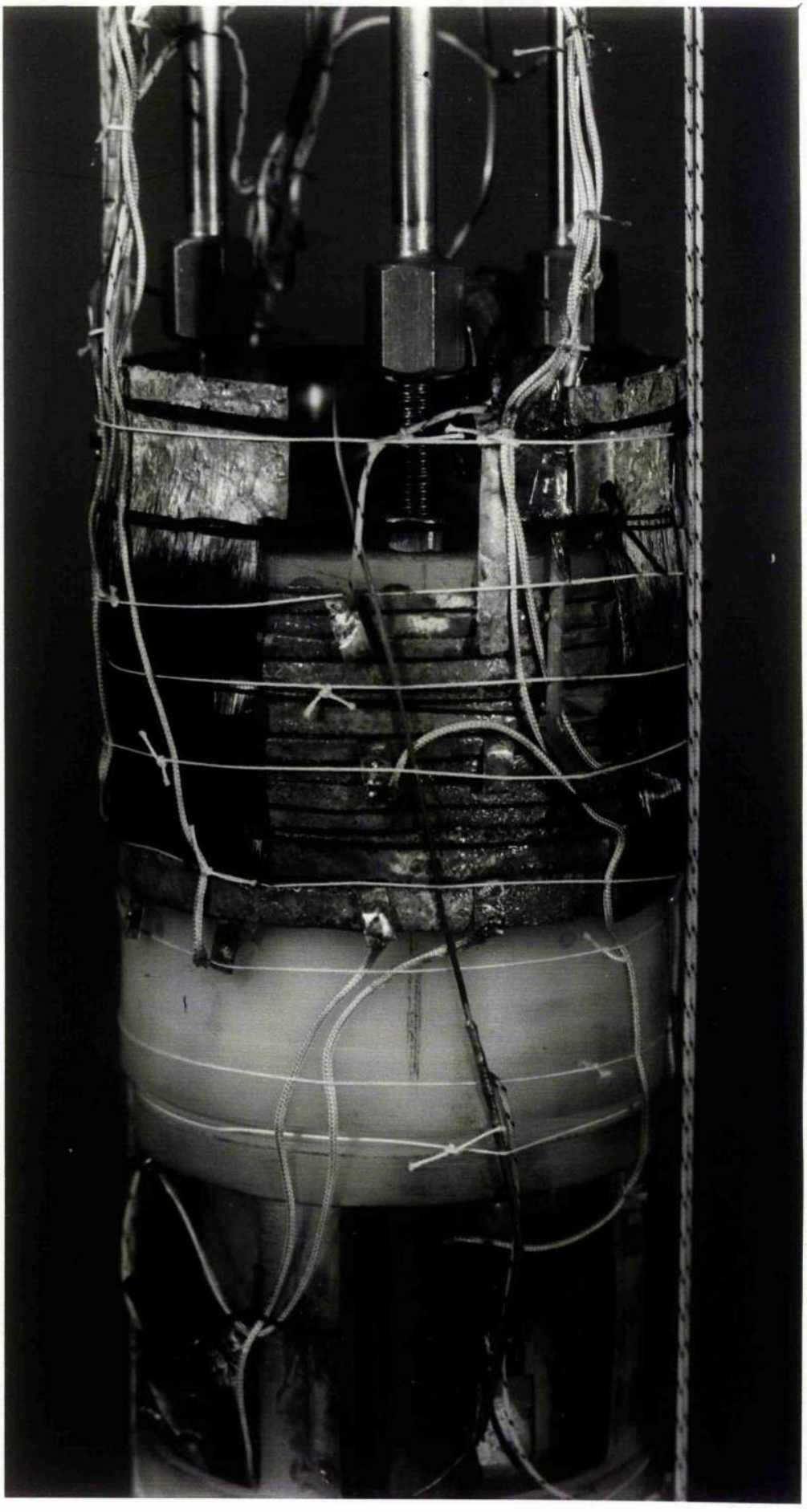

route, thermal contact was established between the helium in the cell-filling capillary and the pills of ferric alum.

The flat strips of copper running between each pair of pills formed the thermal anchors for the electrical leads. The thermal impedances above and below this thermal anchor consisted of 10 cm lengths of .002" diameter Pb-coated manganin wire.

Three screened leads were taken through the guard salt to the experimental cell. Commercial miniature coaxial cable could not be used here, as the conductors would have had too low a thermal impedance. Instead, coaxial leads were made from lengths of 1mm diameter german silver capillary, through which was threaded a teflon sleeve carrying a .002" diameter Pb-coated manganin wire. The capillary, forming the screen of the cable, was soldered directly to the end of one of a pair of copper strips running between two salt pills. The centre conductor was soldered to the other copper strip. By virtue of the earthed coil-foil strips running between each pair of salt pills, the centre conductors were shielded to a certain extent within the guard salt.

Plate 5.6.1. shows a close-up photograph of the guard salt, in which prominent features are the ends of the copper strips protruding from between the salt pills, and the coil-foil strips running up to the split ring of copper at the top of the salt.

5.7 THE EXPERIMENTAL CELL

(a) The Cell Supports

The nylon piece forming the base of the guard salt had on the underside a threaded section into which a nylon supporting structure for the experimental cell was screwed. The details of the arrangement

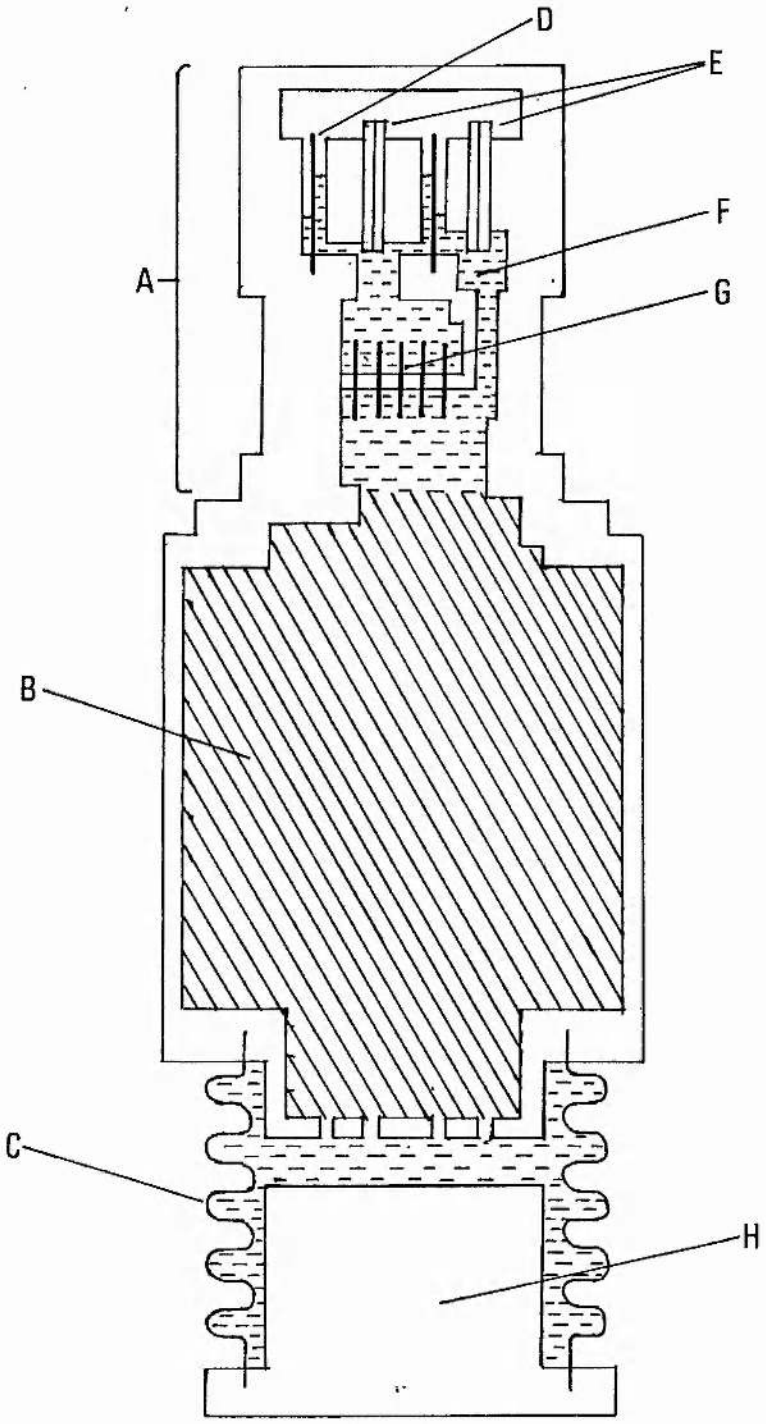

Figure 5.7.1.

A scale drawing of the experimental cell (actual size).

A: Experimental region.

B: Salt chamber.

C: Stainless steel bellows.

D: Beaker.

E: Level sensing capacitors.

F: Liquid helium sample.

G: Sintered copper heat exchangers.

H: Epibond plug.

can be seen schematically in figure 5.4.1., whilst the supporting structure itself is seen more clearly in plates 5.4.2. and 5.6.1. Detailed examination of the photographs reveals that the four nylon struts are slightly bowed outwards, this being the result of over-pressurising the cell during one run. To guard against a repetition of this occurrence, four graphite rods were inserted, one adjacent to each strut. The rods were held in position with G.E. varnish and greatly increased the compressure strength of the supporting structure without contributing significantly to its thermal conductance.

(b) The Experimental Region

The experimental cell was made in several sections from Epibond 100A epoxy resin. These were glued together with Epibond 121 epoxy and 951 hardener. A schematic diagram of the cell is given in figure 5.7.1. The experimental region was built at the Ohio State University by D.B. Crum and had already been used in an experiment on the flow of the helium film below 1K. (Crum et al 1973). This part of the cell was very kindly supplied by Professor J.T. Tough. The following details of the experimental region have been taken from the thesis of D.B. Crum (Ohio State University 1973) and are included in order to make the presentation of this work more complete.

The beaker was made from a short piece of $\frac{3}{4}$" o.d. stainless steel tubing of wall thickness .02". One end of the tubing was cast into a piece of Epibond 100A, forming part of the bottom of the bucket. The other end of the tube was polished to a mirror finish on a lathe. After polishing, the tube had an o.d. of 1.910 cm and an i.d. of 1.867 cm. Thermal contact between the helium in the bucket and that in the outer chamber was improved by glueing strips of

Figure 5.7.2.
The dimensions of the shielded capacitor plate.

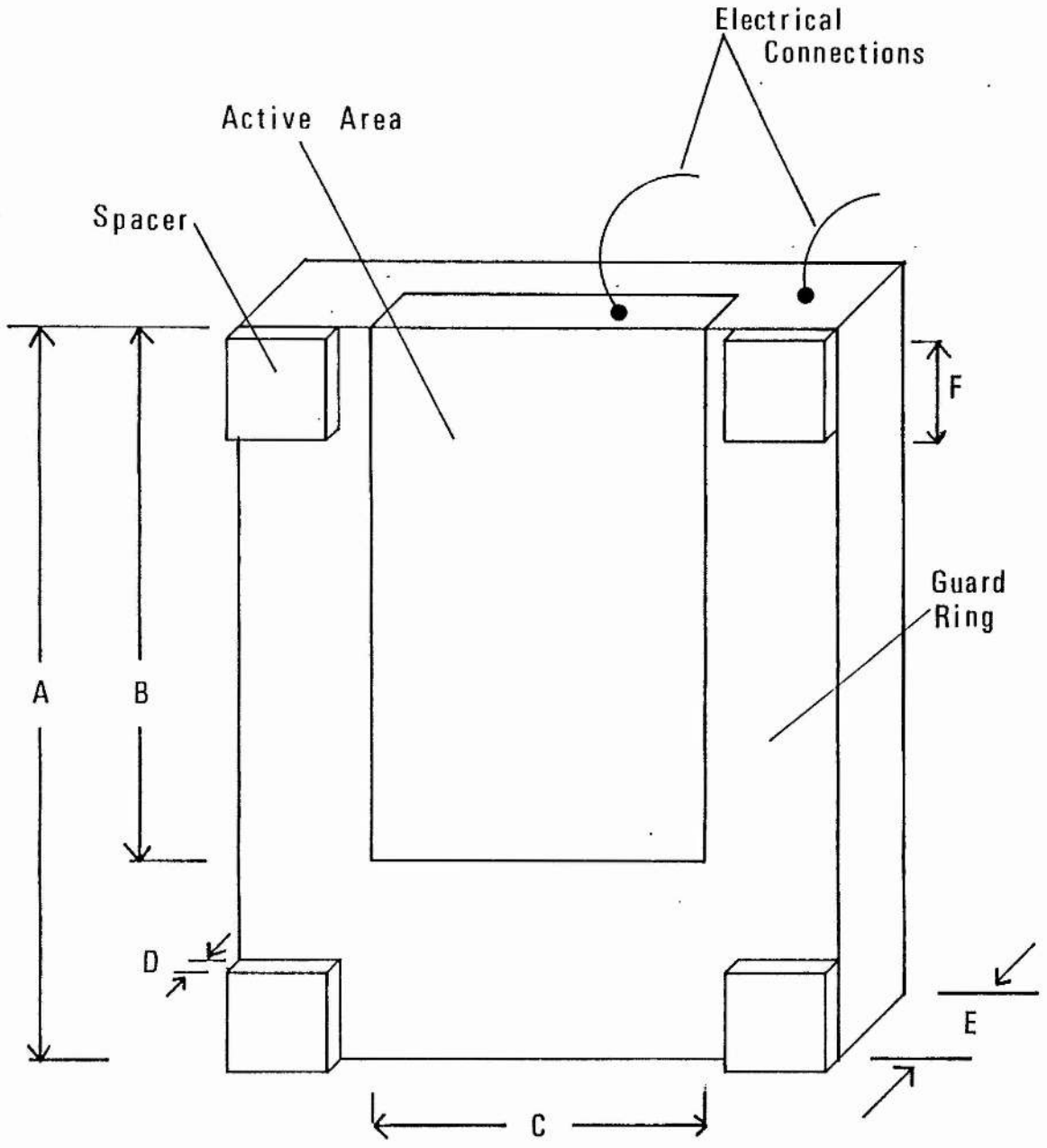

A : 0·753"

B : 0·592"

C : 0·236"

D : 0·0054"

E : 0·061"

F : 0·08"

sintered copper foil through the bottom of the bucket. Five sheets of foil were used, each of size 2.2 x 2.0 x .024 cm , with an "average hole diameter" of 7.5μm. A copper to helium interface of area ∿600 cm^2 was provided by these strips inside the beaker, whilst the area of the interface in the outer chamber was ∿1000 cm^2. The bucket was checked for leak-tightness on a helium-sensitive mass spectrometer. The volume of the bucket was reduced by packing 36-gauge copper wires loosely between the sintered copper strips.

(c) The Level-Sensing Capacitors

Two parallel plate capacitors were used to measure the position of the helium levels inside and outside the beaker. The dielectric constant of liquid ^4He differs from that of vacuum by ∿6%, and hence a change in the liquid levels leads to an easily detectable change in capacitance. The capacitors were made from optical quality quartz plates which were cleaned with a series of solvents and then coated with an evaporated layer of gold, ∿1000Å thick. An active area was marked out on one of each pair of the plates by scratching a line ∿.003" wide in the gold film. The dimensions of the capacitor plates are shown in figure 5.7.2. The spacers between the plates were again made from quartz, and were all cut from the same piece to ensure that the gap would be uniform. The spacer was placed at each corner of one of the plates, the other plate was placed on top and several turns of very fine nylon thread were wound round the plates at the top and bottom. The thread was secured with a touch of G.E. varnish. A three-terminal capacitor was thus formed, with the unmarked plate as the "high" terminal, the active area as the "low" terminal and the surrounding area as the guard ring.

The capacitors made tight push-fits into slots in pieces of epibond, as shown in figure 5.7.1. The epibond mount for the beaker capacitor in fact occupied much of the volume in the beaker, leaving an annulus of cross sectional area 0.757 cm^2 for the liquid. Electrical contact was made to the tops of the capacitor plates by fastening on 42-gauge copper wires with silver-loaded conducting epoxy. These wires were lead out through small holes drilled in the cell wall, which were then sealed with Epibond 121.

Shortly after the experimental region was installed in the cell, the outer level capacitor developed a short circuit. It was found that a flake of gold had become detached from the quartz and had formed a bridge between the high and low plates. The capacitor was removed from the cell and replated. The most successful technique found for marking out the active area was to cover the plate with a thin sheet of filter paper and mark out through the filter paper with a razor blade.

(d) The Salt Chamber

The main refrigerant, chrome potassium alum, was contained in an Epibond chamber of volume ∿170 ccs situated immediately below the experimental region and communicating directly with it. When full, the chamber held 170 gms of salt. The salt was in the form of 1 mm granules and was prepared by grinding down large crystals with a pestle and mortar, rehydrating them by covering the mortar with a damp cloth and then screening the granules for size with a number of graded sieves.

Located on the outside of the experimental region were four bundles of 50-gauge copper wires. These fed through the cell wall at points that were subsequently sealed with Epibond 121, and formed

5.7.1. The magnetic cooling stages of the cryostat.

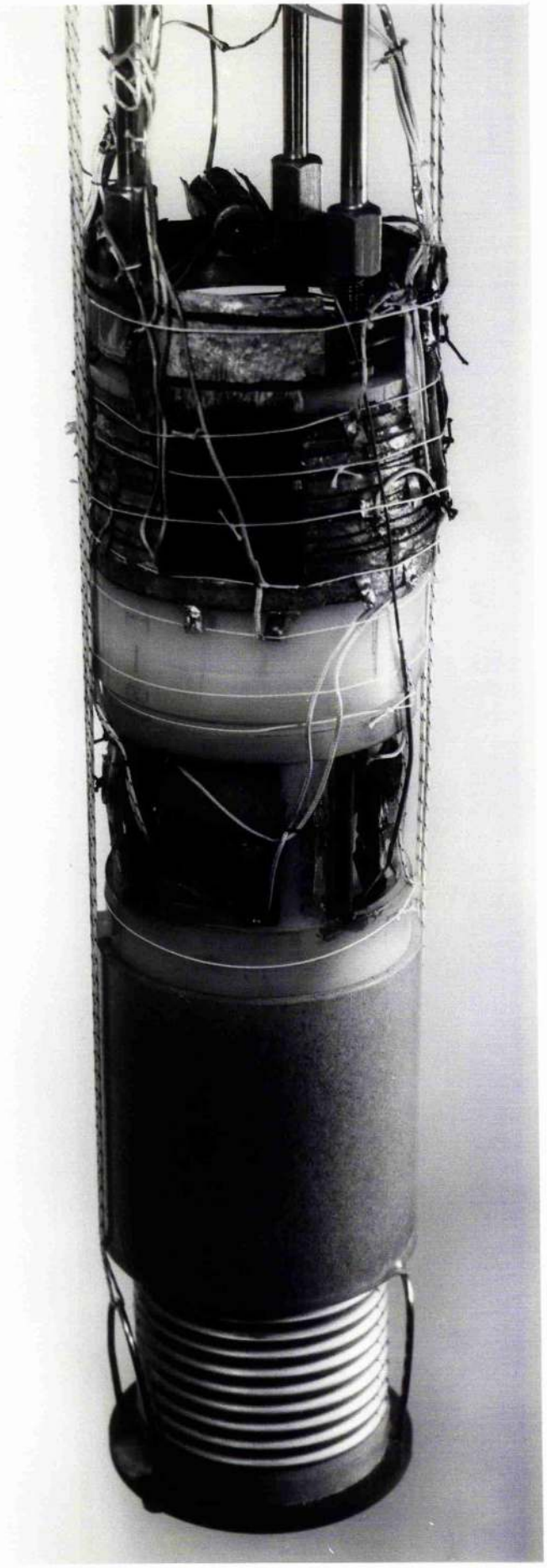

5.8.1. The cryostat top plate, showing the bellows assembly with the hydraulic link in position.

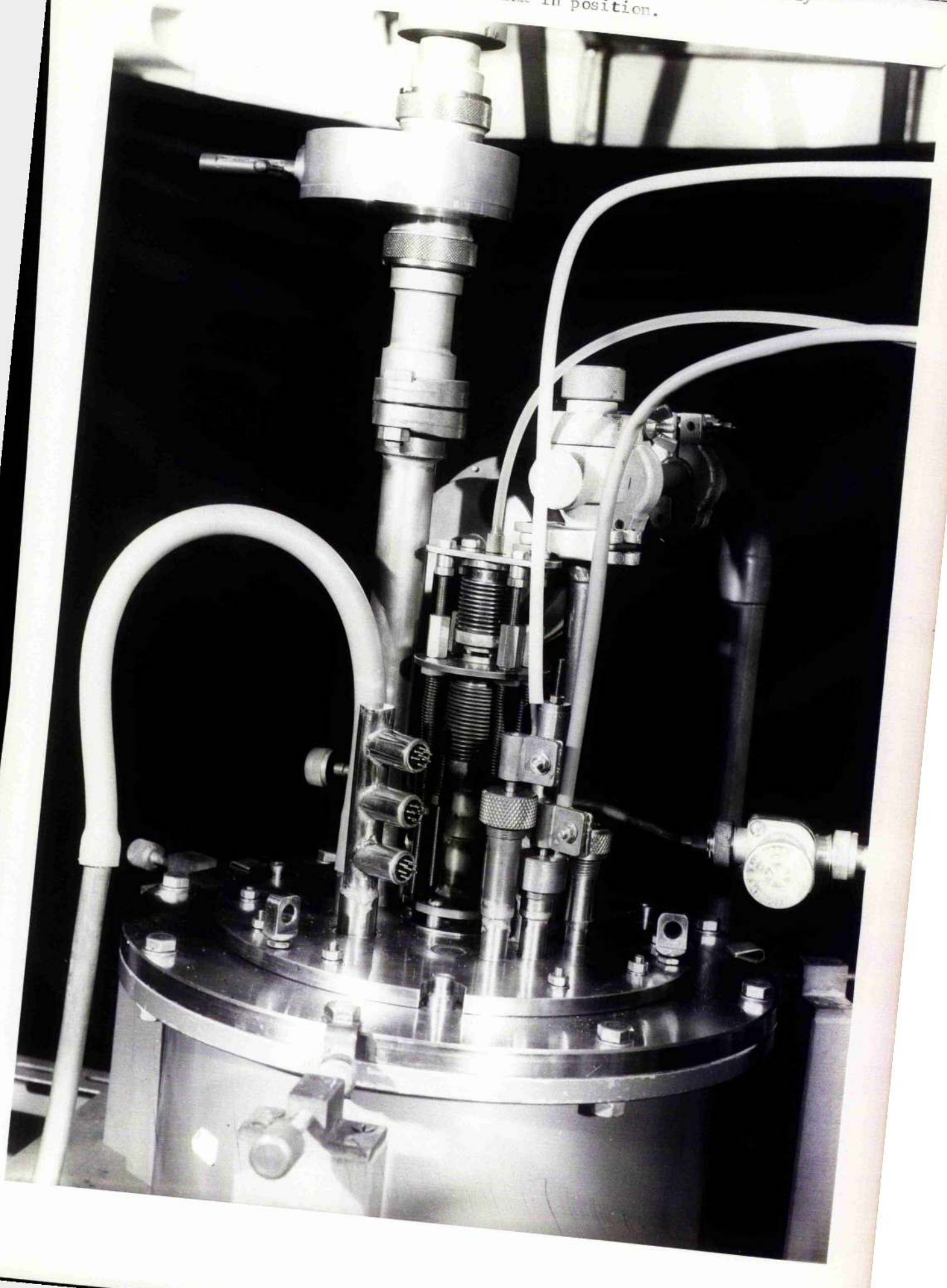

a fine mesh of 20,000 wires inside the salt chamber. During the packing of the salt, care was taken to distribute the granules evenly throughout this mesh. The purpose of the wires was to reduce the thermal time constants in the cell at very low temperatures, and also to provide thermal contact between the helium in the cell and the thermometers. These were mounted outside the cell on copper lugs, hard soldered to the ends of the wire bundles. More details of the thermometers and thermometer mounts will be given in section 6.1.

When the packing of the salt chamber was complete, the base of the cell, consisting of a stainless steel bellows set in epoxy end pieces, was glued on using Epibond 121. A photograph of the fully assembled cell in position beneath the guard salt is given in plate 5.7.1.

5.8 THE BELLOWS ACTUATION MECHANISM

One way of operating a bellows at low temperature is to encase it within a liquid-helium-filled chamber which can be pressurised by means of a pump situated in the laboratory. Such a system is complex, and involves a second helium filling capillary, with all the attendant thermal anchors and isolation spirals. A much simpler system was employed in the present cryostat. The bellows were supported on a 1/8" thick Tufnol cradle fitted with stainless steel lifting hoops. Commercially obtained braided dacron fishing line of 12 lb breaking strain was used to connect the hoops to a steel stirrup arrangement installed around the 1K pot. One length of fishing line looped round twice was used for each hoop, such that the bellows operating load was spread over eight lengths of line. Specially milled slots were provided in the copper piece of the vortex fridge to allow the lines to pass through. Plate 5.7.1. shows the bellows cradle quite

Figure 5.8.1.

The bellows arrangement at the cryostat top plate.

a: light oil. b: three point support. c: phosphor-bronze top bellows.
d: long nut. e: stainless steel wire. f: cryostat top plate.
g: flexible plastic tubing h: phosphor-bronze driving bellows.
i: brass plate. j: spring held in compression. k: brass rod.
l: vacuum space. m: telescopic brass tubing.

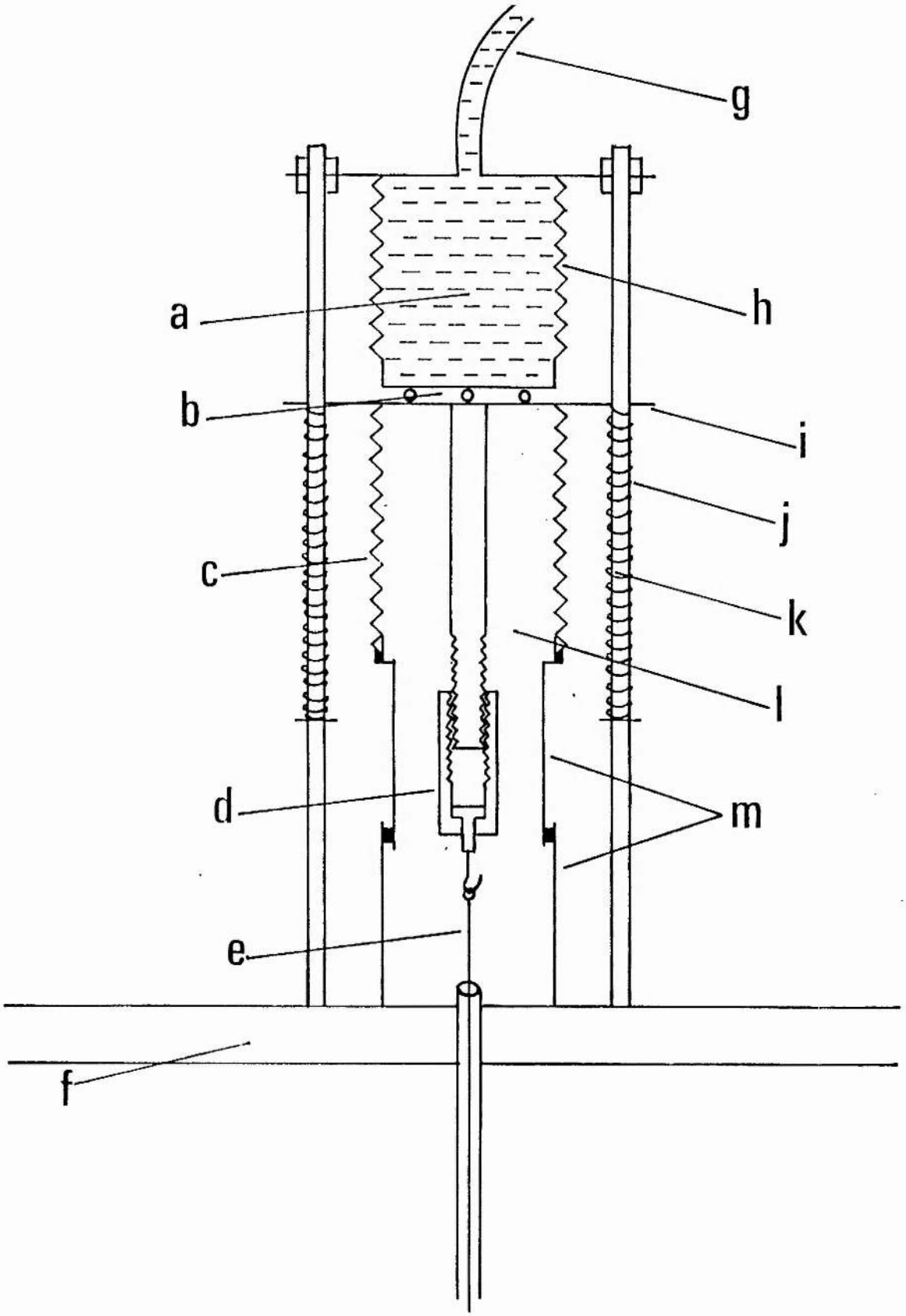

clearly whilst the arrangement of the stirrups around the 1K pot can be seen in plate 5.5.1. The stirrups were thermally anchored to the 1K pot with lengths of copper braid and were bolted to a Tufnol arm, positioned between the 1K pot and the vacuum chamber flange. A stainless steel wire, located centrally in this arm, was carried through the flange to the cryostat top plate in a 1/8" diameter tube, which formed an extension of the vacuum space. The bottom end of the wire was thermally anchored at 4.2K to the underside of the flange.

The arrangement at the cryostat top plate is shown schematically in figure 5.8.1. The top bellows could either be moved through a step displacement, or very slowly driven up or down by a hydraulic link attached to a 100 speed synchronous motor. The motor drove a micrometer through a 10:1 reduction gear. The micrometer compressed a phosphor-bronze bellows filled with light oil. This bellows was linked hydraulically by a length of flexible plastic tubing, to the driving bellows shown in the figure. Plate 5.8.1. shows the bellows assembly at the cryostat top plate with the hydraulic link in position. The actuation mechanism described above was found to operate with a minimum of vibration and thermal conductance. The maximum load on the bellows system occurred when the cell contained ^{4}He at atmospheric pressure whilst the vacuum chamber was evacuated. The effective cross sectional area of the cell bellows was 17.4 cm^2, giving a load of 40.5 lbs. The components of the actuation mechanism were tested with a load of 60 lbs, to allow for the extra force of 18 lbs needed to fully compress the cell bellows.

5.9 THE CELL FILLING SYSTEM

The liquid sample was formed from 6 moles of specially purified

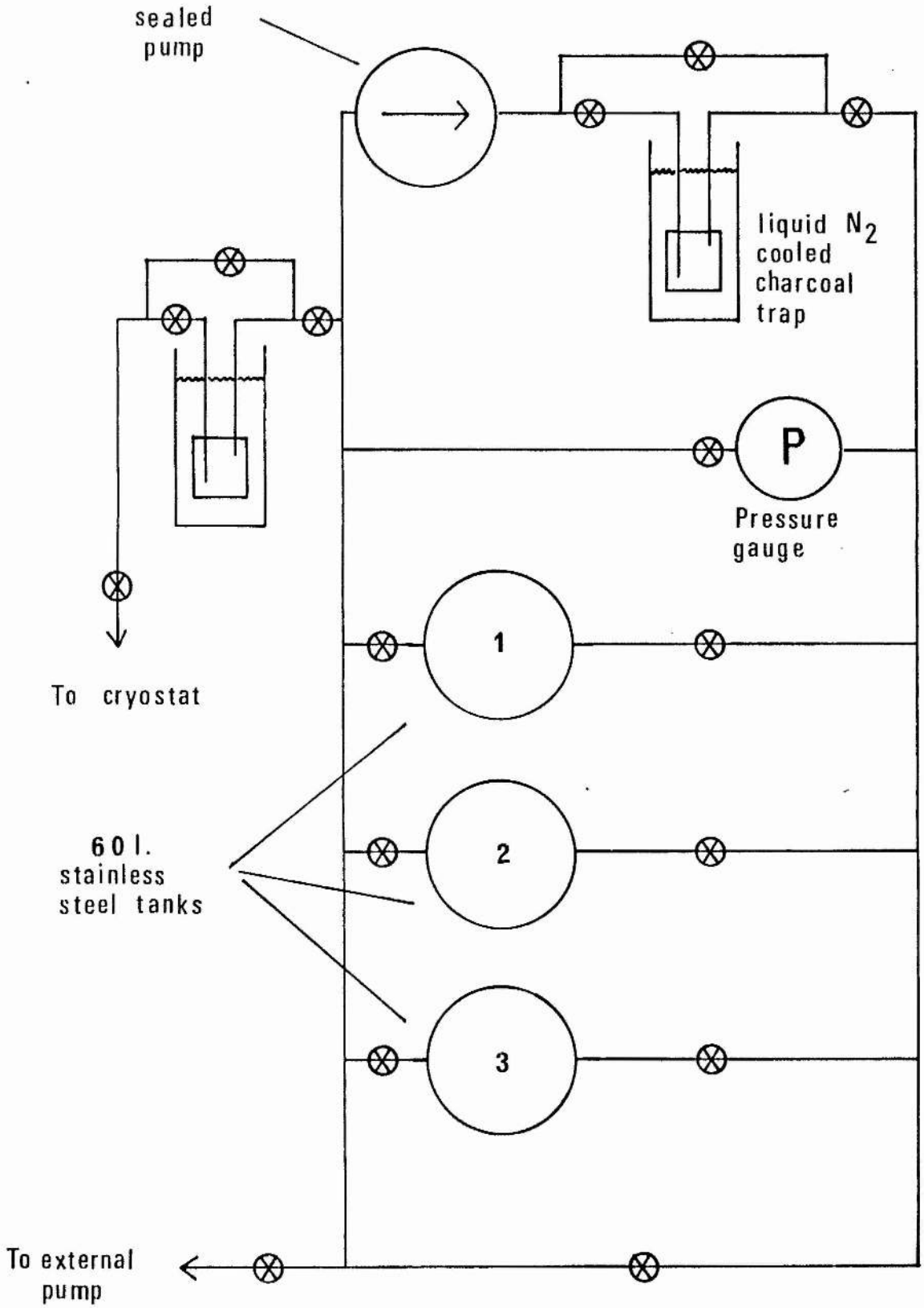

Figure 5.9.1.

Schematic diagram of the gas handling system.

^{4}He gas, purchased from the US Bureau of Mines. The gas was stored at slightly below atmospheric pressure in three 60ℓ stainless steel tanks. These were situated in the laboratory and were connected to the cryostat via a gas handling system, shown schematically in figure 5.9.1. A sealed pump and two liquid-nitrogen-cooled charcoal traps allowed the gas to be circulated and purified prior to being condensed into the cell. Small plugs of glass wool were inserted in the pumping lines on either side of the charcoal traps to prevent dust being carried through into the rest of the system. The pressure could be monitored at several points using a Wallace and Tiernan gauge type FA 145, measuring up to 3 atmospheres in divisions of 2 torr.

On entering the cryostat the gas was condensed in a copper spiral situated in the main helium bath. The liquid sample was then carried through the inner vacuum chamber to the experimental cell via a succession of isolation spirals and sintered copper heat exchangers.

CHAPTER SIX

OPERATIONAL DETAILS OF THE APPARATUS

6.1 THE MEASUREMENT OF TEMPERATURE

(a) The 1K Pot and Vortex Fridge

Speer 220Ω carbon resistance thermometers were mounted in the cell filling capillary heat exchangers on the 1K pot and vortex fridge. The lid of each heat exchanger contained a hole into which the resistor made a tight push-fit. The resistor bodies were lightly smeared with a thermal contact agent, Apiezon 'N' grease, prior to mounting. Heat leaks into the thermometers from the electrical leads were eliminated by careful thermal anchoring of the leads.

The resistance values were measured with a modified Oxford Instruments Resistance Thermometer Bridge, the excitation voltage of which could be varied over the range 3.5 mV rms to 18μV rms. The power dissipated in the sensors was ∿2pW at a temperature of ∿1K.

The resistors were calibrated against the 1958 ^{4}He vapour pressure scale. The 1K pot was pumped down to the lowest attainable temperature of 1.14K and then sealed off. The resistance bridge was set off balance. As the pot warmed, the balance point was reached and the vapour pressure was read from a manometer to an accuracy of $\pm$ .1 torr, using a cathetometer. Calibration points were taken in this way up to a temperature of 2.2K. The rate of warming was in general sufficiently slow for the thermometers to remain in thermal equilibrium with the pot. It was not possible to regulate the temperature with the pump for each calibration point; the vapour pressure was monitored at a point on the pumping line external to the cryostat and any flow of

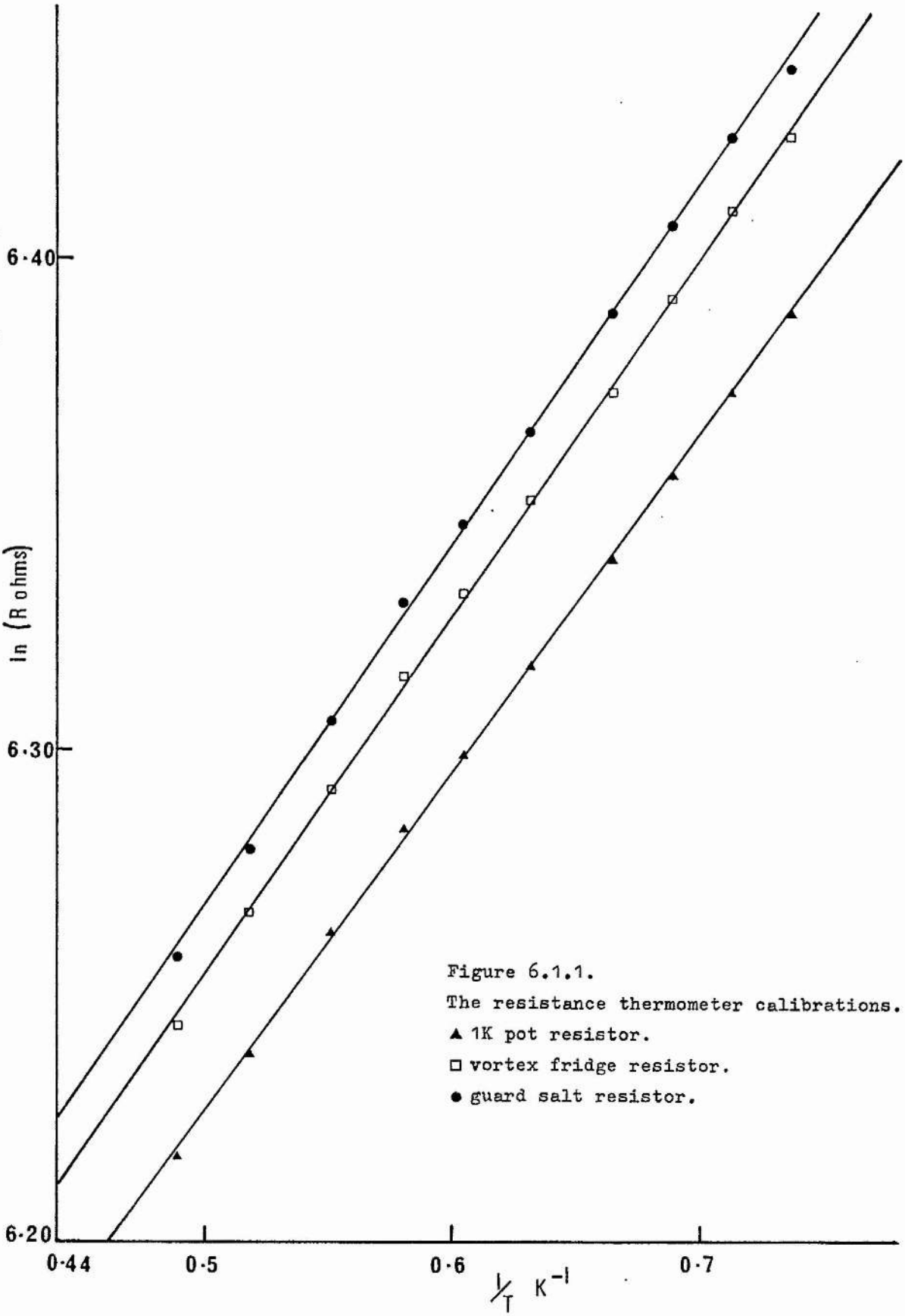

Figure 6.1.1.
The resistance thermometer calibrations.
▲ 1K pot resistor.
□ vortex fridge resistor.
● guard salt resistor.

vapour in the line caused a pressure drop that interfered with the vapour pressure determination.

The calibrations obtained are shown in figure 6.1.1 and are seen to conform to the relationship

$$\ell n\ R = \frac{A}{T} + B \qquad (6.1.1)$$

where R is the electrical resistance and A and B are constants. From studies of Speer carbon resistance thermometers in the literature it can be seen that no single functional form adequately describes the resistance versus temperature characteristic over the temperature range 20 mK to 2K. (Black, Roach and Wheatley 1964). The relationship given in equation 6.1.1. does, however, remain accurate to within 5% down to 0.6K.

(b) The Guard Salt

A Speer 220Ω carbon resistor was soldered to one of the thermal anchoring strips running through the body of the salt. Non superconducting solder was used to avoid loss of thermal contact at low temperatures. The resistance was measured with the bridge system described above and the power dissipated in the thermometer was $\sim 10^{-14}$W at a temperature of ~50 mK. The temperature resolution was better than $\pm$ .5mK at this temperature and no self-heating effects were observed. The thermometer was calibrated down to 1K along with the 1K pot and vortex fridge thermometers by the method described above. The calibration curve is shown in figure 6.1.1.

(c) The Cell

An absolute determination of the cell temperature from the magnetic susceptibility of C.M.N. (cerium magnesium nitrate) was not possible owing to the limited space in the dewar. The cell temperature was

therefore measured by two 'secondary' thermometers,

(i) The Resistance Thermometer

A sliced carbon resistor in a gold plated copper mount, calibrated down to 4mK, was very kindly supplied by C.N.R.S. (Grenoble). The mount was screwed into a copper lug hard soldered to one of the wire bundles emerging from the salt chamber. The resistance was measured with a second Oxford Instruments bridge, modified to operate at an excitation voltage of 7μV rms. Power dissipation in the sensor was $\sim 5 \times 10^{-16}$W at the lowest temperatures. Temperature resolution was better than $\pm$ 0.8mK.

Oda et al (1974) have measured the thermal resistance of carbon thermometers down to 30 mK. An extrapolation of their results indicates that, at 10mK, the power dissipation in the sensor must be kept below 10^{-14}W for the resistance change due to self-heating to remain below 1%. No self-heating effects were observed at the power levels used in the present experiments.

The resistor was one of a matched set having a resistance versus temperature characteristic that lay parallel to the curve

$$\ell n\, T(mK) = 8.631 - \{2.938 + 8.298\, \ell n\, R^*(k\Omega)\}^{\frac{1}{2}}, \qquad (6.1.2)$$

over the range 4mK to 600mK. The measured resistance R_m was related to R^* by

$$R_m = AR^* + B. \qquad (6.1.3)$$

By bringing the cell into thermal equilibrium with the 1K pot at several different temperatures, the constants A and B were determined as 1.90 and -446.17Ω respectively.

(ii) The Capacitance Thermometer

During flow experiments, an excitation voltage of ± 30V was applied to the level sensing capacitors. This induced an emf of 0.25mV across the resistance thermometer which caused serious self-heating at temperatures below 60mK. The resistance thermometer was also affected by the magnetic field of the main solenoid. A second thermometer, specially chosen for its insensitivity to these disturbing influences, was therefore mounted on the cell. This was a Corning type 110 capacitance thermometer, as described by Lawless (1971).

The thermometer was made from a glass-ceramic, $SrTiO_3$, the dielectric constant of which is strongly temperature dependent over the entire range 300K to 7mK, whilst remaining completely insensitive to applied magnetic fields of up to 14×10^4 Gauss (Rubin and Lawless, 1971). In the temperature region 5.2K to 1.1K, the capacitance falls linearly with decreasing temperature, but then levels out to a broad minimum at ∿100mK. Below 80mK the capacitance increases rapidly with decreasing temperature. Lawless, Radebough and Soulen (1971) reported a 1/T dependence of the capacitance over the range 80mK to 25mK, whilst Bakalyar et al (1972) observed a linear increase of capacitance with decreasing temperature over the range 35mK to 7mK.

The capacitance thermometer used in the present experiments was mounted in a close fitting hole drilled in a copper lug, thermal contact being made through a thin layer of G.E. varnish. The lug was hard soldered to one of the wire bundles emerging from the salt chamber. The "low" lead to the thermometer was screened for most of its length inside the cryostat. Capacitance measurements were made with a General Radio 1615A Capacitance Bridge and a Brookdeal 9501

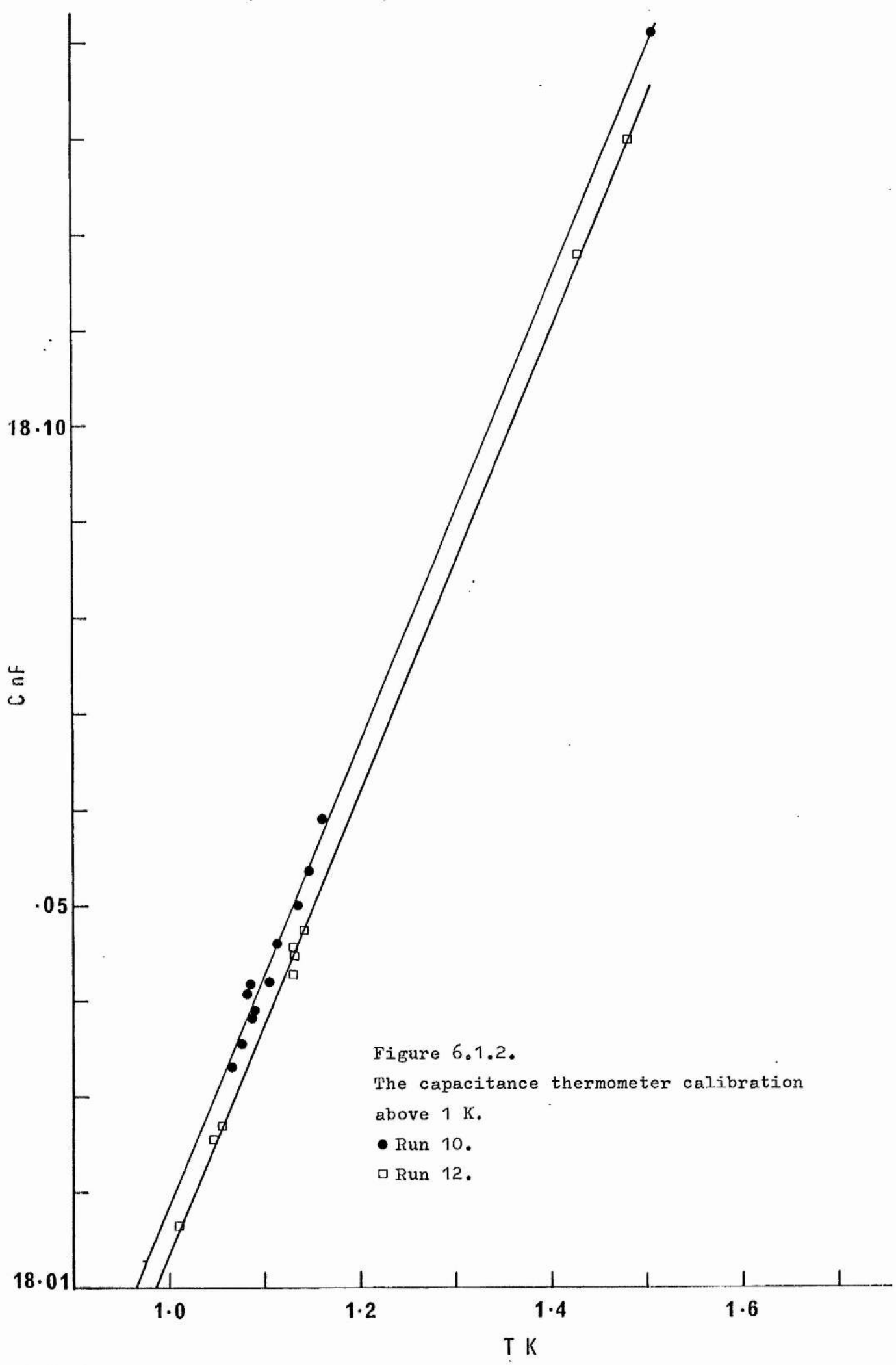

Figure 6.1.2.
The capacitance thermometer calibration above 1 K.
● Run 10.
□ Run 12.

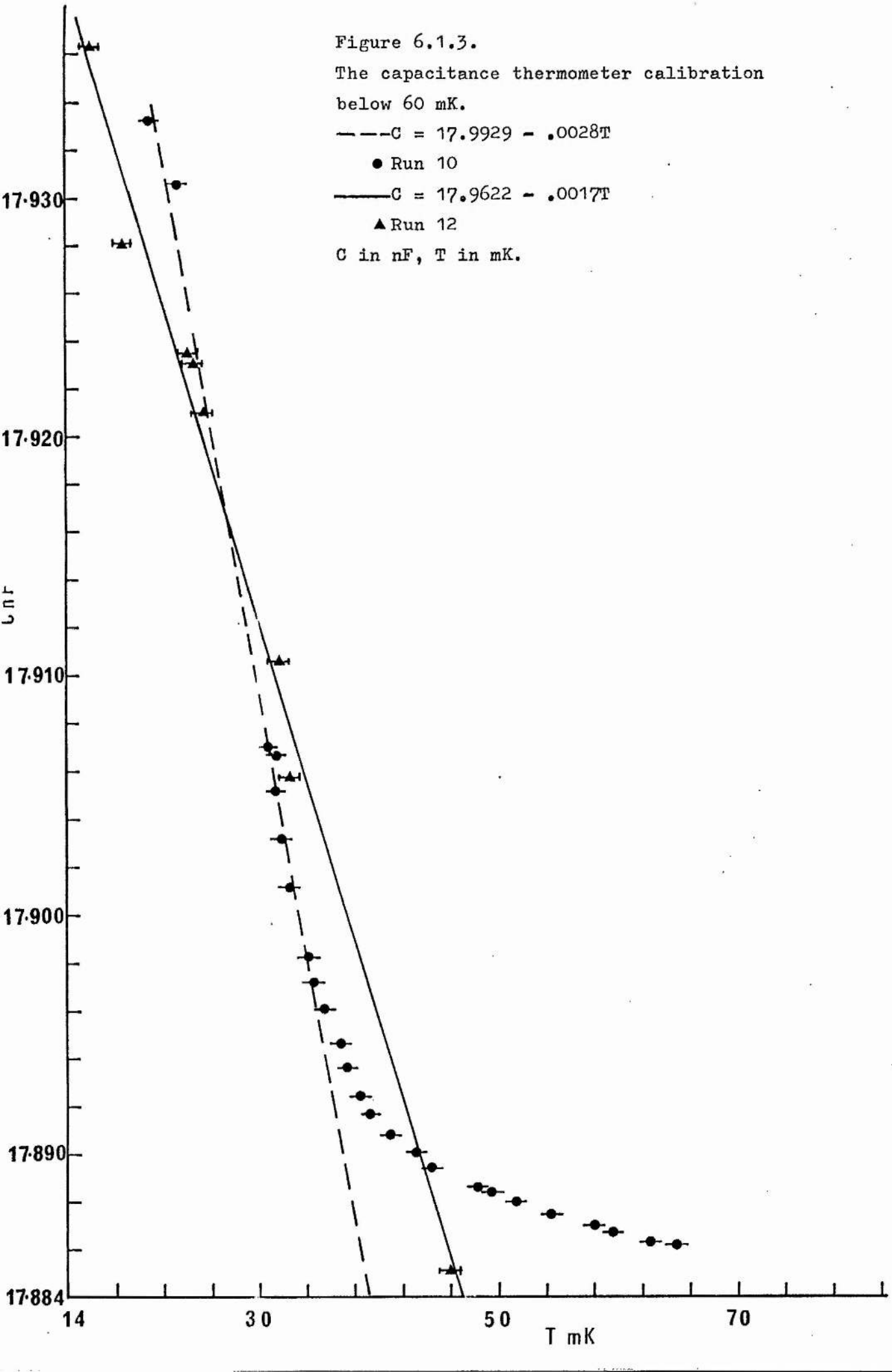
Figure 6.1.3.
The capacitance thermometer calibration
below 60 mK.
---C = 17.9929 - .0028T
● Run 10
——C = 17.9622 - .0017T
▲ Run 12
C in nF, T in mK.
17·930
17·920
17·910
17·900
17·890
17·884
14
30
50
70
T mK

lock-in amplifier as null detector. An oscillator incorporated in the lock-in amplifier provided the excitation voltage of 7mV rms at 1520 c/s, causing a power dissipation in the sensor of 3pW. Self-heating effects were not observed, showing that the thermal resistance of the thermometer was considerably smaller than that of a carbon resistor. The thermometer was therefore unaffected by electromagnetic pick-up. Changes in capacitance of $\pm$ .05pF in 17nF could be resolved by the bridge system, corresponding to a temperature resolution of $\pm$ .02mK below 40mK and $\pm$0.2mK above 1K.

This thermometer could not be used as the primary thermometer on the cell, since its capacitance versus temperature characteristic was found to change on thermal cycling and also if subjected to large voltage transients. The thermometer was therefore calibrated against the cell carbon resistor at the start of each run over the temperature ranges 1.0K and 1.6K and 16mK to 60mK, in the absence of electromagnetic pick-up and applied magnetic fields. It was then used to monitor the rate of cooling of the cell in the full applied field, prior to each demagnetisation, and also to monitor the cell temperature during flow experiments at very low temperatures.

Calibration curves for temperatures above 1K are given in figure 6.1.2. and it can be seen that the capacitance values have shifted by a constant amount, (5pF) between runs. The low temperature calibrations for different runs are given in figure 6.1.3. Between the runs the thermometer was thermally cycled once to room temperature and back, and twice to 77K and back. The linear dependence of capacitance on temperature below 35mK reported by Bakalyar et al was

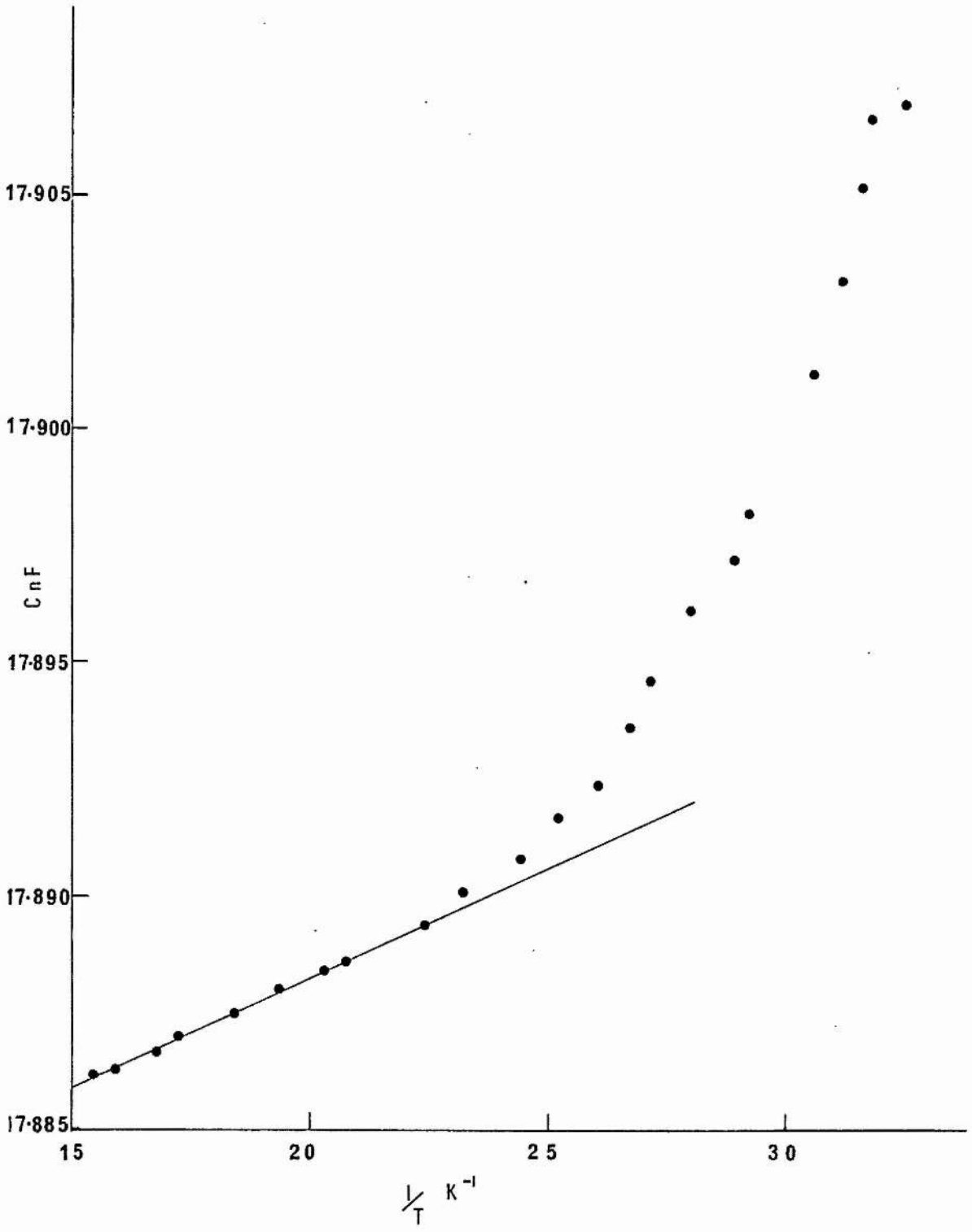

Figure 6.1.4.
The low temperature calibration of the capacitance thermometer.
A plot of capacitance versus T^{-1}. • Run 10.

observed, but the sensitivity was seen to change on thermal cycling. Part of the data is replotted in figure 6.1.4. as capacitance versus T^{-1}. A linear dependence is observed over the temperature range 45mK to 65mK, in partial agreement with the findings of Lawless et al.

6.2 THE MEASUREMENT OF LIQUID LEVELS IN THE CELL

The values of the two parallel plate capacitors described in section 5.7 were measured in the three terminal mode by two independent bridge systems. In three terminal measurements, the effect of strong capacitance to ground is simply to reduce the sensitivity of the detector without contributing to the value of the unknown capacitance. The bridge system used with the "beaker" capacitor comprised a modified A.S.L. ratio arm transformer bridge, model 1055, driven from a Hewlett Packard oscillator, model 3300A, with a P.A.R. type Jb-5 lock-in amplifier and P.A.R. 112 preamplifier as null detector. The standard capacitor used with the bridge was a General Radio type 1403-G air gap capacitor, of 10pF nominal value. The excitation voltage applied to the unknown capacitor was of amplitude $\pm$ 40V peak to peak and frequency 1.9 kc/s. At low temperatures, the loss across the unknown was exceedingly small and no heating effects due to the operation of the bridge were detected. With the lock-in amplifier at full gain, changes in the liquid level as small as 300Å could be resolved. This sensitivity was too high for normal operation, a resolution of $\pm$ 0.5μm being adequate in most experiments. The off balance signal from the bridge was linear to better than .01% and was recorded on one channel of a Servoscribe 2-pen chart recorder. The time constant of the lock-in amplifier was set at 0.1s for all the

measurements. Some typical output traces are reproduced in Chapter 7, figures 7.1.1 to 7.1.4.

The value of the "cell" capacitor was monitored with the same General Radio capacitance bridge and Brookdeal lock-in amplifier that were used with the capacitance thermometer. The internal oscillator of the lock-in amplifier did not provide a high enough excitation voltage to give adequate resolution of the liquid level, so an external Advance type H-1 oscillator was used instead. The excitation voltage was of amplitude $\pm$ 30V peak to peak and frequency 3.7 kc/s. The signal to noise ratio was improved by the use of a Brookdeal type 5001 pre-amplifier and type 5011 active filter. This latter instrument was used in the "notch" mode at 1.9 kc/s, to reduce the effects of pick-up from the "beaker" bridge system. With both measurement systems operating simultaneously, the "cross-talk" was insufficient to cause overloading of the mixers in the lock-in amplifiers. The output from the "cell level" bridge was recorded on the other channel of the Servoscribe 2-pen chart recorder.

6.3 THE CELL FLUSHING PROCEDURE

As mentioned in section 3.4, the presence of solid air on the beaker rim can cause greatly enhanced superfluid film transport. For this reason the experimental cell had to be thoroughly flushed out with pure ^{4}He gas prior to a run. The procedure adopted was to pump on the cell through a liquid nitrogen-cooled charcoal trap and then back-fill the cell with pure ^{4}He gas. The cycle was repeated until the partial pressure of air in the cell was less than 0.02torr. Unfortunately the presence of the isolation spirals in the cell-filling capillary rendered the pumping speed extremely low, and thus the whole

cell flushing operation could take many days. The calculations detailed in Appendix A were carried out to establish the optimum pumping and back filling times for each cycle. These were found to be 2.81 hours and 2.65 hours respectively. 12 complete cycles were necessary if the cell was initially full of air and these could be conveniently executed over a period of 5 days.

6.4 COOLING THE CRYOSTAT FROM ROOM TEMPERATURE TO 1K

Once the dewar wall had been evacuated, the air was pumped out of the main dewar space, which was then back-filled with ^{4}He gas. The 1K pot and vortex fridge were treated similarly. The inner vacuum chamber was pumped out to a pressure of $\sim$10 torr and then sealed off; prolonged pumping at room temperature would have caused dehydration of the guard salt. The nitrogen jacket of the main dewar was then filled and the whole system was left to cool down for $\sim$12 hours. With the guard salt at 77K the air remaining in the inner vacuum chamber was pumped out with a diffusion pump and the chamber was back-filled with either ^{4}He or ^{3}He gas to a pressure of $\sim 10^{-1}$ torr. The advantage of using ^{3}He as a thermal exchange medium was that any residual gas left in the vacuum chamber would not cause heat leaks by forming a superfluid film.

The transfer of liquid helium from the storage dewar was then commenced and the progress of the cooling was followed by monitoring the exchange gas pressure and the value of the capacitance thermometer on the cell. If the exchange gas pressure fell below 10^{-4} torr, thermal contact to the tail of the cryostat was lost; in these circumstances extra gas was added in small quantities until cooling recommenced.

When the main bath was eventually filled with liquid helium, the boil-off rate was initially quite high. It was usually necessary to top up the bath three times during the next two hours before the boil-off rate stabilised at a low value.

With the tail of the cryostat cooled to 4.2K, the exchange gas was pumped out of the inner vacuum chamber with a diffusion pump. A pumping time of 12 hours was necessary to achieve a good thermally insulating vacuum. The Penning gauge on the pumping line then registered a pressure of $\sim 10^{-6}$ torr. A helium-sensitive mass spectrometer leak detector was used to back the diffusion pump during this stage; any leaks into the inner vacuum chamber immediately became obvious.

The 1K pot was then filled from the main helium bath. The best method of filling was to pump on the pot with the needle valve "cracked" open, such that the pot temperature was held at $\sim$1.6K. A rapid rise in this temperature took place when the pot became full.

With the 1K pot and vortex fridge operating, the liquid sample was condensed into the cell from the external gas handling system. This process was performed slowly, so that the temperature of the vortex fridge heat exchanger never exceeded 1.4K. If the cell had been filled with liquid at 4.2K,many days would have been needed to cool the sample to 1K by conduction through the thermal link. During the filling process, the bellows on the cell were held fully compressed so that only the minimum volume of liquid necessary for the operation of the thermal link was condensed. The level sensing capacitors were used to monitor the filling procedure. As the liquid level approached the top of the cell, the pressure in the condensing tank was maintained below 1 atmosphere to avoid overfilling the system;

condensation stopped automatically when the liquid level reached some point in the isolation spiral above the 1K pot where the vapour pressure equalled the pressure in the condensing tank.

6.5 THE CALIBRATION OF THE LEVEL-SENSING CAPACITORS

A detailed calibration procedure was described by Crum (Thesis 1973) in which he showed that the sensitivities of the capacitors to changes in the liquid level were uniform to within $\pm$ 1% over most of their length. A repetition of this detailed calibration was not considered to be necessary as the beaker capacitor had not been disturbed in any way during its installation in the present cell.

A simple two-point calibration procedure was employed to check that the sensitivity of the capacitor had not changed. The "full" and "empty" capacitance values were found by suitable movements of the cell bellows, and their difference was divided by the length of the active area to give the sensitivity. The result of 0.217 pF cm^{-1} was in agreement with the value found by Crum. Unfortunately this calibration did not remain valid for the whole of the data-taking period; the earth connection to the guard ring apparently broke away prior to the run in which the major part of the results was taken. The rectification of this fault would have entailed machining off the top of the cell to gain access to the capacitors. This major operation was not undertaken as the capacitor still functioned perfectly well, albeit with a slightly higher nominal value and sensitivity. The sensitivity was redetermined as 0.245 pF cm^{-1} by the method outlined above.

The cell level capacitor, which had been replated, was not used for accurate flow rate measurements; the replating operation was not

entirely successful, in that there occurred regions of low sensitivity where, presumably, flaking of the gold had recommenced. Also a short circuit developed between the active area and the guard ring soon after the cell was installed in the cryostat, causing the capacitance and sensitivity to increase by approximately a factor of 2. The function of the cell level capacitor was therefore restricted to that of providing qualitative monitoring of the cell level except in the driven flow experiments as described in section 8.2. Its sensitivity was estimated as $\sim$0.46 pF cm^{-1}.

It was important to determine the capacitance values at which the helium just covered the beaker rim, so that the distance from the rim to the liquid surfaces during flow experiments could be calculated. This was achieved by raising the level to the tops of the capacitor plates and then progressively lowering the cell bellows in small steps. At first, no change occurred in the capacitance values since liquid was held up between the plates by surface tension forces. When the surface tension rise was exceeded, both capacitors showed an immediate response to further bellows movements. The position of the liquid surface was at this point above the beaker rim. The bellows movements were continued until a slow response on the beaker capacitor indicated that the outer level now lay below the rim and that superfluid film transfer was taking place. The capacitance changes were recorded on chart, and the exact position of the beaker rim could be calculated.

6.6 THE ENERGISATION OF THE SOLENOID

Thermal contact was established between the cell, guard salt and vortex fridge prior to magnetisation of the salts, and the persistent mode switch heaters were energised. The current was then slowly

increased in the main solenoid at a rate in accordance with the manufacturer's instructions. The warming of the cell was considerably less than that of the guard salt owing to the relatively large volume of liquid helium in thermal contact with the main salt. Once the full field had been reached, however, the guard and cell quickly reached thermal equilibrium through the short length of helium-filled capillary connecting the two. The cell temperature never exceeded 1.6K during a magnetisation process.

The time needed to develop the full field was ∿40 minutes and the excess boil-off from the main bath due to the heat input from the magnet leads was ∿1.5ℓ. When magnetisation was complete, the persistent mode switch heaters were de-energised, trapping the flux in the solenoid, and the current in the main leads was quickly reduced to zero. The leads were then lowered into the helium bath as described in section 5.3, until such time as demagnetisation of the salts was required. The cell bellows were left in the compressed position to allow the slow removal of the heat of magnetisation to take place through the helium-filled capillary.

6.7 THE DEMAGNETISATION PROCEDURE

Once the desired starting temperature of the magnetic cooling cycle had been attained, thermal contact between the cell, the guard salt and the vortex fridge was broken. It was important to execute the bellows movement very slowly at this point, as eddy currents could cause significant warming of the cell. To improve the vibrational isolation of the cryostat, all pumping lines, save that to the 1K pot, were sealed and disconnected, and all the pumps operating in the laboratory were turned off. The magnet leads were retrieved from the

main bath and the current was quickly swept up to match the persistent current trapped in the solenoid. Dynamic control of the solenoid was then regained by energising the persistent mode switch heaters.

The solenoid current was swept down quite slowly over a period of ∿1 hour, mainly to render the demagnetisation as reversible as possible. As the temperature of the cell and guard fell below ∿40mK, eddy current heating effects in the copper thermometer mounts became apparent with the increase in the Kapitza boundary resistances; the temperatures of the thermometers increased sharply, but decreased again as soon as the sweep was halted. For this reason the last few amps were swept down very slowly. The magnet was always put into the persistent mode before the power supply was switched off since on several occasions a voltage spike was generated which caused significant heating of the salts. The magnet leads were then disconnected and lowered into the main bath as smoothly as possible to avoid causing vibrational heating of the cell.

6.8 EXPERIMENTAL PROCEDURES AFTER DEMAGNETISATION

The behaviour of the cell thermometers immediately after a demagnetisation revealed that an appreciable thermal time constant existed within the experimental cell for temperatures below 40mK. The time constant τ_s increased with decreasing temperature, approximately according to the relationship

$$\tau_s = 1.142 \times 10^{+4}\ T^{-2.23} \qquad (6.8.1)$$

where τ_s is in minutes and T is in mK. Calculations showed that this behaviour was most probably due to thermal relaxation between regions of the salt not reached by the brush of very fine copper wires and those regions in close proximity to the wires. The latter regions

would tend to be slightly warmer owing to the influx of heat from the liquid in the experimental region. The conduction of this heat to the more remote, colder regions of salt could only take place through the helium filled interstitial spaces between the salt granules. Such narrow channels are effectively superleaks at very low temperatures and present very high thermal impedances. This factor, together with the high thermal capacity of the salt, gives rise to a time constant of the same order of magnitude as that observed. Similar calculations showed that, in comparison with this effect, the other thermal time constants within the system, in particular those between the thermometers and the helium, were negligible.

Once thermal equilibrium was well established throughout the cell, preliminary checks were carried out to ensure that movements of the cell bellows did not give rise to serious frictional heating. Typically, a step displacement of the bellows of ∿2mm caused the cell temperature to rise by ∿0.6mK, whilst driving the bellows slowly through the same distance produced a slightly smaller temperature rise of ∿0.4mK.

The temperature stability of the cell was good, the rate of rise of temperature being approximately 2mK per hour at the lowest temperatures, rising to 5mK per hour at temperatures above 30mK. These figures agree well with the predictions of section 4.5.

The useful "lifetime" of the guard salt depended strongly on whether or not the vortex fridge was in operation; if the vortex fridge was turned off immediately after a demagnetisation, then the guard warmed to 0.5K in the space of ∿1.5 hours. With the vortex

fridge running however, the lifetime was extended to over 7 hours, which again agrees well with the predictions of section 4.5.

Apart from causing slightly high warming rates, the incidence of 4.2K radiation on the experimental cell had a further undesirable effect, detected during a demagnetisation in which the cell was cooled below 15mK. After the demagnetisation, the resistance thermometer indicated a steady bottom temperature of ∿15mK, but according to the capacitance thermometer, the cell temperature continued to fall steadily for a further 20 minutes. Any difference between the thermal relaxation times of the two thermometers would be of the order of seconds. It is thought that the effect was due to the low temperature increase in the Kapitza boundary resistances between the thermometers and the helium sample. The small heat leak into the thermometers from 4.2K radiation would be accompanied by a temperature drop across the boundary resistances, causing the thermometers to read slightly high. It seems that the Kapitza resistances in the carbon thermometer system were somewhat greater than those in the capacitance thermometer system, so that one thermometer "bottomed out" before the other. The extremely high thermal resistivity of the carbon itself at very low temperatures could also have a role to play in this respect. Unfortunately, the calibration of the capacitance thermometer had shifted immediately prior to this particular demagnetisation, and a further shift took place soon after the completion of the demagnetisation, presumably due to voltage transients. This meant that the lowest temperature attained by the cell could not be inferred from the capacitance value. However, an estimate based on the starting conditions of the demagnetisation, indicated that the bottom temperature should have been ∿11.5mK. This figure was corroborated by substituting the thermal

Figure 6.9.1.
Flows from large level differences; the sequence of bellows movements.

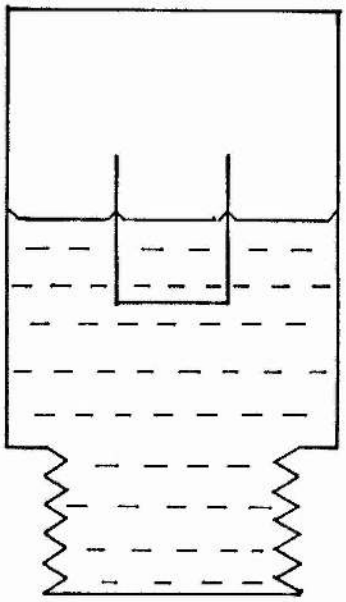

1

Equilibrium at 8 mm rim height

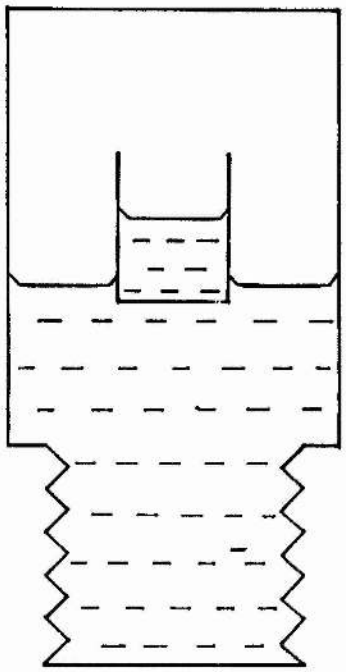

2

Outflow

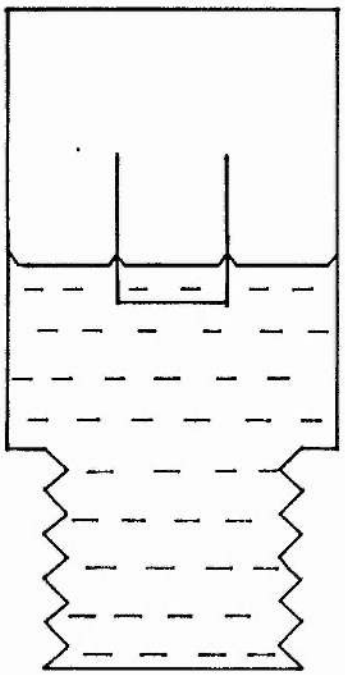

3

Equilibrium at 12 mm rim height

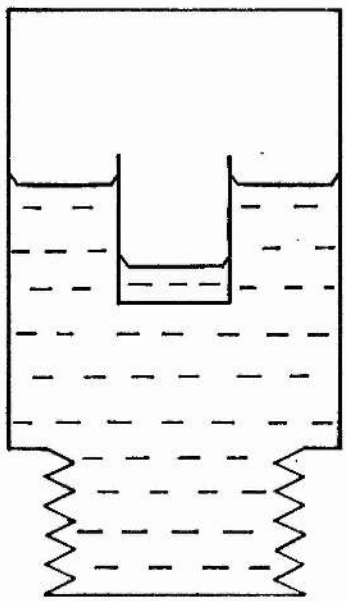

4

Inflow

time constant of the salt, as shown on the capacitance thermometer, into the empirical relation between the time constant and temperature, given in equation 6.8.1.

In some of the early runs the duration of the "experimental time", in which data could be taken at steady temperatures, was artificially curtailed by the need to refill the 1K pot. The higher temperatures of the 1K pot and vortex fridge during the refilling operation caused rapid warming of the guard salt. In later runs, the technique was adopted of increasing the power to the vortex fridge whilst refilling the pot, such that the vortex fridge was at all times maintained below 1K. The warming of the guard salt was now only minimal, and no heating of the cell was detected.

6.9 THE EXPERIMENTS

(a) Flows From Large Level Differences

Two types of experiment were performed on the flow of the superfluid helium film over the surface of the beaker. In the first type, the position of the bellows was adjusted to bring the inner and outer liquid levels into equilibrium at a distance of $\sim$8mm below the beaker rim. A step displacement of the bellows was then made such that an "outflow" from the beaker was initiated, terminating in inertial oscillations about an equilibrium rim height of $\sim$12mm. The step displacement was then reversed, so that the ensuing "inflow" caused the liquid levels to equilibrate at their original position. The sequence of bellows movements and the various configurations of the levels are shown schematically in figure 6.9.1.

During the flows and the inertial oscillations that followed, a chart recording was made of the off-balance signal from the "beaker level" bridge system. The zero of the lock-in amplifier was

offset to the left hand edge of the chart roll. The sensitivities of the chart recorder and amplifier were then adjusted such that by use of the zero suppression switch on the recorder, three sweeps across the chart could be executed before rebalancing of the bridge was necessary. In this way changes in off-balance sensitivity due to slight changes in the contact resistances of the bridge decade switches were kept to a minimum. The off-balance sensitivity could be deduced from the chart record, and this information, together with a knowledge of the capacitor sensitivity and the cell geometry, enabled the superfluid transfer rate to be calculated.

After each cycle of inflow and outflow the cell temperature was measured on the carbon resistance thermometer. The capacitance bridge oscillator had to be turned off during this procedure to prevent self-heating of the thermometer. The cell was then heated by means of a small resistance coil wound around the end of one of the copper wire bundles, and the inflow and outflow measurements were repeated at the new temperature. These "large level difference" experiments were carried out over the temperature range 20mK to 1.62K, and yielded information on the critical flow of the superfluid film, the behaviour of "metastable" rates and the damping of the inertial oscillations. The results are given in Chapters 7 and 8.

(b) Driven Flow at Small Level Differences

The second type of experiment consisted of equilibrating the liquid levels at a rim height of ~12mm, and then driving the outer level very slowly up or down at constant speed by means of the synchronous motor. Once the steady state was attained, the beaker level rose or fell at the same rate.

The amount of dissipation accompanying the flow could be inferred from the difference between the two levels. The motor speed could be adjusted to produce transfer rates well below the "critical" value, and the occurrence of dissipation during these "subcritical" flows could be studied as a function of the transfer rate.

The off-balance signals from both bridge systems were recorded using the two-pen chart recorder. The amplifiers were operated at 1/5 of the sensitivity used in the first type of experiment since inertial oscillations were often superimposed on the steady flow; these were not easily averaged unless several cycles were present on each section of the recorded trace. The amplifier sensitivities were adjusted such that both pens moved through equal distances for equal displacements of the liquid levels. The bridge balance points were not adjusted during an experiment, all rebalancing operations being performed with the zero suppression switch on the chart recorder. The experiments were performed between rim heights of 11 and 13mm since this region of the cell capacitor was free from irregularities caused by flaking of the gold film. The duration of a typical experiment was $\sim$4 minutes, and steady state conditions were usually obtained after the first two minutes. A record of a typical driven flow experiment is given in figure 8.2.1. The 0.3s time constant on the cell-level amplifier reflects the smoothness of the drive.

At the end of a suitable period of steady state flow, the motor drive was switched off and any level difference accompanying the flow subsequently decayed. The ensuing inertial oscillations were recorded so that the new equilibrium position of the levels could be deduced. From the chart record, the level difference at any point during the flow

could be calculated along with the transfer rate at that instant. The experiment was repeated at several temperatures between 11mK and 1.2K, for a range of subcritical and critical transfer rates. A discussion of the results is given in Chapter 8.

6.10 EMPTYING THE EXPERIMENTAL CELL

The 1K pot was allowed to boil dry and the vortex refrigerator was turned off. ^{4}He exchange gas was introduced into the inner vacuum chamber to bring the cell to a temperature of 4.2K and a pressure of 1 atmosphere. The cell-filling capillary was pumped on through a liquid nitrogen cooled charcoal trap, and the pure ^{4}He gas was collected in the three stainless steel storage tanks for re-use. If the cell pressure fell below 1 atmosphere due to cooling, additional exchange gas was introduced, or power was supplied to the cell heater. The cell was usually pumped out at 4.2K for at least 12 hours, such that the final pressure after evaporation of all the liquid was less than 1/20 atmosphere. By this means, overpressurisation of the cell on warming to liquid nitrogen temperature was avoided. For a similar reason, the cell pressure was reduced below $\frac{1}{4}$ atmosphere before warming from liquid nitrogen to room temperature was carried out.

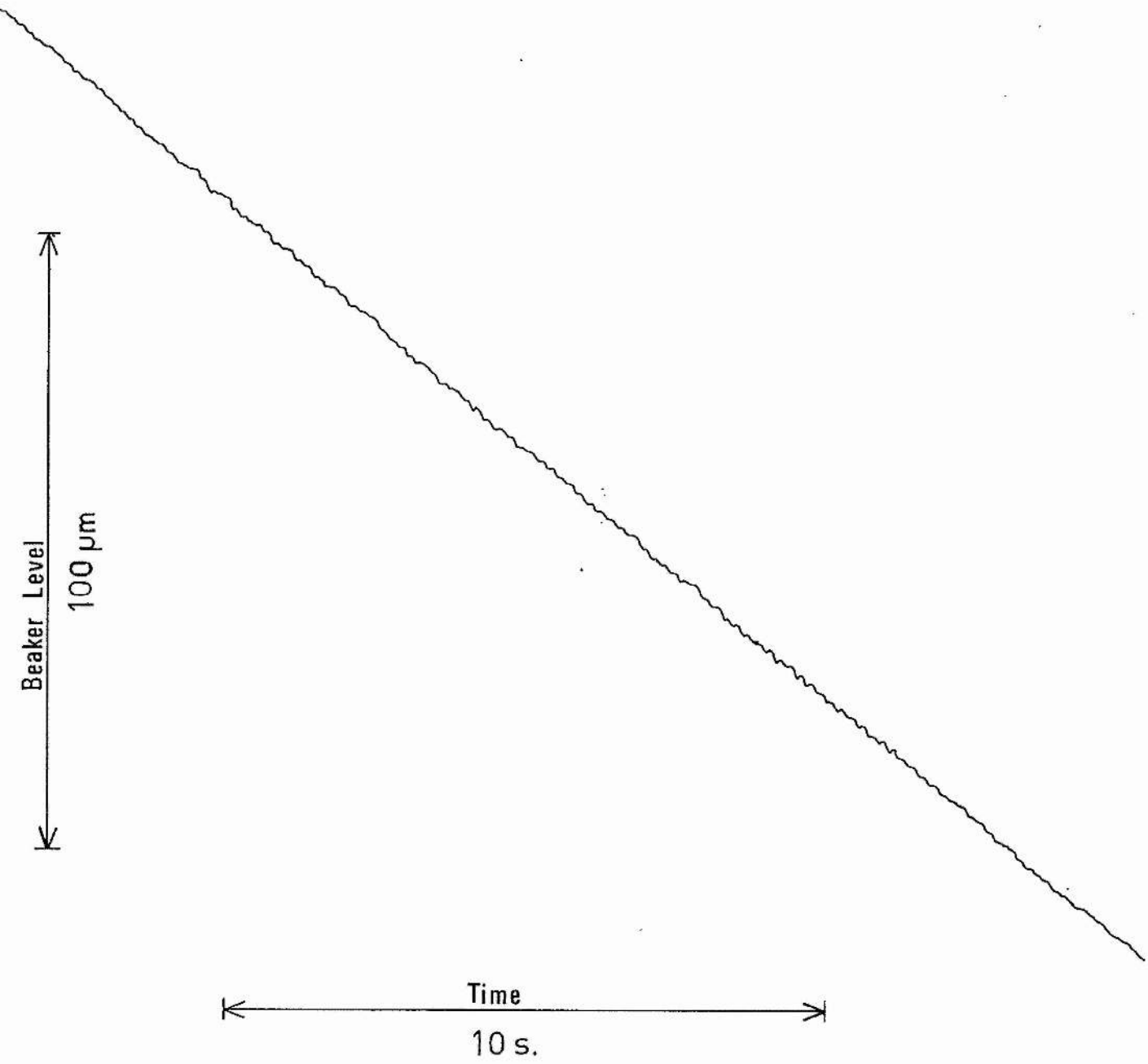

Figure 7.1.1.
Reproduction of a chart record showing the rate of change of the beaker level with time.

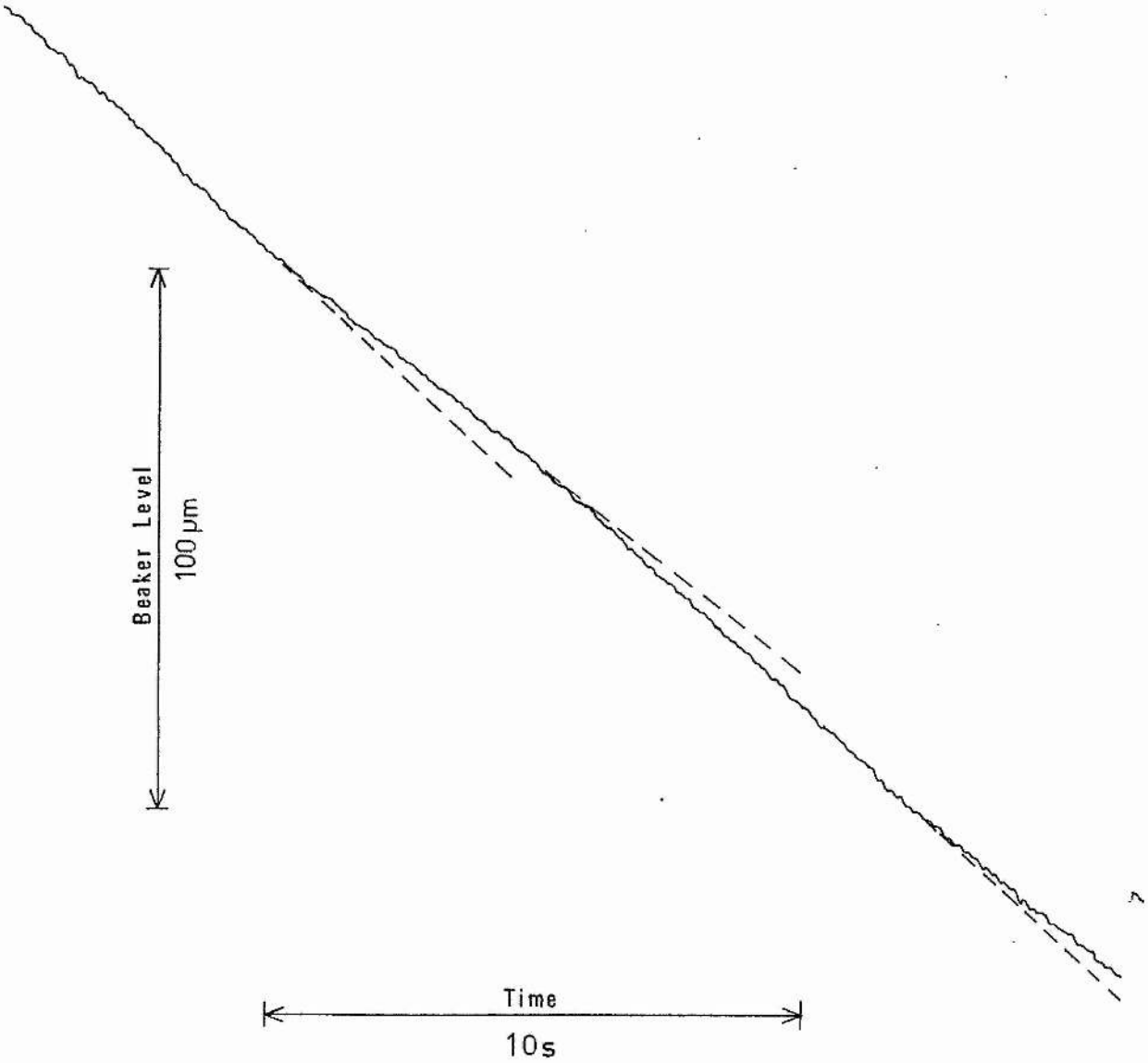

Figure 7.1.2.
Reproduction of a chart record showing transitions in the flow rate.

CHAPTER SEVEN

FILM TRANSFER RATES AT LARGE LEVEL DIFFERENCES

7.1 INTRODUCTION AND GENERAL OBSERVATIONS

In this chapter, the results of the experiments described in section 6.9.(a) will be presented. Both inflows and outflows, that is, flows into and out of the beaker, were studied over the temperature range 20mK $\lesssim T \lesssim$ 1.62K. Results were not taken below 20mK by this method since it was feared that the large Kapitza boundary resistances occurring at these low temperatures could lead to local heating of the film in the region of dissipation.

A portion of a chart record showing the rate of change of the beaker level with time following a step displacement of the outer level is reproduced in figure 7.1.1. The time constant on the lock-in amplifier was set at 0.1s for all these experiments. The quietness of the trace reflects the satisfactory performance of the cryostat anti-vibration mountings.

A common feature of all the experiments was that the film transfer did not proceed at one well-defined "critical" velocity. Rather, during a single flow the transfer rate switched abruptly from one value to another. This observation corroborates those made by earlier workers, as discussed in sections 3.3 and 3.9. The average lifetime of one of these "metastable" rates was $\sim$15s and the transitions in flow rate took place in $\sim$0.5s. A clear example of this type of flow behaviour is given in fig. 7.1.2, which is a reproduction of a chart recording showing three closely spaced rate changes.

At temperatures below $\sim$480mK the inner and outer liquid levels

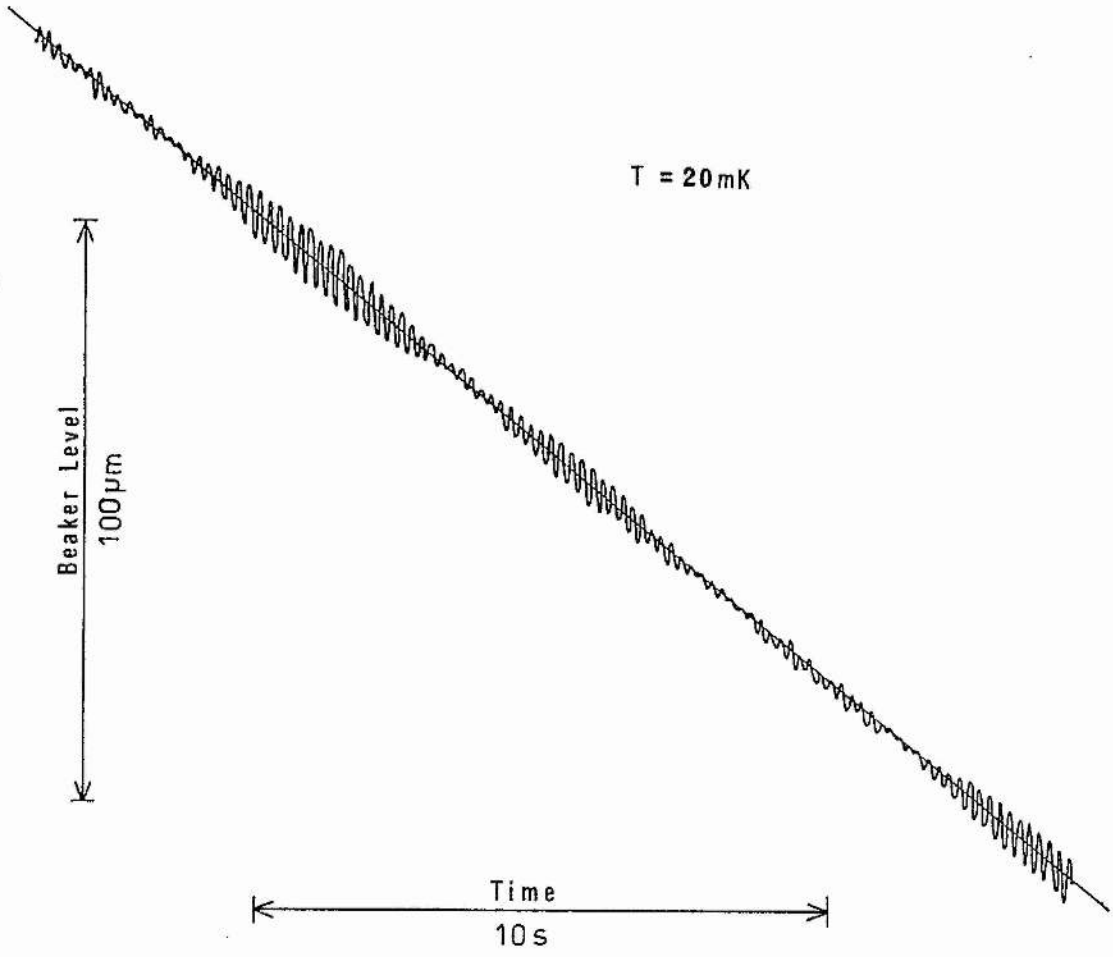

Figure 7.1.3.
Modulated oscillations on the beaker level, reproduced from a chart recording.

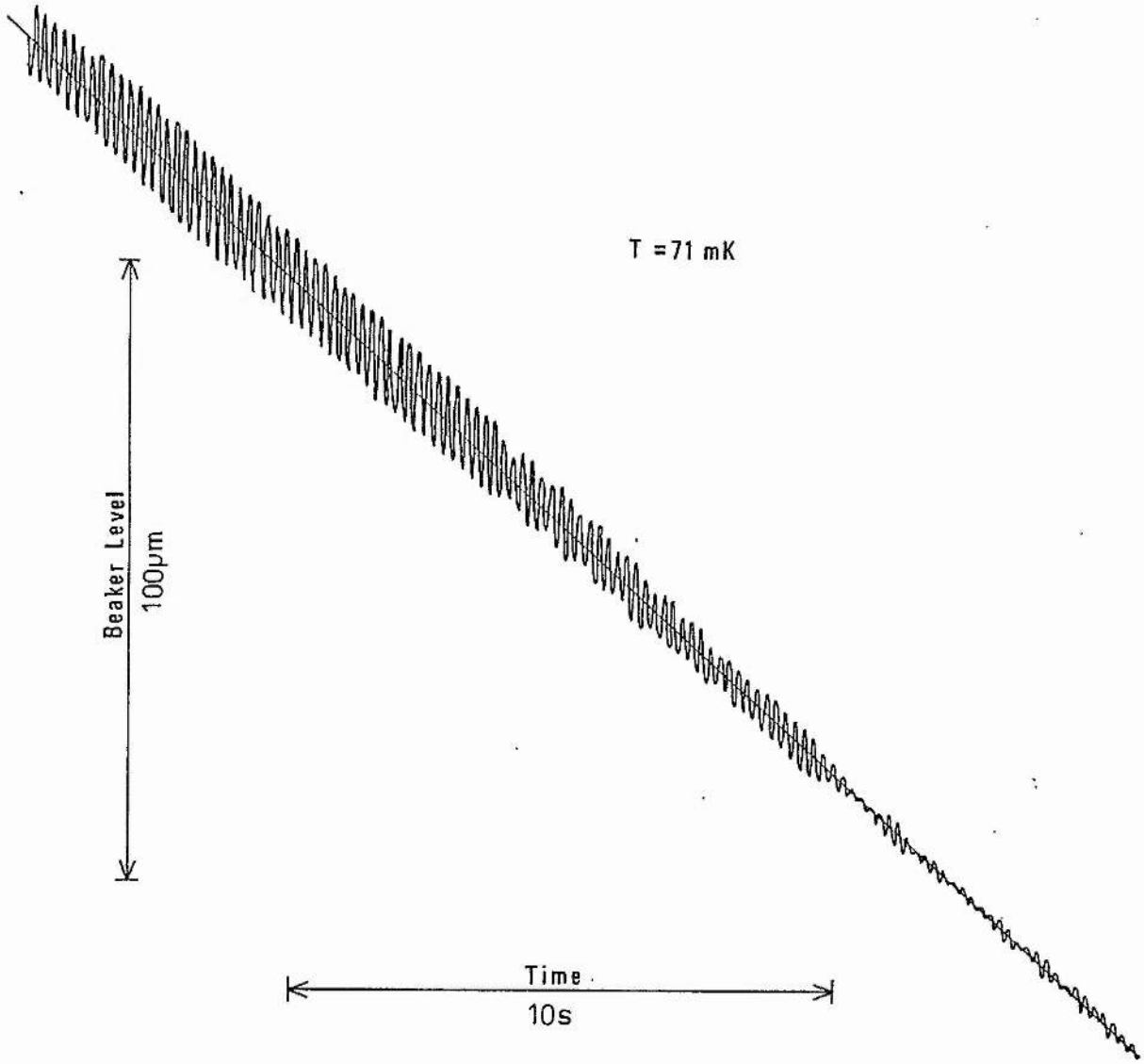

Figure 7.1.4.
Portion of a chart recording showing unmodulated oscillations on the beaker level.

occasionally exhibited oscillations of characteristic frequencies 5.75Hz and 7Hz respectively. Their amplitude was typically 6μm peak to peak, but often appeared to be modulated at a much lower frequency. An example from a recording of the beaker level is given in figure 7.1.3. In many observations of this effect the characteristic frequency of 5.75Hz was always observed, but the modulation frequency varied considerably and was quite often completely absent, as shown in figure 7.1.4. This implies that the modulation cannot be the result of a beating phenomenon between two closely spaced frequencies.

Above 480mK the amplitude of the oscillations fell below the resolution of the detectors on normal gain settings. However, with the detectors at full gain at 1.13K, the oscillations were observed to be still present, with a virtually constant amplitude of 0.2μm peak to peak. This temperature dependent attenuation is a strong indication that the effect is real rather than instrumental.

The oscillations could be due to standing third sound waves in parts of the superfluid film covering the inside surfaces of the experimental cell. As an example the frequency f of such a standing wave in the film covering the surface of the beaker is calculated in Appendix B. For a rim height of ∿1cm, f is found to be ∿6.8Hz, which is very close to the observed frequencies. Since the oscillations on each liquid level were of different frequency and could occur independently of each other it is not possible that a third sound wave in the film joining the two levels could be the origin of the phenomenon. However, the dimensions in the example are fairly typical of other features of the cell geometry, such as the level sensing capacitors, and the heights of various pieces of epibond, and it is

possible that two different third sound resonances, one inside the beaker and one outside, were giving rise to the observed effects. One puzzling feature was that the frequencies of the oscillations were independent of the position of the bulk liquid levels. From equation B9 one would expect the frequency of a third sound wave to vary inversely as $\sqrt{H}$.

Other possible origins of the oscillations are surface waves or U-tube oscillations within the level sensing capacitors. However, simple calculations show that the highest frequency given by these modes would be $\sim$3.5Hz and indeed, oscillations of this frequency were at times observed on the outer liquid level, interspersed with sections of 7Hz oscillations.

7.2 THE DEPENDENCE OF σ ON THE RIM HEIGHT

A general feature of the results was that, as a flow progressed, be it inflow or outflow, the metastable rates became distributed about progressively lower mean values. This can be understood in terms of a gradual change in the film profile as the liquid levels approach equilibrium. The limiting velocity is assumed to occur at the beaker rim where the film is thinnest. The film thickness d at this point therefore determines the value of the observed volume transfer rate. d itself depends on the distance from the rim to the nearest reservoir level. Let this distance be H, and note that for outflows, H is the rim height of the inner level and vice versa. It can be seen from section 6.9 that during an outflow H increases from $\sim$8mm to $\sim$12mm, whilst for an inflow H increases from $\sim$4mm to $\sim$8mm. This increase in H causes the film to thin at the beaker rim and brings

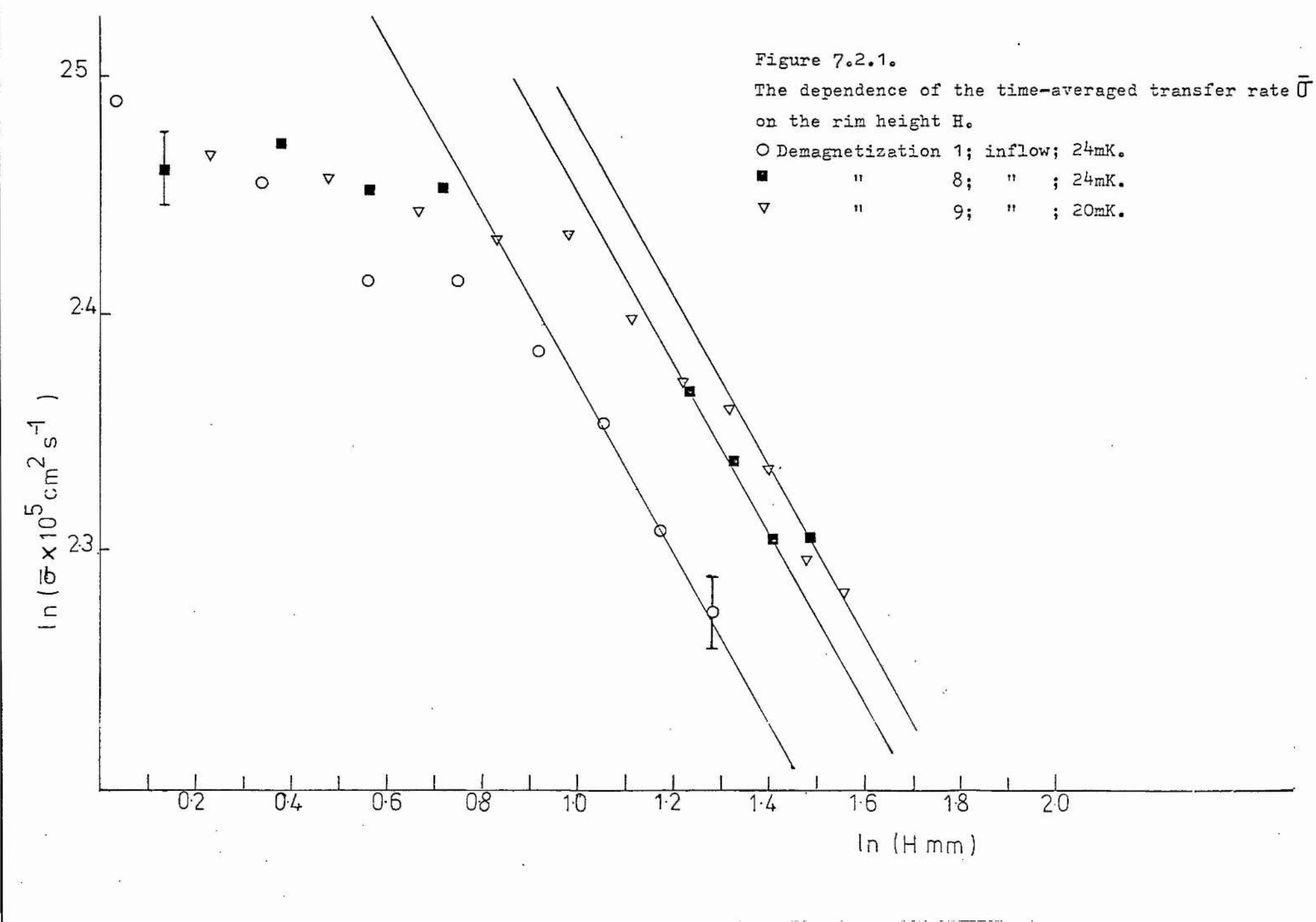

Figure 7.2.1.
The dependence of the time-averaged transfer rate $\bar{\sigma}$ on the rim height H.
○ Demagnetization 1; inflow; 24mK.
■ " 8; " ; 24mK.
▽ " 9; " ; 20mK.

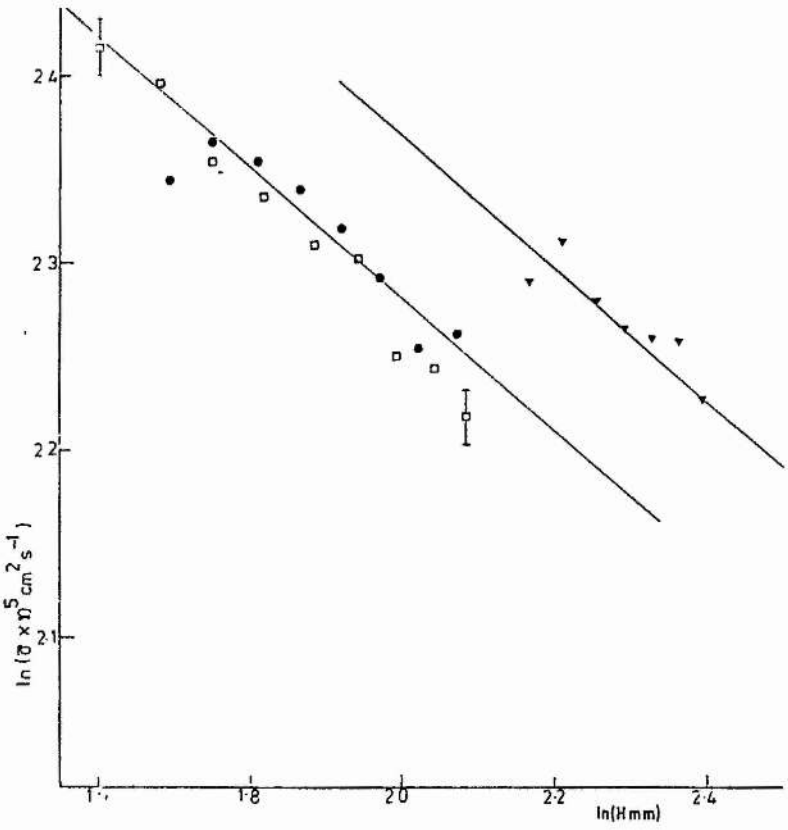

Figure 7.2.2.
The dependence of the time-averaged transfer rate $\bar{U}$ on the rim height H.
□ Demagnetization 1; outflow; 25mK.
▼ " 1; " ; 32mK.
● " 1; inflow ; 33mK.

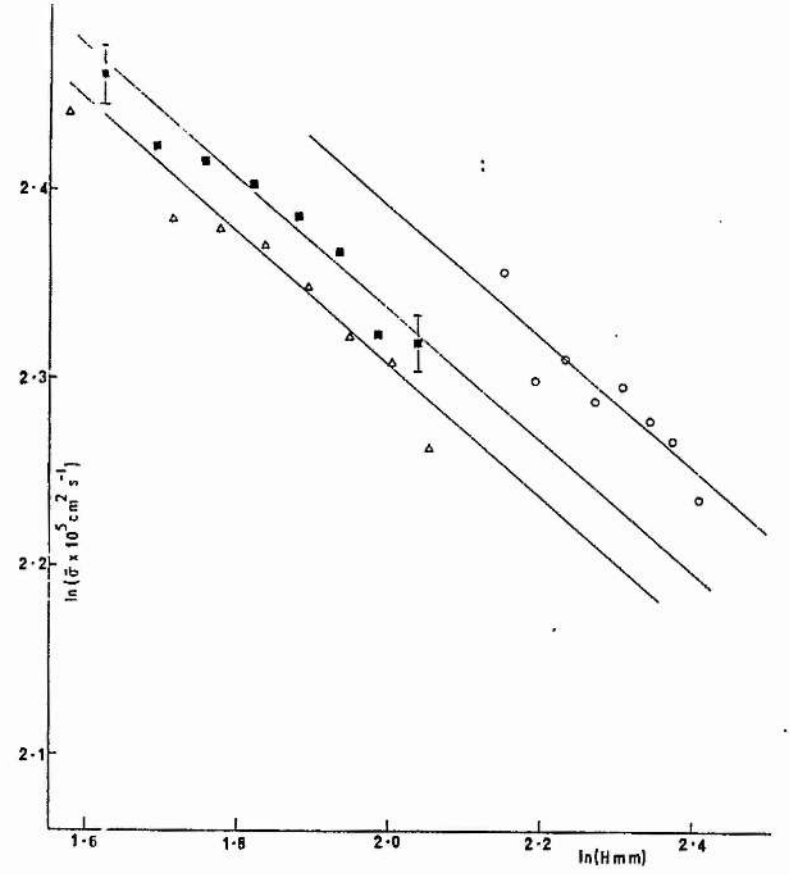

Figure 7.2.3.
The dependence of the time-averaged transfer rate $\bar{U}$ on the rim height H.
○ Demagnetization 1; outflow; 36-46mK.
△ " 1; inflow ; 50-72mK.
■ " 1; " ; 83-99mK.

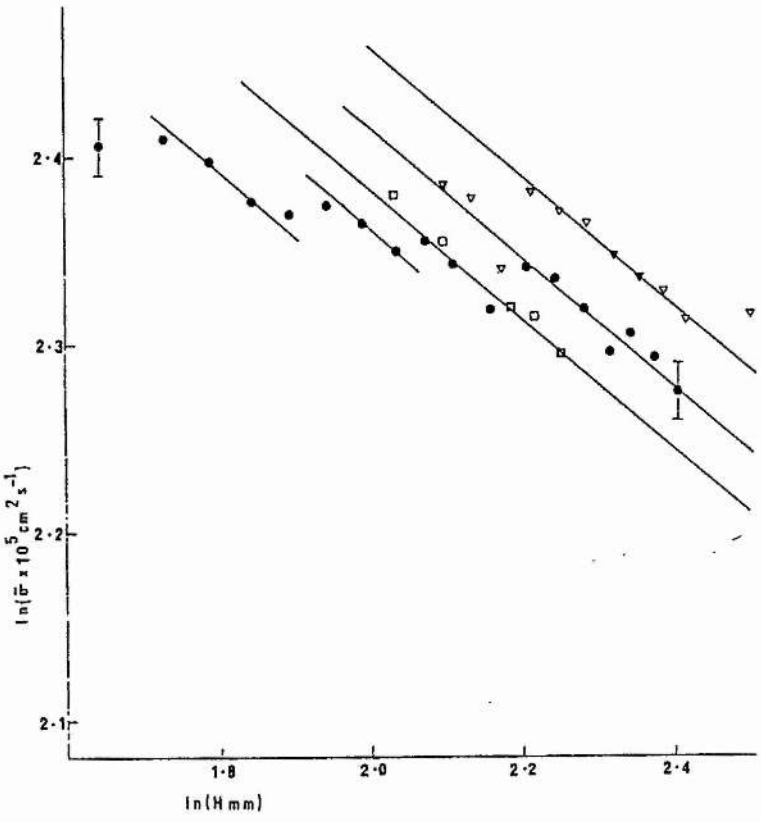

Figure 7.2.4.
The dependence of the time-averaged transfer rate $\bar{U}$ on the rim height H.
● Demagnetization 8; outflow; 26mK.
□ " 8; inflow ; 37mK.
▽ " 8; outflow; 147mK.

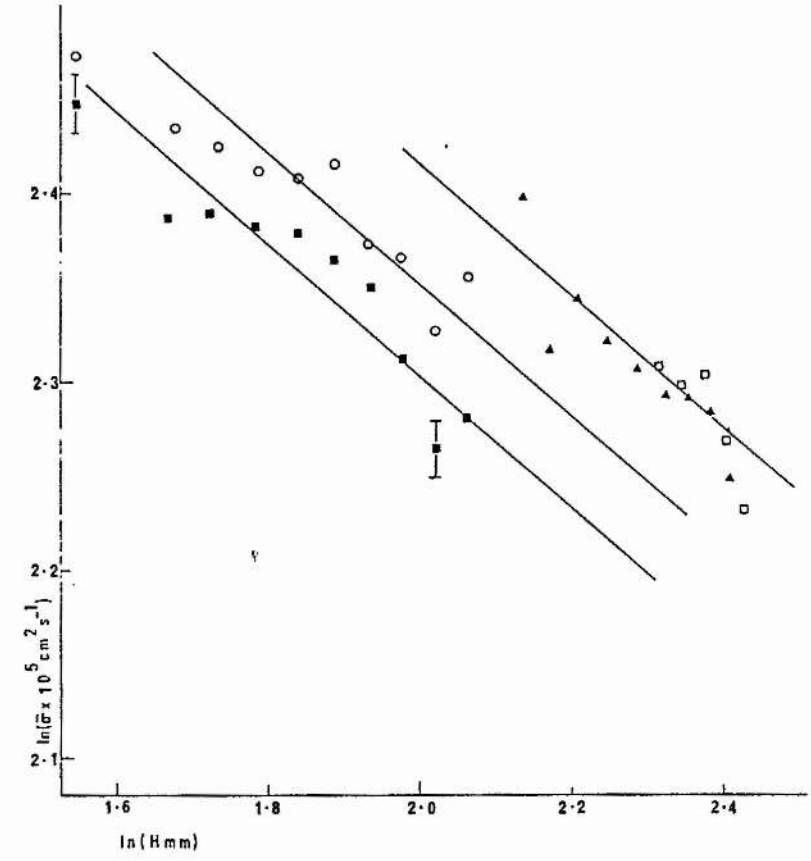

Figure 7.2.5.
The dependence of the time-averaged transfer rate $\bar{U}$ on the rim height H.
□ Demagnetization 8; outflow; 50mK.
■ " 8; inflow ; 61mK.
▲ " 8; outflow; 71mK.
○ " 8; inflow ; 131mK.

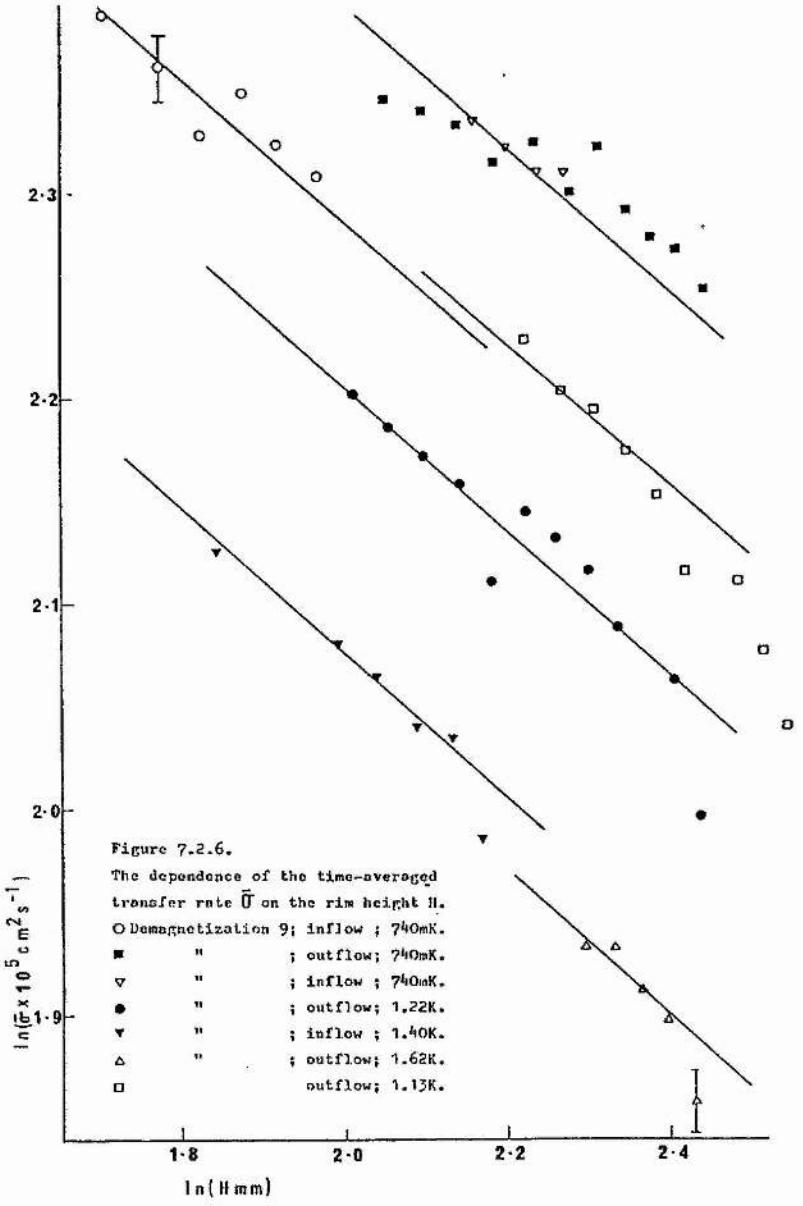

Figure 7.2.6.
The dependence of the time-averaged transfer rate $\bar{U}$ on the rim height H.
○ Demagnetization 9; inflow ; 740mK.
■ " ; outflow; 740mK.
▽ " ; inflow ; 740mK.
● " ; outflow; 1.22K.
▼ " ; inflow ; 1.40K.
△ " ; outflow; 1.62K.
□ outflow; 1.13K.

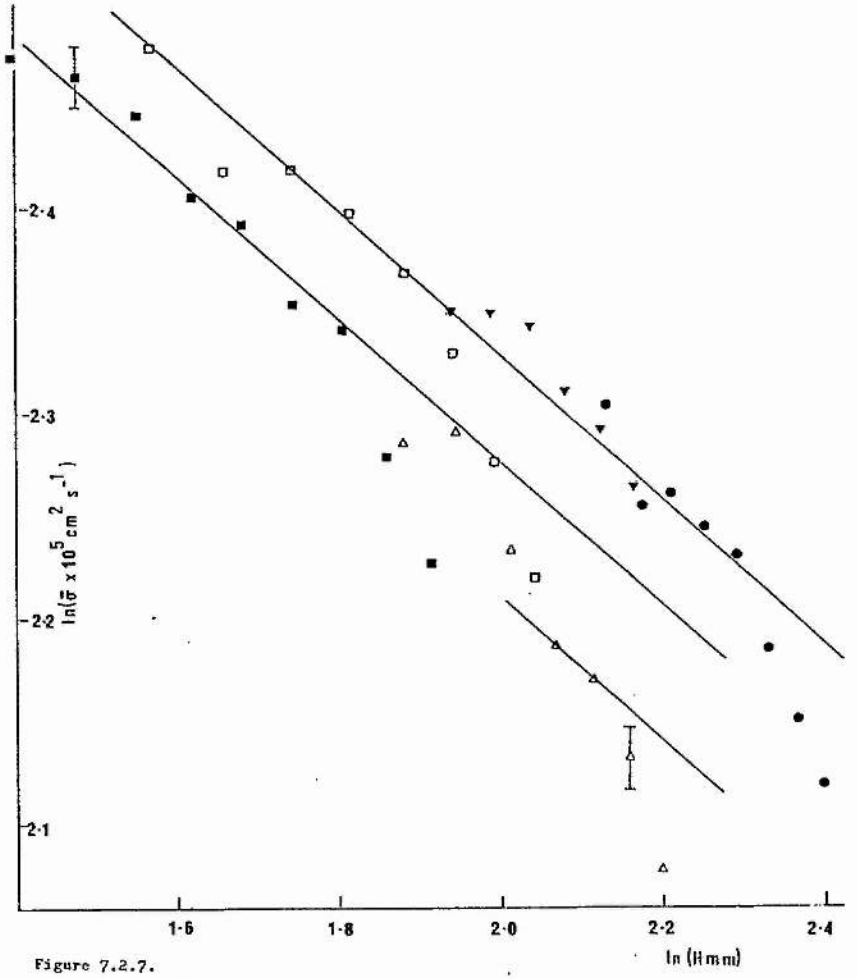

Figure 7.2.7.
The dependence of the time-averaged transfer rate on the rim height H.
▼ Demagnetization 1; inflow ; 780-820mK.
□ " ; " ; 980-990mK.
■ " 9; " ; 1.00 K.
● " 1; outflow; 1.05 K.
△ inflow ; 1.12 K.

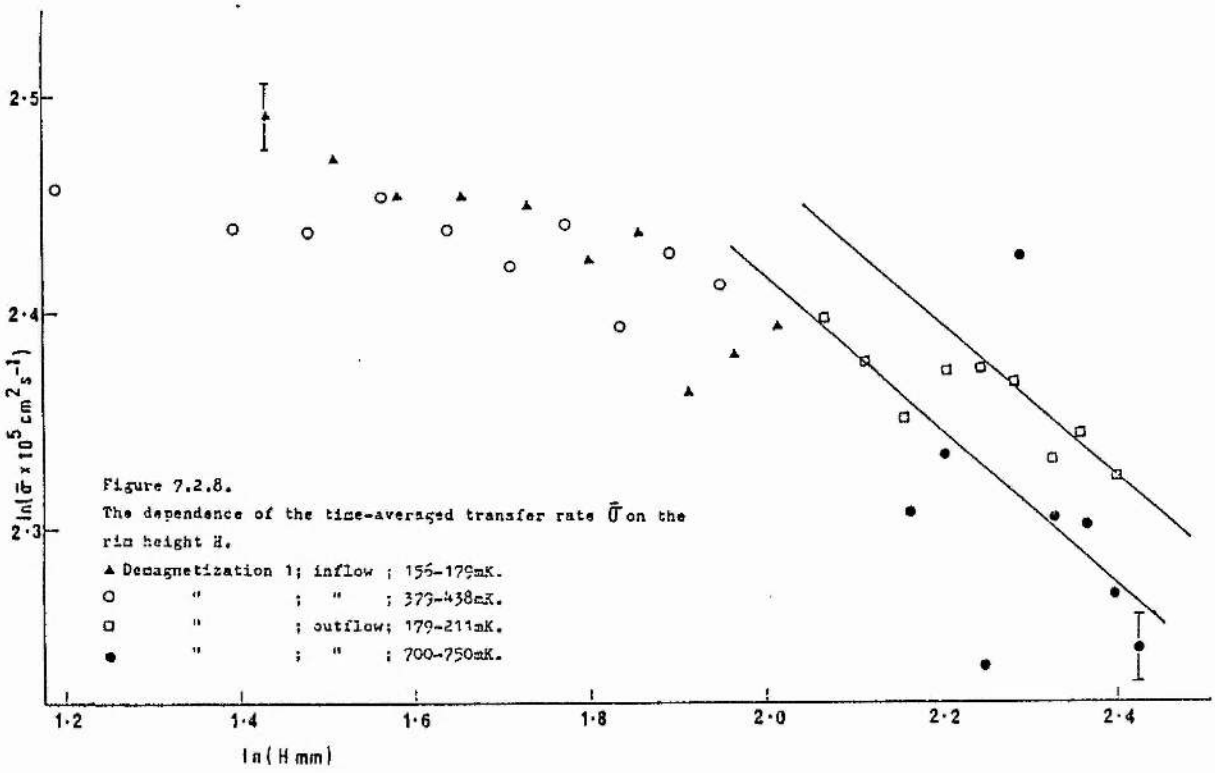

Figure 7.2.8.
The dependence of the time-averaged transfer rate $\bar{U}$ on the rim height H.
▲ Demagnetization 1; inflow ; 156-179mK.
○ " ; " ; 379-438mK.
□ " ; outflow; 179-211mK.
● " ; " ; 700-750mK.

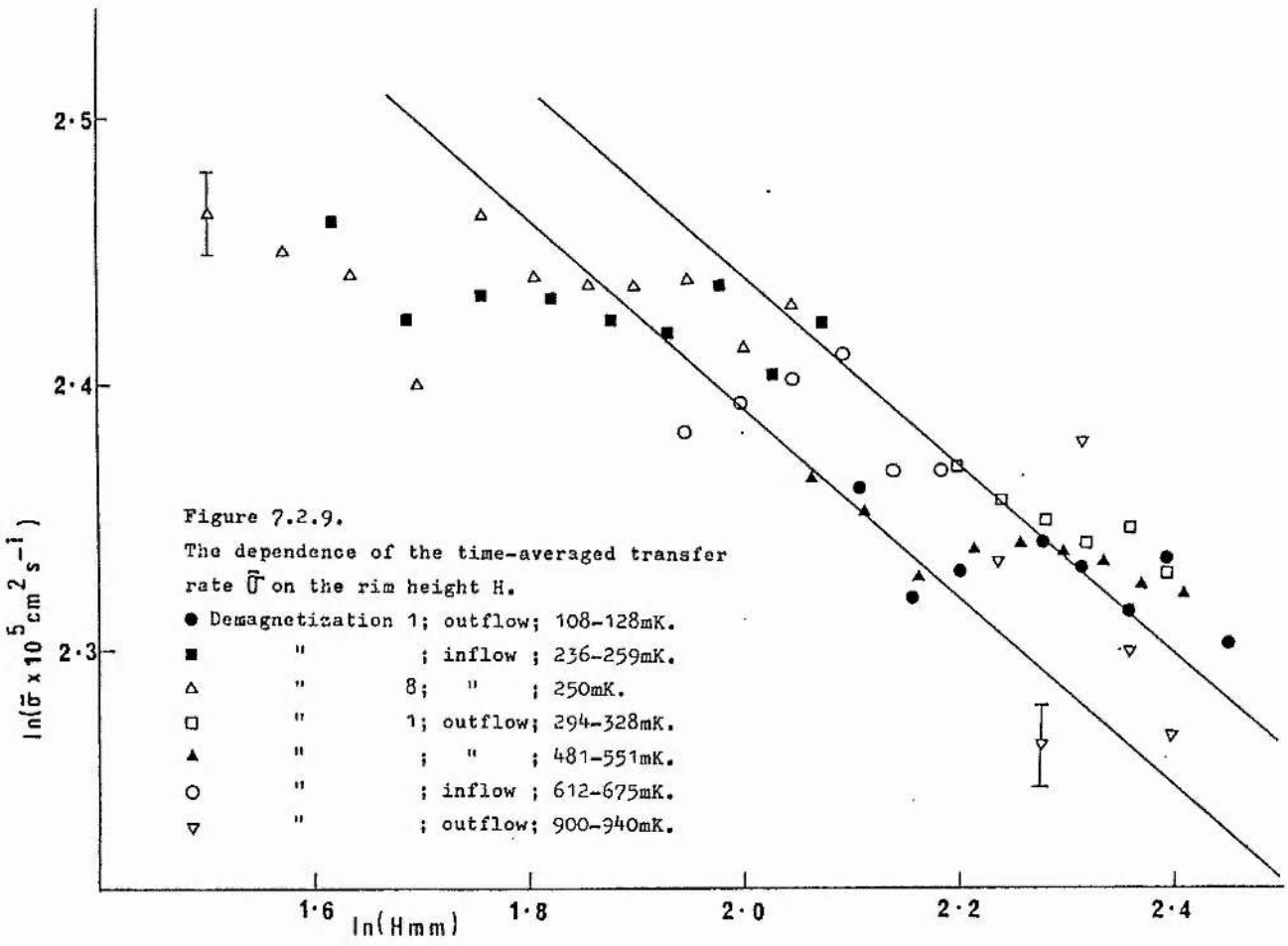

Figure 7.2.9.
The dependence of the time-averaged transfer rate $\bar{U}$ on the rim height H.
● Demagnetization 1; outflow; 108-128mK.
■ " ; inflow ; 236-259mK.
△ " 8; " ; 250mK.
□ " 1; outflow; 294-328mK.
▲ " ; " ; 481-551mK.
○ " ; inflow ; 612-675mK.
▽ " ; outflow; 900-940mK.

about the gradual drop in the transfer rate. Also, the variation of H over different ranges during inflows and outflows causes σ to vary over different ranges, and this behaviour must be compensated for if intercomparison of inflows and outflows is to be possible.

From equation (1.8.1.)

$$\sigma = \frac{\rho_s}{\rho} v_c d,$$

and assuming that the film thickness is given by equation (1.7.3) as

$$d = \frac{k}{H^{1/n}},$$

then

$$\sigma = \frac{\rho_s}{\rho} v_c \frac{k}{H^{1/n}}. \qquad (7.2.1)$$

In particular,

$$\sigma H^{1/n} = \frac{\rho_s}{\rho} v_c k, \qquad (7.2.2)$$

which is the transfer rate, normalised to unit rim height. This quantity will henceforth be referred to as σ_N.

An independent determination of n will be made from the present results, but before this is possible, a suitable method must be adopted for reducing the profusion of metastable rates to representative average values. It would have been impractical to measure every single metastable rate occurring during a flow experiment. Instead time-averages were taken. These were measured from the chart roll over consecutive periods of about 50s, and it was found that about seven such readings could be made during a typical experiment. These time-averaged values of σ will be referred to as $\bar{\sigma}$. For each flow experiment carried out, a plot of ℓn H versus $\ell n\ \bar{\sigma}$ was constructed, where H is the rim height at the mid-point of the time average. The results are shown in figures 7.2.1. to 7.2.9. From equation 7.2.1.

such a plot should be a straight line of gradient $-1/n$ and intercept $\ell n(\frac{\rho_s}{\rho} v_c k)$, for a flow that proceeds at constant v_c and T. Changing the temperature should cause a change in the intercept but not the gradient.

Inspection of the results shows that two types of behaviour are manifested. For temperatures in the ranges $20mk \lesssim T \lesssim 150mK$, and $740mk \lesssim T \lesssim 1.625K$ (figures 7.2.1. to 7.2.7.), a linear relationship between $\ell n\ \bar{\sigma}$ and ℓn H would indeed seem to fit the experimental data satisfactorily, with one or two exceptions which will be discussed below. The gradient of the line is the same for both inflows and outflows and appears to remain independent of temperature. The best fit to the data is obtained with $n = 2.85 \pm .25$. Where appropriate, this line has been superimposed on the experimental points in the figures. For rim heights of less than $\sim$3mm figure 7.2.1. shows that n increases with increased film thickness. This is in accordance with the Lifshitz theory of the retarded Van der Waals potential. Unfortunately it would appear that at the smallest rim heights n far exceeds the upper limit of 4 set by the Lifshitz theory.

Figures 7.2.8 and 7.2.9. show, with two exceptions, the data taken in the central temperature region $150mK \lesssim T \lesssim 740mK$. On the whole, these flows exhibit no particular dependence of $\bar{\sigma}$ on H; indeed some of the flows have points which appear to be almost randomly scattered, far in excess of the experimental error in measuring $\bar{\sigma}$. For other flows the value of $\bar{\sigma}$ remains constant irrespective of the value of H. It would seem improbable that in this temperature region the film profile becomes independent of H. Rather, it would appear that the selection of metastable rates for some reason is no longer

governed by the rim height. Instead of remaining within a fairly narrow band around a rim-height-dependent mean value, the metastable rates now appear to be free to vary over a much wider range, giving an apparent random character to the time-averaged transfer rate. For the sake of consistency, the data from this central temperature region will be analysed in exactly the same way as the results from the more orderly regions on either side.

7.3 COMPARISON OF INFLOWS AND OUTFLOWS

Previous work on film transfer (section 3.3) has shown that, for thick-walled beakers, the nature of inflows and outflows is rather different. For outflows, the region of dissipation is concentrated at the inner edge of the beaker rim whilst for inflows it can extend for a considerable distance down the inner wall of the beaker. This means that for the same difference in the liquid levels, the chemical potential gradient is much greater for an outflow than it is for an inflow. This in turn causes the transfer rate to be different in the two cases. The beaker used in these experiments was comparatively thin-walled (0.216mm) and one would not in this case expect to see any substantial differences between inflows and outflows. With reference to figures 7.2.1. to 7.2.9., if comparisons are made between inflows and outflows occurring over the same range of rim height and at the same temperature then this is indeed seen to be true. Unfortunately there are not many instances where the same rim height ranges are covered, owing to the cyclic method employed in taking the results (section 6.9). However, in figure 7.2.2. it can be seen that the data from the outflow at 25mK lies scattered around essentially the same line as that from the inflow at 33mK. Also, in figure 7.2.4., the 26mK data and the 37mK data agree tolerably over a restricted range of H.

Again, in figure 7.2.6., the inflow and outflow at 740mK show good agreement.

7.4 THE DEPENDENCE OF v_c ON THE RIM HEIGHT

In the above discussion, much emphasis has been placed on the importance of only comparing flow data that have been taken over the same region of H. This argument will now be developed more fully.

With reference to figure 7.2.6. consider the points O and ∇ (both inflows at 740mK). They are seen to lie around lines of the same gradient but completely different intercepts. From equation 7.2.1. the intercept is the quantity $\frac{\rho_s}{\rho} v_c k$, and since the only difference between the two flows is the range of rim height it seems that there is a strong dependence of v_c on the value of the rim height at which the flow is started. In particular, v_c increases with increasing H, which is the same as decreasing film thickness d. This behaviour could be connected with the $d^{-\frac{1}{4}}$ dependence of v_c discussed in section 3.2. However, the data are suggestive of a more complicated phenomenon; at the start of a flow the metastable rates are distributed about a mean value of v_c which seems to remain constant for moderate changes in the rim height, but which can then apparently jump discontinuously to new values. This "step-like" behaviour is most clearly seen in the outflow data at 26mK, displayed in figure 7.2.4. The flow covers a large range of rim heights and v_c increases discontinuously three times as H increases. As most of the other flows cover smaller ranges of H, this behaviour of v_c only shows up when comparisons are made between different flows. Apart from the case at 740mK cited earlier, other examples are : (i) the outflows at 25 and 32 mK in figure 7.2.2.; (ii) the inflows at 24 and 33mK (from demagnetization 1) in figures

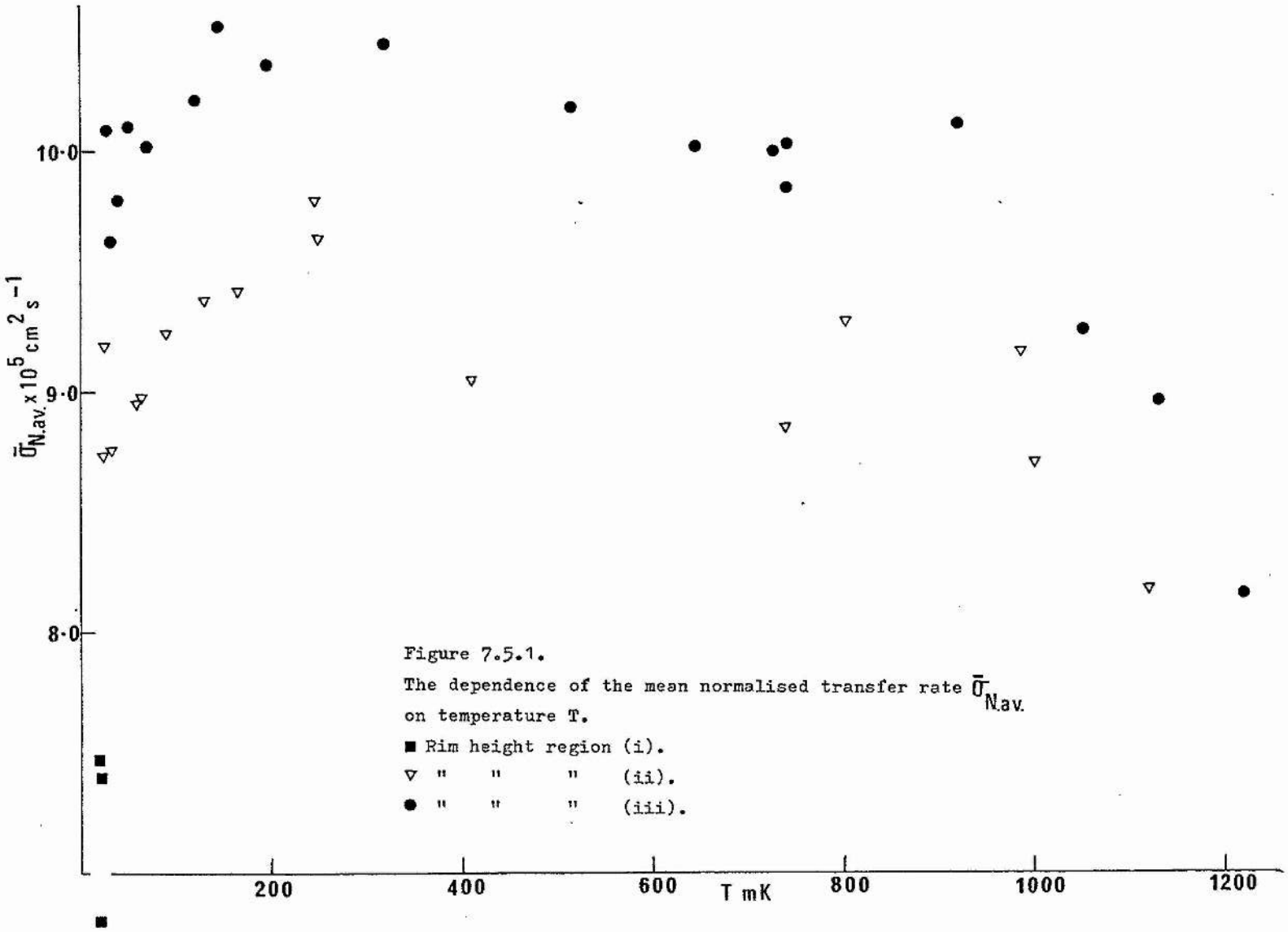

Figure 7.5.1.
The dependence of the mean normalised transfer rate $\bar{\sigma}_{N.av.}$ on temperature T.
■ Rim height region (i).
▽ " " " (ii).
● " " " (iii).

7.2.1. and 7.2.2. The small temperature differences are of no great consequence. Bearing in mind that at similar temperatures inflows and outflows are directly comparable in this experiment, many more instances of discontinuous increases of v_c with increasing H can be found in the data.

7.5 NORMALISATION OF σ

Following the discussion of section 7.2. the time-averaged transfer rate normalised to unit rim height is taken as the quantity

$$\bar{\sigma}_N = \bar{\sigma} H^{1/n} . \qquad (7.5.1.)$$

The best fit to the data was given by $n = 2.85 \pm .25$, which contrasts with the result of $n = 3.7$ obtained by Crum et al. This discrepancy could be a consequence of the differing film velocities in the two experiments.

For each of the flows shown in figures 7.2.1. to 7.2.9. the data points were normalised according to equation (7.5.1.). The values of $\bar{\sigma}_N$ obtained for each flow were then averaged, yielding a flow rate $\bar{\sigma}_{N.av.}$ characteristic of temperature and rim height region. A plot of $\bar{\sigma}_{N.av.}$ against temperature is shown in figure 7.5.1., where different symbols are given to flows occurring over the three rim height ranges (i) 2.9mm to 4.5mm, (ii) 4.5mm to 7.8mm, (iii) 7.8mm to 11mm.

It can be seen from the figure that the data from rim height ranges (ii) and (iii) falls on two roughly parallel curves whilst the three points from region (i) are strongly suggestive of the start of a third curve at much lower σ. This observation is particularly striking for temperatures less than 250mK where the results are less

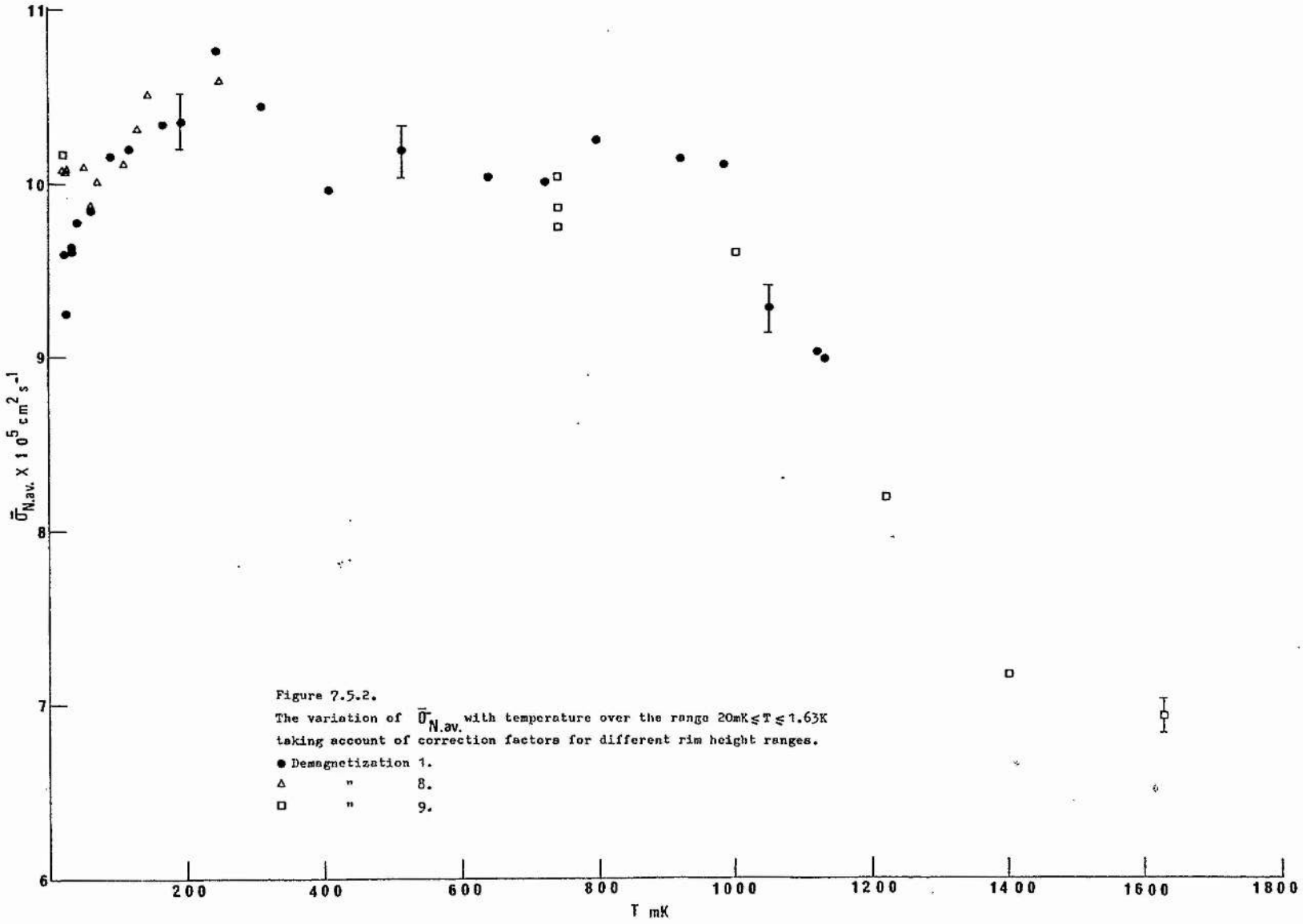

Figure 7.5.2.
The variation of $\bar{\sigma}_{N.av.}$ with temperature over the range $20mK \leq T \leq 1.63K$ taking account of correction factors for different rim height ranges.
● Demagnetization 1.
△ " 8.
□ " 9.

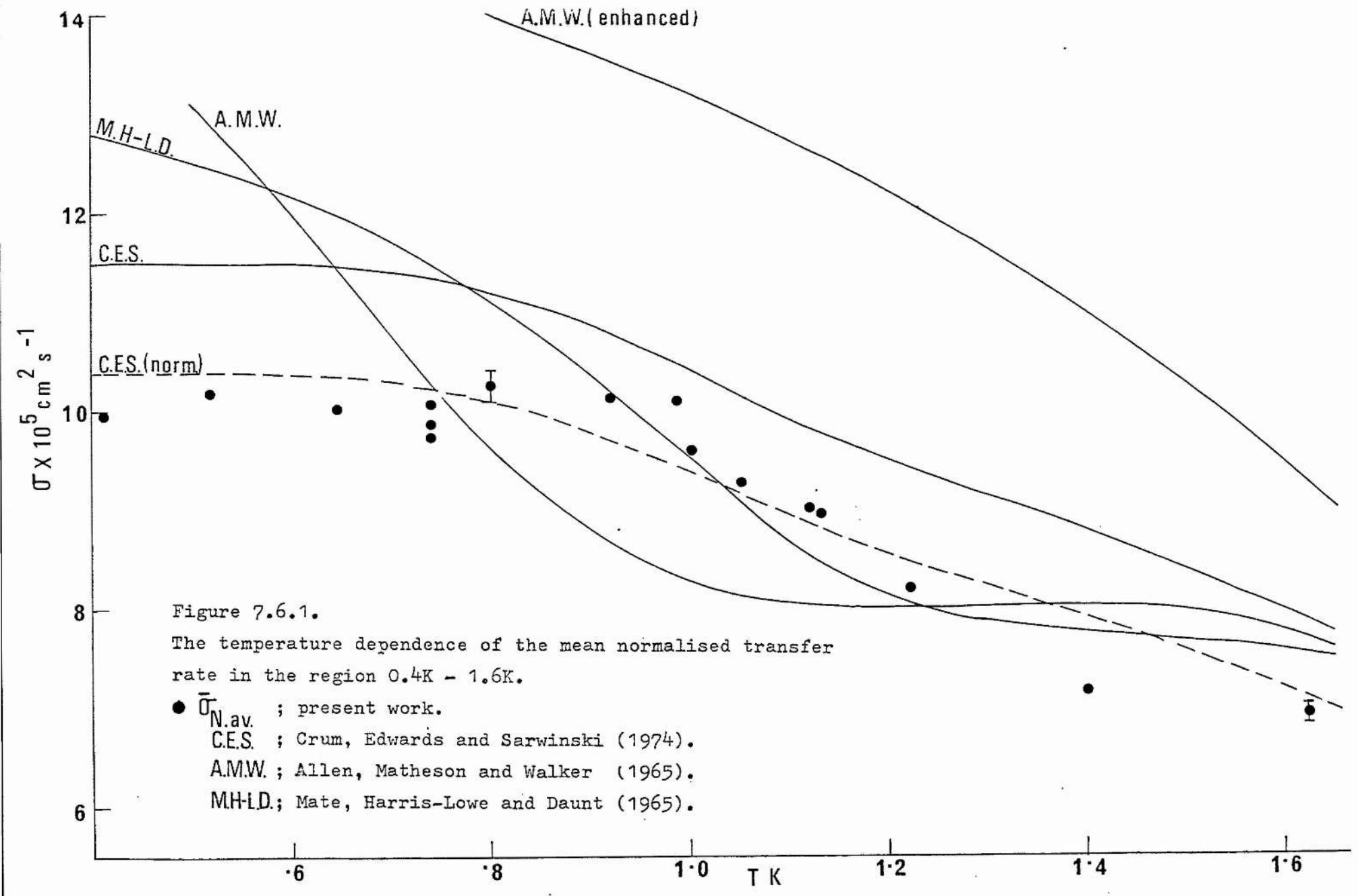

Figure 7.6.1.
The temperature dependence of the mean normalised transfer rate in the region 0.4K - 1.6K.

- ● $\bar{\sigma}_{N.av.}$; present work.
- C.E.S. ; Crum, Edwards and Sarwinski (1974).
- A.M.W. ; Allen, Matheson and Walker (1965).
- M.H-L.D.; Mate, Harris-Lowe and Daunt (1965).

scattered. It would thus seem that within each of the three rim height ranges specified above, there are no discontinuities of v_c, and furthermore, the same temperature dependence of v_c is observed in each range, as shown by the parallel nature of the curves. To allow for the discontinuous changes in v_c between the ranges it is necessary to introduce empirical factors, and to this end the data in region (i) has been multiplied by 1.36 whilst that in region (ii) has been multiplied by 1.10. The final curve for the variation of $\bar{\sigma}_{N.av.}$ with temperature is given in figure 7.5.2.

7.6. THE FORM OF THE $\bar{\sigma}_{N.av.}/T$ CURVE

With reference to figure 7.5.2., the salient features of the curve are (i) the initial steep rise in σ as the temperature falls from 1.6K to 1K, (ii) the almost abrupt levelling out into a plateau region between 1K and 400mK, (iii) a sudden increase to a maximum in the region of 250mK, (iv) a steady fall in σ below 250mK and an apparent upward trend below 25mK, shown by half of the data. These parts of the curve will each be discussed in turn.

(i) The initial rise in σ between 1.6K and 1K.

The results in this region are in qualitative agreement with those of previous workers. In figure 7.6.1. the smoothed curves from the work of three other groups are superimposed on the present results over the temperature interval 1.65K to 0.4K. There can be no doubt that over this temperature interval the film transfer rate increases by between 43% and 70%. Further than this general observation, quantitive comparison between the curves is, at first sight, poor. This is partly because the present results are normalised to 1cm rim height, whilst the other curves are for un-normalised results at differing rim heights.

In the experiments of Crum, (Thesis 1973) all flows were started at a rim height of 4.8mm and the rates measured were those that occurred during the first 200s of flow, corresponding to a fall in the liquid level of 1.78mm. The mean rim height of the reported data is therefore 5.7mm If this rim height is used in the normalisation equation 7.5.1. with n = 2.85, then a correction factor of 0.82 is obtained. Furthermore, as the very same beaker has been used in the present work, then the various correction factors for different rim height ranges should also be applicable. From section 7.5. it can be seen that all the data of Crum was taken over rim height region (ii), and should therefore be multiplied by a further factor of 1.10. The dotted curve in figure 7.6.1. shows the corrected data which is in fair agreement with the present results.

Quite good agreement is obtained with the results of Mate et al over the region where σ is increasing, although quite different behaviour is observed at lower temperatures. In fact the curves that show the largest increase in σ at low temperature are for flow over glass, whilst in the present work and that of Crum et al, which show curves levelling out into a plateau region, a stainless steel substrate was used.

(ii) Differences between the dissipation regimes above and below 1K.

With reference to figure 7.5.2. it would seem , from the abrupt nature in which the plateau region is entered below 1K, that this temperature marks a transition between different types of dissipative behaviour. This speculation is supported by the curves of $\ell n\, \sigma / \ell nH$ for this temperature region, displayed in figures 7.2.6. and 7.2.7.. At temperatures below 980mK the transfer rate is completely independent

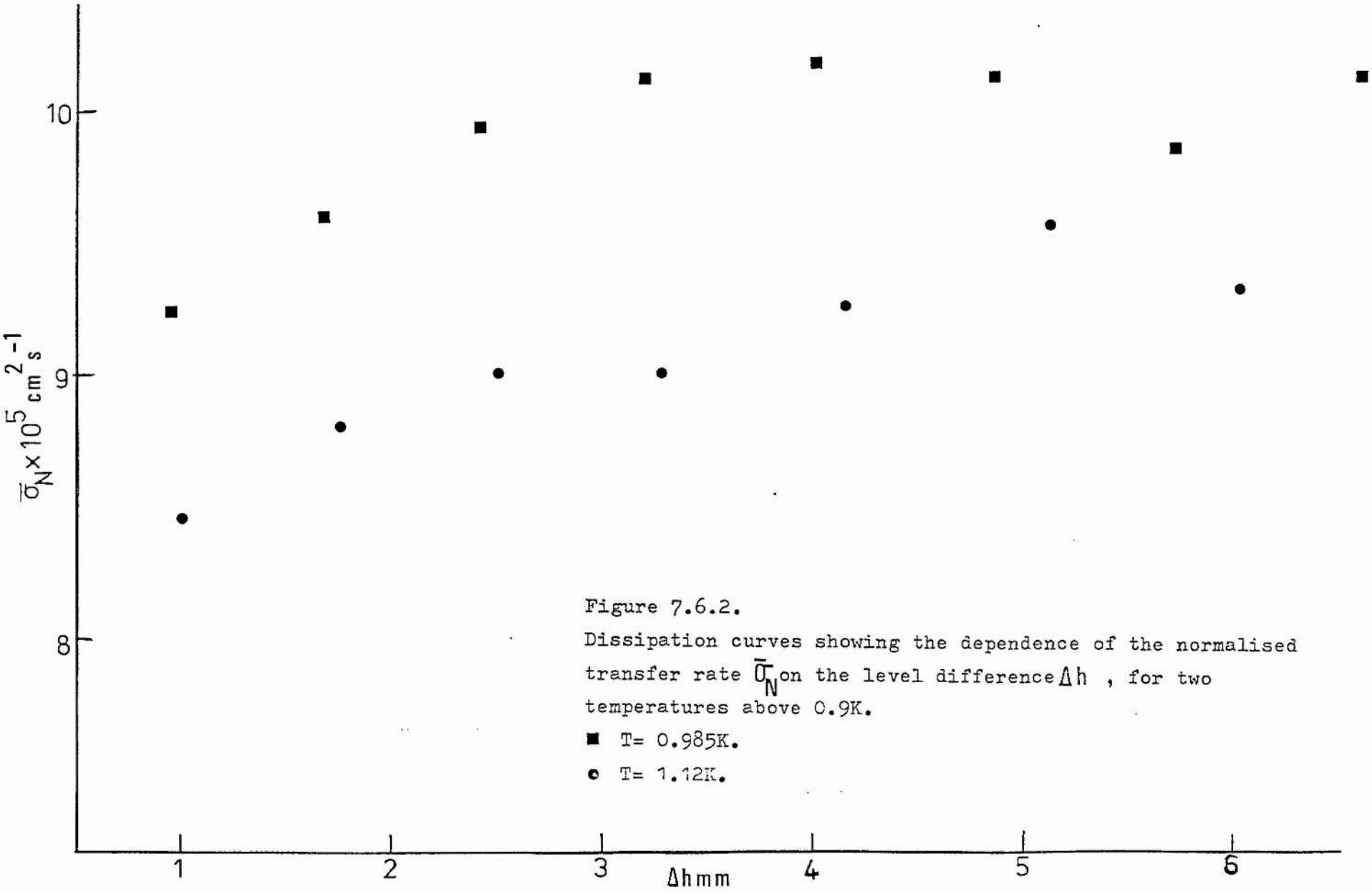

Figure 7.6.2.
Dissipation curves showing the dependence of the normalised transfer rate $\bar{\sigma}_N$ on the level difference Δh , for two temperatures above 0.9K.

■ T= 0.985K.

● T= 1.12K.

of the level difference between the reservoirs. The fall in σ during a flow is accounted for satisfactorily by the thinning of the film as the rim height slowly increases. However, for temperatures above 980mK, an anomalous drop of σ occurs towards the end of each flow, giving the impression that as the levels approach equilibrium, σ is now dependent on the level difference Δh. If the rim height dependence is removed by the normalisation technique described in section 7.5, this variation of σ with level difference is revealed more clearly. Figure 7.6.2. shows two such "dissipation curves" for the data at 0.985K and 1.12K.

As discussed in section 3.7., other workers have observed similar behaviour at temperatures above 1K and have successfully fitted their results to the form of equation 3.7.1.-

$$\Delta\mu = \kappa V f_o \exp\left(\frac{-\beta}{v_s}\frac{\rho_s}{\rho}\frac{1}{kT}\right)$$

by the choice of suitable values for the adjustable parameters f_o and β. The present results were therefore plotted as $\ell n\ \Delta h$ versus $\frac{1}{\sigma_N}$. This should yield a straight line of gradient $-\beta d\left(\frac{\rho_s}{\rho}\right)^2\frac{1}{k\,T}$ and intercept $\ell n\{\frac{\kappa A}{g}\ \ell f_o\}$, as long as negligible error is incurred by the implicit assumption of constant film thickness d over the length ℓ of the dissipation region. From equation 3.7.1., if the variation of v_s with cross sectional area A along the film is to be allowed for, then the correct level difference accompanying any flow is given by integration over the length of the film:

$$\Delta h = \frac{\kappa}{g} f_o \int_{\text{film length}} A \exp\left(\frac{-\beta}{v_s}\frac{\rho_s}{\rho}\frac{1}{kT}\right)\, d\ell \qquad 7.6.1.$$

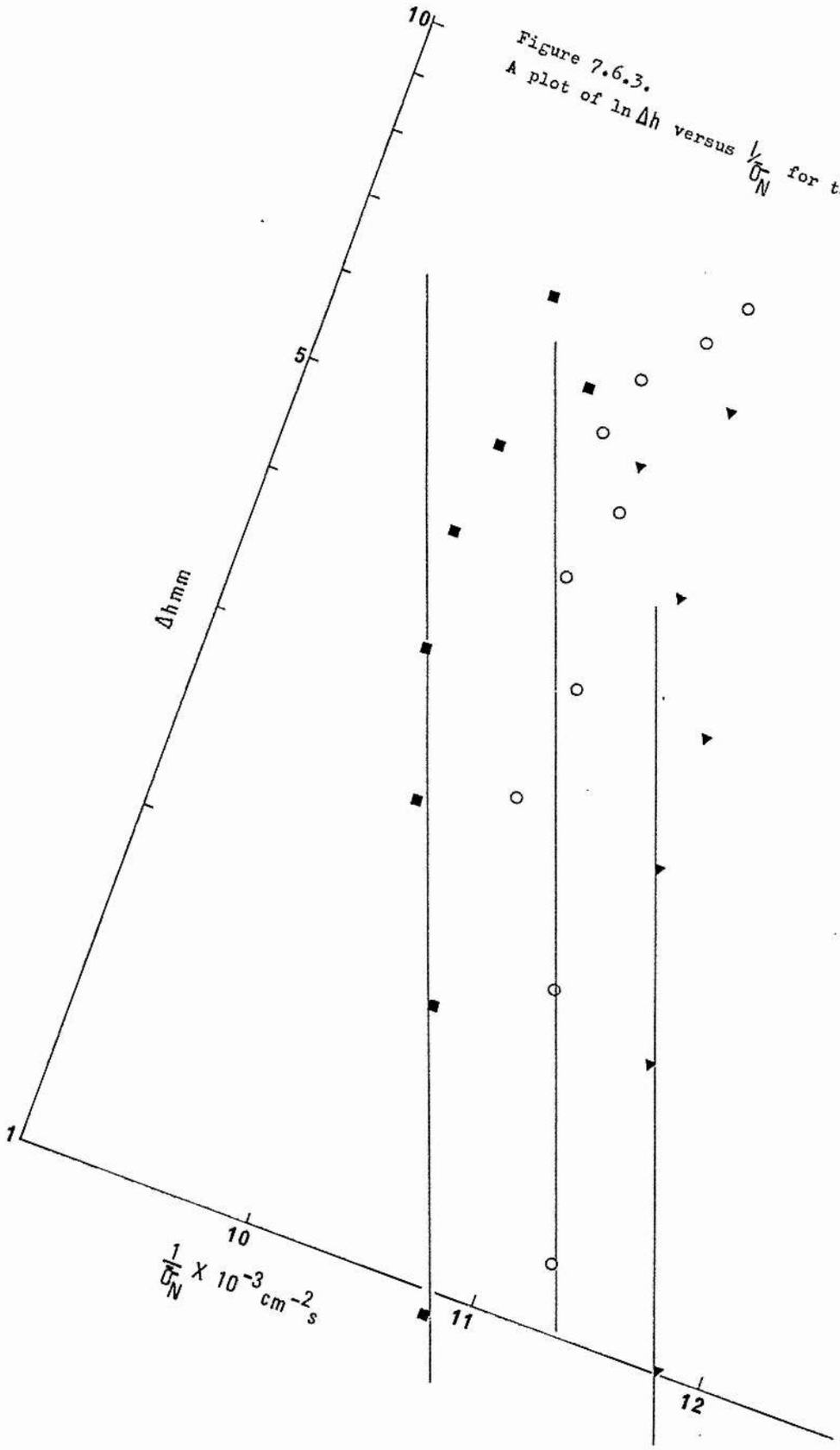

Figure 7.6.3.
A plot of $\ln \Delta h$ versus $\frac{1}{\sigma_N}$ for temperatures between 0.985K and 1.12K
■ Demagnetization 1;inflow;.985 K
○ " 9; " ;1.00K
▼ " 1; " ;1.12K

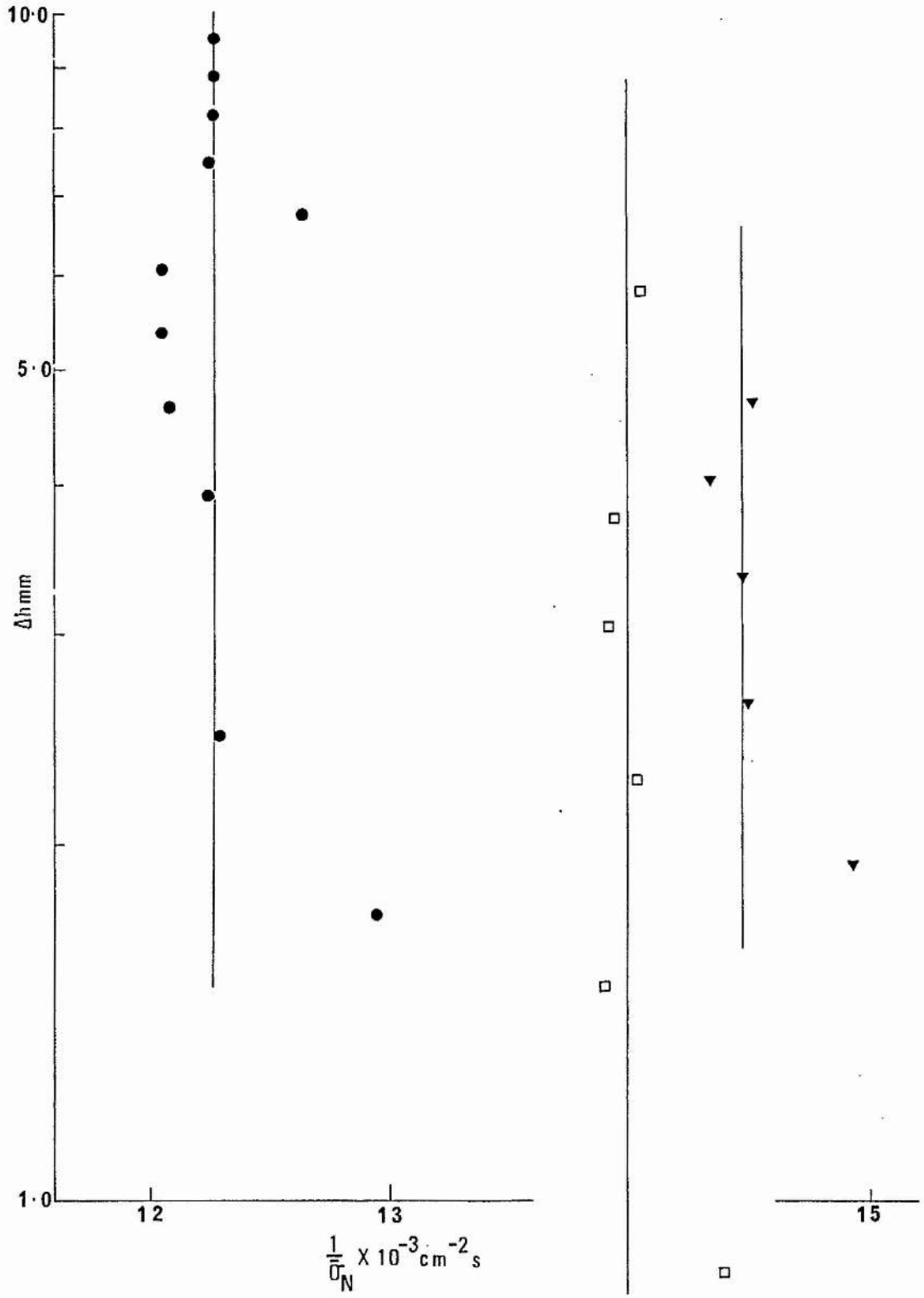

Figure 7.6.4. A plot of $\ln \Delta h$ versus $1/\bar{\sigma}_N$ for temperatures between 1.22K and 1.63K. Demagnetization 9; ● outflow 1.22K; □ inflow 1.4K; ▼ outflow 1.62K.

Figure 7.6.5.
A plot of $\ln \Delta h$ versus $\frac{1}{\sigma_N}\left(\frac{\rho_s}{\rho}\right)^2 \frac{1}{T}$, revealing the temperature dependence of f_0.

△ 1.62K.
■ 1.40K.
● 1.22K.
▽ 1.12K.
○ 1.05K.
▲ 1.00K.
□ 0.985K.

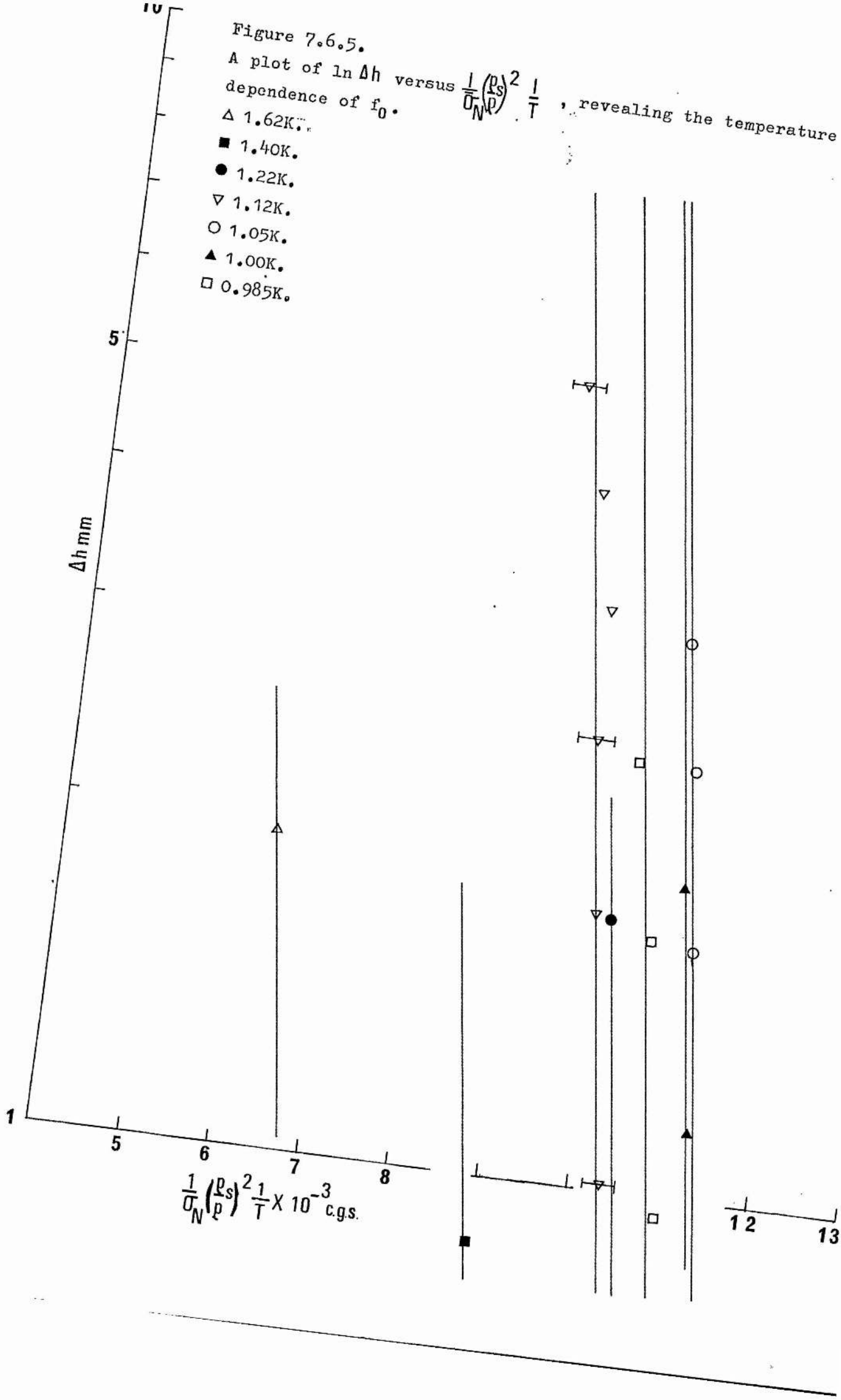

T K	β c.g.s.	v_B cms^{-1}	ℓf_0 c.g.s.
·985	$(6{\cdot}7 \pm {\cdot}7) \times 10^{-14}$	494 ± 52	$(4{\cdot}8 \pm 4{\cdot}0) \times 10^{16}$
1·00	"	486 ± 51	$(8{\cdot}8 \pm 7{\cdot}4) \times 10^{16}$
1·05	"	463 ± 48	$(9{\cdot}7 \pm 8{\cdot}2) \times 10^{16}$
1·12	"	430 ± 45	$(2{\cdot}0 \pm 1{\cdot}6) \times 10^{16}$
1·22	"	389 ± 41	$(2{\cdot}6 \pm 2{\cdot}1) \times 10^{16}$
1·40	"	324 ± 34	$(2{\cdot}2 \pm 1{\cdot}6) \times 10^{15}$
1·625	"	249 ± 26	$(1{\cdot}1 \pm {\cdot}7) \times 10^{14}$

Table 7.6.1.
The values of the parameters β, v_B and ℓf_0, as a function of temperature. The values of β and ℓf_0 at temperatures 1.22K, 1.40K and 1.625K are speculative.

The plots are shown in figures 7.6.3. and 7.6.4.. With reference to figure 7.6.3. it is apparent that, despite the rather limited amount of data, reasonable functional agreement with the form of equation 3.7.1. is obtained for transfer rates below a certain value. Above this value, however, there is evidence for the existence of a completely different type of dissipation regime in that the transfer rate no longer shows any systematic dependence on Δh, but varies about an apparently constant mean value. This "critical velocity" type behaviour is shown more clearly in the data of figure 7.6.4., and it is precisely this type of behaviour that is observed for all values of Δh at temperatures below 985mK.

From figures 7.6.3. and 7.6.4. it is easy to select the data points in each flow which lie in the "subcritical" regime. These points can be used to investigate the temperature dependence of the quantities f_o and β. Writing equation 3.7.1. in terms of the transfer rate σ gives

$$\Delta h = \frac{\kappa A}{g} \ell f_o \exp\{-\frac{\beta d}{\sigma}(\frac{\rho_s}{\rho})^2 \frac{1}{k_B T}\} . \qquad (7.6.2.)$$

If f_o and β were temperature independent then a plot of $\ell n\ \Delta h$ versus $\frac{1}{\sigma}(\frac{\rho_s}{\rho})^2 \frac{1}{T}$ for all the data should yield a single straight line. Figure 7.6.5. reveals that this is not in fact the case. The parameter f_o is quite strongly temperature dependent in that the points from flows at different temperatures lie around lines of differing intercepts. The quantity β may be weakly temperature dependent, but there is insufficient data to reveal any such behaviour. Accordingly, the points in figure 7.6.5. have been fitted to a set of parallel straight lines, the parameters of which are tabulated in table 7.6.1.

The overall lack of data in this rather important "subcritical" regime is a product of two factors. The geometry of the experimental cell was such that the area of the outer liquid reservoir was approximately equal to that of the beaker reservoir. Consequently, if subcritical behaviour started below, say, a 3mm level difference, the distance moved by each liquid level to the equilibrium position was only 1.5mm, which halved the time available for measurements. Coupled to this restriction is the fact that metastable rates were still in evidence at these small level differences: the curve of the beaker level versus time, obtained as raw data, was insufficiently smooth to yield meaningful values of the transfer rate from direct measurements of the gradient. Rather, time averaged values of the flow rate were taken over periods of ∿50s, during which time the inner level had moved through 400-500μm. Thus, from the onset of sub-critical behaviour at a level difference of 3mm, a maximum of three time-averaged measurements of σ could be made.

Returning to table 7.6.1., it should be noted that since the length of the dissipation region is not accurately known, no estimates of its extent have been made. Rather, the product ℓf_o is treated as a single adjustable parameter of the model. The quantity V_B shown in the table is related to β by

$$V_B = \beta \frac{\rho_s}{\rho} \frac{1}{kT} , \qquad (7.6.3.)$$

and, having the dimensions of velocity, is referred to as the "barrier velocity". The value for β of 6.7×10^{-14} cgs units found in these experiments is somewhat smaller than the values found by other workers over similar temperature ranges, (2.9×10^{-13}; Saunders [illegible] 1974, $2 \rightarrow 3 \times 10^{-13}$; Campbell et al 1976), and implies that the onset of

dissipation for the flows described here was much "softer", or more gradual. Also, given a reasonable estimate of ℓ as lying somewhere between 0.1mm and 10mm, the values of f_o found here are 7-10 orders of magnitude lower than those found by the above workers. f_o is seen to increase with decreasing temperature over the range 1.625K to 1.05K, which agrees with the observations of others, although the magnitude of the increase is much smaller. However, below 1.05K, f_o falls with decreasing temperature, which trend is actually in agreement with the predictions of thermal fluctuation theories.

The gradual onset of dissipation witnessed in these experiments is perhaps significant when making comparisons with the work of others. For level differences as large as several millimetres the transfer rate is observed to be still increasing quite rapidly with Δh until the transition is made into the critical regime; the dissipation then takes a different form and σ remains more or less constant. However, if the onset of dissipation were more sudden, corresponding to the larger value of β observed by others, the dissipation curve given by equation 7.6.2. would have virtually levelled out for a Δh of several millimetres, and it is possible that the transition into the "critical" regime would not be noticeable. The low value of β found in this experiment may well be connected with the use of a metal substrate; the increased surface roughness could produce locally high superfluid velocities, leading to a lowering of the energy barrier to vortex formation.

It should be noted that the temperature dependence of $\bar{\sigma}_{N.av.}$ over the region T > 985mK shown in figure 7.6.1. is calculated from values of σ occurring in the "critical" regime, whilst it is possible that the

results of the other experiments shown in the figure are for σ in the "subcritical" regime. This could go some way towards explaining the lack of agreement between the results.

(iii) The "plateau" region between 400mK and 980mK.

The existence of this region of "critical"type dissipation below 1K wherein the mean transfer rate shows no pronounced temperature dependence is of considerable interest. The dissipation is presumably still caused by the nucleation and growth of superfluid vortices and their subsequent transportation across the stream. However the very low temperatures would seem to preclude both the thermal nucleation and stream-crossing mechanisms described in Chapter 2. Given that vortices can be nucleated mechanically in some way at very low temperatures, subsequent pinning of one end of a vortex line to the substrate would cause the line to cross the stream under the influence of the Magnus force. Such an approach has recently been suggested by Harris-Lowe (1977). It is possible that the results obtained in the "plateau" region are representative of this process. The characteristics of this type of dissipation are the presence of a multiplicity of metastable transfer rates during any one flow, and an apparent insensitivity of the metastable rates, or the mean rate, to changes in the temperature or in the chemical potential difference between the ends of the film.

An attempt was made to see if the metastable rates took on a series of evenly-spaced preferred values, following the discussion of section 3.3. Direct measurements of σ were taken from the recorded off-balance signal of the capacitance bridge. The relative accuracy

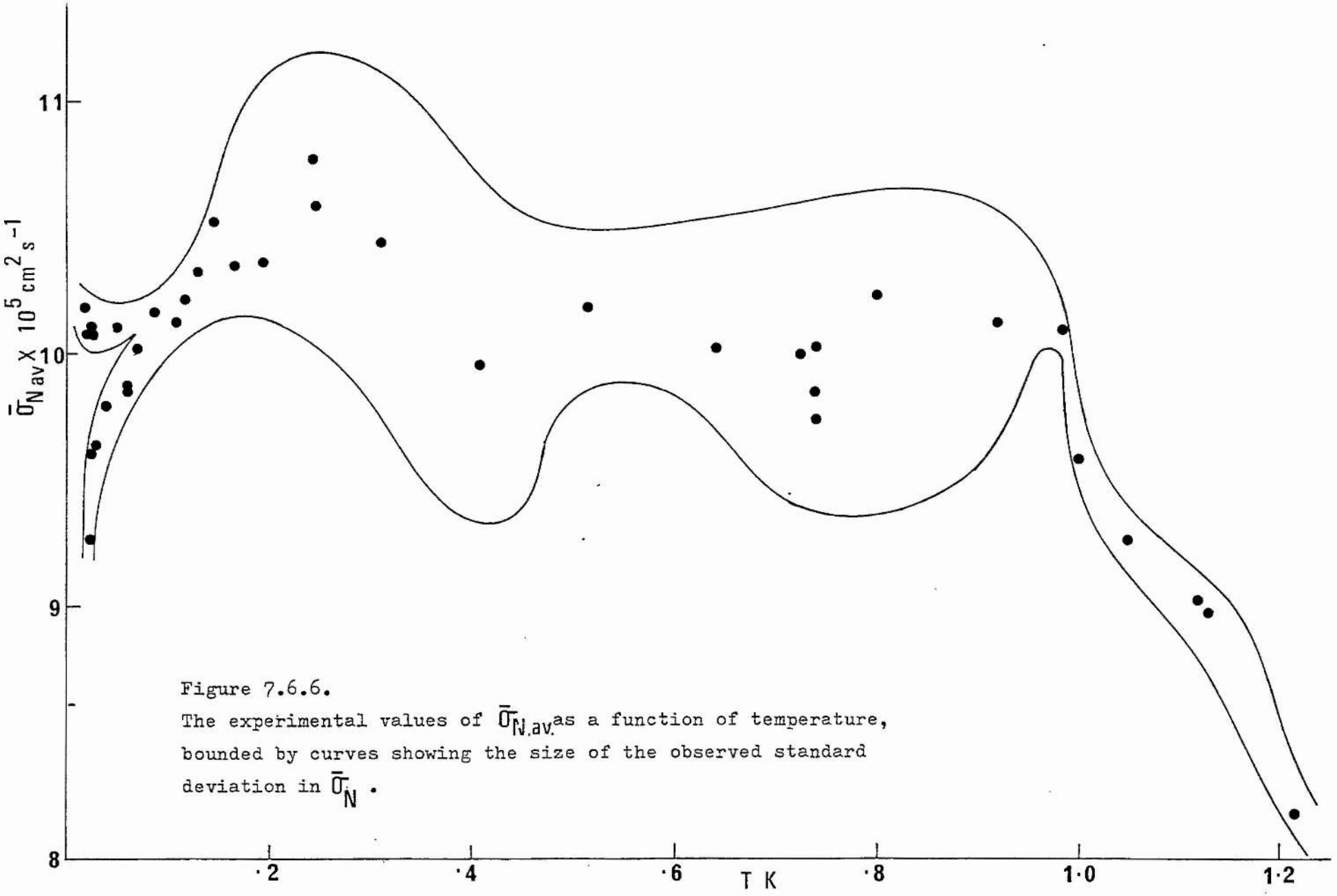

Figure 7.6.6.
The experimental values of $\bar{\sigma}_{N.av.}$ as a function of temperature, bounded by curves showing the size of the observed standard deviation in $\bar{\sigma}_N$.

of these measurements was estimated to be $\pm$ 2% for comparisons between different flows and between widely separated sections of the same flow. Over short sections of one flow, between re-balancing operations of the bridge, the accuracy was approximately $\pm$ 0.5%. One hundred and fourteen direct measurements of the transfer rate were made and no evidence for a "preferred rate" structure was found. The rates were fairly evenly distributed over a wide range of values and it must be concluded that if a preferred rate structure does exist then the spacing between rates is closer than the 4% resolution of the present experiment.

The actual spread in values of the metastable rates is greatest in the temperature region between 200mK and 940mK. Figure 7.6.6. shows the mean normalised transfer rate, $\bar{\sigma}_{N,av.}$ over the temperature region 0 to 1.25K and superimposed on this is an area whose width is equal to the observed standard deviation of $\bar{\sigma}_N$ about the mean value. The relative experimental error associated with measuring $\bar{\sigma}$, was $\pm$ 1.5% and it can be seen that the observed standard deviation is much greater than this. In the temperature regions $T < 150mK$ and $T > 980mK$, the standard deviation of $\bar{\sigma}_{N,av.}$ was found to be of the same order as the experimental error. This is not to say that metastable rates do not occur in these temperature regions, they are easily observed over short sections of flows as discontinuous changes of the transfer rate from one stable value to another. The magnitude of the jump in flow rate far exceeds the increased experimental accuracy of $\pm$ 0.5% appropriate to such short regions. However, the spread in the values of σ is for some reason much reduced, leading to only small variations in the time average $\bar{\sigma}$.

Figure 7.6.7.
The temperature dependence of the mean normalised transfer rate below 250mK.
— — — Crum, Edwards and Sarwinski (normalised).

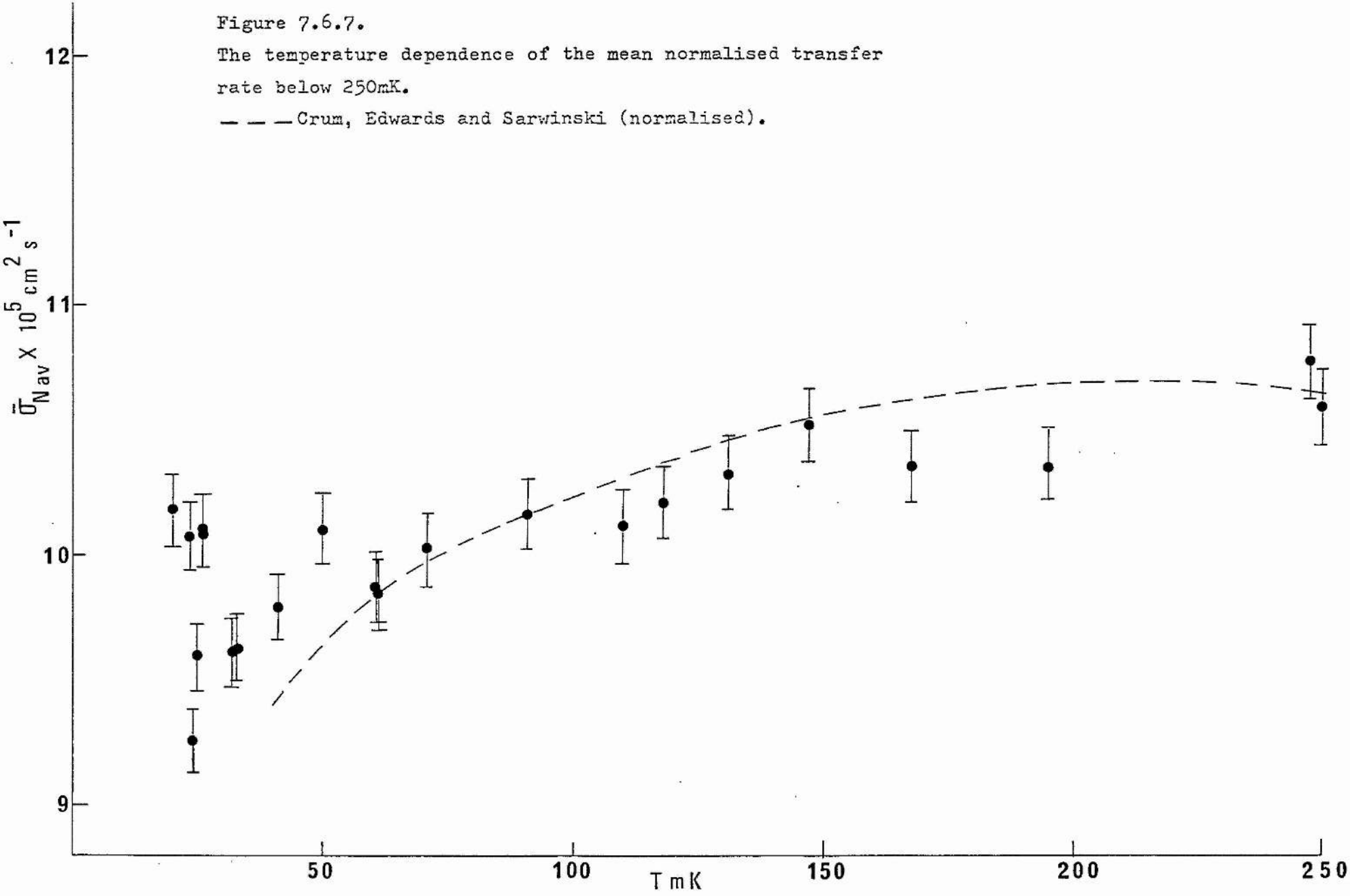

(iv) The temperature region 400mK to 200mK .

Although the scatter of metastable rates is still very large in this region, the mean rate appears to increase quite rapidly with decreasing temperature to a maximum in the vicinity of 250mK. A similar trend was observed by Crum et al but the effect was not as pronounced as in the present data. No other experimental observations of this phenomenon have been made, and any speculation as to the mechanisms at work could well be postponed until a more detailed study has been carried out. A correlation that may be appropriate is that the amplitude of the 5.75Hz oscillations on the inner liquid level, described in section 7.1., grows rapidly below 480mK, over the same temperature interval as the mean flow rate is increasing.

(v) The drop in transfer rate below 250mK.

The portion of figure 7.5.2. for temperatures below 250mK is shown on an expanded scale in figure 7.6.7. The dashed line in the figure shows the results of Crum et al for this temperature region, normalised according to the discussion of section 7.6.(i). Remarkably good agreement is obtained for temperatures above 60mK, considering the notorious irreproducibility of experiments on the flowing helium film. The fall in the value of σ with decreasing temperature has been interpreted by Crum et al as evidence for the formation on the surface of the film of a layer of ^{3}He. This is normally contained as an impurity in commercially available ^{4}He at a concentration of 2 parts in 10^7. As mentioned in section 3.9 the existence of such a surface state was first proposed by Andreev (1966) in order to explain the observed temperature dependence of the surface tension of dilute ^{3}He-^{4}He mixtures.

The total surface area covered by the superfluid film in the experimental cell used by Crum was estimated as $57cm^2$, whilst the volume of liquid contained in the cell was approximately 28ccs. Assuming that the ^4He he used contained 0.2ppm of ^3He, there would be sufficient ^3He to produce about 3.3 monolayers at the lowest temperatures. In the present experiments, the film area was approximately the same as above, but the volume of liquid in the cell was larger by a factor of 5. Specially purified ^4He was used, a sample of which was analysed subsequent to the experiments and found to contain ^3He at a concentration of 3 parts in 10^8. (The analysis was carried out by the US Bureau of Mines, Amarrillo, Texas, using a mass spectrographic technique.) The increased liquid volume balances out the reduced ^3He concentration to a certain extent, in that the number of monolayers of ^3He to be expected at the lowest temperatures is only reduced to 2.5.

The present results would therefore seem to closely corroborate those of Crum et al down to a temperature of 60mK for similar concentrations of ^3He at the surface of the film. Below 60mK a curious divergence of results appears, which is seemingly linked to the history of the helium in the cell. Those results which show a continuing downward trend as the temperature is reduced to 24mK were all taken after the first demagnetisation at the very beginning of the experimental run. The results which show a levelling out of the transfer rate at $\sim$60mK, followed by a possible slight increase at the lowest temperature were taken after the eighth and ninth demagnetisations at the end of the run. A period of 23 days separates the two sets of data during which time the liquid in the cell was maintained at a temperature below 1.6K.

At temperatures above 60mK, the two sets of data fall about a common line. This suggests that the divergence of the results at lower temperatures is due to a fall in the ^{3}He concentration over the course of the experiment. A detailed mechanism for the transport of ^{3}He out of the cell is hard to find, but could in some way be connected with the continual flow of film up the walls of the cell filling capillary towards the warmer parts of the cryostat. Alternatively, the ^{3}He could for some reason be preferentially adsorbed on the large surface area of the paramagnetic salt granules present in the cell.

In between taking these two sets of data on film transfer at large level differences, a study was made of the driven flow behaviour of the film, the results of which will be presented in chapter 8. It will be seen that the findings are in very good agreement with the upper of the two curves in figure 7.6.7. suggesting that in fact the reduction in the ^{3}He impurity level occurred shortly after the first demagnetisation. In the light of the experience gained here it would perhaps be advisable to conduct any future investigations into film transfer at very low temperatures with a small volume of highly purified ^{4}He contained in a sealed capsule.

7.7. SUMMARY

At all temperatures in the range .02K to 1.62K the film transfer rate exhibits an array of metastable values. To within the resolution of the present experiment (4%) these values do not form any kind of reproducible "preferred rate" structure.

In the temperature intervals 20mK $\lesssim T \lesssim$ 150mK and .74K $\lesssim T \lesssim$ 1.62K, the variation of the time-averaged transfer rate with rim height suggests that the film thickness at the rim should be calculated using a

van der Waals' exponent, n, of 2.85 $\pm$ .25. However, in the temperature range 150mK $\lesssim$ T $\lesssim$ 740mK the spread in values of the metastable rates is much greater, and the mean rate shows no systematic dependence on the rim height.

As the temperature is lowered from 1.6K to 1K, the mean transfer rate increases by 43%. This increase does not continue below 1K. Instead, an abrupt transition is made into a plateau region which extends down to 400mK.

Below 1K there is no dependence of the transfer rate on the level difference Δh, for Δh in the range 8mm to 0.5mm. This "critical velocity" type behaviour is also present above 1K for level differences in excess of roughly 3mm. However, as the level difference falls below $\sim$3mm a sharp transition into a "subcritical" dissipation regime now takes place. In this regime the transfer rate varies with the level difference in accordance with the functional form of equation 3.7.1. The parameters β and f_o for film flow over stainless steel are found to be considerably smaller than those reported for flow over glass.

Good agreement with the results of Crum et al is obtained for the fall in transfer rate with temperature over the interval 250mK to 60mK. Below 60mK it would appear that for low concentrations of ^{3}He impurity, the transfer rate stops falling and eventually increases slightly at the lowest temperatures. For higher concentrations of ^{3}He the fall in the transfer rate continues to the lowest temperatures investigated.

7.8 CONCLUSIONS

It seems possible that over the entire temperature range .01K to 1.6K, one basic dissipation mechanism is at work characterised by the properties of film flow in the so-called "critical" regime. The flow rate has a range of metastable values whose mean is essentially

independent of temperature and level difference, as witnessed in the region 400mK to 1K. Above 1K and below 400mK the basic mechanism becomes modified in some way so as to cause the mean critical rate to become temperature dependent.

The occurrence of high metastable rates at level differences as small as 500μm implies that the onset of dissipation is extremely sudden, and must only take place when certain critical conditions are met in the film. If the critical factor were solely the superfluid velocity, it is difficult to see how, above 1K, the mean critical transfer rate suddenly becomes strongly temperature dependent. On the other hand it is possible that the critical factor is in some way connected with the density of vortex lines in the film. As the film transfer rate increases, the rate of production of vortex lines could increase with very little attendant dissipation, until at a certain line density the pinning of the vortices sets in, causing them to sweep across the stream and give rise to dissipative effects.

Above 1K there could exist an additional, temperature-dependent, nucleation mechanism, connected in some way with the increased proportion of normal fluid in the film. The critical vortex density would now be achieved at smaller superfluid velocities and the temperature dependence of the additional nucleation mechanism would bring about the observed temperature dependence of the mean critical rate. For vortex densities below the critical value a certain amount of dissipation would still be expected above 1K, since the anisotropic scattering of normal fluid excitations off the vortex covers would cause these "free" vortices to cross the stream. This would account for the existence of a subcritical dissipation regime above 1K.

Below 250mK, the basic dissipation mechanism could be modified in a different way. The number of ^{3}He atoms at the surface of the film increases progressively with decreasing temperature. This has the effect of reducing the surface tension, which could lower the nucleation energy of a hollow-cored vortex-line. This in turn could reduce the velocity at which the critical vortex line density is achieved. The mean transfer rate will therefore fall with temperature. The origin of the suspected rise in the transfer rate at extremely low temperatures, for small ^{3}He impurity levels, remains open to speculation.

CHAPTER EIGHT

DRIVEN FLOW AT SMALL LEVEL DIFFERENCES AND THE DAMPING OF THE INERTIAL OSCILLATIONS

8.1 INTRODUCTION

The standard film flow experiment of creating a relatively large difference between the reservoir levels and observing its subsequent decay with time yields information on the transfer rate under basically non-equilibrium conditions. There is no way of knowing that the same results would be obtained in a steady-state situation. Also, any information on the dependence of the transfer rate on the level difference is usually compressed into a short section towards the very end of a flow and is consequently difficult to analyse. It was therefore considered desirable to carry out the experiments as described in section 6.9.(b) where a particular level difference could be selected and held constant by driving the outer liquid level either up or down at the appropriate rate, and the corresponding steady state film transfer rate recorded.

The results of these experiments are of particular interest in the low temperature region below 1K. In the previous chapter it was seen that flows from large level differences at these temperatures revealed no detectable dependence of the transfer rate on the level difference for $\Delta h \gtrsim 500\mu$. It is of fundamental importance to establish whether this "critical velocity" type behaviour is maintained right down to zero level difference or whether in fact the onset of dissipation is more gradual.

Below 30mK the appearance of large Kapitza boundary resistances

could cause anomalous results in film flow experiments. For a steady state transfer rate of 10^{-4} $cm^2 s^{-1}$ at a level difference of 1cm, the rate of energy loss in the dissipation region of the film is approximately 1.4×10^{-9} W per unit length of perimeter. If, within this region the dissipated kinetic energy is transformed directly to thermal excitations, that is, normal fluid, this will be immobilised by its own viscosity. The presence of the large Kapitza boundary resistance between film and substrate will then cause the appearance of a substantial temperature differential, which could be as great as 100mK for the passage of 10^{-9} W into a substrate at 20mK. It was therefore considered important to perform driven flow experiments at level differences below 500μm, which, by comparison with the results of flows at large level differences, would reveal the presence of any "film heating" effects in the latter data.

Above 1K, the results of Chapter 7 show that the film transfer rate becomes dependent on the level difference Δh, for $500\mu m \lesssim \Delta h \lesssim 3mm$, according to the relation

$$\Delta h = \frac{\kappa A}{g} \ell f_o \exp\{-\frac{\beta d}{\sigma} (\frac{\rho_s}{\rho})^2 \frac{1}{k_B T}\} . \qquad (7.6.2)$$

Driven flow experiments were carried out above 1K to test for the continuation of this functional form in the region $0 \lesssim \Delta h \lesssim 500\mu m$.

In the first part of this chapter the results of the experiments at temperatures below 1K will be presented. In the light of these results, the damping of the inertial oscillations over the same temperature range will then be discussed. The final section of the chapter will be concerned with the driven flow results above 1K and a comparison will be made with the oscillation damping in this region.

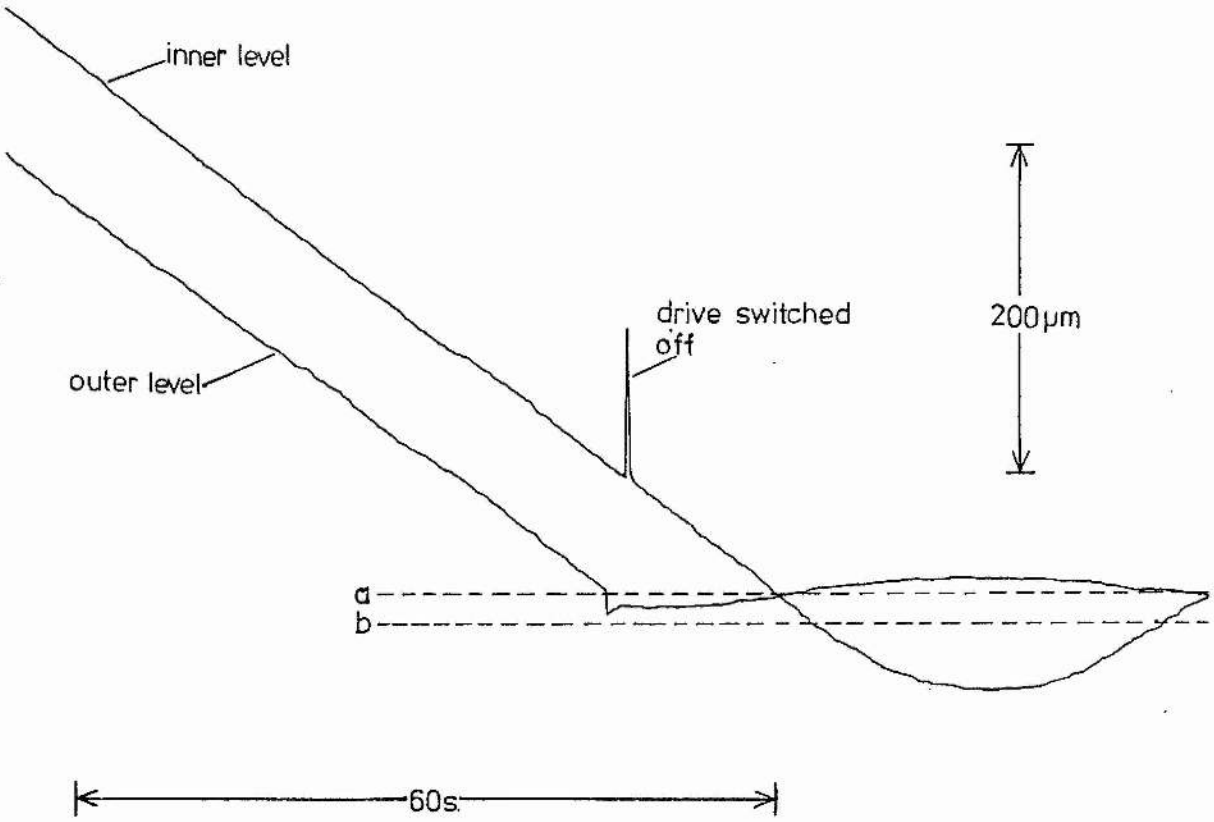

Figure 8.2.1.
A reproduction from a chart record of a typical driven flow experiment, showing the positions of the inner and outer liquid levels as a function of time.

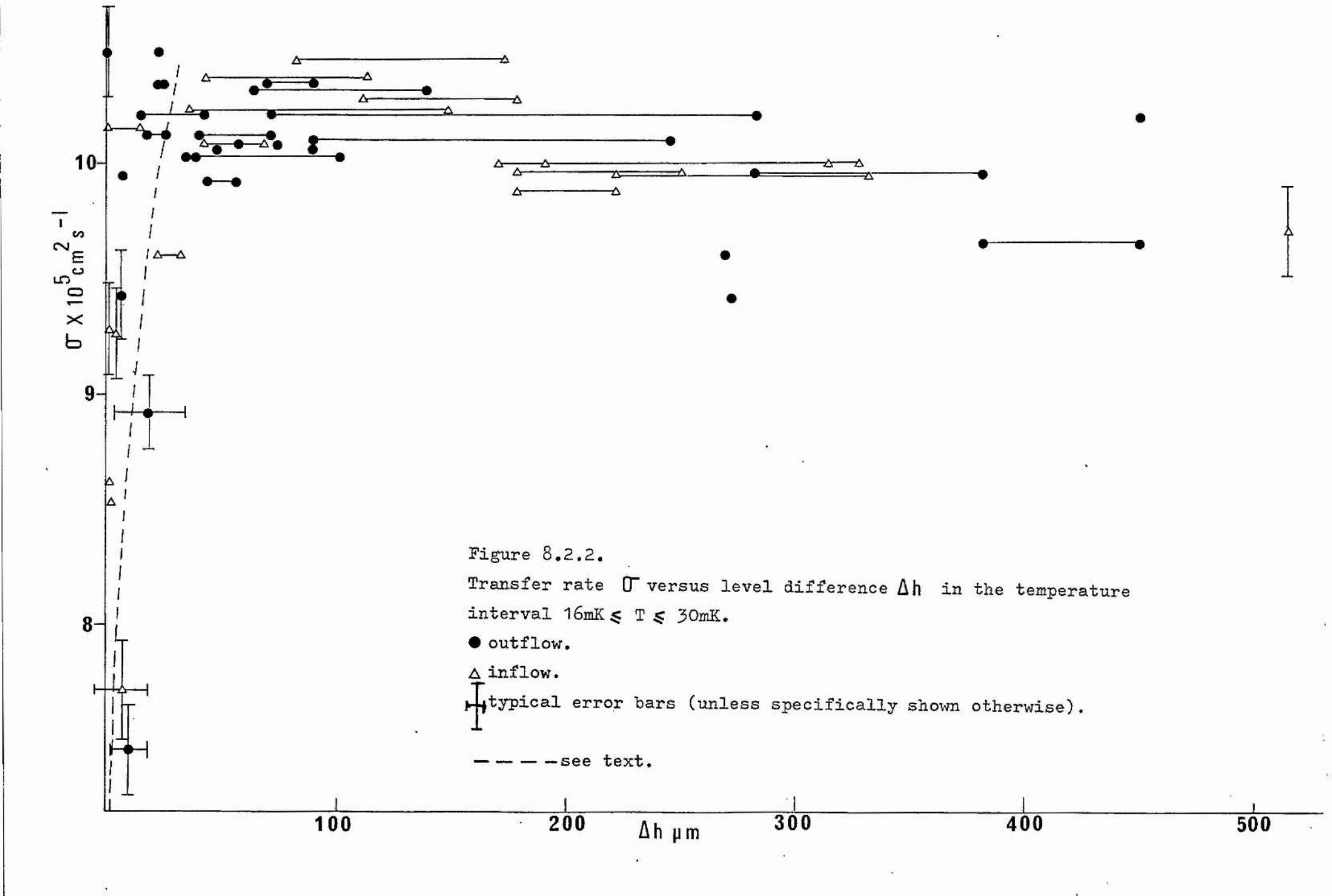

Figure 8.2.2.

Transfer rate σ versus level difference Δh in the temperature interval $16mK \leq T \leq 30mK$.

● outflow.

△ inflow.

typical error bars (unless specifically shown otherwise).

– – – –see text.

8.2 DRIVEN FLOW BELOW 1K

A reproduction from the chart record of a typical driven flow experiment as described in section 6.9(b) is given in figure 8.2.1.. The equilibrium positions of the liquid levels were determined from the damped inertial oscillations by taking the means of successive maxima and minima and fitting the best straight line through these points by a least squares method. With this knowledge, the value of the level difference at any point in the driven portion of the flow could be computed to an accuracy of $\pm$ 3μm. The associated transfer rate could be measured to a relative accuracy of $\pm$ 1%. Each experiment of the type illustrated in figure 8.2.1. yielded one data point on a plot of the dissipation curve (transfer rate versus level difference), and it therefore took a great deal of experimental time to establish the relationship between σ and Δh over the range $0 < \Delta h \lesssim 500\mu m$, at any one temperature. It was not possible to cover all temperature ranges in the same detail, and indeed it was in some cases necessary to combine data from adjacent temperature ranges.

The most detailed picture of the shape of the dissipation curve was built up from data taken at temperatures between 16 and 30mK. The results are shown in figure 8.2.2. The scatter is substantial, but was not found to be caused by the slight spread in the temperature and rim height values of the different data points. (Driven flow experiments were carried out at rim heights over the range 11.175mm to 13.182mm). Two types of behaviour are apparent in different regions of the curve. For $\Delta h < 40\mu m$ the transfer rate is sensitive to variations in the level difference and increases extremely steeply with increasing Δh. In this "subcritical" region the value of Δh

is always non-zero, but the scatter of points makes it impossible to characterise the dependence of Δh on σ by a particular functional form. For $\Delta h > 40\mu m$ or $\sigma > 10^{-4}$ $cm^2 s^{-1}$, essentially the same type of critical flow behaviour is observed as is found for flows from large heads at all temperatures below 1K. Each flow experiment yields a particular metastable rate which can remain constant as Δh is increased through a certain range during the course of the flow. This is indicated in figure 8.2.2. by pairs of points with different Δh values connected by solid lines. These should not be confused with error bars. The rates are sometimes observed to be stable to within $\pm \frac{1}{2}\%$ as the level difference changes by as much as $200\mu m$.

The mean metastable rate seems to go through a slight maximum at a level difference of $\sim 130\mu m$ after which it drops very slowly with increasing Δh. This does not mean that the film actually slows down as the "driving force" is increased. Rather, the implication is that, as Δh is increased, the dissipation region spreads out, causing a fall in the gradient of the chemical potential. Since it is this quantity that is equal to the force on unit mass of superfluid then a reduction in the transfer rate is to be expected. A relevant observation made during flow experiments at large level differences was that a high metastable rate would often occur immediately prior to the onset of the inertial oscillations at the end of the flow. The level difference at which this high rate appeared was usually $\sim 200\mu m$, which agrees quite well with the position of the maximum in figure 8.2.2.

The results of the driven flow experiments in the nine other

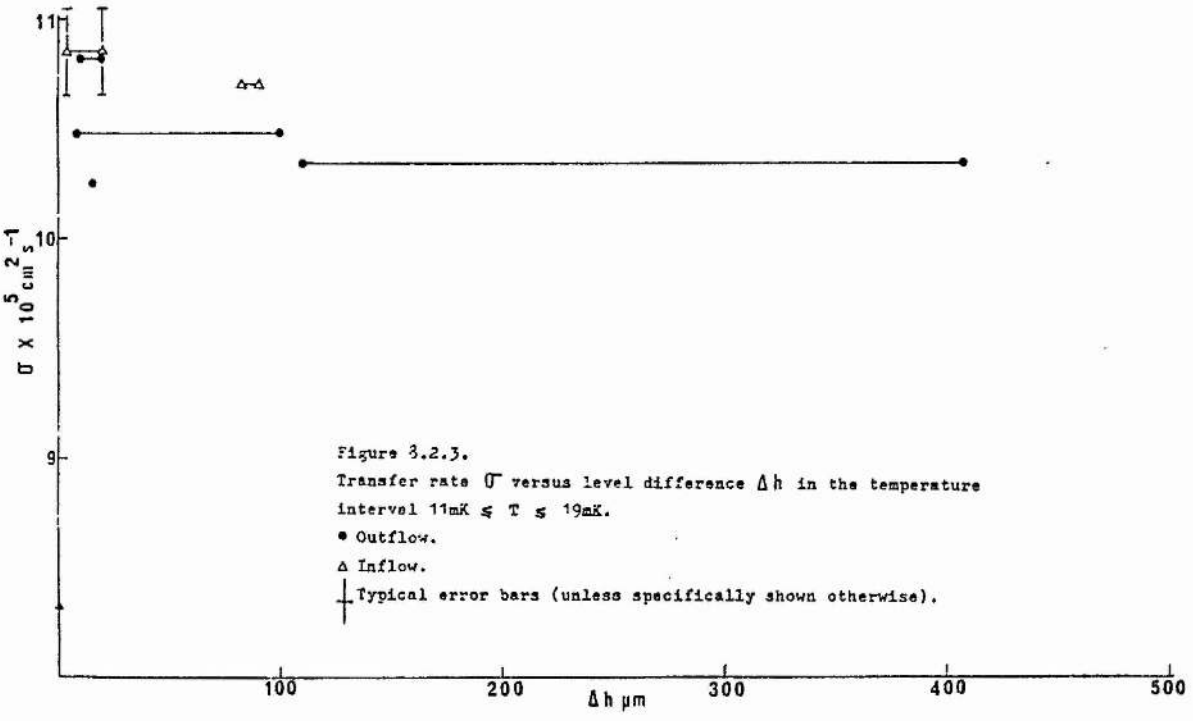

Figure 8.2.3.
Transfer rate Γ versus level difference Δh in the temperature interval 11mK $\leq$ T $\leq$ 19mK.
• Outflow.
△ Inflow.
┼ Typical error bars (unless specifically shown otherwise).

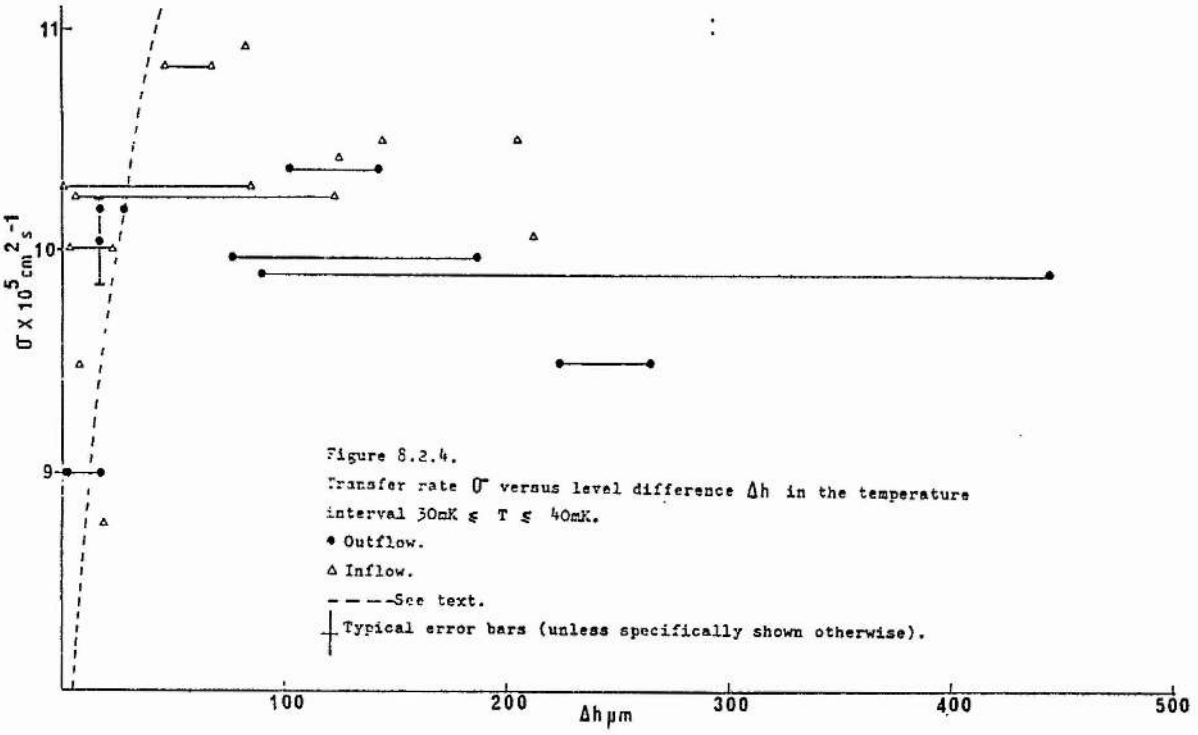

Figure 8.2.4.
Transfer rate Γ versus level difference Δh in the temperature interval 30mK $\leq$ T $\leq$ 40mK.
• Outflow.
△ Inflow.
– – – See text.
┼ Typical error bars (unless specifically shown otherwise).

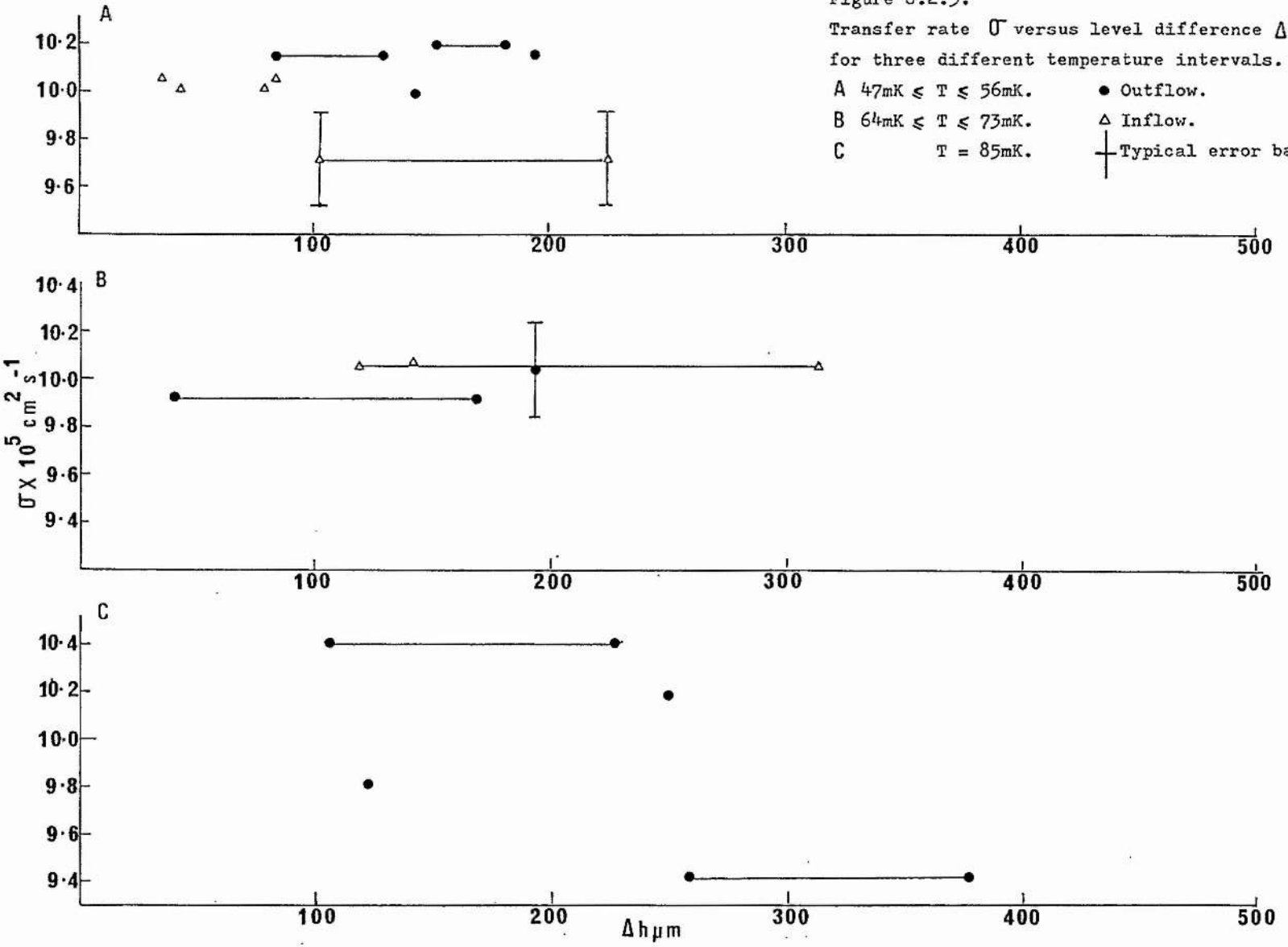

Figure 8.2.5.
Transfer rate σ versus level difference Δh for three different temperature intervals.

A 47mK ≤ T ≤ 56mK. ● Outflow.

B 64mK ≤ T ≤ 73mK. △ Inflow.

C T = 85mK. ┼ Typical error bars.

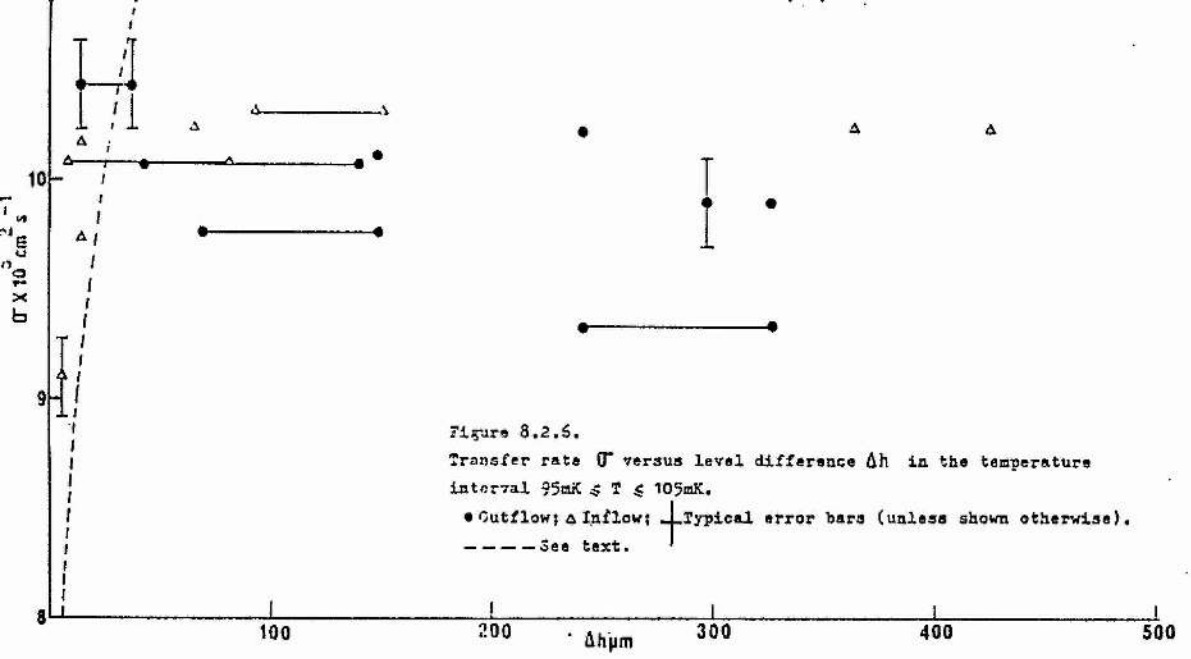

Figure 8.2.6.
Transfer rate Γ versus level difference Δh in the temperature interval 95mK $\lesssim T \lesssim$ 105mK.
• Outflow; △ Inflow; ┼ Typical error bars (unless shown otherwise).
– – – – See text.

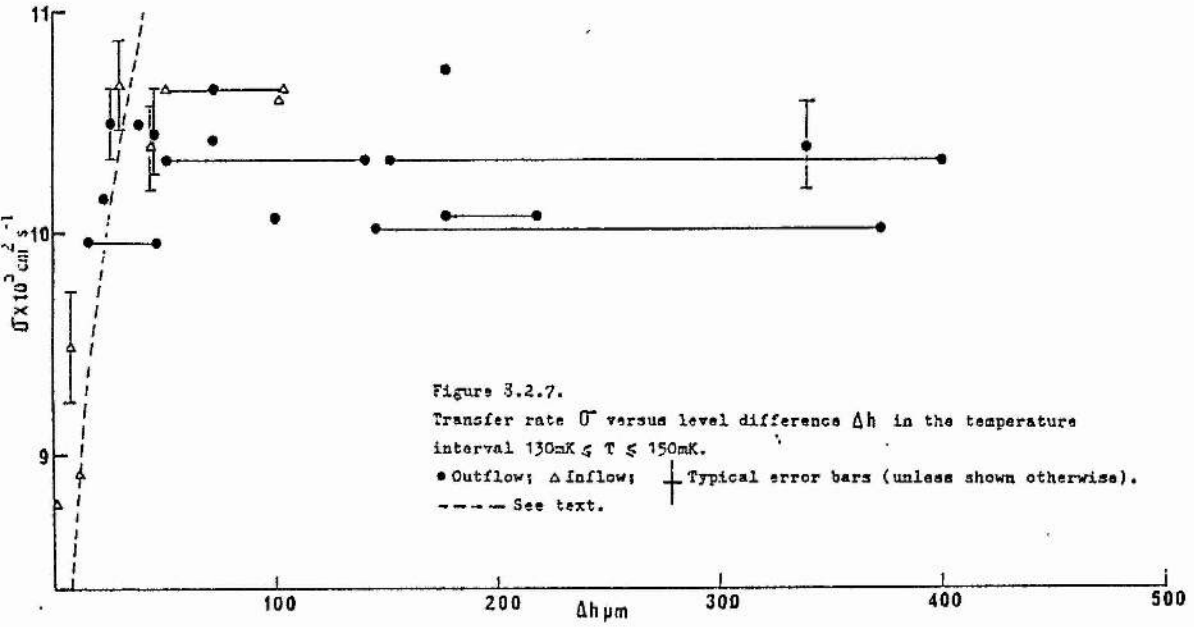

Figure 8.2.7.
Transfer rate Γ versus level difference Δh in the temperature interval 130mK $\lesssim T \lesssim$ 150mK.
• Outflow; △ Inflow; ┼ Typical error bars (unless shown otherwise).
– – – – See text.

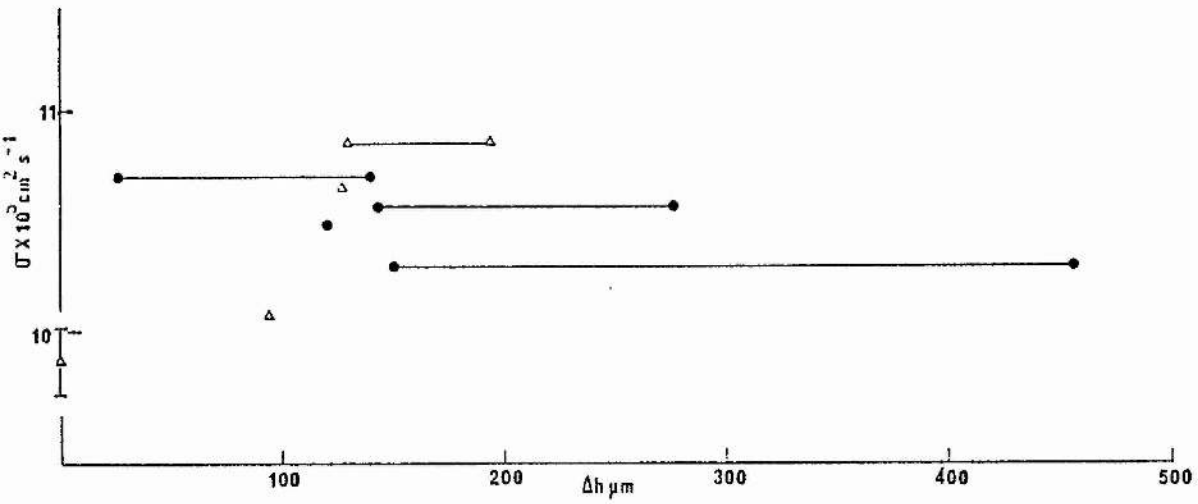

Figure 8.2.8.
Transfer rate Γ versus level difference Δh in the temperature interval 156mK $\lesssim T \lesssim$ 206mK.
• Outflow; △ Inflow; ┼ Typical error bars (unless shown otherwise).

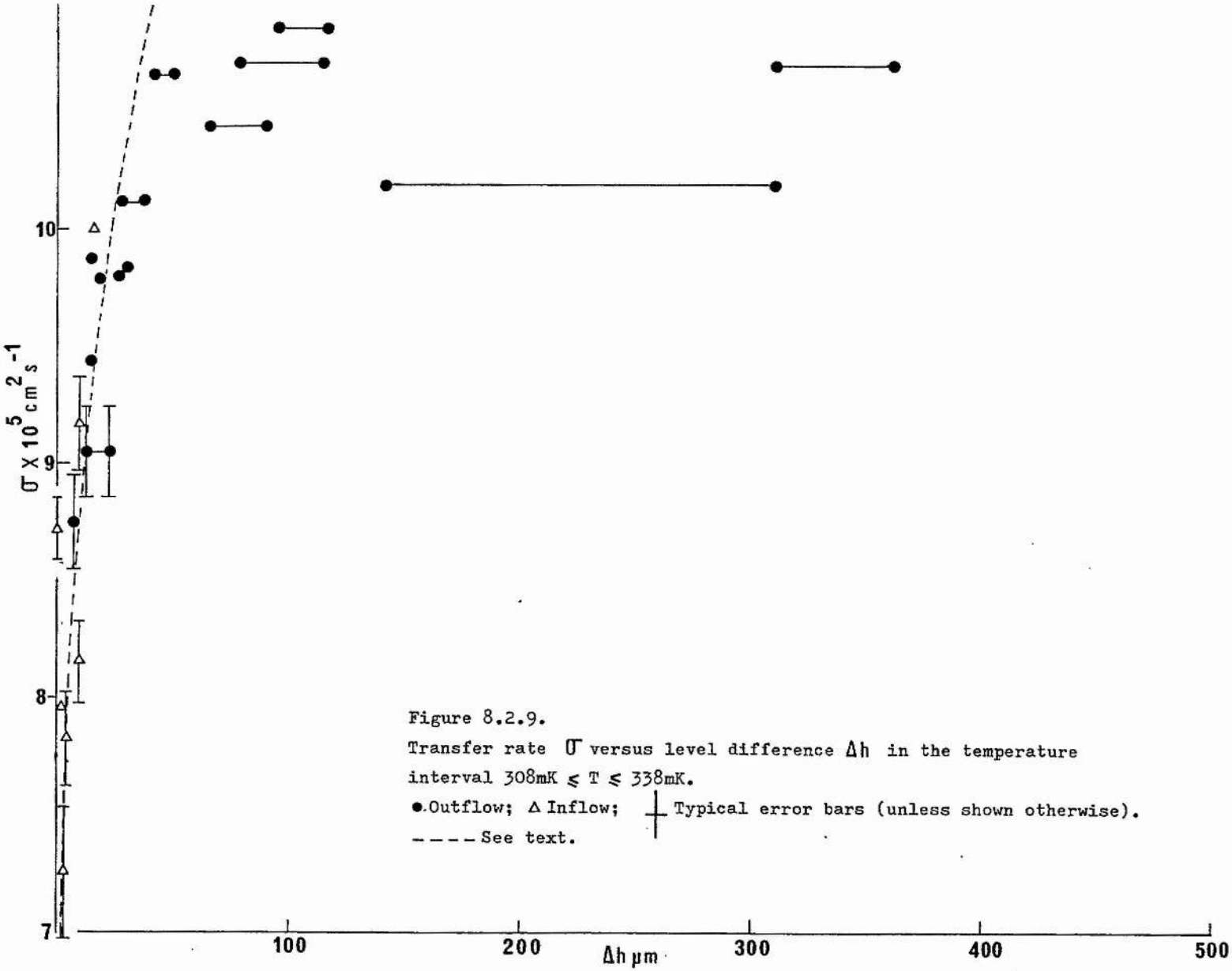

Figure 8.2.9.
Transfer rate Γ versus level difference Δh in the temperature interval 308mK $\leq$ T $\leq$ 338mK.
● Outflow; △ Inflow; ┼ Typical error bars (unless shown otherwise).
– – – – See text.

Figure 8.2.10.

The temperature dependence of Γ ; a comparison between the results of driven flow experiments and experiments at large level differences.

■ Driven flow results.

○ Large level difference results.

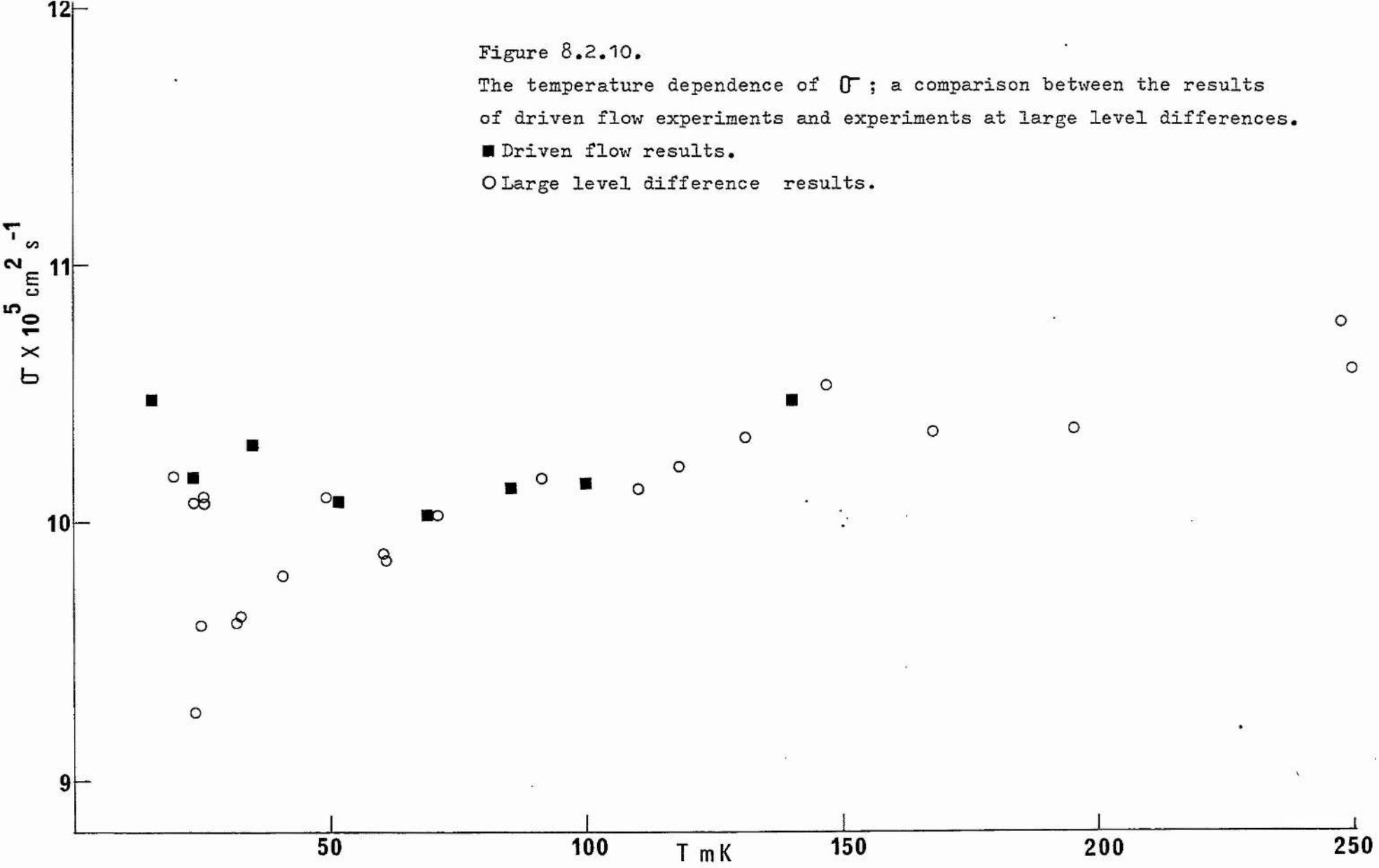

temperature regions studied are given in figures 8.2.3. to 8.2.9. Some of the dissipation curves are obviously incomplete, but the data is useful in assessing the general temperature dependence of the mean metastable rate, averaged over the region of the maximum in the critical regime ($\Delta h \sim 130\mu m$). This quantity, referred to as $\bar{\sigma}_{max}$, is shown in figure 8.2.10 superimposed on the results of figure 7.6.7. for flow from large heads. The agreement is seen to be remarkably good. This is somewhat fortuitous in that the driven flow experiments were carried out at larger rim heights than the flows from large level differences. The values of $\bar{\sigma}_{max}$ should therefore be smaller than those of $\bar{\sigma}_{N.av.}$, and it appears that another discontinuity in v_c must exist between the two rim height ranges, such that the normalisation factor is exactly cancelled. Below 70mK the driven flow results show the same levelling out and slight increase as was seen in the later experiments from large level differences. However it would be wrong to lay too much importance on some of the values of $\bar{\sigma}_{max}$ at the lower temperatures as insufficient metastable rates were observed to give an accurate mean.

The good agreement between these results from the two different types of experiment is an indication that the film heating effects discussed in section 8.1. are in fact absent. Quite apart from the numerical agreement, one would not expect to observe the same temperature dependence of $\bar{\sigma}$ if the strongly temperature dependent Kapitza resistance were playing a dominant role in one experiment and not the other. It therefore follows that any dissipation process occurring in the film must remain entirely within the superfluid; the dissipated flow energy must be initially stored as rotational and potential energy in the vortex system. The final degradation into

Figure 8.2.11.
A plot of ln Δh versus $\frac{1}{\sigma}$ for driven flow data in the temperature interval 308mK $\leq$ T $\leq$ 338mK.
——— See text.

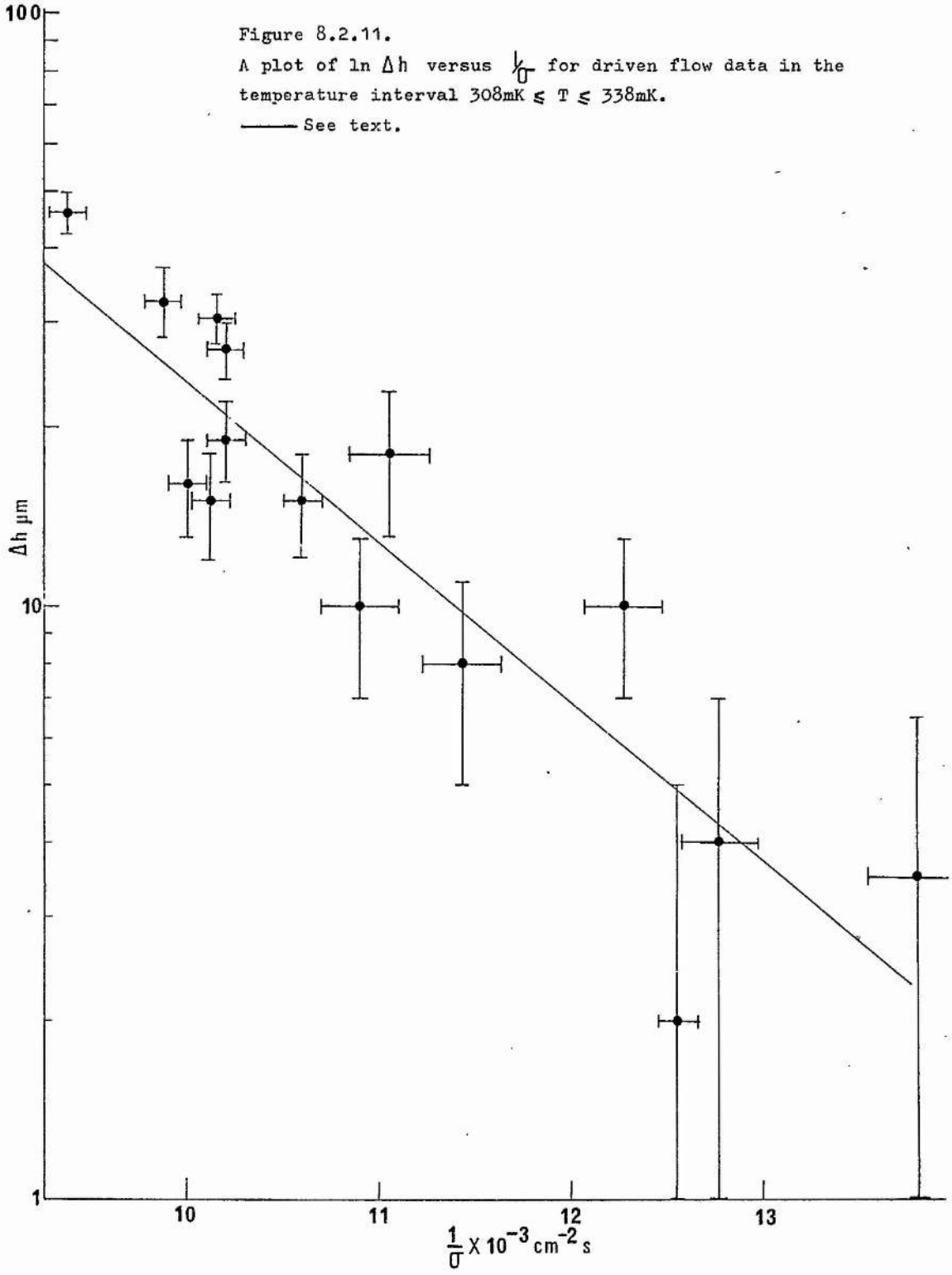

heat must take place in the liquid reservoirs, not in the film.

The most clearly defined dissipation curve for level differences <40μm is to be found in figure 8.2.9. for the temperature range 308mK ≲ T ≲ 338mK. An attempt can be made to parameterise this curve to the same functional form as was used in section 7.6.(ii), for temperatures above 1K. From equations 7.6.2. and 7.6.3.

$$\Delta h = \frac{\kappa A}{g} \ell f_o \exp\{-\frac{d}{\sigma}(\frac{\rho_s}{\rho}) v_B\} . \qquad (8.2.1.)$$

A plot of $\ell n\, \Delta h$ versus $\frac{1}{\sigma}$ is given in figure 8.2.11. where the straight line fitted to the data has the parameters $\ell f_o = 7 \times 10^{10}$ cgs and $v_B = 220 \text{cm s}^{-1}$ ($\beta = 9.8 \times 10^{-15}$ cgs). It should be stressed that the restricted range of values of Δh and the scatter in the data render the comparison of one functional form with another virtually impossible; an equally good fit could have been obtained with a function of the type

$$\Delta h = Ce^{\alpha\sigma} , \qquad (8.2.2.)$$

with C and α as adjustable parameters. Equation 8.2.1. was simply chosen as a convenient approximation to the data which allowed direct comparison with the type of subcritical dissipation observed above 1K. It can be seen from the lower value of β found here that the onset of dissipation is more gradual at these lower temperatures. It is also noteworthy that according to a thermal fluctuation type theory the value of ℓf_o at these temperatures should be much smaller than the observed value of 7×10^{10} cgs (cf. section 2.3.(c)). The curve of equation 8.2.1. with the values of v_B and ℓf_o given above has been superimposed where appropriate as a dashed line on the driven flow data shown in figures 8.2.2. to 8.2.9. It can be seen that in most cases the fit is not unreasonable, which would suggest that the

dissipation mechanism operating in the subcritical regime is the same at all temperatures below 1K.

8.3 THE DAMPING OF THE INERTIAL OSCILLATIONS BETWEEN 1K and 20mK

The existence of subcritical dissipation, as demonstrated in the previous section, leads one to expect that the inertial oscillations occurring at the end of any flow experiment should be gradually damped out. This is indeed observed to be the case. Furthermore, it should be possible, by assuming the functional form of equation 8.2.1. for the subcritical dissipation curve, to calculate independent values for the parameters v_B and f_o from the magnitude of the damping. As discussed in section 7.6.(ii), equation 8.2.1. can be improved to allow for the variation in v_s as the cross-sectional area A of the film changes. Using equation 1.8.1., equation 8.2.1. can be written as

$$\frac{g\Delta h}{\ell} = \kappa A f_o \exp\{-\frac{v_B}{v_s}\} . \qquad (8.3.1.)$$

If ℓ is allowed to become an incremental length $\Delta\ell$, then 8.3.1. becomes

$$\underline{\nabla}\mu = \kappa A f_o \exp\{-\frac{v_B}{v_s}\} , \qquad (8.3.2.)$$

which is an expression for the frictional force exerted on unit mass of superfluid flowing with velocity v_s. The energy loss over successive half-cycles of the inertial oscillations can then be computed using 8.3.2. and the damping of the oscillations estimated. By varying the parameters f_o and v_B, the degree of damping can be adjusted until a good fit to the experimental observations is obtained. I am indebted to J. Armitage for this approach and also for carrying out these calculations.

The experimental results for the damping at various temperatures

Figure 8.3.1.
The damping of the inertial oscillations below 1K for a mean rim height of 12.3mm. The logarithm of the level difference at the extrema of the oscillation is plotted against time, in the form of half periods.

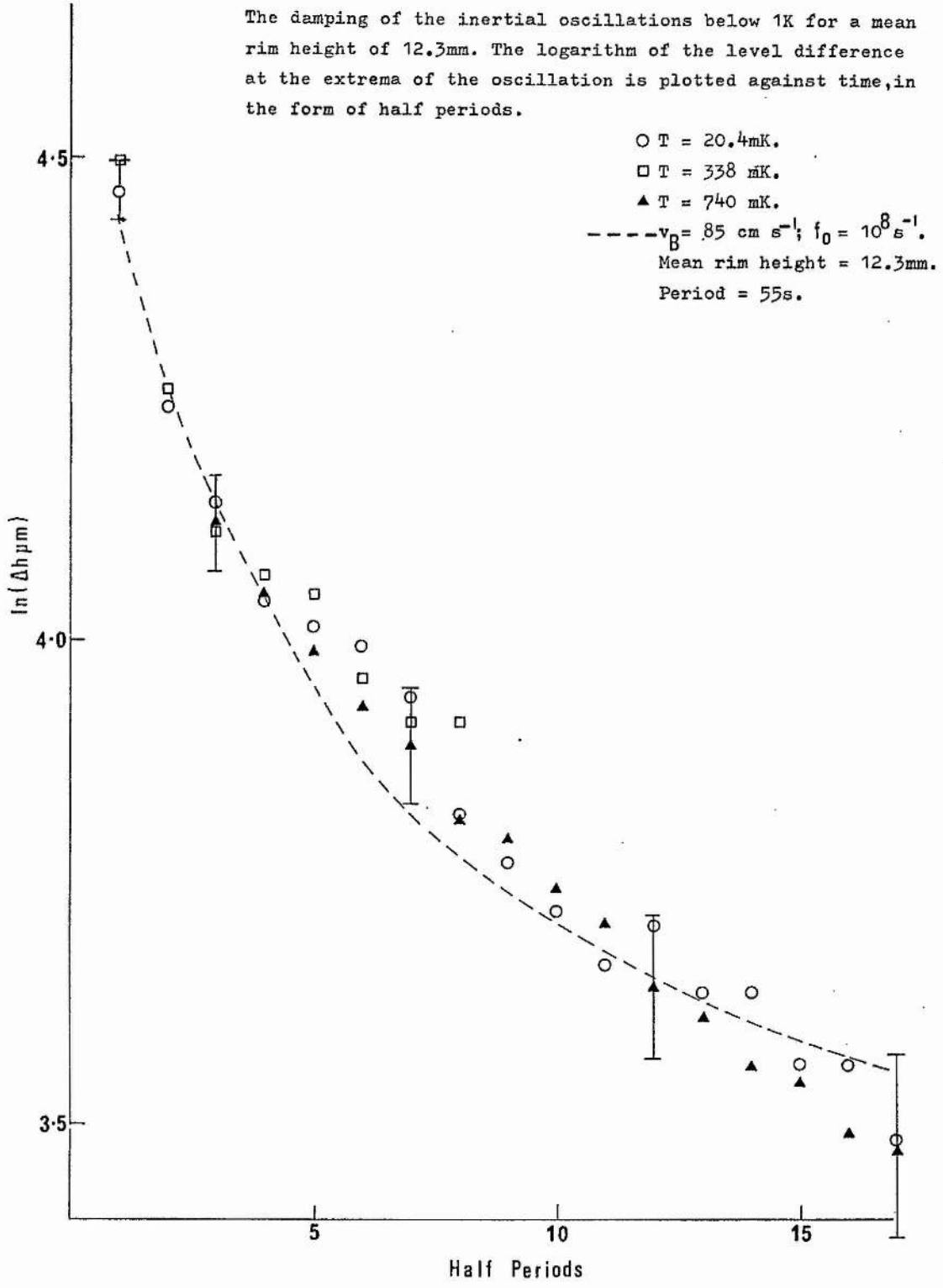

Figure 8.3.2.
The damping of the inertial oscillations below 1K for a mean rim height of 8mm. The logarithm of the level difference at the extrema of the oscillation is plotted against time, in the form of half periods.

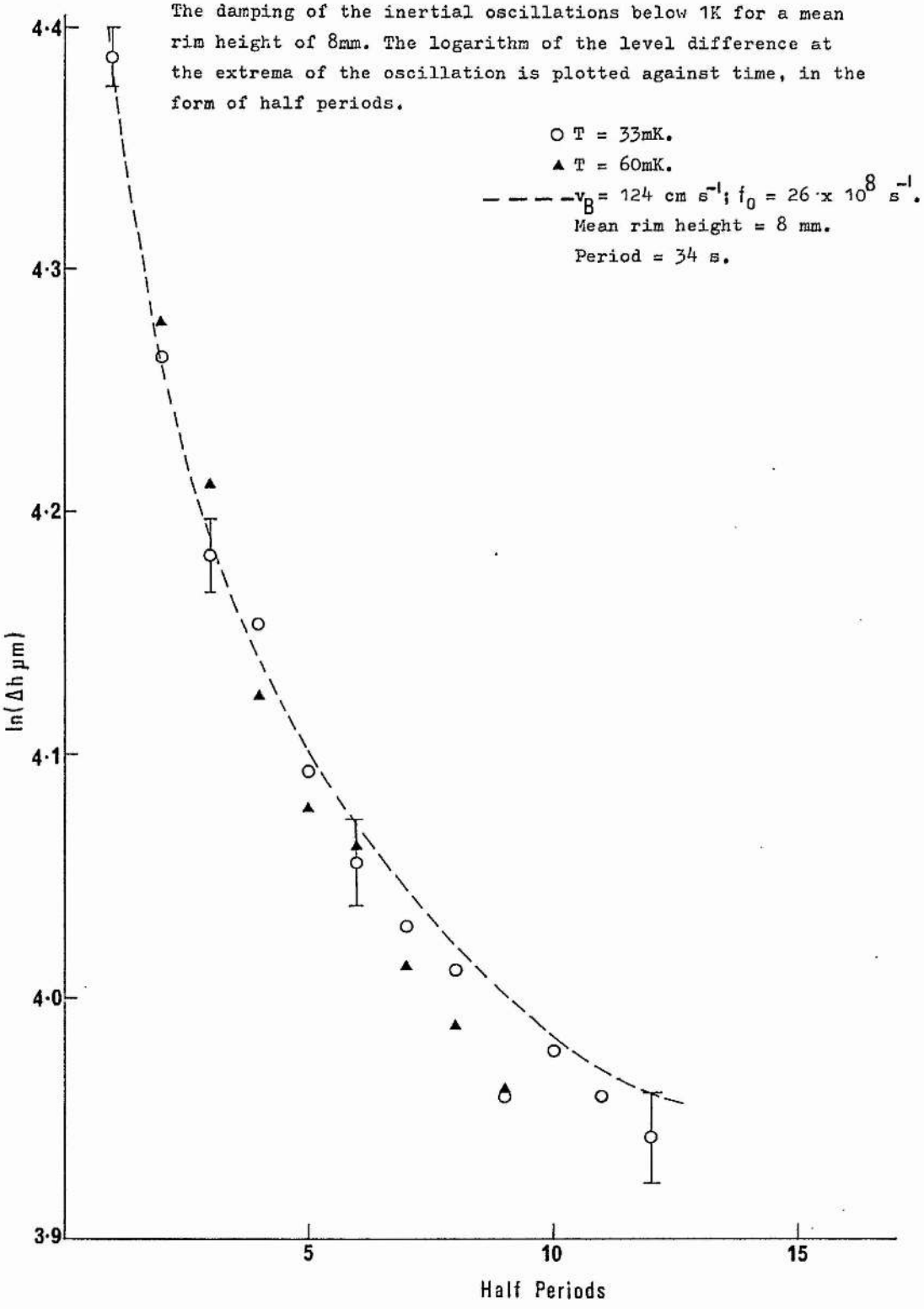

below 1K are shown in figures 8.3.1. and 8.3.2. The logarithm of the level difference at the extrema of the oscillation, expressed in μm, has been plotted against time, shown in the form of half periods. In the first figure the mean rim height of the oscillations is 12.3mm, giving a period of 55s, whilst in the second figure the mean rim height and period are 8mm, and 34s respectively. Direct comparison between the damping in the two figures cannot be made as the superfluid velocity is varying over different ranges in each case. For the purposes of comparison within each figure, the oscillations commencing at smaller amplitudes have been displaced sideways by an integral number of half cycles such that the first point coincides with an equivalent point on the other oscillation. It can be seen that the damping is non-exponential and is essentially the same over the entire temperature range 20mK to 740mK. This is in agreement with the observation that the subcritical portion of the driven flow dissipation curve is the same at all of the temperatures investigated below 1K. The dashed lines on the figures represent the calculations of J. Armitage, with the values for the parameters f_o and v_B as indicated. It was not possible to obtain a good fit over the entire duration of the oscillations. The parameters were therefore chosen to give the best fit at large amplitudes. It is not understood why their values should vary with the rim height. Direct comparison cannot be made between the values of f_o and v_B found here and those found to fit the driven flow data in section 8.2., since in the latter case the "constant film thickness" approximation was made. Consequently the values of f_o and v_B found by Armitage have been used to calculate the form of the driven flow dissipation curve, according

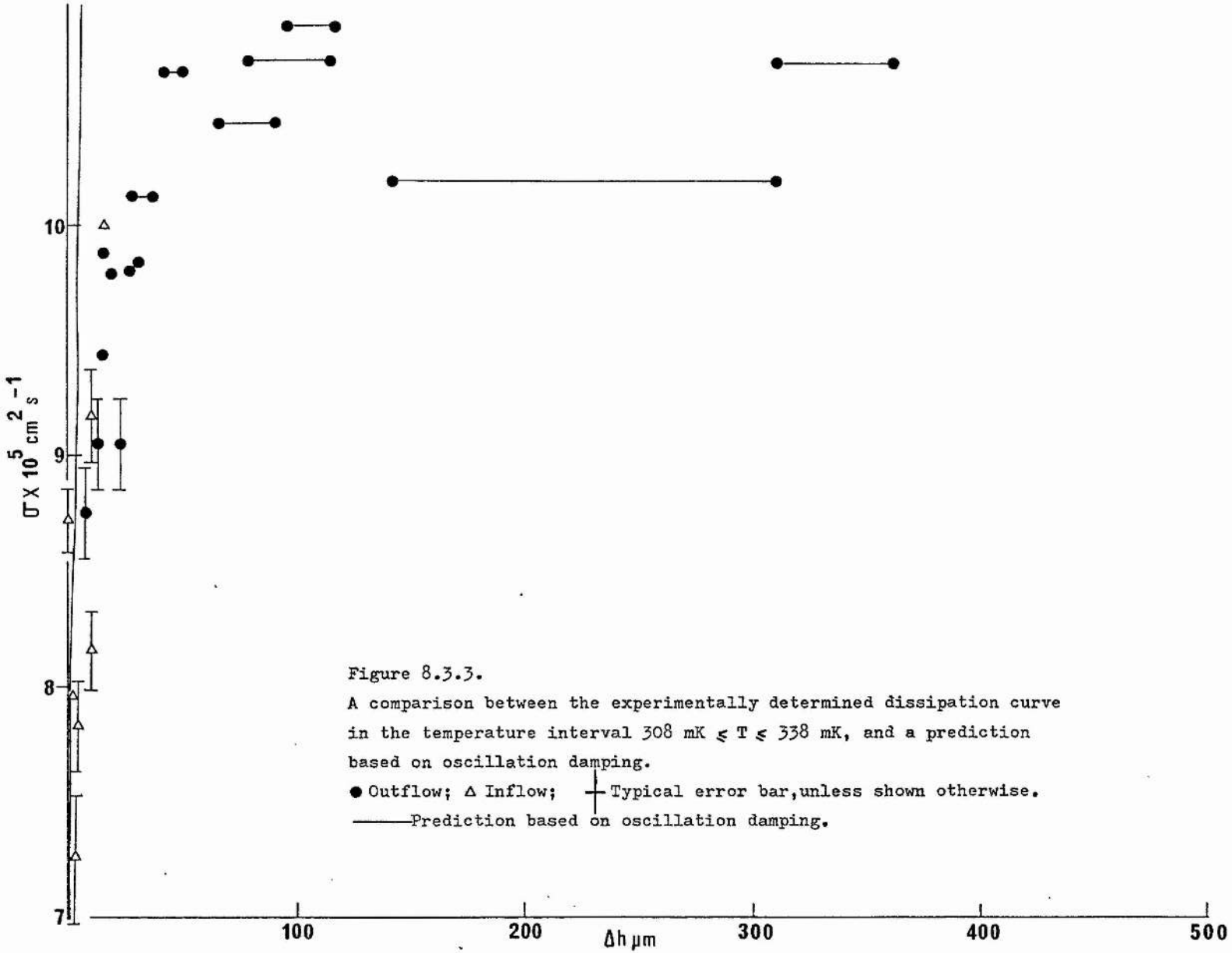

Figure 8.3.3.

A comparison between the experimentally determined dissipation curve in the temperature interval 308 mK $\lesssim T \lesssim$ 338 mK, and a prediction based on oscillation damping.

● Outflow; △ Inflow; ┼ Typical error bar, unless shown otherwise.

——— Prediction based on oscillation damping.

to the integrated form of equation 8.3.2. :

$$\Delta h = \frac{\kappa f_o}{g} \int_{film} A e^{-\frac{v_B}{v_s}} \, d\ell. \qquad (8.3.3.)$$

The results for $v_B = 85 cm\,s^{-1}$, $f_o = 10^8\ s^{-1}$, which values are appropriate to a temperature of 338mK and a rim height of 12.3mm, are shown in figure 8.3.3., superimposed on the experimental driven flow data obtained in this temperature and rim height region. The agreement is reasonable at low transfer rates but is seen to become progressively worse as σ increases. This is perhaps not surprising in that the transfer rate during the inertial oscillations rarely exceeded $5 \times 10^{-5}\ cm^2 s^{-1}$, which is well below the range of transfer rates covered in the driven flow experiments. There is no fundamental theoretical reason for choosing the functional form of equation 8.3.2. to fit to the oscillation damping. Above 1K one might argue for the existence of a thermal fluctuation dissipation mechanism but below 1K this ceases to be relevant and it is simply a matter of convenience to parameterise the frictional force in this way. If this functional form is wrong, then the error is bound to be revealed in an extrapolation of the type made in figure 8.3.3. It is in fact encouraging that the discrepancy is no greater than it is. It would be reasonable to conclude that below 1K the same dissipation mechanism is at work during both steady state driven flow and the inertial oscillations, and that by experimenting with different functional forms for the frictional force, it should be possible to improve the agreement.

Figure 8.4.1.
The damping of the inertial oscillations at a temperature of $\sim$11mK. The logarithm of the level difference at the extrema of the oscillation is plotted against time, in the form of half periods. The solid line represents exponentially damped sinusoidal oscillations with a damping constant k of 2.28 x $10^{-3}s^{-1}$.
Mean rim height = 12.57 mm.
Period = 57s.

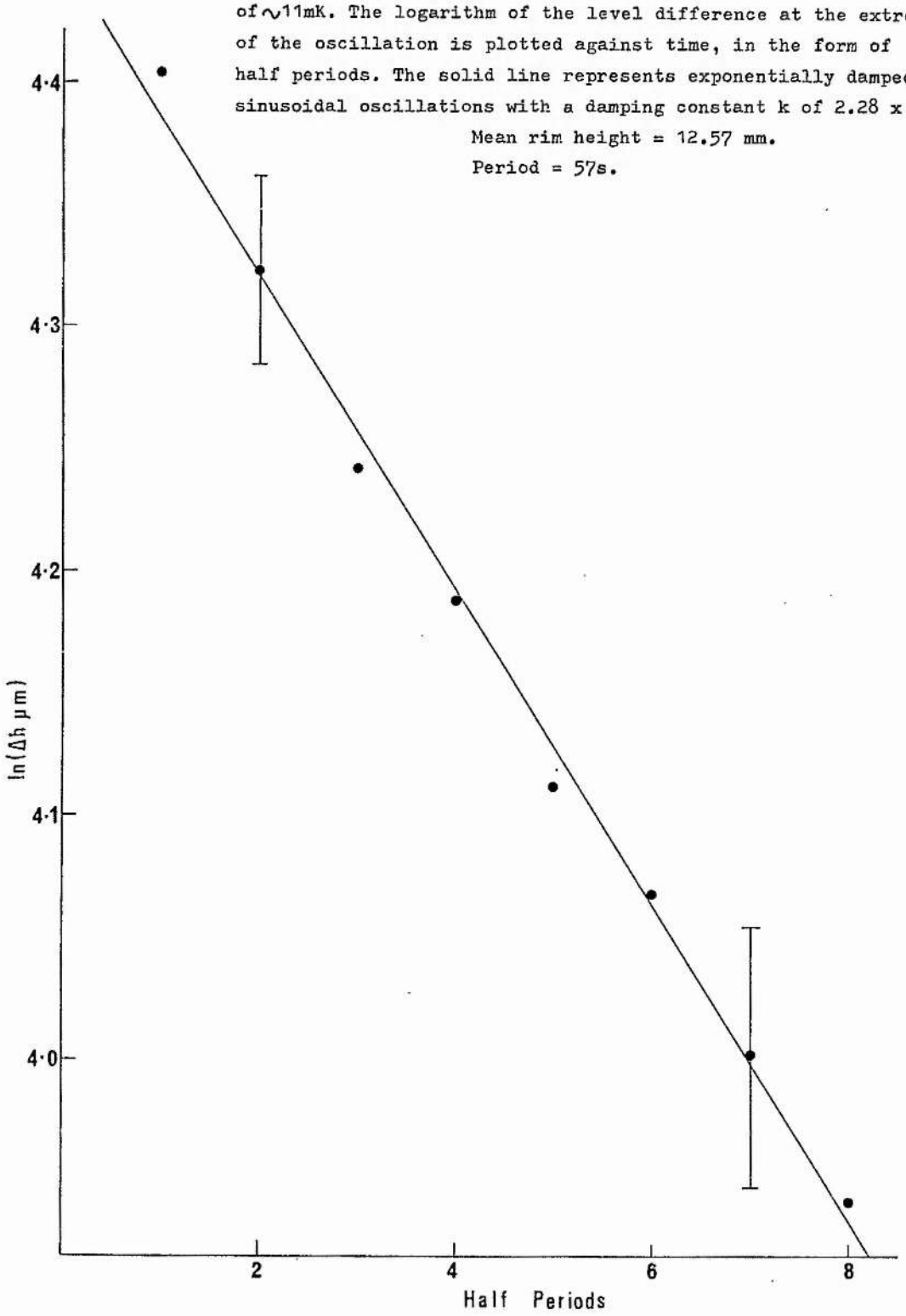

8.4 THE DAMPING OF THE INERTIAL OSCILLATIONS BELOW 20mK

At the lowest temperature attained in this series of experiments, estimated to be ∿11mK (cf. section 6.8.) the character of the damping was seen to change. Figure 8.4.1. shows a logarithmic plot of the level difference at the extrema of the oscillation versus time. By comparison with figures 8.3.1. and 8.3.2. it is apparent that the heavy non-linear damping observed during the first few half cycles for temperatures in the range 20mK $\leqslant T \lesssim$ 740mK is virtually absent at ∿11mK. The damping is now almost purely exponential, which implies that the frictional force F_s on unit mass of superfluid is linear in the superfluid velocity:-

$$F_s = 2k\, v_s \,. \qquad (8.4.1.)$$

The equation of motion for the two reservoirs linked by a superfluid film is that of a damped oscillator:-

$$\ddot{y} + 2k\dot{y} + \omega_o^2 y = 0, \qquad (8.4.2.)$$

where y is the level difference and ω_o is the undamped angular frequency, given by

$$\omega_o = \{\frac{\rho_s}{\rho} \frac{g\pi r}{A^*} (\int_0^H \frac{dH}{d})^{-1}\}^{\frac{1}{2}} \,. \qquad (8.4.3.)$$

d is the film thickness, H is the rim height, r is the beaker radius and A^* is the reduced area, defined as

$$A^* = \frac{A_{in} A_{out}}{A_{in} + A_{out}} \,, \qquad (8.4.4.)$$

A_{in} and A_{out} are the areas of the inner and outer liquid reservoirs respectively.

The solution of equation 8.4.2. is

$$y = y_o e^{-kt} \sin\omega t, \qquad (8.4.5.)$$

where

$$\omega^2 = \omega_o{}^2 - k^2 \ . \qquad (8.4.6.)$$

The damping constant k of the oscillations shown in figure 8.4.1. is $(2.28 \pm .14) \times 10^{-3}$ cgs which, on substitution into equation 8.4.1. yields for the frictional force on unit mass of superfluid

$$F_s = (4.56 \pm .28) \times 10^{-3} \ v_s \text{ dynes gm}^{-1}. \qquad (8.4.7.)$$

The form of the steady state, driven flow dissipation curve in this new regime can be calculated from equation 8.4.2. Setting

$$\ddot{y} = 0 \text{ and } \dot{y} = \frac{2\pi r\sigma}{A^*} \ ,$$

we get $$\frac{2k}{\omega_o^2} \cdot \frac{2\pi r}{A^*}\sigma = y. \qquad (8.4.8.)$$

Substituting for ω_o from equation 8.4.3. gives

$$y = \left(\frac{4k}{g}\frac{\rho}{\rho_s}\int_0^H \frac{dH}{d}\right)\sigma. \qquad (8.4.9.)$$

The film profile during these inertial oscillations is assumed to take the form found by Crum et al.

$$d = \frac{293 \times 10^{-8}}{H^{1/3.7}} \text{ cm.} \qquad (8.4.10)$$

Equation 8.4.9. can therefore be evaluated, using the mean rim height of 12.574mm appropriate to the oscillations of figure 8.4.1. The form of the subcritical dissipation curve at this rim height is found to be

$$y = 3.34 \times \sigma, \qquad (8.4.11.)$$

where y is the level difference in cm and σ is the film transfer rate in $cm^2 s^{-1}$.

The driven flow results obtained in this very low temperature region are shown in figure 8.2.3. The data is sparse, but would admit to the subcritical dissipation taking the form of equation 8.4.11.,

Figure 8.5.1.

Transfer rate Γ versus level difference Δh at a temperature of 1.14K.

● Outflow; △ Inflow; ┼ Typical error bar (unless shown otherwise).

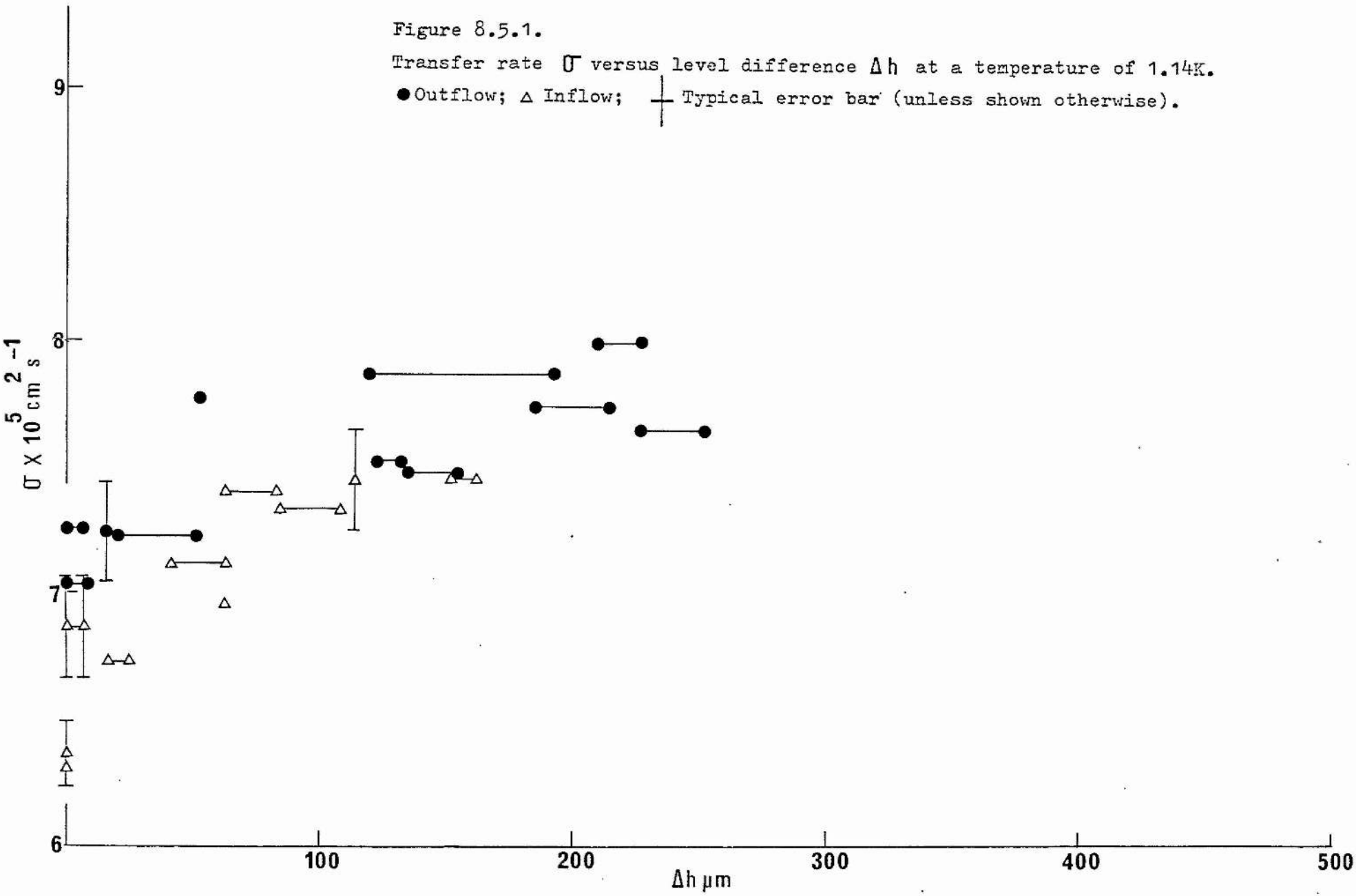

in that such a curve would give hardly resolvable level differences even at high transfer rates. (For $\sigma = 10^{-4}$ cm^2 s^{-1} the level difference would be 3.3μ, which could just be resolved from zero within the present experimental error.)

As was discussed in sections 7.6.(v) and 8.2 an unexpected trend in the temperature dependence of the critical flow rate accompanies the change in subcritical behaviour below 20mK. Observations made in both driven flow and large level difference experiments show that at temperatures in this region, the critical transfer rate increases slightly with decreasing temperature. It is hoped that these indications of the possible existence of a new type of dissipation regime will stimulate further experimental work in the temperature range below 10mK.

8.5 DRIVEN FLOW ABOVE 1K

A series of driven flow experiments was carried out at a temperature of 1.14K to compare subcritical behaviour above 1K with that observed below 1K. It was also hoped to show that the functional form of the subcritical dissipation curve found in section 7.6.(ii) for level differences in the range $500\mu m \lesssim \Delta h \lesssim 3mm$ was also valid at very small level differences.

The results are shown in figure 8.5.1. where it can be seen that an entirely different behaviour to that found at lower temperatures now prevails. The transition between subcritical and critical regimes at $\Delta h \sim 40\mu$ is no longer evident. Instead the subcritical regime persists over the whole range of Δh covered. Furthermore, the metastable rates characteristic of critical flow are now present in the subcritical region, although their stability to large changes in

Figure 8.5.2.

A plot of $\ln \Delta h$ versus $\frac{1}{\sigma}$, for both driven flow and flow from large level differences, at temperatures of 1.14K and 1.12K respectively.

● Inflow from a large level difference.

△ Driven flow.

—— See text.

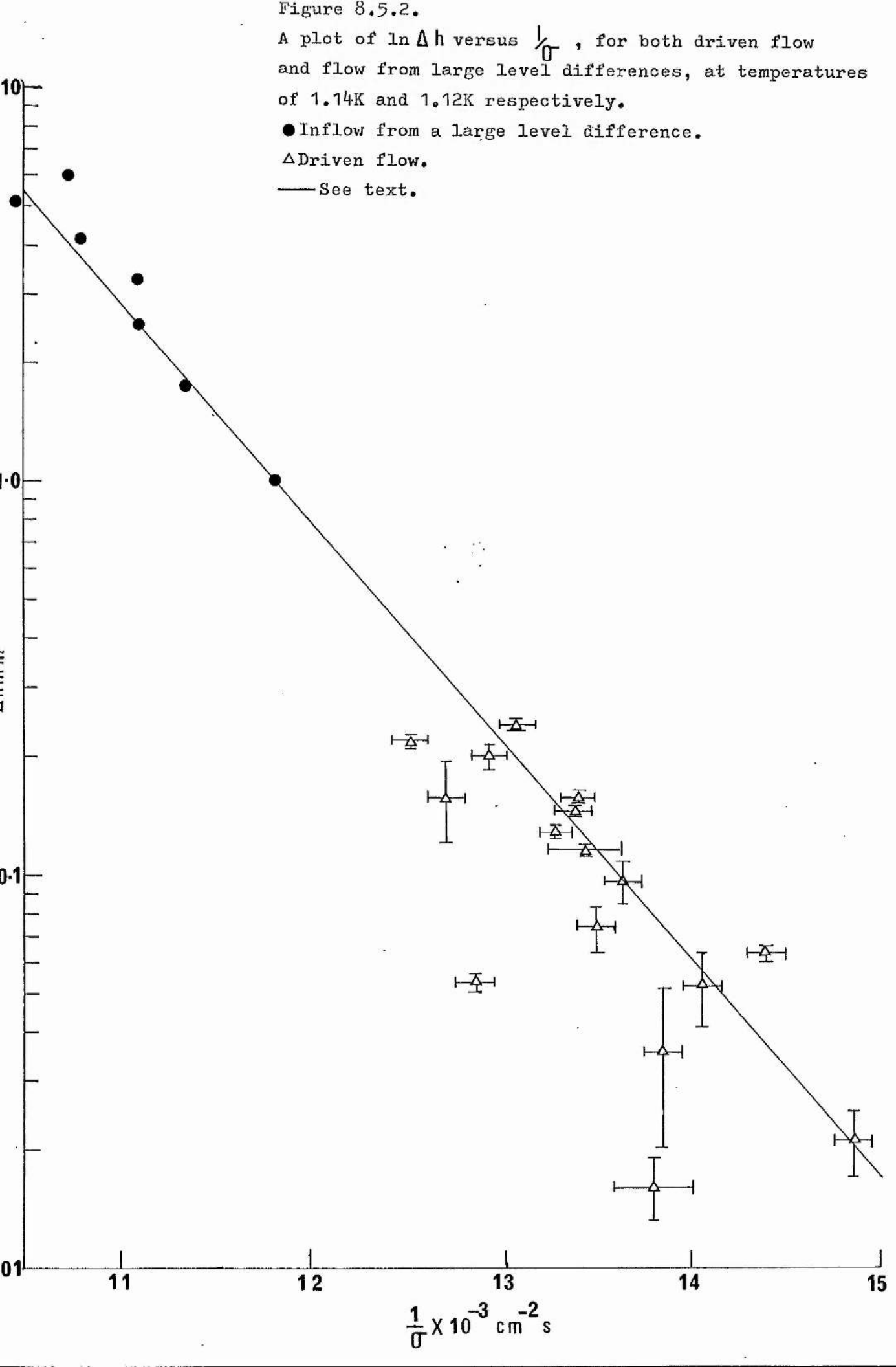

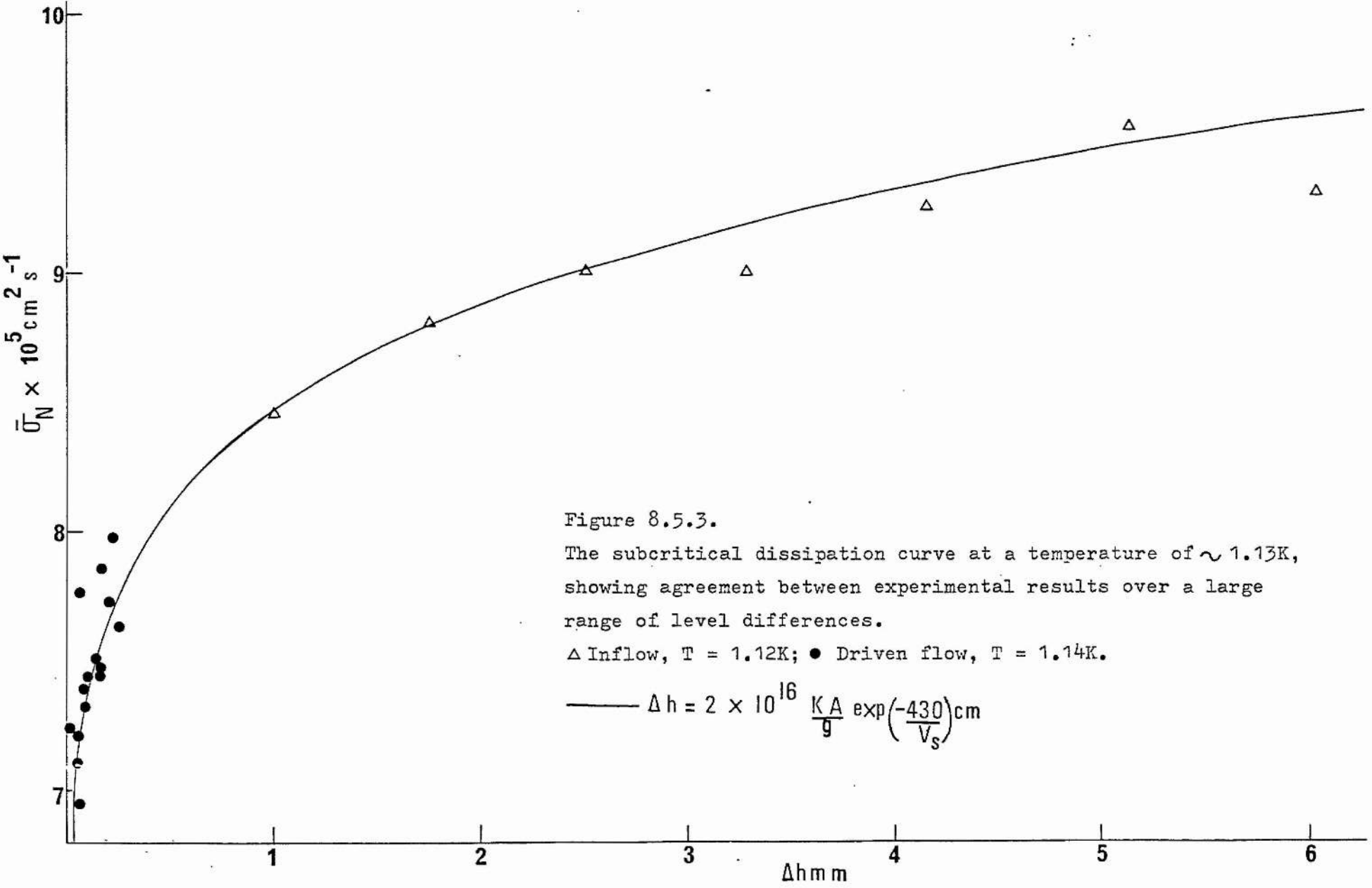

Figure 8.5.3.

The subcritical dissipation curve at a temperature of $\sim$ 1.13K, showing agreement between experimental results over a large range of level differences.

△ Inflow, T = 1.12K; ● Driven flow, T = 1.14K.

——— $\Delta h = 2 \times 10^{16} \frac{KA}{g} \exp\left(\frac{-430}{V_s}\right) \text{cm}$

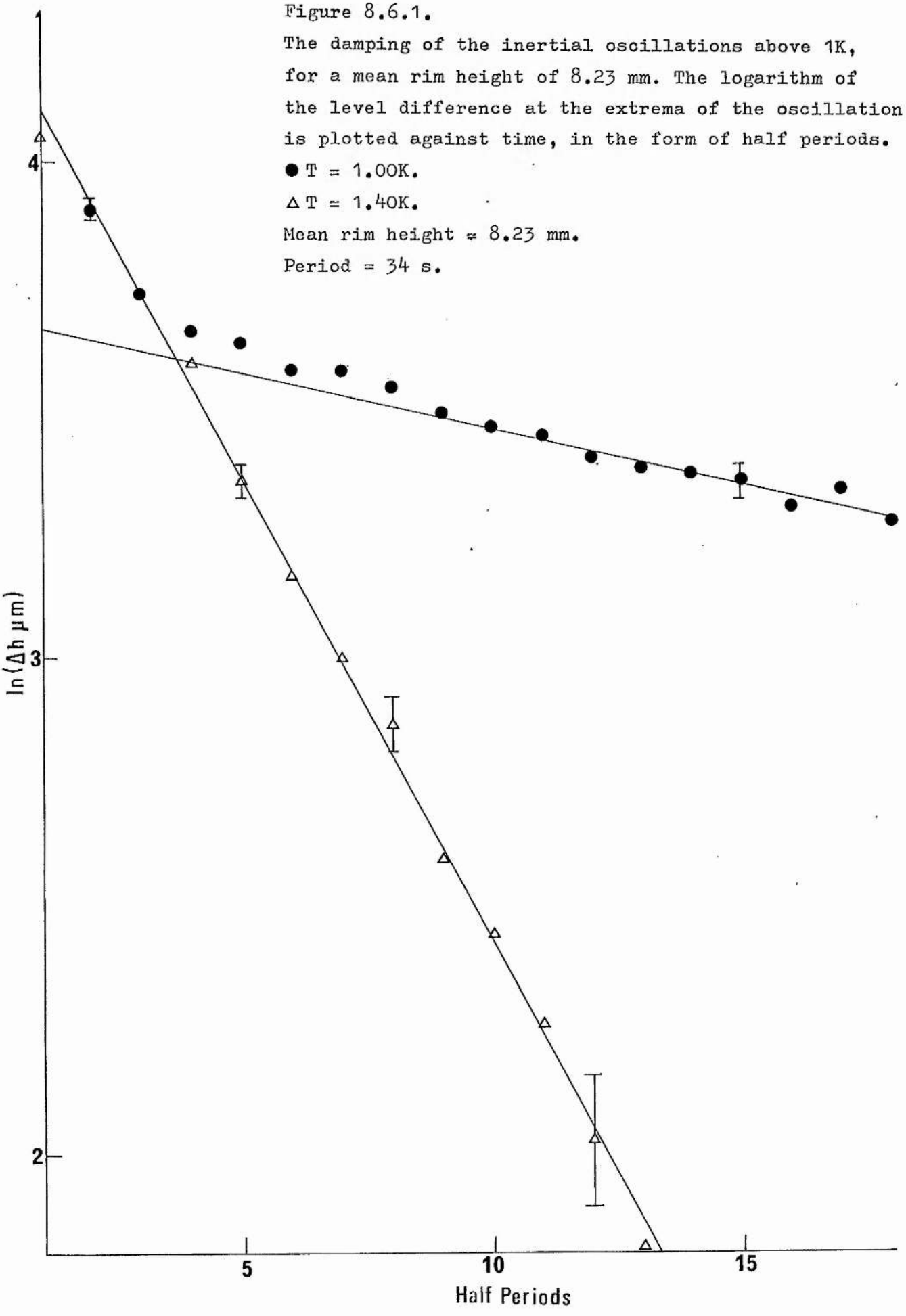

Figure 8.6.1.
The damping of the inertial oscillations above 1K, for a mean rim height of 8.23 mm. The logarithm of the level difference at the extrema of the oscillation is plotted against time, in the form of half periods.
● T = 1.00K.
△ T = 1.40K.
Mean rim height = 8.23 mm.
Period = 34 s.

Figure 8.6.2.
The damping of the inertial oscillations above 1K, for a mean rim height of 12.33 mm. The logarithm of the level difference at the extrema of the oscillation is plotted against time, in the form of half periods.
● T = 1.20K.
△ T = 1.62K.
Mean rim height = 12.33 mm.
Period = 56 s.

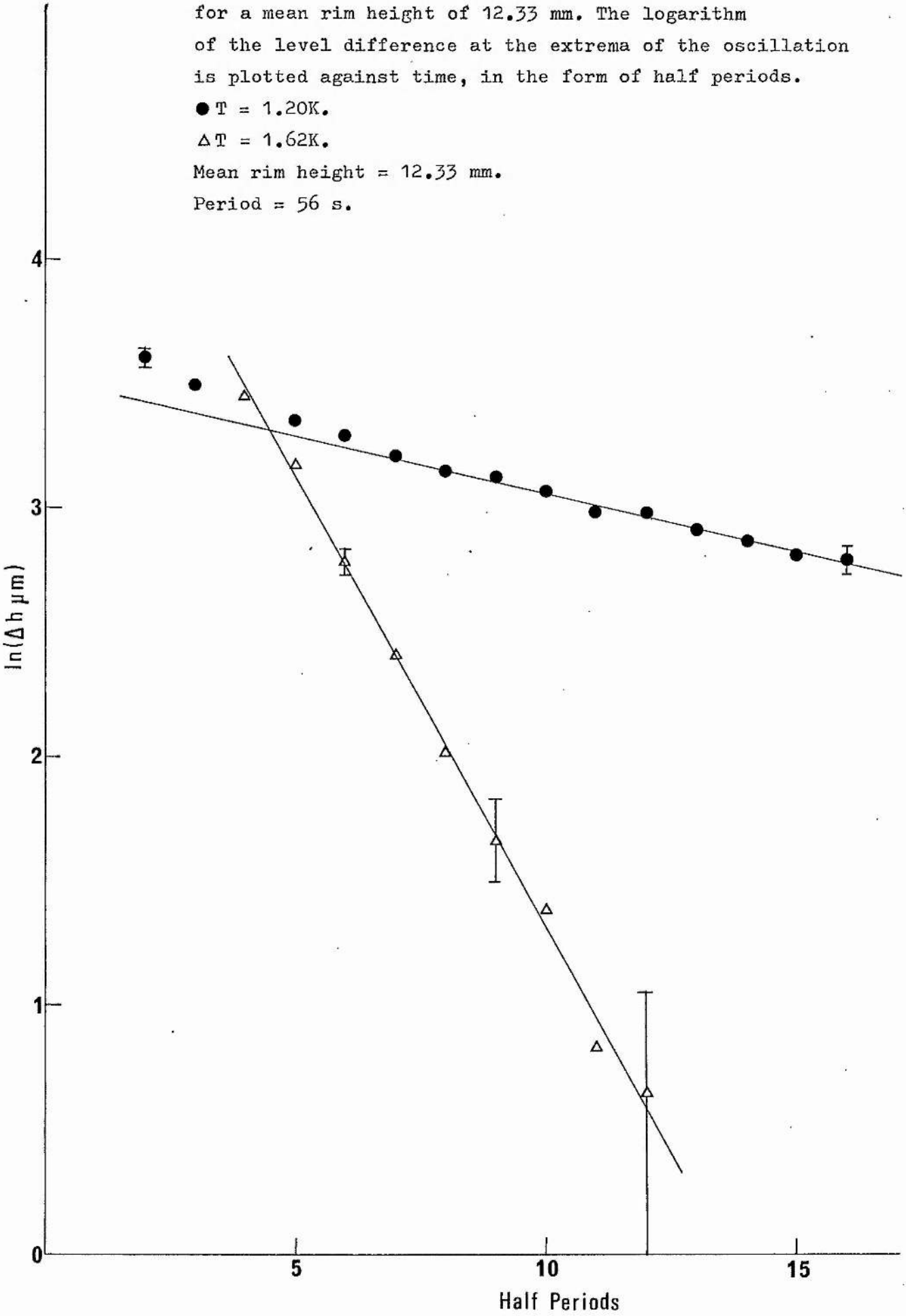

Δh is reduced. This causes the data to fall in a broad band rather than lie on a well defined curve.

To test the functional dependence of the mean rate on the level difference, the data of figure 8.5.1. has been plotted in figure 8.5.2. as $\ell n\ \Delta h$ versus $\frac{1}{\sigma}$. Included in the same graph is the data from figure 7.6.3. for subcritical flow at the same temperature but from a large level difference. The solid line is that found in section 7.6.(ii) to best represent this large level difference subcritical data. (The parameters ℓf_o and β for a temperature of 1.12K are given in table 7.6.1. It can be seen that an extrapolation of the line represents the driven flow data quite well. This confirms that the subcritical dissipation observed at $\sim$1.13K in both driven flow and flow from large level differences can be characterised by

$$\Delta h = \frac{\kappa A}{g} = 2 \times 10^{16} \exp\left(\frac{-430}{v_s}\right) . \qquad 8.5.1.$$

Figure 8.5.3. shows the data plotted as $\bar{\sigma}$ versus Δh with the curve of equation 8.5.1. superimposed.

8.6 DAMPING OF THE INERTIAL OSCILLATIONS ABOVE 1K

In figures 8.6.1. and 8.6.2. the damping of the inertial oscillations at four temperatures spanning the range $1.0K \lesssim T \lesssim 1.625K$ is displayed in the same manner as in figures 8.3.1. and 8.3.2. It can be seen that at the lower two temperatures the first few half cycles exhibit heavy non-linear damping which disappears in favour of exponential damping at smaller amplitudes (and consequently, smaller superfluid velocities). At the higher temperatures, the damping becomes exponential at all amplitudes.

The occurrence of exponential damping in this temperature region is in agreement with the observations of other workers, as described in section 3.8, and with the predictions of Robinson, as described in section 2.4. Quantitative comparison of the magnitude of the damping constant with the Robinson theory cannot be made in this instance as the thermal conductance between the inner and outer liquid reservoirs was not measured. Such a comparison is not, however, thought to be necessary, since the applicability of the theory has been sufficiently well demonstrated by several groups, in the temperature region above 1K.

It is of interest to note that whilst the oscillation damping is dominated by irreversible heat exchange rather than intrinsic dissipation in the superfluid itself, the opposite is true of the driven flow experiments carried out above 1K. The size of the damping constant k is consistent with this statement. In figure 8.6.2. a straight line fit has been made to the latter half of the 1.2K data, corresponding to the region dominated by Robinson type dissipation. The value of k is found to be 1.68×10^{-3} cgs. The expression for the size of the fountain head accompanying steady state driven flow in the Robinson regime is identical to that given in equation 8.4.9.

$$y = \left(\frac{4k}{g}\frac{\rho}{\rho_s}\int_0^H \frac{dH}{d}\right)\sigma \ . \qquad (8.4.9.)$$

However it should be stressed that in this case no dissipation is taking place in the film itself; the fountain head merely maintains a zero chemical potential difference across the film by balancing the term due to the temperature difference between the reservoirs. For the rim height H = 12.321mm appropriate to the oscillations at

1.2K, the coefficient of σ in equation 8.4.9 can be evaluated to give

$$y = 2.45\sigma \ , \qquad (8.6.1.)$$

where y is in cm and σ is in $cm^2\ s^{-1}$. Thus for a transfer rate of $8 \times 10^{-5}\ cm^2 s^{-1}$ the fountain head due to Robinson type dissipation would be $\sim$2μm. This is in fact a tiny fraction of the actual level difference observed at this transfer rate, as can be seen from figure 8.5.3. Intrinsic superfluid dissipation is thus the dominant process at the transfer rates occurring in the driven flow experiments.

8.7 SUMMARY AND CONCLUSIONS

The driven flow experiments described in this chapter are the first measurements of their type to be made below 1K. They reveal that below 1K the "critical" dissipation regime does not persist to zero level difference. Instead, at a level difference of $\sim$40μm a transition is made into a "subcritical" regime. Thus it appears that even for small flow rates there is always a finite amount of dissipation in the superfluid.

The onset of dissipation in this new regime is much more gradual than is observed in the subcritical regime above 1K. Presumably, this is due to there only being one vortex nucleation mechanism at work below 1K, whilst above 1K it is thought that an additional temperature dependent mechanism may operate. The subcritical portions of the dissipation curves for all driven flow experiments between 20mK and 340mK are seen to be similar. This apparent temperature independence is also seen in the damping of the inertial oscillations, which is the same at temperatures between 740mK and 20mK. The detailed mechanism at work in this subcritical

dissipation region remains open to speculation but in view of the observed temperature independence, and the very low temperatures, it seems unlikely that a thermal fluctuation type process could operate.

At the lowest temperature attained, ∿11mK, it is thought that a different type of subcritical dissipation regime exists. The damping of the inertial oscillations is now exponential, implying that the frictional force on unit mass of superfluid is directly proportional to the superfluid velocity. The constant of proportionality is found to be $(4.56 \pm .28) \times 10^{-3}$ dynes $gm^{-1} cm^{-1} s$.

The critical dissipation regime observed in the driven flow experiments for $\Delta h \gtrsim 40\mu m$ shows the same characteristics as the critical regime observed in flows from large heads below 1K. In particular the temperature dependence of the mean flow rate below 250mK is the same in both cases. This implies that film heating effects are absent and that the degradation of flow energy into heat takes place in the liquid reservoirs rather than the film itself.

Above 1K, the results of the driven flow experiments showed that the subcritical dissipation curve appropriate to flows from large level differences is also valid in the region $\Delta h \lesssim 250\mu m$. However the exponential damping of the inertial oscillations indicates that at lower transfer rates the dominant dissipation mechanism is of the Robinson type.

The results of this study of superfluidity at very low temperatures point to many areas in which further work is necessary. In particular, more experiments on driven flow and oscillation damping could lead to a better understanding of the basic subcritical dissipation mechanism below 1K. Transitions between subcritical and critical

regimes are also of considerable interest, whilst the modified subcritical behaviour seen below 20mK would provide an especially demanding, and hopefully fruitful, field of research.

APPENDIX A

DETERMINATION OF THE OPTIMUM CELL FLUSHING CYCLE

Let the pressure at the top of the filling capillary be P_1, the pressure in the cell be P_2 and the volume of the cell be V. Let the filling capillary be of total length ℓ and bore 2R. For laminar flow of gas through the capillary, the rate of mass transfer Q through a short section of length $\Delta\ell$ over which the pressure drop is ΔP is given by

$$Q = \frac{\pi\rho R^4 \Delta P}{8\eta\Delta\ell} \quad . \tag{A.1}$$

η is the viscosity of the gas and ρ is the density, which is assumed to remain constant over the short length $\Delta\ell$. Writing ρ as

$$\rho = \frac{Pm}{kT} \quad , \tag{A.2}$$

where P is the gas pressure, m is the mass of a molecule and k is Boltzmann's constant, gives on substitution into equation A.1,

$$\frac{\Delta P}{\Delta\ell} = \frac{8Q\eta kT}{\pi R^4 Pm} \quad . \tag{A.3}$$

The total pressure drop across the capillary is thus found by integration of equation A.3;

$$\int_1^2 P\, dP = \int_1^2 \frac{8Q\eta kT}{\pi R^4 m}\, d\ell \quad , \tag{A.4}$$

or

$$P_2^{\,2} - P_1^{\,2} = \frac{16Q\eta kT\ell}{\pi R^4 m} \quad . \tag{A.5}$$

Now, the total mass M of gas contained in the cell is given from the ideal gas law by

$$M = \frac{mP_2V}{kT} \quad . \tag{A.6}$$

The rate of change of M with the cell pressure P_2 is therefore given by

$$dM = \frac{mV}{kT} dP_2 \ . \qquad (A.7)$$

However dM can also be written as

$$dM = -Qdt \ . \qquad (A.8)$$

Equating A.8 and A.7 and substituting for Q from A.5 gives

$$\frac{dP_2}{(P_2^2 - P_1^2)} = - \frac{\pi R^4}{16V\eta\ell} dt \ . \qquad (A.9)$$

The pressure P_1 will be held constant at some low value during pumping whilst the cell pressure P_2 falls with time. The length of time t_p necessary to reduce P_2 to some predetermined value $P_2(t_p)$ is found by integration of A.9 to be

$$t_p = \frac{8V\eta\ell}{P_1\pi R^4} \ell n\left[\frac{P_1 + P_2(t_p)}{P_1 - P_2(t_p)} \frac{\alpha}{\beta}\right] \ , \qquad (A.10)$$

where
$$\alpha = P_1 - P_2(o) \ , \qquad (A.11)$$

and
$$\beta = P_1 + P_2(o) \ . \qquad (A.12)$$

The same equation can be used to calculate the time t_b needed to backfill the cell (with pure ^{4}He gas) to a predetermined pressure $P_2(t_b)$. The pressure P_1 is again essentially constant, but now refers to the pressure of the cylinder of pure ^{4}He. $P_2(o)$ becomes the cell pressure prior to the backfilling operation which is by definition $P_2(t_p)$. The total time τ taken to complete a single cycle of pumping followed by backfilling can therefore be calculated as a function of $P_2(t_p)$, the lowest pressure to which the cell is pumped in the cycle. Now the number n of such cycles is determined by the condition that, starting from a situation where the cell contains 100% air, the final partial pressure of the air in the cell must be $<2 \times 10^{-2}$ torr. Thus,

if the dilution factor obtained in each cycle is α, then n is given by

$$\alpha^n = \frac{.02}{760} = 2.63 \times 10^{-5} . \qquad (A.13)$$

α is given by

$$\alpha = \frac{P_2(t_p)}{P_2(o)} \qquad (A.14)$$

where $P_2(o)$ is 1 atmosphere. From A.13 and A.14 we therefore have for the number n of cycles

$$n = \frac{\ell n[2.63 \times 10^{-5}]}{\ell n[\frac{P_2(t_p)}{P_2(o)}]} \qquad (A.15)$$

which again is a function of $P_2(t_p)$. The total time τ_o needed to complete the n cycles is given by

$$\tau_o = n(P_2(t_p))\ \tau(P_2(t_p)) \qquad (A.16)$$

which was calculated for several values of $P_2(t_p)$.

The values used for the various parameters of the system were as follows: $V = 160cm^3$; $\ell = 650cm$; $R = .011cm$; $\eta = 190\mu poise$; P_1 during pumping cycle = 1torr; P_1 during backfilling cycle = 760torr; $P_2(o)$ during pumping cycle = 760torr; $P_2(o)$ during backfilling cycle = $P_2(t_p)$ during pumping cycle; $P_2(t_b)$ during backfilling cycle = 0.95×760torr. τ_o was seen to exhibit a minimum for $P_2(t_p) = 305$torr. Substitution of this value into equation A.10 gives the pumping and backfilling times of a single cycle as $t_p = 2.81$ hours and $t_b = 2.65$ hours. Substitution of $P_2(t_p) = 305$torr into equation A.15 gives the number of cycles as 12.

APPENDIX B

CALCULATION OF THE FREQUENCY OF A STANDING THIRD SOUND WAVE IN THE FILM COVERING THE SURFACE OF THE BEAKER

The velocity U_3 of third sound is given by

$$U_3 = \left[\frac{\rho_s}{\rho} fd\right]^{\frac{1}{2}} , \tag{B.1}$$

where f is the force per unit mass at the surface of the film and d is the film thickness. For the case of third sound, f is thought to be dominated by the Van der Waals term, and can therefore be written as

$$f = \frac{3\alpha}{d^4} , \tag{B.2}$$

where α is the Van der Waals constant. From equation (1.7.3), the film thickness at a height z above the bulk level can be expressed as

$$d = \left(\frac{\alpha}{gz}\right)^{1/3} . \tag{1.7.3}$$

Substituting into equation B.1 for f and d yields

$$U_3 = \left[3\frac{\rho_s}{\rho} gz\right]^{1/2} . \tag{B.3}$$

Thus, at any point in the surface of the film, height z above the bulk liquid, the instantaneous wavelength of a third sound wave of frequency f can be written as

$$\lambda(z) = \frac{U_3(z)}{f} = \frac{1}{f}\left(3\frac{\rho_s}{\rho} gz\right)^{1/2} . \tag{B.4}$$

The change $d\phi$ in the phase angle ϕ with an incremental change dz in z can be written as

$$d\phi = \frac{dz}{\lambda(z)} \cdot 2\pi . \tag{B.5}$$

The total phase change in going from one liquid level to the other is given by integration of equation B.5:-

$$\Delta\phi = 2\pi \int_{\text{film length}} \frac{dz}{\lambda(z)} = 4\pi \int_o^{\text{rim}} \frac{dz}{\lambda(z)} \quad . \tag{B.6}$$

It would be reasonable to assume that the same boundary conditions exist at both bulk liquid surfaces, in which case the minimum value of $\Delta\phi$ will be π. Substitution in B.6 for $\Delta\phi$ and $\lambda(z)$ gives

$$\pi = 4\pi \int_o^{\text{rim}} \frac{f}{(3\frac{\rho_s}{\rho} gz)^{1/2}} dz \quad , \tag{B.7}$$

or

$$\frac{1}{4} (3\frac{\rho_s}{\rho} g)^{1/2} = 2f [z^{\frac{1}{2}}]_o^{\text{rim}} \quad . \tag{B.8}$$

If the rim height is H, then the frequency of the standing wave is given by

$$f = \frac{1}{8} (3\frac{\rho_s}{\rho} \frac{g}{H})^{1/2} \quad . \tag{B.9}$$

For $\frac{\rho_s}{\rho} \sim 1$ and $H \sim 1\text{cm}$, f takes the value of 6.8Hz.

REFERENCES

Allen J.F. (1960) Nature (London) 185, 831.

Allen J.F. (1963) Proc. Enrico Fermi School of Phys., Varenna, p.305, Academic Press, London.

Allen J.F. and Armitage J.G.M. (1966) Phys. Lett. 22, 121.

Allen J.F., Armitage J.G.M. and Saunders B.L. (1974) "Low Temperature Physics" L.T.13. Plenum Press 1, 258.

Allen J.F. and Matheson C.C. (1966) Proc. Roy. Soc. (London) A290, 1.

Allen J.F., Matheson C.C. and Walker C.M. (1965) Phys. Lett. 19, 199.

Allen J.F. and Misener A.D. (1938) Nature (London) 141, 75.

Allen J.F. and Misener A.D. (1939) Proc. Roy. Soc. A172, 467.

Ambler E. and Hudson RP(1955) Reports on Prog. in Phys. 18, 251.

Ambler E. and Kurti N. (1952) Phil. Mag. 43, 260.

Anderson A.C., Reese W. and Wheatley J.C. (1963) Rev. Sci. Instr. 34, 1386.

Anderson P.W. (1966) Rev. Mod. Phys. 38, 298.

Andreev A.F. (1966) Sov. Phys. J.E.T.P. 23, 939.

Arkhipov R.G. (1958) Sov. Phys. J.E.T.P. 6, 90.

Atkins K.R. (1950a) Proc. Roy. Soc. A203, 119.

Atkins K.R. (1950b) Proc. Roy. Soc. A203, 240.

Bakalyar D., Swinehart R. and Weyhmann W. (1972) Rev. Sci. Instr. 43, 1221.

Banton M.E. (1974) Journ. Low Temp. Phys. 16, 211.

Bertman B. and Kitchens T.A. (1968) Cryogenics 8, 36.

Black W.C., Roach W.R. and Wheatley J.C. (1964) Rev. Sci. Instr. 35, 587.

Bowers R. and Mendelssohn K. (1950) Proc. Phys. Soc. A63, 1318.

Burge E.J. and Jackson L.C. (1951) Proc. Roy. Soc. A205, 270.

Campbell L.J. (1970) Journ. Low Temp. Phys. 3, 175.

Campbell L.J. (1972) Journ. Low Temp. Phys. 8, 105.

Campbell L.J. (1975) "The Helium Liquids", S.U.S.S.P. XV. (Armitage and Farquhar Eds.) Academic Press, p.161.

Campbell L.J, Hammel E.F., Hoffer J.K. and Keller W.E. (1976) Journ. Low Temp. Phys. 24, 527.

Cannon W.C., Chester M. and Jones B.K. (1972) Journ. Low Temp. Phys. 9, 307.

Chandrasekhar B.S. and Mendelssohn K. (1955) Proc. Phys. Soc. (London) A68, 857.

Chester M. and Ziff R. (1971) Journ. Low Temp. Phys. 5, 285.

Clow J.R. and Reppy J.D. (1967) Phys. Rev. Lett. 19, 291.

Cohen M. and Feynman R.P. (1957) Phys. Rev. 107, 13.

Crum D.B. (1973) Thesis, Ohio State University.

Crum D.B., Edwards D.O. and Sarwinskii R.E. (1974) Phys. Rev. A9, 1312.

Daunt J.G. and Mendelssohn K. (1939) Proc. Roy. Soc. A170, 423, 439.

Daunt J.G. and Mendelssohn K. (1946) Nature (London) 157, 829.

De Klerk D. (1956) Handbuch der Physik (Springer-Verlag) 15, 38.

Donnelly R.J. and Roberts P.H. (1971) Phil. Trans. Roy. Soc. London, A271, 41.

Eselson B.N. and Lasarev B.G. (1951) Dokl. Akad. Nauk. SSSR, 81, 537.

Eselson B.N. and Lasarev B.G. (1952) Zh. Eks. Teor. Fiz. 23, 552.

Feynman R.P. (1953) Phys. Rev. 91, 1301.

Feynman R.P. (1954) Phys. Rev. 94, 262.

Feynman R.P. (1955) Prog. Low Temp. Phys. (Gorter ed.) 1, 17.

Feynman R.P. and Cohen M. (1956) Phys. Rev. 102, 1189.

Fineman J.C. and Chase C.E. (1963) Phys. Rev. 129, 1.

Frenkel J. (1940) Journal of Physics U.S.S.R. 2, 345.

Galkiewicz R.K. and Hallock R.B. (1974) Phys. Rev. Lett. 33, 1073.

Galkiewicz R.K., Telschow K.L. and Hallock R.B. (1977) Journ. Low Temp. Phys. 26, 147.

Giauque W.F., Stout J.W., Egan C.J. and Clark C.W. (1941) Journ. Amer. Chem. Soc. 63, 405.

Glaberson W.I. and Donnelly R.J. (1966) Phys. Rev. 141, 208.

Gopal E.S. (1963) Ann. Phys. (N.Y.) 25, 196.

Graham G.M. (1977) Journ. Low Temp. Phys. 27, 177.

Graham G.M. and Vittoratos E. (1974) Phys. Rev. Lett. 33, 1136.

Gribbon P.W.F. and Jackson L.C. (1963) Can. Journ. Phys. 41, 1047.

Grimes L.G. and Jackson L.C. (1959) Phil. Mag. 4, 1346.

Guo H.M., Edwards D.O., Sarwinski R.E. and Tough J.T. (1971) Phys. Rev. Lett. 27, 1259.

Hallock R.B. and Flint E.B. (1973) Phys. Rev. Lett. 31, 1383.

Ham A.C. and Jackson L.C. (1957) Proc. Roy. Soc. A240, 243.

Harris-Lowe R.F. (1977) Journ. Low Temp. Phys. 28, 489.

Harris-Lowe R.F. and Turkington R.R. (1971) Journ. Low Temp. Phys. 4, 525.

Harris-Lowe R.F. and Turkington R.R. (1973) Journ. Low Temp. Phys. 10, 369.

Harris-Lowe R.F., Mate C.F., McCloud K.L. and Daunt J.G. (1966) Phys. Lett. 20, 126.

Harrison S.J. and Mendelssohn K. (1974) Proc. 13th Int. Conf. on Low Temp. Phys. Plenum Press N.Y. p.298.

Hebert G.R., Chopra K.L. and Brown J.B. (1957) Phys. Rev. 106, 391.

Heer C., Barnes C. and Daunt J. (1954) Rev. Sci. Instr. 25, 1088.

Henkel R.P., Kukich G. and Reppy J.D. (1968) Proc. 11th Int. Conf. on Low Temp. Phys. (eds. Allen, Finlayson and McCall) St Andrews Univ. p.178.

Henshaw D.G. (1958) Phys. Rev. Lett. 1, 127.

Hoffer J.K., Fraser J.C., Hammel E.F., Campbell L.J., Keller W.E. and Sherman R.H. (1974) Proc. L.T.13, Plenum Press, p.253.

Hull J.R. and Hull R.A. (1941) Journ. Chem. Phys. 9, 465.

Iordanskii S.V. (1965) Soviet Physics J.E.T.P. 21, 467.

Kapitza P. (1938) Nature (London) 141, 74.

Keller W.E. (1970) Phys. Rev. Lett. 24, 569.

Keller W.E., Hammel E.F., Campbell L.J. and Jones D.M. (1969) Proc. 11th Int. Conf. on Low Temp. Phys. (eds. Allen, Finlayson and McCall) St Andrews Univ. p.182.

Keller W.E. and Hammel E.F. (1965) Cryogenics 5, 245.

Keller W.E. and Hammel E.F. (1966a) Phys. Rev. Lett. 17, 998.

Keller W.E. and Hammel E.F. (1966b) Physics 2, 221.

Keller W.E. and Hammel E.F. (1974) Proc. 13th Int. Conf. on Low Temp. Phys. (Timmerhaus, O'Sullivan and Hammel, eds.) Plenum Press, N.Y. p.263.

Kontorovich V.M. (1956) Soviet Phys. J.E.T.P. 3, 770.

Kukich G., Henkel R.P. and Reppy J.D. (1968) Phys. Rev. Lett. 21, 197.

Kwoh D.S. and Goodstein D.L. (1977) Journ. Low Temp. Phys. 27, 187.

Lamb H. "Hydrodynamics" (1965) Dover Publications, N.Y. 6th Ed. p.241.

Landau L.D. (1941) Journ. of Phys. U.S.S.R. 5, 71.

Landau L.D. (1947) Journ. of Phys. U.S.S.R. 11, 91.

Langer J.S. and Fisher M.E. (1967) Phys. Rev. Lett. 19, 560.

Langer J.S. and Reppy J.D. (1970) Prog. Low Temp. Phys. 6, 1.

Lavrova V.V., Rachitskii D.G., Fisher L.M. and Yudkin V.A. (1973) Cryogenics, July, p.438.

Lawless W.N. (1971) Rev. Sci. Instr. 42, 561.

Lawless W.N., Rade Braugh R. and Soulen R.J. (1971) Rev. Sci. Instr. 42, 567.

Lesensky L. and Boorse H.A. (1952) Phys. Rev. 87, 1135.

Liebenberg D.H. (1971a) Phys. Rev. Lett. 26, 744.

Liebenberg D.H. (1971b) Journ. Low Temp. Phys. 5, 267.

Lifshitz E.M. (1956) Sov. Phys. J.E.T.P. 2, 73.

Little W.A. (1964) Prog. in Cryogenics 4, 99.

London H. (1939) Proc. Roy. Soc. A171, 484.

Mate C.F., Harris-Lowe R. and Daunt J.G. (1965) Proc. 9th Int. Conf. on Low Temp. Phys. Plenum Press N.Y. p.206.

McFee R. (1958) Rev. Sci. Instr. 30, 98.

Mehl J.B. and Zimmerman W. (1965) Phys. Rev. Lett. 14, 815.

Mendoza E. (1961) Experimental Cryophysics p.165.

Notarys H.A. (1969) Phys. Rev. Lett. 22, 1240.

Oda Y., Fujii F. and Nagano H. (1974) Cryogenics, Feb., 84.

Olijhoek J.F., Van Alphen W.M., de Bruyn Ouboter R. and Taconis K.W. (1967) Physica, 35, 483.

Olijhoek J.F., Hoffer J.K., Van Beelen H., de Bruyn Ouboter R. and Taconis K.W. (1973a) Physica, 64, 289.

Olijhoek J.F., Van Beelen H., de Bruyn Ouboter R. and Taconis K.W. (1973b) Physica, 69, 38.

Onsager L. (1949) Nuovo Cimento Suppl. 6, 2249.

Palevsky H. et al (1957) Phys. Rev. 108, 1346.

Picus G.S. (1954) Phys. Rev. 94, 1459.

Probert D. (1964) Nature, 283.

Rayfield G.W. and Rief F. (1964) Phys. Rev. 136 A, 1194.

Reppy J.D. and Depatie D. (1964) Phys. Rev. Lett. 12, 187.

Roberts P.H. and Donnelly R.J. (1970) Phys. Lett. 31A, 137.

Robinson J.E. (1951) Phys. Rev. 82, 440.

Rollin B.V. (1936) Proc. VII Int. Congress of Refrigeration 1, 187.

Rubin L.G. and Lawless W.N. (1971) Rev. Sci. Instr. 42, 571.

Sabisky E.S. and Anderson C.H. (1973) Phys. Rev. A7, 790.

Saunders B.L. (1974) Ph.D. Thesis. Univ. St Andrews.

Schiff L.T. (1941) Phys. Rev. 59, 838.

Schmid L.P. and Smart J.S. (1954) U.S. Naval Ordnance Rep. No. 3640.

Seki H. (1962) Phys. Rev. 128, 502.

Smith B. and Boorse H.A. (1955) Phys. Rev. 99, 346.

Staas F.A. and Severijns A.P. (1969) Cryogenics 9, 422.

Telschow K., Rudnick I. and Wang T.G. (1975) Journ. Low Temp. Phys. 18, 43.

Tisza L. (1938) Nature, 141, 913.

Van Alphen W.M., Van Haasteren G.J., de Bruyn Ouboter R. and Taconis K.W. (1966) Phys. Lett. 20, 474.

Van Dijk H. and Durieux M. (1958) Physica 24, 1.

Van Spronsen E., Verbeek H.J., de Bruyn Ouboter R., Taconis K.W. and Van Beelen H. (1973) Phys. Lett. A45, 49.

Van Spronsen E., Verbeek H.J., Van Beelen H., de Bruyn Ouboter R. and Taconis K.W. (1974) Physica 77, 570.

Verbeek H.J., Van Spronsen E., Mars H., Van Beelen H., de Bruyn Ouboter R. and Taconis K.W. (1974a) Physica 73, 621.

Verbeek H.J., Van Spronsen E., Van Beelen H., de Bruyn Ouboter R. and Taconis K.W. (1974b) Physica 77, 131.

Vilches O.E. and Wheatley J.C. (1966a) Phys. Rev. 148, 509.

Vilches O.E. and Wheatley J.C. (1966b) Rev. Sci. Instr. 37, 819.

Vinen W.F. (1963) "Liquid Helium" (G. Careri ed.) Academic Press N.Y. p.336.

Wagner F. (1973) Journ. Low Temp. Phys. 13, 185.

Wagner F. (1976) Journ. Low Temp. Phys. 23, 771.

Wang T.G. and Rudnick I. (1974) Proc. 13th Int. Conf. on Low Temp. Phys. (Timmerhaus, O'Sullivan and Hammel, eds.) Plenum Press N.Y. p.239.

Waring R.K. (1955) Phys. Rev. 99, 1704.

Williams G.A. and Packard R.E. (1974) Phys. Rev. Lett. 32, 587.

Arnold P.G., Bendt P.J. & Kerr E.C.

Yarnell J.L. (1959) Phys. Rev. 113, 1379.

Zinov'eva K.N. and Boldarev S.T. (1969) Sov. Phys. J.E.T.P. 29, 585.